Yuan, Qiheng (2020) *Variability analysis of wind and solar energy for optimal power system integration.* PhD thesis.

.

Variability analysis of wind and solar energy for optimal power system integration

Qiheng Yuan

Degree of Doctor of Philosophy

School of Engineering

College of Science and Engineering

University of Glasgow

April 2020

To my family

Statement of Originality

I certify that the thesis presented here for examination for a PhD degree of the University of Glasgow is solely my own work other than where I have clearly indicated that it is the work of others (in which case the extent of any work carried out jointly by me and any other person is clearly identified in it) and that the thesis has not been edited by a third party beyond what is permitted by the University's PGR Code of Practice.

The copyright of this thesis rests with the author.

No quotation from it is permitted without full acknowledgment.

I declare that the thesis does not include work forming part of a thesis presented successfully for another degree.

I declare that this thesis has been produced in accordance with the University of Glasgow's Code of Good Practice in Research.

I acknowledge that if any issues are raised regarding good research practice based on a review of the thesis, the examination may be postponed, pending the outcome of any investigation of the issues.

Signature:

Date: 30/March/2020

Acknowledgment

I would like to thank my supervisor Dr. Keliang Zhou, who provides continuous support for my PhD research. His guidance helps me in all the time of this research and writing this thesis. I would like to thanks my supervisor Dr. Jin Yang, who took over me after Dr. Keliang Zhou left the University of Glasgow. Without his support, it is not possible to finish my research work and this thesis. I would like to thank Dr. Jing Yao, Dr. Wenzhou Lu and Weicong Luo, who help me master geography software and participate in the publications.

I would like to thank all the departments of science and engineering school at the University of Glasgow. They do the fantastic work of helping all the postgraduate research students to research in their area of interest.

In addition, I also want to thank all my friends at the University of Strathclyde, the University of Edinburgh and the University of Manchester. They bring me a lot of happy time in my PhD period and I hope they all go well in the future.

At last, I would like to express the deepest appreciation to my father Lianqing Yuan and my mother Rui Wang. They give all their love to me and raise me as a man. They always support my decisions unconditionally. This thesis will be a gift to all my family members.

Abstract

The development of renewable energy has made a significant contribution to the mitigation of global climate change and environmental pollution. In particular, the installed capacity of intermittent wind and solar power in the world has increased significantly in the past decade, and this growth is expected to be maintained in the future. Due to the intermittence and uncontrollability of wind and solar energy, the integration of wind and solar energy into power systems brings significant impacts on the operation and profit of power systems.

This thesis focuses on exploring the wind and solar power variability and its impacts on power system integration. Chapter 2 proposes a new measure to assess the variability of wind power, solar power and mixed wind-solar at one site, and the variability of interconnected wind and solar power from different sites in both the time domain and frequency domain. In the time domain, the measure mainly includes inter-annual variation, smoothness coefficient and correlation coefficient; while in the frequency domain, it mainly includes frequency spectrum analysis, fluctuation rate, and cumulative energy distribution index. The implications of the proposed measure are explored to facilitate power system integration. Without loss of generality, enormous wind and solar data collected at various locations and spanning a long period are employed to assess the variability of wind and solar power, which are taken from National Renewable Energy Laboratory (NREL) databases. The measurement results indicate that the variability of solar power highly depends on the latitude of its geographic location; the interconnection of wind power can effectively reduce the variability of wind power in the high-frequency range; the intermittent wind/solar power in the time domain can be treated as a Quasi-Time-Invariant (QTI) source of power harmonics in the frequency domain.

Based on the proposed variability measure, Chapter 3 investigates the impacts of the wind and solar power variability on the sizing of the standalone wind/solar power systems. Taking the impacts of wind and solar power variability into consideration, big data simulations of the six Satandalone Wind Power (SAWP) and six Standalone Photovoltaic power (SAPVP) systems with the same residential load demand at the six sites were carried out to reveal the dependency between the sizing of the system components (i.e., the battery and the wind turbines/PV panels) and the power supply reliability. Case studies of optimal sizing of the SAWP system at Chicago and optimal sizing of the SAPVP system at Houston

were carried out to demonstrate the feasibility of the proposed methods, which aims is to minimize the system cost while satisfying the requirement of power supply reliability.

The chapter 4 attempts to employ the cumulative energy distribution index to evaluate the variability costs for the integration of high penetration level wind/solar power into power grids. Big data simulations of the Electric Reliability Council of Texas power system (ERCOT) in 2018 reveal the impacts of grid flexibility on wind/solar energy curtailment rate and capacity factor at different penetrations. The maximum wind/solar energy penetration can be roughly determined according to the requirements of the wind/solar power capacity factor and energy curtailment of the power systems with specific flexibility. A case study of 70% grid flexibility with 20 wind farms and 10 solar plants interconnected ERCOT power system shows that the developed large time scale variability costs index can be used to estimate the variability cost when wind and solar energy penetration is between 30% to the maximum penetration.

Contents

List of Figures

List of Tables

List of Symbols

A_S	Size of the PV panel
A_W	The blade swept area of wind turbine
B_{ac}	Active battery capacity
B_n	Nominal battery capacity
B^*	The most cost-effective final battery capacity
C_{Bi}	Initial cost of battery bank
C_{Bm}	Maintenance cost of battery bank
CF_{RE}	Capacity factor of renewable energy
$CF_{RE\text{-}set}$	Specified minimum renewable power capacity factor
CF_S	Capacity factor of solar energy
CF_W	Capacity factor of wind energy
$CF_{W\&S}$	Capacity factor of hybrid wind and solar energy
C_{Pi}	Initial cost of PV panel
C_{Pm}	Maintenance cost of PV panel
CR_{RE}	Renewable energy curtailment rate
$CR_{RE\text{-}set}$	Specified maximum renewable energy curtailment
CR_S	Solar energy curtailment rate
CR_W	Wind energy curtailment rate
$CR_{W\&S}$	Curtailment rate of hybrid wind and solar energy
C_V	Variability costs
C_{Wi}	Initial cost of wind turbine
C_{Wm}	Maintenance cost of wind turbine
COE_S	COE of SAPVP system
COE_W	COE of SAWP system
C_P	Power coefficient
C_{Pmax}	Maximum power coefficient
d	Day of the year
DoD	Depth of discharge of the battery

$D_{RE(y)}(j)$	Cumulative energy distribution index for renewable energy
$D_{REgen}(j)$	Cumulative energy distribution index for generated renewable energy in the power grid
$D_{S(y)}(j)$	Cumulative energy distribution index for solar energy
$D_{Sgen}(j)$	Cumulative energy distribution index for generated solar energy in the power grid
$D_{W(y)}(j)$	Cumulative energy distribution index for wind energy
$D_{Wgen}(j)$	Cumulative energy distribution index for generated wind energy in the power grid
$D_{W\&S(y)}(j)$	Cumulative energy distribution index for hybrid wind and solar energy
$D_{W\&Sgen}(j)$	Cumulative energy distribution index for generated hybrid wind and solar energy in the power grid
$e_L(i)$	Energy of i-th order load energy harmonic for the year y
$e_{M(y)}(i)$	Energy of i-th order generation-load mismatch energy harmonic for the year y
$e_{Mavg}(i)$	Average energy of i-th order generation-load mismatch energy harmonic for the year y
$e_{RE(y)}(i)$	Energy of i-th order renewable energy harmonic for the year y
$e_{REgen}(i)$	Generated energy of i-th order renewable energy harmonic in the power grid
$e_{S(y)}(i)$	Energy of i-th order solar energy harmonic for the year y
$e_{Savg}(i),$	Average energy of i-th order solar energy harmonic for the year y
$e_{W(y)}(i)$	Energy of i-th order wind energy harmonic for the year y
$e_{Wavg}(i)$	Average energy of i-th order wind energy harmonic for the year y
$e_{W\&S(y)}(i)$	Energy of i-th order hybrid wind and solar energy harmonic for the year y
$E_{RE}(y)$	Total annual renewable power generation for the year y
$E_S(y)$	Total annual solar power generation for the year y
$E_W(y)$	Total annual wind power generation for the year y
$E_{W\&S}(y)$	Total annual hybrid wind and solar power generation for the year y
$f(i)$	Frequency of the i-th order harmonics
F_G	Grid flexibility
$F_S(y)$	Fluctuation rate of solar power for the year y
F_{Savg}	Average fluctuation rate of solar power from the year y_0 to Y
$F_{RE}(y)$	Fluctuation rate of renewable power for the year y

F_{REavg}	Average fluctuation rate of renewable power from the year y_0 to Y
$F_W(y)$	Fluctuation rate of wind power for the year y
F_{Wavg}	Average fluctuation rate of wind power from the year y_0 to Y
$F_{W\&S}(y)$	Fluctuation rate of hybrid wind and solar power for the year y
$F_{W\&Savg}$	Average fluctuation rate of hybrid wind and solar power from the year y_0 to Y
G_{min}	Minimum generation level of the power system
h	Original height
$h_S(i)$	DFT of $P_{N\text{-}S}$ at frequency domain point i
$h_{RE}(i)$	DFT of $P_{N\text{-}RE}$ at frequency domain point i
$h_{REgen}(i)$	DFT of $P_{N\text{-}REgen}$ at frequency domain point i
$h_W(i)$	DFT of $P_{N\text{-}W}$ at frequency domain point i
$h_{W\&S}(i)$	DFT of $P_{N\text{-}W\&S}$ at frequency domain point i
H	Objective height
I_{avg}	Annual average solar irradiation
$I_{RE}(y)$	Ratio of the total renewable energy in the year y to the average for the years y_0 to Y
$I_S(y)$	Ratio of the total solar energy in the year y to the average for the years y_0 to Y
$I_W(y)$	Ratio of the total wind energy in the year y to the average for the years y_0 to Y
$I_{W\&S}(y)$	Ratio of the total hybrid wind and solar energy in the year y to the average for the years y_0 to Y
L	Geographical latitude
m_B	Margin factor of battery bank capacity
m_S	Margin factor of PV panel
m_W	Margin factor of wind turbine
N_B	Required number of the battery bank
$N_{\text{Interconnected}}$	Sample size for the output power data of interconnected wind and solar sites
N_S	Sample size for solar irradiation data
N_{Single}	Sample size for the output power data of single wind or solar site
N_W	Sample size for wind speed data

p_{RE}	Renewable energy penetration
p_S	Solar energy penetration
p_W	Wind energy penetration
$p_{W\&S}$	Hybrid wind and solar energy penetration
$P_{ava\,RE}(i)$	Available renewable power
$P_{ava\,S}(i)$	Available solar power
$P_{ava\,W}(i)$	Available wind power
$P_{ava\,W\&S}(i)$	Available wind and solar power
P_{BES}	Balancing energy services prices
$P_{cur\,RE}(i)$	Curtailed renewable power
$P_{cur\,S}(i)$	Curtailed solar power
$P_{cur\,W}(i)$	Curtailed wind power
$P_{cur\,W\&S}(i)$	Curtailed wind and solar power
$P_G(i)$	Gross power generation of the power system
$P_{G\,min}$	Minimum power output of the power system
$P_{Interconnected}$	Output power of interconnected wind and solar sites
P_L	Load demand
P_{Lavg}	Average annual residential load
$P_{L\,peak}$	Approximate peak load demand
$P_{Net\,load}$	Net load
$P_{N\text{-}RE}(i)$	Nominalized annual renewable power generation
$P_{N\text{-}REgen}(i)$	Nominalized generated renewable power in the power grid
$P_{N\text{-}S}(i)$	Nominalized annual solar power generation
$P_{N\text{-}Sgen}(i)$	Nominalized generated solar power in the power grid
$P_{N\text{-}W}(i)$	Nominalized annual wind power generation
$P_{N\text{-}Wgen}(i)$	Nominalized generated wind power in the power grid
$P_{N\text{-}W\&S}(i)$	Nominalized annual hybrid wind and solar power generation
$P_{N\text{-}W\&Sgen}(i)$	Nominalized generated hybrid wind and solar power in the power grid
$P_{rat\,RE}(i)$	Rated renewable power output

$P_{rat\ S}(i)$	Rated solar power output
$P_{rat\ W}(i)$	Rated wind power output
$P_{rat\ W\&S}(i)$	Rated wind and solar power output
P_{RE}	Annual renewable power generation
$P_{REgen}(i)$	Generated power from renewable power in the power grid
P_S	Solar power output
$P_{Sgen}(i)$	Generated solar power in the power grid
P_{Single}	Output power of single wind or solar site
P_W	Wind power output
$P_{Wgen}(i)$	Generated wind power in the power grid
$P_{W\&S}$	Hybrid wind and solar power output
$P_{W\&Sgen}(i)$	Generated power from hybrid wind and solar power in the power grid
$\bar{P}_{Interconnected}$	Average output power of interconnected wind and solar sites
$\bar{P}_L$	Average load demand
$\bar{P}_S$	Average solar power output
$\bar{P}_{Single}$	Average output power of single wind or solar site
$\bar{P}_W$	Average wind power output
ΔP	Generation-load power mismatch
q_H	Hourly energy component
r	Correlation coefficient
R_{RE}	Power supply reliability of standalone renewable energy systems
R_S	Power supply reliability of SAPVP systems
R_{set}	Specified minimum required power supply reliability
$R_{S\ min}$	Minimum system reliability of SAPVP system
R_W	Power supply reliability of SAWP systems
$R_{W\ min}$	Minimum system reliability of SAWP system
$R_{W\&S}$	Power supply reliability of standalone hybrid wind and solar power systems
S	Smoothness coefficient of interconnected wind and solar power
S_i	Solar irradiation of i-th sample

S_I	Solar irradiation
SoC_{ini}	Initial state of charge
SoC_{max}	Maximum state of charge
SoC_{min}	Minimum state of charge
T	Period
T_{op}	Operating time
T_{out}	Total power outage time
T_S	Sampling time interval
T_V	Selected time scale
v_{avg}	Average wind speed
v_h	Wind speed at original height
v_H	Wind speed at objective height
v_i	Cut-in wind speed
v_o	Cut-off wind speed
v_r	Rated wind speed
W_i	Wind speed of i-th sample
z	Solar zenith angle
α	Size factor
β	Ratio of wind and solar power generation directly transferred to the load
γ	Correction coefficient
δ_{FREmax}	Upper bound of $F_{RE}(y)$
$\delta_{FRE\,min}$	Lower bound of $F_{RE}(y)$
$\delta_{FS\,max}$	Upper bound of inter-annual variation of solar power
$\delta_{FS\,min}$	Lower bound of inter-annual variation of solar power
$\delta_{FW\,max}$	Upper bound of inter-annual variation of wind power
$\delta_{FW\,min}$	Lower bound of inter-annual variation of wind power
$\delta_{IRE\,max}$	Upper bound of $I_{RE}(y)$
$\delta_{IRE\,min}$	Lower bound of $I_{RE}(y)$

$\delta_{IS\,max}$	Upper bound of inter-annual variation of solar power
$\delta_{IS\,min}$	Lower bound of inter-annual variation of solar power
$\delta_{IW\,max}$	Upper bound of inter-annual variation of wind power
$\delta_{IW\,min}$	Lower bound of inter-annual variation of wind power
ε	Exponential coefficient
η_{PV}	Power generation efficiency of PV panel
η_W	Power generation efficiency of Wind turbine
λ	Surface roughness
ρ	Air density
$\sigma_{\text{Interconnected}}$	SD of interconnected wind and solar power
σ_S	SD of solar irradiation
σ_{Single}	SD of single wind or solar power output
σ_W	SD of wind speed
ϕ	Solar declination angle

Abbreviations

COE	Cost of Energy
DFT	Discrete Fourier transform
DHI	Diffuse Horizontal Irradiance
DNI	Direct Normal Irradiance
ERCOT	Electric Reliability Council of Texas
FFT	Fast Fourier Transform
FRCC	Florida Reliability Coordinating Council
GHI	Global Horizontal Irradiance
GNI	Global Normal Irradiance
ISO-NE	ISO New England
MISO	Midcontinent Independent System Operator
MPPT	Maximum Power Point Tracking
NREL	National Renewable Energy Laboratory
NSRDB	National Solar Radiation Data Base
NYISO	New York energy law
PJM	PJM interconnection
PSD	Power Spectra Density
PV	Photovoltaic
QTI	Quasi-Time-Invariant
SAPVP	Standalone Photovoltaic Power
SAWP	Standalone Wind Power
SD	Standard Deviation
SERC	SERC Reliability Corporation
SPP	Southwest Power Pool
RPS	Renewable Portfolio Standards
WIND	Wind Integration National Dataset

Chapter 1

Introduction

Since 1960, human activities have become the main factor in climate change [1-4]. A growing consensus over the dangers posed by climate change has prompted people and governments worldwide to seek ways to generate that energy while minimizing carbon emissions and other environmental impacts. Over the past 40 years, the global population grew from 4 billion to more than 7 billion people [5]. The increase in the proportion of middle class living in cities further increases the global energy consumption and carbon emissions. Fortunately, the development of renewable energy offers a viable option for the mitigation of carbon emissions and energy deficit. Rapid technological progress, combined with falling costs enables renewable energy, especially wind and solar power, to provide an answer to the Energy Trilemma as shown in Figure 1.1 [6-9].
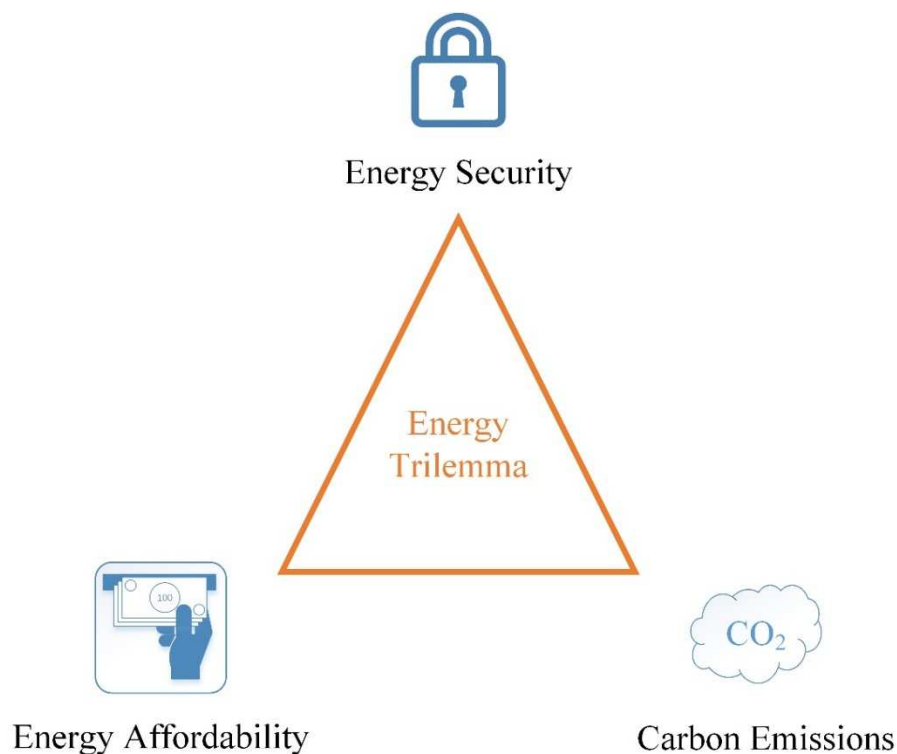
Figure 1.1 The Energy Trilemma.

1.1 Development of renewable energy

The issues of climate change and energy deficit significantly boost renewable energy integration. The global renewable energy capacity (including hydropower) reaches 6674 TWh in the year of 2017 with 4065 TWh hydropower, 1128 TWh wind power, 584 TWh solar power and 585 TWh other renewable power as shown in Figure 1.2 [10]. It can be seen that, besides hydropower, the installed capacity of wind and solar power has increased significantly in recent years which far exceeds the installed capacity of other renewable power. In addition, due to the limited potential of hydro resources, the global growth rate of hydropower is estimated at about 2.4% in the future [11-13]. On the other hand, the abundant wind and solar resources are bound to cause wind and solar power to become the emphasis of future renewable energy development.
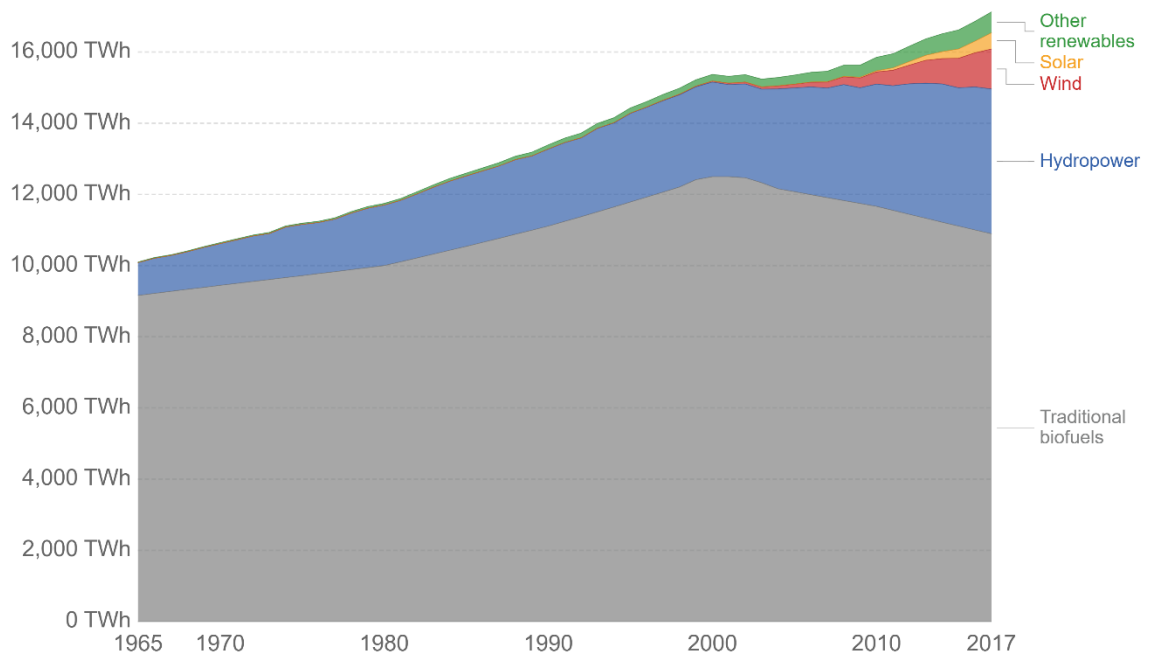
Figure 1.2 Global energy consumption [10].

In fact, many regions have taken strong initiatives to increase their renewable energy capacity in a certain period. For example, in Europe, ETP Smart Grids proposed the Strategic Research Agenda 2035 which expected more than 34% of the gross electrical energy consumption would be supplied by renewable energy by 2035 [14]. In China, China National Energy Administration established The 13th Renewable Energy Development Five Year Plan which announced that 680 GW renewable energy capacity will be installed by 2020, and the

share of renewable energy in total primary energy consumption will increase to 15% by 2020 and to 20% to 2030 [15]. Also, in the United States, 29 states adopted Renewable Portfolio Standards (RPS) that mandated a certain proportion of renewable energy in the overall energy consumption, and most states' targets are between 10% to 50% [16]. Among these plans, the new installation of wind and solar power occupies the majority of renewable energy development goals. By the end of 2019, the top 10 countries of wind and solar power installed capacity are shown in Table 1.1. China has the largest installed capacity of wind and solar power by far, followed by the USA.

Table 1.1
The top 10 countries of wind and solar power installed capacity in 2019 [17].

Wind power		Solar power	
Country	**Installed capacity (TWh)**	**Country**	**Installed capacity (TWh)**
China	406	China	224
USA	300	USA	107
Germany	126	Japan	73
UK	65	Germany	47
India	63	India	46
Brazil	56	Italy	24
Spain	55	Australia	17
France	34	Spain	15
Canada	30	UK	13
Sweden	22	South Korea	13

1.2 Motivation and problem formulation

Renewable energies are quickly becoming significant sources of electricity supply. However, due to their intermittent and undispatchable nature, variable renewable energies (primarily wind and solar power) will increase the operational costs and reliability of electricity systems because system operators have to resort to additional flexible resources (such as storage technologies or dispatchable electrical generators) to balance fluctuations and uncertainties in the output of wind and solar power. Otherwise, the unbalance between the wind and solar power supply and the time-varying load demand will cause power outages in the case of insufficient wind and solar power, or will bring power losses in the case of excessive solar and wind power [18]. It can be said that, the mitigation of wind and solar

power variability will impose prominent impacts on operation reliability and system economy of electrical power systems.

1.3 Review of wind and solar power integration

It is a big challenge to effectively cope with the variability of wind and solar power for integrating high levels of renewable generation into electricity systems. It is a must to better understand and depict the wind and solar power variability for its effective mitigation.

1.3.1 Variability analysis of wind/solar power

Variability of wind and solar power is a multi-faceted spatial and temporal concept described by a range of measurable parameters on different timescales or in different magnitude variation range, such as statistical distribution, persistence, frequency, correlation, and so on. Regarding the cost and reliability of a system with high renewables penetrations, these distinct characteristics may give rise to a range of different implications for power system integration. Generally speaking, variability analysis can be classified into time domain analysis and frequency domain analysis.

a. Time domain

YH. Wan analyzed the wind power of 6 sites in Texas, Lowa and Minnesota at 1 second, 1 minute and 1-hour time scale [19]. It found that wind power variations on hourly timescales were much larger than the sub-hourly variations, reaching up to 70% of the entire rated capacity of the wind farm, although it was discovered that such events were very infrequent. Meanwhile, there are some studies approved that the change in wind speed is complex and is affected by the terrain [20-22]. They found wind speed-ups in complex terrain are reduced when compared to those found above isolated hills or ridges in the USA, Canada, UK.

Solar power variability is affected by many environmental factors and it is hard to find how solar power changes at different time scales. E. Friis-Christensen and K. Labitzke presented that the changes in solar irradiation are periodic which can be a one-year cycle or a multi-year cycle [23, 24]. Some studies have confirmed that cloud, volcano and internal climate oscillations will cause solar power variability [25-29]. In addition, measurements

show that 10 to 20% of solar irradiance will be absorbed by the stratospheric ozone that implied geographical latitude might affect solar power [30-33].

In the time domain, wind power and solar power vary in different time scales [34]. The step-change analysis of the power produced by wind and solar plants and the duty ratio of power ramp is used to evaluate the wind and solar power variability [35-37].

Geographical distribution and power source interconnection are essential directions for studying wind and solar power variability. H. Holttinen and G. Sinden studied the reduction of wind variability due to geographic dispersion on a one-hour level in the Nordic countries and the UK [38-40]. They point out as geographical distance increase, interconnected wind farms show a smoothing effect on wind power variability. The smoothing effect of solar power variability due to geographical spreading has been explored in Germany as well [41]. A similar smoothing effect also was found for seven interconnected solar plants in Spain [42].

Correlation analysis is also often used to explore wind and solar power variability. Some studies identified a weak correlation between wind power generation and load demand in Ireland [43], Germany [44] and Finland [45]. In addition, G. Giebel and L. Landberg also confirm this weak correlation based on a European scale with about 60 sites of 3-hour wind data resolution [46, 47]. Moreover, some studies found the negative correlation between wind and solar power in Sweden [48], Iberian Peninsula [49] and the USA [50]. These imply that wind and solar power are two utterly different energy sources and hybrid wind and solar energy may reduce overall variability.

b. Frequency domain

Some studies found the Power Spectra Density (PSD) in the frequency domain of the power output of wind turbine and Photovoltaic (PV) panel followed a Kolmogorov spectrum at high frequency as shown in Figure 1.3, while the PSD of output power from interconnected wind and solar plants decreased rapidly at high frequency [51-55]. In addition, the red line in Figure 1.3 is the fitting curve of the wind power in the frequency domain that follows the $f^{-5/3}$ Kolmogorov curve. Thus, according to $f^{-5/3}$ Kolmogorov power spectrum of the wind power generators, the power density of wind power significantly decreases the growth of the frequency.

In addition, the PSD of interconnected disperse wind or solar power is found to blow the $f^{-5/3}$ Kolmogorov curve in high frequency band. That also implies that geographical dispersion and wide-area interconnection could help reduce overall variability and help the long term integration of wind energy to power systems.
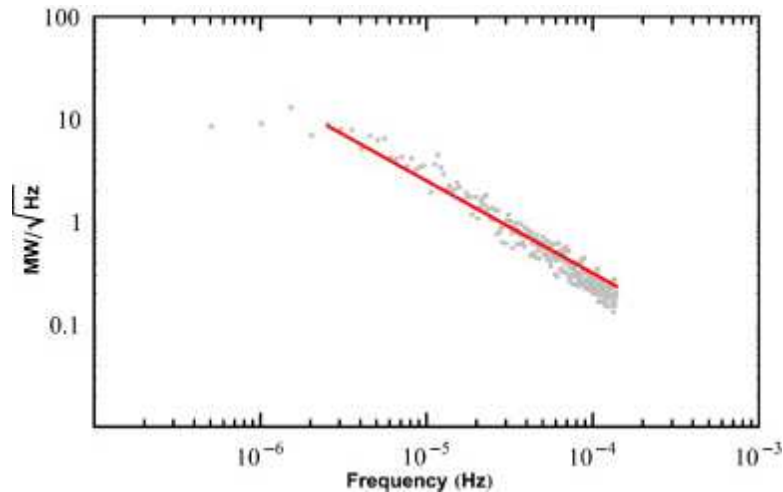
Figure 1.3 Wind power output shows the Kolmogorov spectrum feature [52].

So far, the variability analysis focuses primarily on the behavior of of wind and solar power. The variability analysis in the time domain qualitatively describes the variations of the wind and solar power. The power spectrum analysis preliminarily demonstrates the power fluctuations and its distribution in the frequency domain. However, for optimal integration of wind and solar power into both standalone power systems and power grids, distinct characteristics of wind and solar variability still need to be identified and assessed, and their specific implications for power system integration need to be determined.

1.3.2 Standalone wind/solar power systems

Standalone wind and solar power are employed by remote household users where the electricity obtained from the power grid is not affordable but has excellent local renewable energy resources. For example, T. Ma et al., H. Fathabadi et al. and AH. AI-Badi et al., investigated the standalone alone wind and solar power system in the remote islands and Al Duqm in Oman [56-59]. They find that with the effective variability mitigation method like energy storage devices, the standalone power system can be powered only by the wind and solar resources. AH. AI-Badi pointed out that when the average wind speed beyond 5.3 m/s, the standalone wind power system can provide a lower cost of energy than the conventional

power resources in Oman. The average wind speed in Oman is more than 5.3 m/s which means it is completely feasible to adopt standalone wind power in Oman. T. Ma introduced pumped hydro storage for the standalone hybrid wind and solar system to a remote island in Hong Kong. The hour-by-hour simulation results indicate that the intermittent nature of the renewables can be compensated which implies that technically the energy storage based renewable power system is an ideal solution to achieve 100% energy autonomy in remote communities. Moreover, standalone wind and solar power are also employed in some special cases. For example, W. He presents a case study of integrating a 20 MW standalone wind farm into an offshore oil and gas platform [60]. He assessed the benefits of fuel consumption and carbon emissions reduction and the stability of this standalone wind power system. The results confirm the feasibility of offshore wind power for offshore drilling platforms. Similarly, AAM. Zin explored the potential of standalone hybrid wind and solar power systems for Iran drilling oil rigs in the desert [61]. He found that for the reliable operating of the standalone hybrid wind and solar power system for the drilling oil rigs, the electricity generation is increased by around 18% to 0.938$/kWh. However, since the stand-alone system can be installed locally, there is no need for expensive transmission costs. Moreover, this study also found that hybrid wind and solar power will reduce 50% dependency on battery.

a. Variability mitigation measures
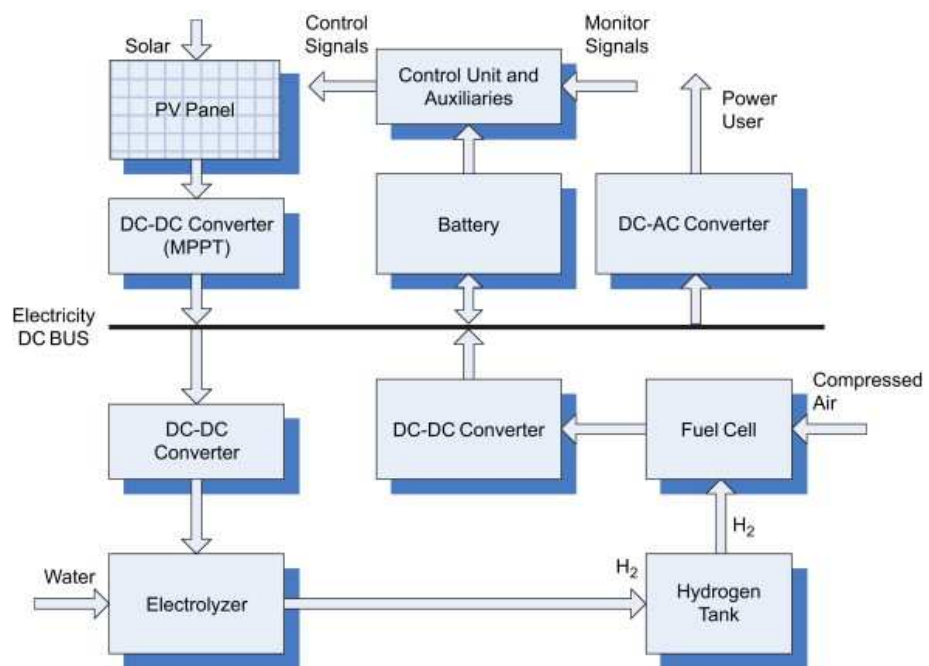
Figure 1.4 A standalone PV-hydrogen power system [62].

A typical Standalone wind/solar power system generally consists of a wind turbine and/or PV panels, an energy storage system, and an end-user load. Basically, the generated wind and solar power should produce sufficient electricity to meet the load demand. However, the mismatch between intermittent wind/solar power and varying load demand would cause power outages in the case of a power supply deficit, and power losses in the case of excessive power supply. To increase the power supply reliability and the system efficiency, the energy storage is incorporated to make the wind and solar power dispatchable. There are many researches try to find an optimal combination of multiple energy storage devices to minimize wind and solar variability. For instance, Figure 1.4 shows a Standalone PV Power (SAPVP) system that includes the battery system for short-term energy storage and a hydrogen system for long-term energy storage [62]. Through two energy storage devices, most of the wind and solar power fluctuations can be buffered. However, due to the efficiency of industrial electrolysis is up to 70% [63] and the efficiency of the fuel cell is between 50% to 60% [64], the gross efficiency of the hydrogen system is usually less than 40%. Meanwhile, most long-term energy storage devices have significant high initial costs and maintenance costs [65-67]. Thus, research on reducing wind and solar power fluctuations through energy management strategies can improve power supply reliability, but generally leads to low system efficiency and poor system economics.

In addition, standby diesel generators can be optionally added into the standalone wind/solar power systems to compensate power outage, but would incur expensive costs of carbon-emitting fuel, operation and maintenance in the life cycle [68-70]. Oversized wind turbines or PV panels also help reduce the power outages at the expense of an extra installed cost of the wind turbine and PV panel [71].

b. Optimal sizing methods

There are many optimal sizing methods proposed for standalone wind/solar power systems. A. S. AI Busaidi directly used average annual load demand to determine the size of wind turbines and PV panels which ignores the variations of annual wind and solar power [69]. R. Hosseinalizadeh implemented iterative algorithms to optimize standalone wind/solar power systems in terms of minimizing the system costs in Iran [72]. This study also set the system reliability must reach 98%. M. Smaoui proposed an optimization methodology based on an iterative technique to optimize the size of standalone wind and solar power systems in order to supply a desalination unit for Kerkennah Island in South Tunisia [73]. The main objective of this optimization was minimizing the system cost. This

study found that the complementary characteristics of the hybrid wind and solar power can reduced system costs because of the reduction of energy storage requirements. R. Belfkira gave a multi-objective optimization method called DIRECT to optimal sizing standalone wind and solar power systems [74]. This study found a global optimum of system costs and energy availability for remote users. C. E. C. Nogueira used linear programming to optimal sizing standalone wind and solar power systems by minimizing the system costs while letting the wind and solar power output meet the load demand [75]. Genetic Algorithm, which usually is used to solve the non-linear problem, is one of the most potent optimization algorithms which has been paid attention in the sizing of standalone wind and solar power system. H. Chen used the adaptive Genetic Algorithm to optimal sizing of the standalone wind and power systems in Taiwan in terms of minimum system costs [76]. Moreover, some researches proposed big data management which includes data integration, data storage, data analytics, data visualization, data transmission and so on to optimal sizing standalone wind/solar power systems as well [77-79].

Table 1.2
Common approach for optimal sizing of standalone wind and solar power systems.

Optimization approaches	References	Disadvantages
Graphic construction method	[80, 81]	Few system parameters are considered
Probabilistic method	[82-84]	Cannot represent the dynamic characteristics of wind and solar power variability
Iterative technique	[72, 73, 76, 85]	Increased computational efforts and errors
Artificial intelligence	[86-88]	Results are only for unique systems, conclusions are not universal
Multi-objective optimization	[74, 89, 90]	Need to set multiple optimization goals

There are various approaches for optimal sizing of standalone wind/solar power systems. Table 1.2 summarised conventional optimization methods with corresponding references and disadvantages. Although different optimization methods are studied for the sizing of standalone wind/solar power systems, it is vague that how the optimal sizing of these standalone systems can be efficiently achieved by using these optimization techniques

without taking the impacts of wind and solar power variability into careful consideration. Given the full or high penetration of random and uncontrollable wind and solar power in standalone systems, it remains an open issue to quantify the wind and solar power variability and the impacts of wind and solar power variability on the optimal sizing of standalone wind/solar power systems, especially on the determination of battery capacity [91, 92].

1.3.3 Grid-connected wind and solar power systems

Global climate change and environmental pollution make lots of international resolution policies and carbon emission reduction goals have been released, which leads to significant growth in variable renewable energy [93-95]. The research on the energy level of grid-connected variable renewable energy mainly focuses on the feasibility of high variable renewable energy penetration and system economics.

a. High variable renewable energy penetration

High variable renewable energy penetration (wind and solar power) will significantly challenge system reliability. P. Denholm studied the combination of wind power generation and high capacity of compressed air energy storage which found that this combination can improve the wind energy penetration to more than 50% in the Midwestern United States under a variety of operating conditions [96]. I. Komusanac carried out that hybrid 1.65 GW of wind power plants and 1.6 GW of solar power plants will increase the renewable energy penetration to 36% in the Republic of Croatia via a simulation model EnergyPLAN [97]. P. Denholm evaluated the life cycle and cycling emissions of dispatchable generators in the high wind penetration power system of Ireland [98]. It found that with an increase in wind power, cycling emissions had an increasing trend and the life cycle of dispatchable generators was reduced significantly. P. Denholm also investigated the impacts of system flexibility on wind and solar energy penetration [99, 100]. It found that with 100% system flexibility of the Texas power system, the maximum wind penetration will be 80% and maximum solar penetration will be 50%. In addition, the maximum wind and solar energy penetration will drop rapidly with the reduction of system flexibility.

Currently, many research work mainly studied the impacts of high penetration of wind and solar energy on system performance. However, the impacts of wind and solar power variability on wind and solar energy penetration is often neglected. Moreover, some studies

find that energy storage can improve wind and solar energy penetration, but the system costs may significantly increase.

b. Integration cost

Variable wind and solar power require additional power system flexibility to integrate into a reliable power grid. The integration of wind and solar power needs more ancillary services which cause integration costs [101]. In the past, the integration costs have been paid by end-users, but utilities have begun to wind operators for costs arising from the integration of high wind and solar penetration in their system[102]. With the increase of wind and solar energy penetration, the cycling and ramping of the operating reserves will undoubtedly increase and lead to higher integration costs. The wind/solar power integration cost can be decomposed to variability costs and uncertainty costs (mainly refers to extra expenses caused by prediction errors) [103]. P. Denholm explored the impacts of the system flexibility on wind/solar power system integration, and the cost of wind and solar power at high penetration is roughly set to 1.2 times the base cost that is very inaccurate [99, 100].
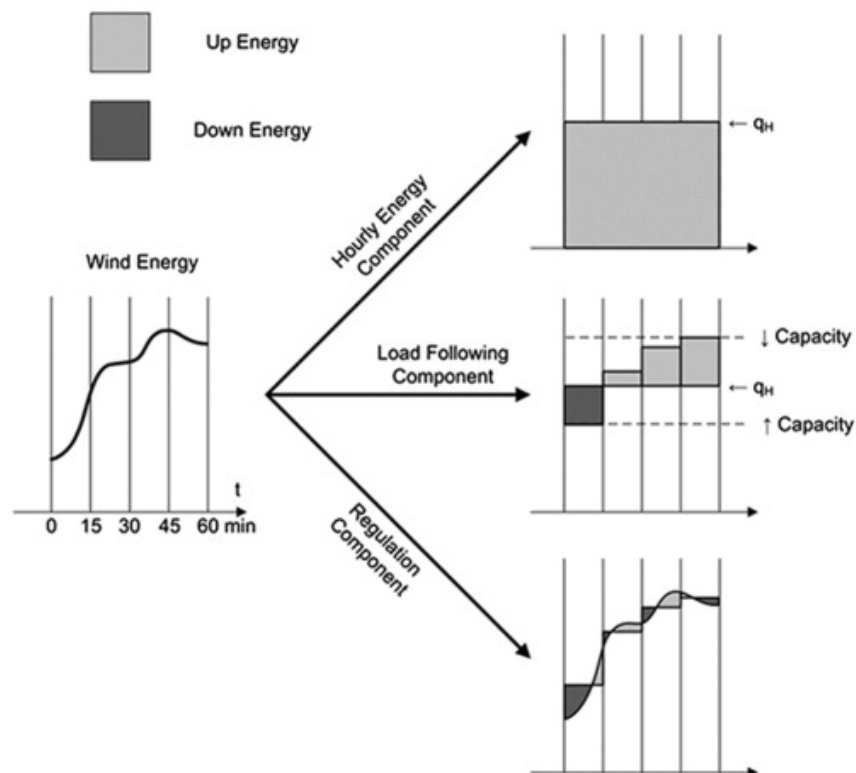
Figure 1.5 Conceptual diagram of how reference [102] partition wind energy into hourly energy, load following, and regulation components.

W. Katzenstein proposed a new approach to decompose wind energy into up energy and down energy to evaluate the sub-hourly variability cost for individual wind farms in Texas as shown in Figure 1.5 [102]. The hourly energy component q_H is the decision variable in the optimization approach and is set at the level that minimizes the total costs of the load following and regulation components. Noted that in that paper, the energy balancing price includes up balancing price and down balancing price for up and down energy regulations. However, this approach is hard to be commonly used because of the limitations of data availability (in lots of regions, Up-regulation price and Down-regulation price are not included in the electricity market). S. Diaf, A. A. Shata, M. A. Ramli and D. Saheb-Koussa gave formulas of the present value of wind and solar power systems but even not cover the integration costs in the total annualized costs [104-107]. L. Hirth presented a new definition of the integration costs as the composition of balancing costs, grid-related costs and profile costs [108]. However, for a high penetration wind/solar power system, the variability cost must be considered for unbiased integration costs. Given the high penetration of intermittent wind and solar power, it remains an open issue to quantify the variability cost.

1.3.4 Energy storage technologies

The integration of high penetration level intermittent energy resources rests on sufficient power system flexibility. Energy storage provides a very common measure to enhance power system flexibility and mitigate power fluctuations. Table 1.3 lists major technical specifications of several common energy storage facilities, such as the typical charge time, capital cost, cycle durability and efficiency of common energy storage [91, 109-117]. It can be seen that some novel energy storage technologies have a very fast ramping rate of charging and higher efficiency. However, the expensive capital cost and restricted operating conditions make these methods unable to be installed on a large scale. Therefore, it is unrealistic to use these energy storage methods to eliminate the high-frequency variations of wind energy. In this section, the widely used energy storage in the standalone power system and grid-connected power system will be specifically introduced.

Table 1.3
Technical parameters for different energy storage method [91, 109-117]

Energy Storage	Capital Cost ($/kWh)	Service Life (years)	Efficiency (%)
Superconducting Magnetic Energy Storage	1000-10000	virtually unlimited	> 90 (high-temperature environment)
Super Capacitor	10000	10 - 15	85 – 95 (self-discharge 50% in 30 – 40 days)
Flywheels	1000 - 5000	15 - 20	80 - 90
Lead-acid battery	100	5 - 15	75 - 90
Lithium-ion battery	300 - 600	14 - 16	90 - 100
Pumped Hydro Storage	5 - 100	30 – 60	65 - 80

a. Lead-acid battery

The lead-acid battery is a very mature battery technology that is widely used in standalone power system. It consists of stacked batteries immersed in a dilute solution of sulfuric acid (H_2SO_4) as an electrolyte. The positive electrode of each battery is composed of lead dioxide (PbO_2), while the negative electrode is composed of sponge lead (Pb). During the discharge, both electrodes are converted to lead sulphate ($PbSO_4$). During the charging cycle, both electrodes return to their initial state [118]. The Lead-acid battery normally has the life cycle of 1200 – 1800 cycles with a round trip efficiency of 75% - 90%. The lifetime of the lead-acid battery strongly depends on the operating temperatures, and the lifetime of the lead-acid battery is approximately 5 – 15 years [119].

b. Lithium-ion battery

The lithium-ion battery is often used in small devices such as mobile phones in the past. However, with the development of lithium-ion batteries, more and more standalone power systems have begun to use lithium=ion batteries as energy storage devices [120]. The operation of lithium-ion batteries is based on the electrochemical reaction between positive lithium ions (Li^+) and anode and cathode active materials. Lithium-ion batteries are made of anode and cathode plates filled with liquid electrolyte materials. The electrode area is defined by a porous separator of polyethylene or polypropylene, which allows lithium ions to pass through. The cathode material is usually based on lithium metal oxides, such as lithium cobalt oxide ($LiCoO_2$), and the anode material is graphite (C). The electrolyte is usually a non-aqueous organic liquid, such as PC, EC or DMC [121].

c. Pumped Hydro Storage

Pumped Hydro Storage is suitable for the large-scale energy storage of grid-connected power system. It works based on the management of the gravitational potential energy of water by pumping water from the lower reservoir to the upper reservoir during periods of low power demand. When the demand for electricity is high, water flows from the upper reservoir to the lower reservoir, thereby starting the turbines to generate electricity. Generally, the lifetime of the Pumped Hydro Storage is about 30 – 60 years with the 65 – 80% round trip efficiency [122].

1.3.5 Energy management for the operation of the renewable power system

Reasonable energy management strategy is the key to system operation optimization. The energy management strategy should ensure high system efficiency and high reliability at the lowest cost. Some key parameters that are widely considered for the optimization of renewable energy management (wind and solar power) are summarized below [123]:

- Potential energy from the primary energy resources, such as wind and solar.

- Capital cost, operating cost, charging cycles and lifetime of the energy storage devices.

- Fuel price if the system includes additional power generators.

a. Standalone power system

The standalone power system normally consists of power generators, energy storage devices and load. The key of optimal energy management strategies for standalone wind and solar power systems is to adjust the power flow for the economic operation. D. Ipsakis et al. proposed three energy management strategies (different operating logic) for a standalone hybrid wind and solar power system with hydrogen fuel cell and lead-acid battery [124]. It compared three energy management strategies via sensitivity analysis which consider some parameters such as state of charge and output/input power of hydrogen fuel cell and lead-acid battery. Moreover, these three different energy management strategies lead to a different lifetime of hydrogen fuel cell and lead-acid battery which can help system operators to select the most suitable strategy. D. Ipsakis et al. also proposed two improved energy management strategies that use a hysteresis band for the same standalone power system [125]. The results showed hysteresis band based energy management strategies could help to reduce the start-up and shut down cycles of the energy storage devices via preventing them from an irregular operation.

Similar, E. Dursun et al. investigate three developed energy management strategies for standalone hybrid wind and solar power systems with proton-exchange membrane fuel cell and battery banks [126]. Due to the price of the proton-exchange membrane fuel cell is high and its membrane lifetime is short, these strategies aimed to increase the operation of the membrane meanwhile ensure the economic operation of the system. After comparison, it found that the third developed strategies can carry out the best results in terms of battery efficiency with an efficiency rating of 85%. The third strategy specifies that when the battery state of charge is within the set limit and the wind and solar power output can meet the load demand, the excess power will operate the electrolyzer. However, when the battery state of charge is below the set limit and the wind and solar power output can meet the load demand, the fuel cell operates to supply the load and charge the battery.

M.S Ismail et al. presented a techno-economic analysis and energy management strategy for a standalone solar power system with a battery bank and a microturbine in Palestine [127]. It found that when microturbine running as a backup charging device of battery, the Cost of Energy for the system is 0.284$/kWh. However, if the microturbine runs in its cogeneration mode to directly supply the load demand, the cost of energy for the system will decrease to 0.263$/kWh. It also proved that using microturbine as a backup source using showed more attractive on the Cost of Energy comparing with a diesel generator.

On the other hand, some studies using intelligent techniques on energy management. S. Abedi and et al. used iterative optimization algorithm to determine the values of energy management strategy parameters and the sizing parameters for standalone wind and solar power with battery bank [128]. These values have to meet the operational constraints of output power, battery state of charge, and the power ramp rate of each device. This energy management strategy is integrated with sizing algorithms to minimize the overall system cost.

It can be seen that, various energy management strategies can effectively improve the economical operation of standalone wind and solar power systems. However, many energy management strategies are only suitable for a specific region. Wind power and solar energy have strong randomness, so wind speed and solar irradiance are different at different locations. Thus, developing energy management strategies without considering the variable nature of wind and solar power in the province, the results will not be universal.

b. Grid-connected power system

Most of the studies for grid-connected renewable energy systems strongly recommended implementing energy management to control the flow of energy among the various energy generation and storage systems from one side of the grid to the other. N. Karami and et al. developed an energy management strategy for a grid-connected solar power system with a fuel cell at the power generator side. By using the MPPT with Perturb and Observe technique for solar power and fuel cell, the system can generate maximum power output [129]. The objective of this energy management strategy is remaining the stable operation of power supply, saving the energy from no load situation and sending the surplus energy to the grid. After modeling 16 different cases, the results showed that the proposed strategy are able to make the proposed system to supply the load demand without interruption.

Kim and et al. examined the environmental and techno-economic feasibility of hybrid wind and solar power systems in Jeju, South Korea [130]. By using the energy management strategy from HOMER, which is a simulation software for renewable energy study, it found the most economically feasible hybrid system. Very similar, G. J. Dalton, D. Saheb-Koussa and et al. also used using the energy management strategy HOMER to found the most economically feasible grid-connected wind/solar power system [131, 132].

A. Ozbilen and et al. discussed the environmental and economic feasibility of hydro and wind plants with a hydrogen storage device in Ontario [133]. The analysis results showed that the system is viable and the payback period is around 17 years for an average electricity price of 4.6 ¢/kWh when the proposed energy management is adopted. This strategy claim that electricity must first be converted to hydrogen and then transferred to storage tanks during excess energy production.

The energy management strategies for grid-connected wind and solar power systems focus on economic feasibility. Similar to standalone wind and solar power system, the variability of wind and solar power will strongly affect the energy management strategies. Moreover, different power grids have different structures and load distribution. Therefore, the variability of wind and solar power and the load demand should be considered for the development of energy management strategies.

1.4 Research objective and content

This research aims to explore the variability of intermittent wind and/or solar energy to facilitate optimal integration of wind and/or solar into off-grid and grid-connected power systems.

The main research contents of this research work include:

- Propose a new measure of wind and/or solar power variability in the time and frequency domain, and utilize it to comprehensively assess the variability of wind and/or solar power data from two NREL databases to gain insights into the variability of wind and/or solar power and its specific implications for power system integration.

- Investigate the impacts of wind/solar power variability on the optimal sizing of standalone winds and/or solar power systems. Case studies of optimal sizing of standalone wind and/or solar systems across North and South America are carried out to demonstrate how to take the variability of wind and/or solar power and its impacts on the power system integration.

- Investigate the impacts of wind/solar power variability on the integration costs of wind and/or solar power into the power grid. A case study of the impact analysis of

wind and solar power variability on wind and solar energy penetration in the Electric Reliability Council of Texas power system (ERCOT) is to be carried out.

1.5 Organization of the thesis

The remaining parts of this thesis are organized as follow:

Chapter 2 – Variability analysis of wind/solar power

This chapter reviewed two previous variability analysis method in the time domain and proposed a factor to evaluate the inter-annual variation of wind/solar power in the time domain. In addition, a frequency spectrum based approach is developed to quantify the wind and solar power variability in the frequency domain. Big data analysis of wind/solar power data at 12 locations across North and South America are carried out to investigate the wind and solar power variability.

Chapter 3 – Optimal sizing of standalone wind/solar power systems

This chapter investigated the impacts of wind/solar power variability on the optimal sizing of standalone winds/solar power systems. The measurement results of wind/solar power variability are applied to the system sizing of standalone wind/solar power systems. Furthermore, big data simulations of six Standalone Wind Power (SAWP) systems at six far apart sites across USA and six Standalone Photovoltaic Power (SAPVP) systems at six sites from latitude 0° to 50° across North and South America with the same residential load demand, provide QTI dependence curves of power supply reliability against the battery capacity and the PV panel/wind turbine size to quantify the impacts of wind/solar power variability on the system sizing. Case studies of optimal sizing of standalone wind/solar systems are carried out to demonstrate how to take the variability of wind/solar power variability and its impacts on the power system integration.

Chapter 4 – Implications of variability on grid-connected wind and solar power

This chapter investigated the impacts of wind and solar power variability on the integration costs of wind and solar power into the power grid. A case study of the impact analysis of wind and solar power variability on wind and solar energy penetration in the Electric Reliability Council of Texas power system (ERCOT) is to be carried out.

Chapter 5 – Conclusions

This chapter drew the conclusions of this thesis. The contributions of this research work have been summarized and the future research ideas are presented.

Chapter 2

Variability analysis of wind/solar power

2.1 Introduction

Variability of wind and solar power has significant impacts on the development of wind and solar power systems. Variability is a multi-faceted spatial and temporal concept described by a range of measurable parameters on different timescales or in different magnitude variation range. In this chapter, a set of methods of the comprehensive analysis of wind and solar power variability is proposed in both the time domain and frequency domain. Regarding the cost and reliability of a system with high renewables penetrations, relevant distinct characteristics of variability are identified to explore their implications for power system integration. Two open-source databases of National Renewable Energy Laboratory (NREL) are employed for this study, where wind speed data collected at six locations uniformly distributed over long distances across the USA during 2007 to 2012 and solar irradiation data collected at six locations evenly from latitude 0°-50° across North and South America during 1998-2017. Big-data analysis is carried out to assess the variability of these wind and solar data. In addition, the impacts of geographical dispersion on wind/solar power variability, and the impacts of grid interconnection on wind/solar power variability are explored.

2.2 Wind and solar data

For the observation and analysis of the variability of wind and solar power, all the wind and solar information data is extracted from the publicly available databases of NREL - Wind Integration National Dataset (WIND) Toolkit and National Solar Radiation Data Base (NSRDB).

WIND Toolkit provides a 5-min interval 80m wind speed data and electrical power output only across the United States, which includes meteorological conditions for more than 126,000 locations from 2007 to 2012 [134]. Note that, the wind power output data of WIND Toolkit is emulated with ten 3MW Vestas V90 wind turbines model in 3TIER model package at every 4 square kilometer area for all potential wind sites in the USA. Details of the data set compilation are available in the report presented by the 3TIER Corporation [135]. 3MW Vestas V90 wind turbines are large commercial wind turbines used in power

grids and the wind tower height is usually between 80m and 100m, which is not suitable for SAWP systems. Thus, wind power output for SAWP systems is emulated with a typical wind turbine model.

NSRDB provides a 30-min interval and 4-km horizontal resolution solar radiation, surface wind speed and meteorological data across North and South America from 1998 to 2017 [136]. The solar power data for our study are emulated with a simplified PV panel model equipped with Maximum Power Point Tracking (MPPT) function using Matlab. Note that NSRDB can only provide earth surface wind speed data.

In this thesis, wind and solar data are extracted from the corresponding highest resolution database in various situations to minimize the uncertainty of results. Table 2.1 lists the detailed database selection for all the research scenarios in this thesis.

Table 2.1
Database selection for different research scenarios.

Research scenario	Adopted database	
	WIND Toolkit	**NSRDB**
Wind power variability analysis	√	
Solar power variability analysis		√
Hybrid wind and solar power variability analysis		√
SAWP systems	√	
SAPVP systems		√
Standalone hybrid wind and solar power systems		√
Grid-connected wind power	√	
Grid-connected wind and solar power	√	√

2.2.1 Wind data

a. Wind power generation

The process of turning the blades of the wind turbine through the wind to convert kinetic energy into electrical energy is called wind power. Wind speed is an important parameter affecting wind power output and wind resource assessment which is a fundamental atmospheric quantity caused by air moving from high to low pressure. Wind

speed increases typically with height above the earth's surface. It is mainly affected by factors such as the roughness of the ground, the presence of obstacles and the difference of land-ocean surface temperature. For a typical 3-blade wind turbine, wind power output P_W from the wind can be theoretical modeled [137] as

$$P_W = \begin{cases} 0 & v < v_i \ or \ v > v_o \\ 0.5\rho A_W v^3 C_P \eta_W & v_i \leq v \leq v_r \\ 0.5\rho A_W v_r^3 C_P \eta_W & v_r < v < v_o \end{cases} \tag{2.1}$$

where v represents the wind speed, the cut-in wind speed normally $v_i \in [1.5, 3.5]$ m/s, the rated wind speed normally $v_r \in [12, 17]$ m/s, the cut-off wind speed v_o is usually set as 25 m/s, the air density ρ is about 1.225 kg/m^3 at sea level and at 15 ℃, A_W presents the blade swept area, η_W is the power generation efficiency of the wind turbine, and C_P is the power coefficient with maximum value $C_{Pmax} = 16/27 \approx 0.593$ [67]. Note that, in this chapter, annual power generation from the wind turbine is assumed to meet 1.1 times a typical residential load (about 5.55 MWh per year) to determine uniform A_W. The detailed information of the typical residential load will be given in Chapter 3 and the 1.1 times is because of the energy flow which will also be described in Chapter 3.
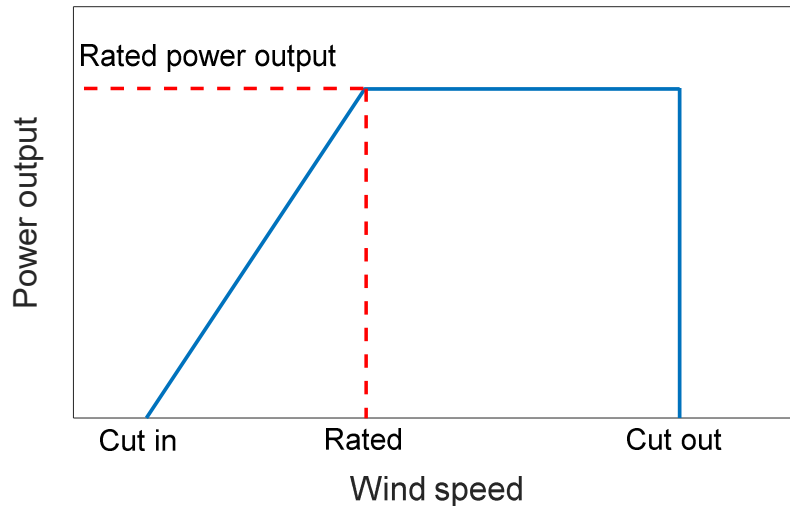
Figure 2.1 Theoretical power curve of a wind turbine.

Considering mechanical wear, minimum power output, safe operation and so on, wind turbines have an output power curve as shown in Figure 2.1. The minimum wind speed of wind turbine operation is called cut-in wind speed. Below cut-in wind speed, the wind

strength is not sufficient to overcome the inertia of the rotor so that wind turbines do not produce any power below this wind speed. The maximum wind speed of the safe operation is called cut-out wind speed. Beyond cut-out wind speed, wind turbines may suffer irreversible damage. The wind speed that wind turbines can produce rated output power is called rated speed. When actual wind speed is between rated wind speed to cut-out wind speed, the control system will regulate wind turbines to produce the rated output power.

b. Database selection

For the simulations and case studies of wind power, all the 5-min interval wind data will be obtained from the WIND Toolkit. In addition, the wind output power used in wind power variability analysis and sizing of SAWP systems is modeled by the Eq. (2.1). However, for grid-connected wind power systems, the wind turbines are usually not designed to completely follow the theoretical wind power curve because of the power ramp rate requirement. 3TIER model has already limited the wind power output to control the power ramp remain within the standard all the time. Therefore, for the study of grid-connected wind power, wind electrical power output data directly uses the wind power data in the WIND Toolkit.

WIND Toolkit is one of the widely used datasets for solar-related studies [138-140]. C. Draxl validated the WIND Toolkit by comparing the wind data of WIND toolkit to the wind data from anemometers at six locations [134]. It found that the bias in 5-minute wind data ranges from -0.97% to 1.8%. In this study, there are no missing wind data for selected locations.

Moreover, because the wind power output is greatly affected by the height of the wind turbine hub, the original wind speed data needs to be converted to the wind speed at required height upon demands. Commonly, extrapolation methods are used to convert wind speed. The vertical extrapolation of wind speed at the wind turbine hub height can be calculated via using the following wind profile power laws

$$v_H = v_h \cdot (\frac{H}{h})^{\frac{1}{\varepsilon}} \qquad (2.2)$$

where v_H is the wind speed at objective height H, v_h is the wind speed at original height h, ε is the exponential coefficient that is recommended value of 0.2 for onshore by the IEC standards [106, 141].

The logarithmic law of wind speed is defined as:

$$v_H = v_h \cdot \frac{\ln(H/\lambda)}{\ln(h/\lambda)} \tag{2.3}$$

where λ is the surface roughness. Logarithmic law has a constraint which is the original height mush be anemometer height so that in this thesis, the original wind speed is converted via Eq. (2.2).

c. Locations selection

Figure 2.2 Six selected locations across the USA for the research of wind power variability and SAWP systems.

Figure 2.3 12 selected locations for interconnected wind power in Colorado State of the USA.

As mentioned above, WIND Toolkit can provide very high-resolution wind power data across the USA for our studies. The wind speed is greatly affected by the terrain so that for wind power studies, the wind power data at different locations with different geomorphological features should be widely selected. Figure 2.2 shows the six selected locations for wind power variability analysis and sizing of SAWP systems. These six locations are evenly distributed along the West Coast, East Coast, Central, and South of the United States. As shown in Figure 2.3, for the analysis of interconnected wind power, 5-min wind power data collected at 12 selected locations in Colorado State will be used.

d. Wind speed data
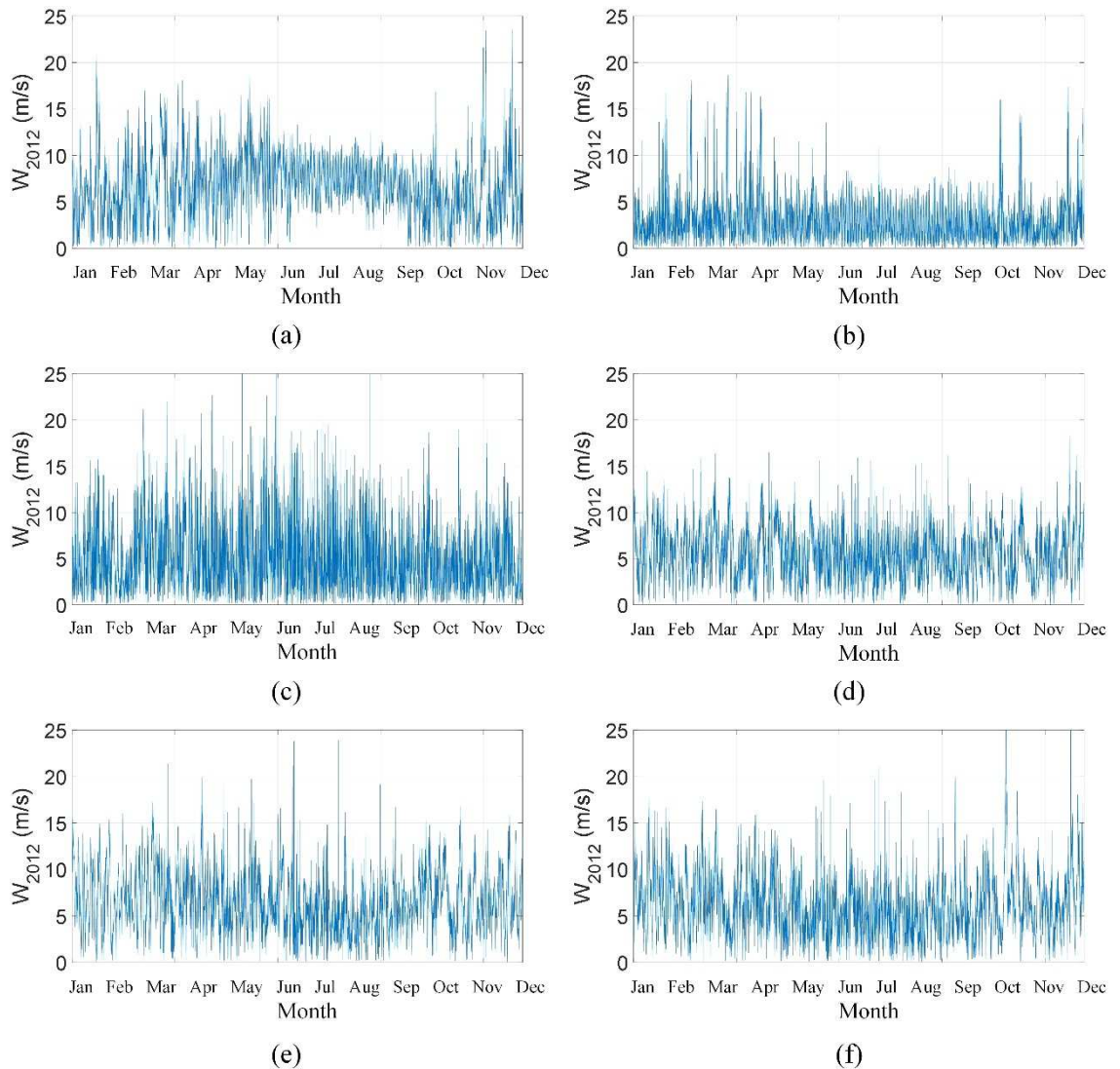
Figure 2.4 Wind speed for the year 2012 W_{2012} at (a) San Francisco, (b) Los Angeles, (c) Denver, (d) Houston, (e) Chicago, (f) New York.

Figure 2.4 gives an example of wind speed data for the year 2012 in San Francisco, Los Angeles, Denver, Houston, Chicago and New York. It can be seen that:

i. The profiles of wind speed at six locations are different from each other, and present high degree of randomness.

ii. Wind speed has less fluctuation in summer at Los Angeles, and more fluctuation in summer at Denver.

    iii.   The profiles of the wind speed of six selected locations do not show the annual distribution of wind speed has any pattern related to its geographical locations (e.g., east coast or west coast).

Note that it is well known that the profile of wind speed data at one location can be thought to be quasi-periodic yearly.

In order to more intuitively observe the wind speed in different locations throughout the year, statistical methods are usually used. The mean value of wind speed and solar irradiation can directly reflect the potential of wind resources. The mean value of wind speed can be described as:

$$v_{avg} = \frac{1}{N_W} \cdot \sum_{i=1}^{N_W} W_i \tag{2.4}$$

where v_{avg} is the average wind speed, W_i is the wind speed of i-th sample, N_W is the sample number of wind speed data.

In addition, Standard Deviation (SD) is a measure of the amount of variation or dispersion of a set of samples in statistics. A low SD means that the sample values are close to the mean of the set, while a high SD indicates that the sample values are spread out over a wider range. Thus, higher SD implies a more significant variation of the samples, and vice versa. SD of wind speed can be formulated as follow:

$$\sigma_W = \sqrt{\frac{1}{N_W} \cdot \sum_{i=1}^{N_W} (W_i - v_{avg})^2} \tag{2.5}$$

where σ_W is the SD of wind speed.

Table 2.2 gives the average value of mean and SD of wind speed from 2007 to 2012 at six selected locations. Ann represents annual and Q1 to Q4 means quarter 1 to 4 (spring, summer, fall, winter). The average annual mean of wind speed provides numerical evidence to show that wind speed has strong randomness and may be affected by local terrain. Moreover, SD of San Francisco is much higher than the other 5 locations which imply the wind power variation in San Francisco is stronger and it leads to the poor reliability of wind power systems in San Francisco.

Table 2.2
The average annual/quarter mean and standard deviation of wind speed from 2007 to 2012.

Location	v_{avg} (m/s)					σ_W (m/s)				
	Q1	Q2	Q3	Q4	Ann	Q1	Q2	Q3	Q4	Ann
San Francisco	7.23	9.17	8.74	6.50	7.91	1.60	2.09	1.83	1.53	1.99
Los Angeles	5.38	5.06	3.86	4.60	4.72	1.29	1.69	1.42	1.14	1.45
Denver	6.62	7.58	6.44	6.33	6.75	1.47	1.73	1.71	1.35	1.62
Houston	7.14	6.90	4.74	6.51	6.51	1.11	1.47	1.27	1.27	1.42
Chicago	8.48	7.75	8.41	6.24	7.71	1.40	1.49	1.14	1.35	1.55
New York	8.16	6.91	6.14	8.04	7.31	1.44	1.42	1.31	1.47	1.58

2.2.2 Solar data

a. Solar power generation

The PV panels convert the sun's irradiation into electricity by exciting electrons in silicon cells using the photons from sunlight is called solar power. Solar irradiance is an important parameter affecting solar power output and solar resource assessment which is radiant energy emitted by the sun, particularly electromagnetic energy. Solar irradiation (received by PV panels) is mainly affected by factors such as the distance from the sun, the weakening of the atmosphere and the covering. Due to most of the commercial PV panel commonly uses MPPT to maximize power extraction under all conditions, the output power of the PV panel is considered to be linearly related to solar irradiation. In addition, this study focus on investigating the wind and solar power variability so that the environmental factors are set to constant to ensure unbiased research. Thus, the dust, shading, aging, snow covering temperature losses and not consider for the PV panels and the ambient temperature is assumed to remain 25℃. Subsequently, the solar power output of P_S in the 100-kW Grid-Connected PV Array model can be simplified as [83]:

$$P_S = S_I \cdot A_S \cdot \eta_{PV} \tag{2.6}$$

where S_I represents the solar irradiation in kW/m^{-2} and A_S represents the size of the PV panel in m^2, η_{PV} denotes the power generation efficiency of the prevalent commercial PV panel which is about 15% at ambient temperature 25℃[142]. Note that, in this chapter, annual

power generation from the PV panel is assumed to meets 1.1 times a typical residential load (about 5.55 MWh per year) to determine uniform A_S. The detailed information of the typical residential load will be given in Chapter 3 and the 1.1 times is because of the energy flow which will also be described in Chapter 3.

b. Database selection

For the simulations and case studies of solar power, all the 30-min interval solar data will be obtained from NSRDB. And all the solar power output data is obtained from the 100-kW Grid-Connected PV Array model in Matlab and its simplified formula is expressed in Eq. (2.6). Note that, the solar power output data from Matlab model is also used in grid-connected solar power systems because of the data limitation. However, due to the low penetration of solar power for most of the power grid, the error of solar output power modeling will not have much impact on power system analysis.

NSRDB is one of the widely used datasets for solar-related studies [143, 144]. There are several previous works that validated NSRDB datasets: M. Sengupta used the solar data of NSRDB from 1998 to 2016 to compare with solar data from 9 ground stations including 7 from the SURFRAD network. GHI and DNI were validated on various temporal scales (hourly, daily, monthly, and yearly) [136]. Furthermore, D. Yang also validated NSRDB data from 1998 to 2016 against ground-based measurements from 7 SURFRAD stations. It revealed that the bias in hourly-averaged NSRDB GHI data ranges from -2.6% to 4.0% [145]. In addition, in this study, perhaps it is because the simulation locations are all around larger cities, so there is no missing data.

Note that solar irradiation consists of Direct Normal Irradiance (DNI), Diffuse Horizontal Irradiance (DHI), Global Horizontal Irradiance (GHI) and Global Normal Irradiance (GNI). GHI is the total irradiance from the sun on a horizontal surface on Earth. It is the sum of DNI and DHI which can be described as:

$$\text{GHI} = \text{DHI} + \text{DNI} \cdot \cos(z) \qquad (2.7)$$

where z is the solar zenith angle. The solar zenith angle is related to the geographical latitude L and it can be described as:

$$\cos(z) = \cos(L) \cdot \cos(\phi) + \cos(L) \cdot \cos(\phi) \qquad (2.8)$$

where ϕ is the solar declination angle. The solar declination angle is the angular distance of the sun north or south of the equator. ϕ varies from 23.45° North to 23.45° South every year. The declination angle is calculated using [146]:

$$\phi = 23.45° \cdot \sin(360° \cdot \frac{284+d}{365}) \tag{2.9}$$

where d is the day of the year. Generally, the solar irradiation used in calculating the output power of solar panels is GHI, so that the solar irradiation mentioned in this thesis refers to GHI.

c. Locations selection
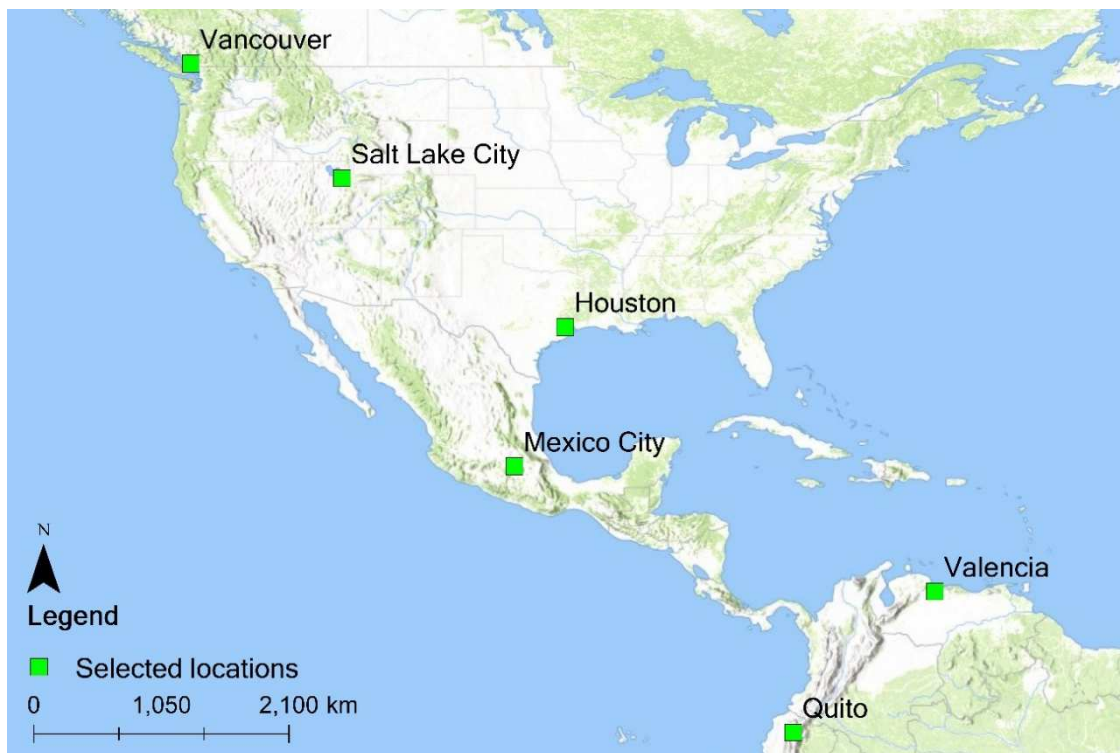
Figure 2.5 Six selected locations across North and South America for the research of solar power variability, SAPVP systems and standalone hybrid wind and solar power systems.

NSRDB can provide a wider geographical context for 30-min interval wind and solar data. Different latitudes have very different sunshine durations on the same day, so it is necessary to explore solar power variation at different latitudes. Figure 2.5 shows six locations have been evenly selected from latitude 0° to 50° with every 10° a step across the North and South America. Note that the daytime in the winter at the regions that located

above latitude 50° is very short and the regions more than latitude 66° even have the polar night [147]. Solar power is not a cost-effective power generation option in these areas, so that these high-latitude locations are not considered in this research.

d. Solar irradiation data
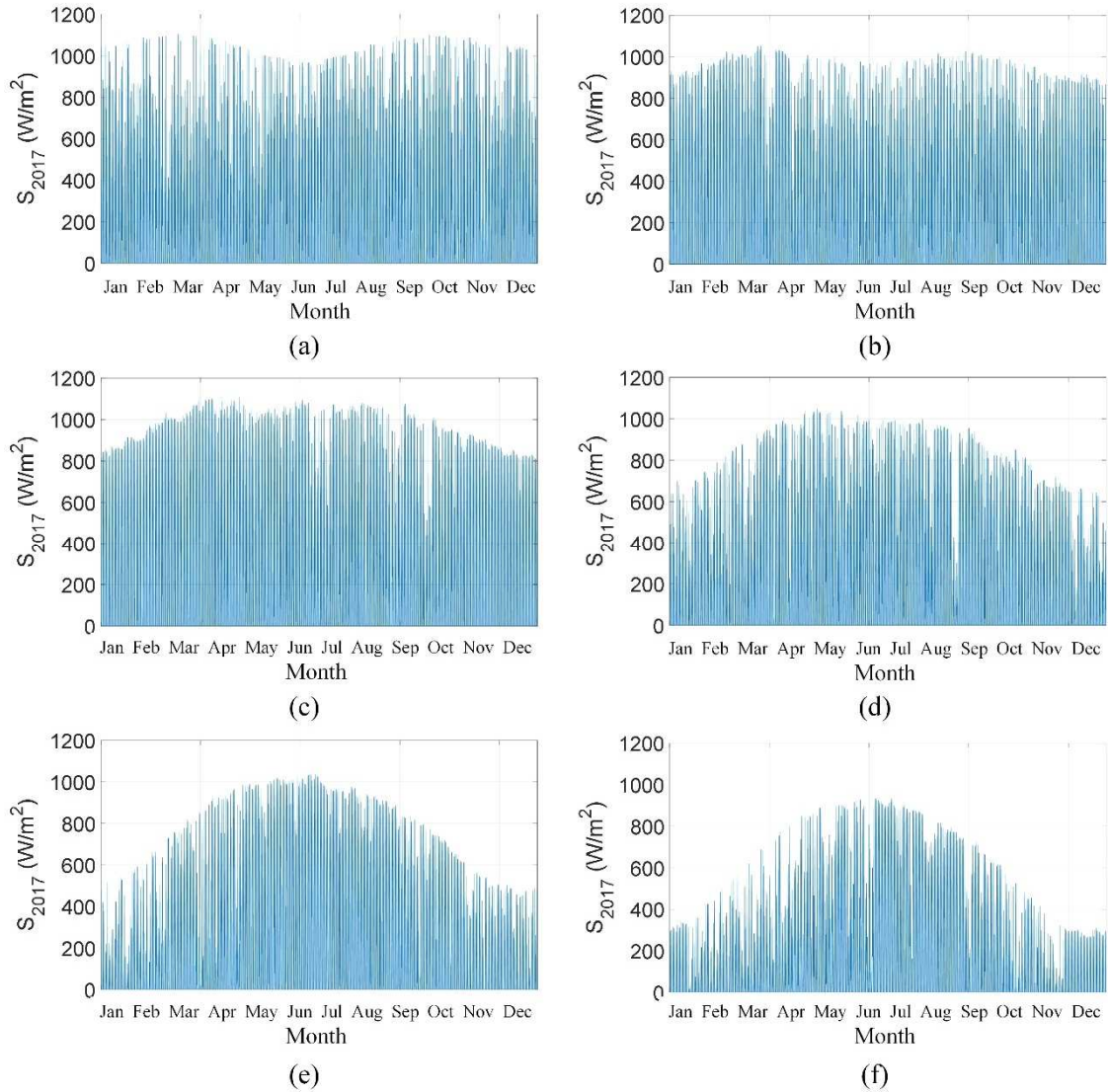
Figure 2.6 Solar irradiance for the year 2017 S_{2017} at (a) Quito, (b) Valencia, (c) Mexico City, (d) Houston, (e) Salt Lake City, (f) Vancouver.

Figure 2.6 gives an example of solar irradiation for the year 2017 at Quito, Valencia, Mexico City, Houston, Salt Lake City and Vancouver. It can be seen that:

    i.   as the latitude increases, the annual maximum solar irradiation decreases, and the annual maximum solar irradiation of Vancouver (Lat 50°) is below 1000 W/m^2;

    ii.   the profile of the solar irradiation at Quito (Lat 0°) looks the flattest, and the solar irradiation in winter reduce significantly with the increase of the latitude which results in the sharper profile of solar irradiation at higher latitudes (the peaks in the summer and the bottoms in the winter);

Note that it is well known that the profile of solar irradiance data at one location can be thought to be quasi-periodic yearly.

From Figure 2.6 it can be seen that solar irradiation is closely correlated to geographic latitude. Generally speaking, the lower the latitude, the higher the solar irradiance, and vice versa. This is because when the latitude is low, the solar zenith angle is large and the distance of solar radiation passing through the atmosphere is short so that less solar irradiation is weakened by the atmosphere. On the contrary, if the latitude is high, the solar zenith angle is small and the distance of solar radiation passing through the atmosphere is long so that more solar irradiation is weakened by the atmosphere which is shown in Figure 2.7. Thus, solar irradiation generally decreases with the increase of the latitude. Moreover, high latitude locations have longer daytime in the summer but shorter daytime in the winter. Therefore, the profile of the solar irradiation at higher latitude regions appears as a convex shape.
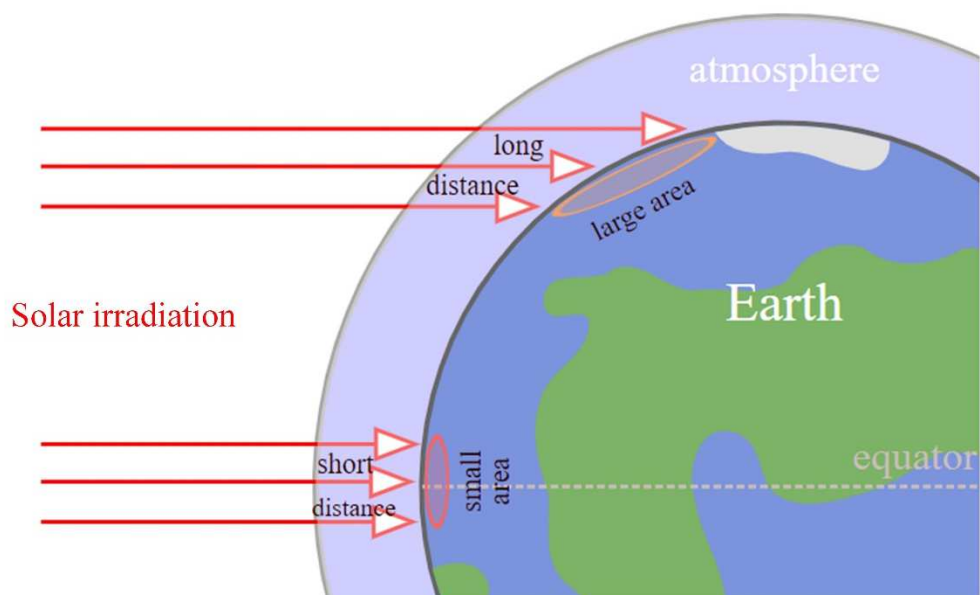
Figure 2.7 Schematic diagram of solar irradiation emits at different latitude regions.

Similarly, the mean value of solar irradiation can directly reflect the potential of solar resources. The mean value of solar irradiation can be described as:

$$I_{avg} = \frac{1}{N_S} \cdot \sum_{i=1}^{N_S} S_i \qquad (2.10)$$

where I_{avg} is the annual average solar irradiation, S_i is the solar irradiation of i-th sample, N_S is the sample size for solar irradiation data.

In addition, in order to simply observe the fluctuation of annual solar irradiation, SD of solar irradiation can be formulated as follow:

$$\sigma_S = \sqrt{\frac{1}{N_S} \cdot \sum_{i=1}^{N_S} (S_i - v_{avg})^2} \qquad (2.11)$$

where σ_S is the SD of solar irradiation.

Table 2.3
Average annual mean and standard deviation of solar irradiation from 1998 to 2017.

Location	I_{avg} (W/m^2)					σ_S (W/m^2)				
	Q1	Q2	Q3	Q4	Ann	Q1	Q2	Q3	Q4	Ann
Quito	214	216	241	224	224	136	137	152	144	284
Valencia	256	222	223	211	227	165	138	138	137	260
Mexico City	252	280	240	217	247	167	175	154	146	322
Houston	158	258	247	147	203	108	151	148	103	263
Salt Lake City	129	280	267	108	196	94	158	157	82	267
Vancouver	70	215	214	50	137	55	117	124	41	200

Table 2.3 gives the average value of mean and SD of solar irradiation from 1998 to 2017 at six selected locations. Ann represents the annual and Q1 to Q4 means quarter 1 to 4. The average annual mean of solar irradiation further provides numerical evidence to show

that solar irradiation is affected by the latitude (relatively high at low latitudes and vice versa). In addition, the annual mean and SD of solar irradiation in each quarter implies that solar radiation in high latitudes is much larger in the second and third quarters than in the first and fourth quarters but also more variable.

2.2.3 Hybrid wind and solar data

a. Database selection

For grid-connected wind and solar power systems, the wind and solar power from the WIND toolkit are usually taken from different geographic locations. Furthermore, solar power usually only takes a small share of the power sources of the power grid, and is often far less than wind power.

For standalone hybrid wind and solar power systems, both the wind turbines and PV panels should be installed in the same location. Although WIND Toolkit can provide higher-resolution wind power data, the scope of data collection is limited to the United States. Thus, the 30-min interval wind speed data in NSRDB is implied for the study of standalone wind and solar power systems. It is worth noting that because the wind speed data of NSRDB is the surface wind speed, in order to unify with the WIND Toolkit data, the 80m wind speed can be converted from the surface wind speed via the extrapolation method.

b. Location selection

Due to the latitude's effect on the solar power as mentioned above, the research of the variability of hybrid wind and solar power and the standalone wind and power systems will also evenly select six locations from latitude 0° to 50° with every 10° a step across the North and South America as shown in Figure 2.5.

2.3 Variability analysis in the time domain

Variability analysis of wind and solar power in the time domain provides operators and designers an intuitive way to understand the characteristics of wind and solar power. Standard Deviation (SD) is one widely used measurable parameter for assessing the variation of the data. Since SD reflects the degree of dispersion of a data set around its average value, the SD value of wind and solar power output can represent the degree of variation of the wind and solar power, or the smoothness of the wind and solar power. In addition, SD can

also be used to evaluate the variation of hybrid of wind and solar power (either in standalone systems or grid-conneccted systems) or interconnection of wind power from disperse geographic locations. In addition, the Pearson correlation coefficient is used to assess the complementary degree between the wind power and the solar power (either in standalone systems or grid-conneccted systems), or between the wind power from dispersing geographic locations. The weaker the correlation between the two sets of data, the stronger the complementarity. In this Section, considering its implications for power system integration, the variability of wind and solar power will be explored from various perspectives in the time domain.

2.3.1 Inter-annual variation

It is well known that the profile of annual wind or solar power at one location can be treated as quasi-periodic yearly. The inter-annual variation of wind and solar power can provide a margin factor to determine the annual fluctuation of wind and solar power supply. In the time domain, the inter-annual renewable energy variations for years y_0 to Y can be expressed as

$$
\begin{cases}
E_{RE}(y) = \sum_{i=1}^{N} P_{RE(y)}(i)T_S \\
I_{RE}(y) = E_{RE}(y) / \left(\sum_{i=y}^{Y} E_{RE}(y) / (Y - y_0) \right) \\
\delta_{IRE\,\max} = \max(I_{RE}(y)) - 1 \\
\delta_{IRE\,\min} = \min(I_{RE}(y)) - 1
\end{cases}
\tag{2.12}
$$

where $E_{RE}(y)$ is the total annual renewable power generation for the year y, $\delta_{IRE\,\max}$ is the upper bound of $I_{RE}(y)$, $\delta_{IRE\,\min}$ is the lower bound of $I_{RE}(y)$. Note that in this thesis, wind and solar power is mainly investigated so that $E_{RE}(y)$ includes total annual wind power generation $E_W(y)$, total annual solar power generation $E_S(y)$, total annual hybrid wind and solar power generation $E_{W\&S}(y)$; $I_{RE}(y)$ is the ratio of the total renewable energy (also includes the ratio of the total wind energy $I_W(y)$, the ratio of the total solar energy $I_S(y)$, the ratio of the total hybrid wind and solar energy $I_{W\&S}(y)$)in the year y to the average for the years y_0 to Y. Eq (2.12) can be used to determine the inter-annual variation of wind and solar power. $\delta_{IRE\,\max}$ can represent the margin of the inter-annual variation which can help the sizing of wind turbines or PV panels in standalone power systems. A larger $\delta_{IRE\,\max}$ indicates a larger size of wind turbines or PV panels are needed to reduce the unbalance between the wind and solar power supply and the load demand.

Chapter 2
Variability analysis of wind/solar power

a. Wind power

Table 2.4 lists the annual wind energy generation at six sites as shown in Figure 2.2 for the years 2007 to 2012. It can be seen from Table 2.4 that Los Angeles and Houston have the largest variations of wind energy generation: the highest energy generation above 6 MWh and lowest energy generation below 5 MWh.

Table 2.4
Annual wind energy generation at the six sites for the years 2007-2012.

$E_W(y)$ (MWh) \ Year	Location					
	San Francisco	Los Angeles	Denver	Houston	Chicago	New York
2007	5.72	5.94	5.77	6.33	5.77	5.44
2008	5.55	5.38	5.66	4.44	5.77	5.44
2009	5.61	4.61	5.05	5.77	5.27	5.66
2010	5.38	6.33	5.33	5.55	5.27	6.27
2011	5.27	5.77	5.61	6.33	5.77	5.38
2012	5.72	5.27	5.83	4.94	5.44	5.16

Table 2.5 gives the inter-annual wind energy variations at the six sites for the years 2007 to 2012. From the data listed in Table 2.5, it is not difficult to know that Los Angeles and Houston have the biggest inter-annual variation (0.83 at the year of 2009 and 0.8 at the year of 2008 separately) which means wind power in Los Angeles and Houston have more significant annual variance. In addition, $\delta_{IW\,max}$ and $\delta_{IW\,min}$ provide the specific upper and lower bounds of inter-annual variation of wind power. Los Angeles and Houston show the larger value than the other four sites which reach +14% and -17%/-20%. Furthermore, these imply that the SAWP systems in Los Angeles and Houston need cost more on wind turbines to ensure that the power supply reliability can meet the requirements during the operating time.

Table 2.5
Inter-annual wind power variations at the six sites for the years 2007-2012.

$I_W(y)$ / Year	Location					
	San Francisco	Los Angeles	Denver	Houston	Chicago	New York
2007	1.03	1.07	1.04	1.14	1.04	0.98
2008	1.00	0.97	1.02	0.80	1.04	0.98
2009	1.01	0.83	0.91	1.04	0.95	1.02
2010	0.97	1.14	0.96	1.00	0.95	1.13
2011	0.95	1.04	1.01	1.14	1.04	0.97
2012	1.03	0.95	1.05	0.89	0.98	0.93
$\delta_{IW\,max}$	+3%	+14%	+5%	+14%	+4%	+13%
$\delta_{IW\,min}$	-5%	-17%	-9%	-20%	-5%	-7%

b. Solar power

Table 2.6 lists the annual solar energy generation at six sites as shown in Figure 2.5 for the years 1998 to 2017. It can be seen from Table 2.6 that solar energy generation is gently fluctuating every year at six sites. There is not a big variation that happened during the study period.

Table 2.7 gives the inter-annual solar energy variations at the six sites for the years 1998-2017. From the data listed in Table 2.7 it can be seen that, the inter-annual variations of solar power are very different from wind power that there is no significant inter-annual variation for six sites. $\delta_{IS\,max}$ and $\delta_{IS\,min}$ of solar power shows that inter-annual variation varies within ±10% which means solar power has better annual stability than wind power. Furthermore, these imply that the SAPVP systems cost less on PV panels to ensure that the power supply reliability can meet the requirements during the operating time.

Table 2.6
Annual solar energy generation at the six sites for the years 1998-2017.

$I_S(y)$ Year	Location					
	Quito	**Valencia**	**Mexico City**	**Houston**	**Salt Lake City**	**Vancouver**
1998	5.66	5.61	5.77	5.66	5.27	5.22
1999	5.49	5.72	5.72	5.88	5.66	5.16
2000	5.66	5.77	5.72	5.77	5.61	5.33
2001	5.88	5.83	5.66	5.50	5.77	5.55
2002	5.94	5.83	5.66	5.50	5.83	6.11
2003	5.66	5.55	5.55	5.38	5.61	5.77
2004	5.72	5.55	5.44	5.27	5.61	5.77
2005	5.55	5.55	5.50	5.77	5.55	5.44
2006	5.44	5.50	5.50	5.55	5.61	5.66
2007	5.49	5.49	5.50	5.22	5.77	5.16
2008	5.27	5.66	5.50	5.61	5.61	5.38
2009	5.44	5.49	5.55	5.38	5.50	5.94
2010	5.33	5.27	5.55	5.66	5.33	5.55
2011	5.55	5.22	5.77	5.94	5.33	5.22
2012	5.49	5.38	5.50	5.66	5.55	5.11
2013	5.66	5.55	5.50	5.55	5.44	5.50
2014	5.61	5.66	5.33	5.44	5.50	5.72
2015	5.72	5.61	5.33	5.33	5.55	5.88
2016	5.44	5.44	5.44	5.50	5.55	5.72
2017	5.27	5.38	5.61	5.55	5.55	5.83

Table 2.7
Inter-annual solar power variations at the six sites for the years 1998-2017.

$I_S(y)$ Year	Location					
	Quito	Valencia	Mexico City	Houston	Salt Lake City	Vancouver
1998	1.02	1.01	1.04	1.02	0.95	0.94
1999	0.99	1.03	1.03	1.06	1.02	0.93
2000	1.02	1.04	1.03	1.04	1.01	0.96
2001	1.06	1.05	1.02	0.99	1.04	1.00
2002	1.07	1.05	1.02	0.99	1.05	1.10
2003	1.02	1.00	1.00	0.97	1.01	1.04
2004	1.03	1.00	0.98	0.95	1.01	1.04
2005	1.00	1.00	0.99	1.04	1.00	0.98
2006	0.98	0.99	0.99	1.00	1.01	1.02
2007	0.99	0.99	0.99	0.94	1.04	0.93
2008	0.95	1.02	0.99	1.01	1.01	0.97
2009	0.98	0.99	1.00	0.97	0.99	1.07
2010	0.96	0.95	1.00	1.02	0.96	1.00
2011	1.00	0.94	1.04	1.07	0.96	0.94
2012	0.99	0.97	0.99	1.02	1.00	0.92
2013	1.02	1.00	0.99	1.00	0.98	0.99
2014	1.01	1.02	0.96	0.98	0.99	1.03
2015	1.03	1.01	0.96	0.96	1.00	1.06
2016	0.98	0.98	0.98	0.99	1.00	1.03
2017	0.95	0.97	1.01	1.00	1.00	1.05
$\delta_{IS\,max}$	+7%	+5%	+4%	+7%	+5%	+7%
$\delta_{IS\,min}$	-5%	-6%	-4%	-6%	-5%	-8%

c. Hybrid wind and solar power

Table 2.8 gives the inter-annual variations of hybrid wind and solar power at the six sites as shown in Figure 2.5 for the years 2017 and Table A.1 to Table A.19 gives the inter-annual variations of hybrid wind and solar power for years 1998-2016 which is listed in Appendix A. *S/W* ratio represents the proportion of solar power out and wind power output in the gross power generation. For example, 0% *S/W* ratio means solar power output accounts for 0% of gross power output and wind power output accounts for 100% of gross power

output; 30% *S/W* ratio means solar power output accounts for 30% of gross power output and wind power output accounts for 70% of gross power output. From the data listed in Table 2.8 and the data in Table A.1 to A.19, it can find that, hybrid wind and solar power will not bring any improvement for inter-annual variations. In fact, hybrid wind and solar power show features of the weighted average of wind and solar power but not mitigation of inter-annual variations. Therefore, hybrid wind and solar power will not bring any cost-benefit for wind turbines and PV panels.

Table 2.8
Inter-annual hybrid wind and solar power variations at the six sites for the year 2017.

$I_{W\&S}(y)$ / S/W ratio	Location					
	Quito	Valencia	Mexico City	Houston	Salt Lake City	Vancouver
0%	1.00	1.16	0.90	1.03	1.12	1.14
10%	0.99	1.14	0.91	1.03	1.11	1.13
20%	0.98	1.12	0.92	1.02	1.10	1.12
30%	0.98	1.10	0.93	1.02	1.08	1.12
40%	0.97	1.08	0.94	1.02	1.07	1.11
50%	0.96	1.06	0.95	1.01	1.06	1.10
60%	0.96	1.04	0.96	1.01	1.05	1.09
70%	0.96	1.02	0.98	1.01	1.04	1.08
80%	0.95	1.00	0.99	1.00	1.02	1.07
90%	0.95	0.98	1.00	1.00	1.01	1.06
100%	0.95	0.97	1.01	1.00	1.00	1.05

2.3.2 Smoothness coefficient

Interconnected wind and solar power is considered as a method to smooth the fluctuation of gross wind power output [51, 148]. In order to measure the smoothing effect of interconnected wind and solar power, the smoothness coefficient *S* is defined in the time domain:

$$S = \frac{\sigma_{Single} - \sigma_{Interconnected}}{\sigma_{Single}} \tag{2.13}$$

where S is the smoothness coefficient of interconnected wind and solar power. σ_{Single} is the SD of single wind or solar power output and $\sigma_{\text{Interconnected}}$ is the SD of interconnected wind and solar power. σ_{Single} and $\sigma_{\text{Interconnected}}$ can be denoted as:

$$
\begin{cases}
\sigma_{\text{Single}} = \sqrt{\dfrac{1}{N_{\text{Single}}} \cdot \sum_{i=1}^{N_{\text{Single}}} (P_{\text{Single}} - \overline{P}_{\text{Single}})^2} \\
\sigma_{\text{Interconnected}} = \sqrt{\dfrac{1}{N_{\text{Interconnected}}} \cdot \sum_{i=1}^{N_{\text{Interconnected}}} (P_{\text{Interconnected}} - \overline{P}_{\text{Interconnected}})^2}
\end{cases}
\tag{2.14}
$$

where P_{Single} is the output power of a single wind or solar site, $\overline{P}_{\text{Single}}$ is the average output power of a single wind or solar site, N_{Single} is the sample size for the output power data of a single wind or solar site; $P_{\text{Interconnected}}$ is the output power of interconnected wind and solar sites, $\overline{P}_{\text{Interconnected}}$ is the average output power of interconnected wind and solar sites, $N_{\text{Interconnected}}$ is the sample size for the output power data of interconnected wind and solar sites.

Larger S means a better smoothing effect on power fluctuation. In addition, if S is negative, it means that the interconnect wind and solar power even bring more power fluctuation that is not expected. Note that most of the wind and solar power variability analysis in the time domain is based on the SD. However, the SD of wind and solar power is mostly affected by the sample size. The larger the sample size, the larger the standard deviation value will be. Thus, the variability analysis in the time domain which is represented by the smoothness coefficient can only provide a very rough reference for the system designers and operators. It is hard to consider its implications for power system integration in practice.

Table 2.9 shows the smoothness coefficient varies with the different number of interconnected wind turbines from 2007 to 2012. It can be seen that S increases with the increase in the amount of interconnected wind power, and this trend is saturated when enough interconnected wind turbines. These imply that, interconnecting wind turbines can mitigate the wind power fluctuation but this mitigation is decayed with the number of connected wind turbines increase.

Table 2.9
S varies with the different number of interconnected wind turbines from 2007 to 2012.

S \ Year	Number of interconnected wind turbines										
	2	3	4	5	6	7	8	9	10	11	12
2007	-0.32	-0.02	0.05	0.12	0.17	0.17	0.19	0.20	0.19	0.18	0.17
2008	-0.21	0.06	0.14	0.19	0.24	0.22	0.23	0.23	0.22	0.22	0.22
2009	-0.18	0.09	0.16	0.22	0.28	0.26	0.27	0.28	0.27	0.27	0.28
2010	-0.13	0.12	0.19	0.23	0.28	0.28	0.27	0.27	0.26	0.26	0.27
2011	-0.14	0.11	0.17	0.21	0.26	0.26	0.26	0.27	0.26	0.26	0.27
2012	-0.18	0.07	0.14	0.20	0.25	0.26	0.26	0.26	0.25	0.25	0.25

Table 2.10
S varies with the different mixed proportions of solar/wind power at Houston from 2007 to 2012.

S \ Year	Mixed proportions of solar/wind power									
	0.1	0.2	0.3	0.4	0.5	0.6	0.7	0.8	0.9	1.0
2007	0.09	0.11	0.05	-0.07	-0.24	-0.43	-0.64	-0.87	-1.10	-1.34
2008	0.11	0.14	0.09	-0.03	-0.20	-0.40	-0.62	-0.85	-1.09	-1.34
2009	0.11	0.14	0.09	-0.02	-0.19	-0.39	-0.60	-0.83	-1.07	-1.32
2010	0.10	0.13	0.07	-0.07	-0.25	-0.46	-0.69	-0.94	-1.19	-1.44
2011	0.11	0.14	0.08	-0.05	-0.24	-0.45	-0.68	-0.93	-1.18	-1.44
2012	0.10	0.11	0.05	-0.09	-0.27	-0.48	-0.71	-0.96	-1.21	-1.46

Table 2.10 shows the smoothness coefficient varies with the different mixed proportion of solar/wind power at Houston from 2007 to 2012. It can be seen that S decreases with the increase of the mixed proportion of solar/wind power, and when the mixed proportion beyond a specific value, S will be negative. These imply that, in Houston, interconnecting wind turbines can mitigate the wind power fluctuation but this mitigation is decayed with the increase in the number of interconnected wind turbines. S of other five selected locations as shown in Figure 2.5 that are Quito, Valencia, Mexico City, Salt Lake City and Vancouver is listed from Table A.20 to Table A.24 in Appendix A. Table A.21, Table A.22 and Table A.23 show the similar pattern of change of S as Table 2.10. However,

Table A.20 and Table A.24 show an increase of *S* before the mixed proportion of solar/wind power reaches 0.3 and 0.2 separately. These imply that when mixing wind and solar power (more wind power) at very high latitude (about Lat 50°) or very low latitude (about Lat 0°) locations, power fluctuations can be reduced. However, because results show that wind and solar hybrids can sometimes reduce power fluctuations and sometimes increase power fluctuations, *S* cannot determine the benefits of wind and solar power complementary.

2.3.3 Correlation coefficient

Correlation coefficient *r* is an essential parameter for evaluating the complementarity of interconnected wind and solar power in the time domain [48, 149]. It can be described as

$$r = \frac{\sum_{i=1}^{n}(x_i - \bar{x}) \cdot (y_i - \bar{y})}{\sqrt{\sum_{i=1}^{n}(x_i - \bar{x})^2} \cdot \sqrt{\sum_{i=1}^{n}(y_i - \bar{y})^2}} \tag{2.15}$$

where *r* is the correlation coefficient of interconnected wind and solar power, x_i and y_i are the individual sample points indexed with *i*, $\bar{x}$ and $\bar{x}$ are the mean value of x_i and y_i, *n* is the sample size.

In this study, x_i and y_i could be interconnected wind power or interconnected wind and solar power which is depend on research objectives. Note that in this study, Pearson's correlation coefficient or called Pearson's *r* is employed that is used for data-based correlation analysis. The correlation coefficient is a parameter that indicates the strength of the linear relationship between two variables. The larger the correlation coefficient, the stronger the correlation between the two variables, and vice versa. For wind and solar power output, the smaller the correlation coefficient means that the peak-cutting and valley-filling occur more between the two resources, that is, the complementarity of two power sources is strong, and vice versa. Furthermore, *r* can vary from 0 to 1, when *r* falls between 0 to 0.4 which means low correlation; when *r* falls between 0.4 to 0.7 which means moderate correlation; when *r* falls between 0.7 to 1 which means high correlation. Note that the correlation coefficient can only reflect the complementarity of the output power amplitude of interconnected wind and solar power. However, considering the complex superposition effect of interconnected wind and solar power, complementarity is difficult to quantify the mitigation of power fluctuations directly.

Figure 2.8 shows *r* varies with the increase of the distance between two wind turbines. It can be easily seen from Figure 2.8 that with the rise in the distance, the correlation between the output power of two wind turbines is significantly decreasing and when the distance beyond 150km, the output power of two wind turbines shows low correlation. These imply that the complementarity of interconnected wind power is significantly affected by distance. The longer the distance between two wind turbines, the stronger the complementarity of the wind power output.
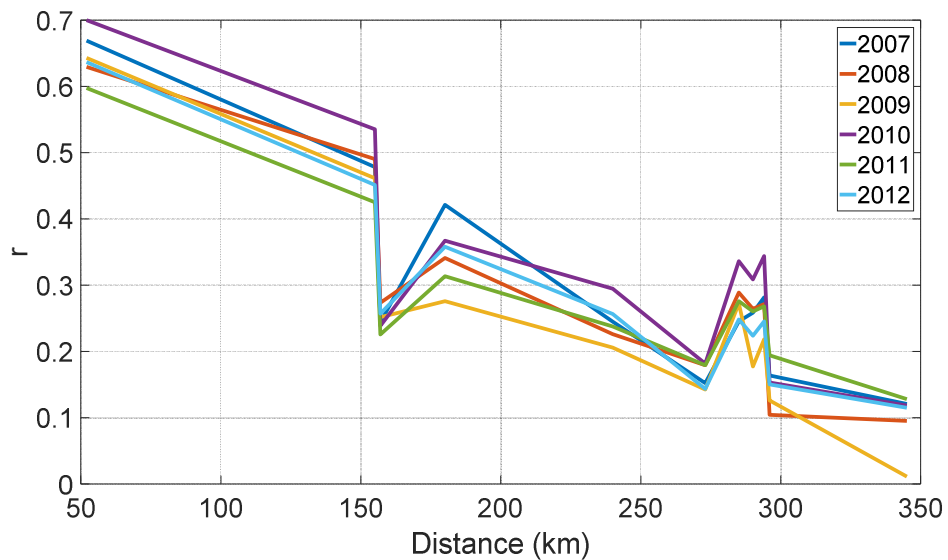
Figure 2.8 Correlation coefficient varies with the distance between two wind turbines from 2007 to 2012.

Figure 2.9 shows the correlation coefficient varies with the different mixed proportions of solar/wind power for six selected locations from 2007 to 2012. The solar/wind mix is 0 which means pure wind power (when solar/wind mix is 0, *r* is self-correlation of wind power which is 1), and the solar/wind mix is 0 which means pure solar power (when solar/wind mix is 1). It can be seen from Figure 2.9 that when solar/wind mix is 1, for all six selected location from 2007 to 2012, all the *r* are below 0.4 which mean wind and solar power have a very low correlation and high complementarity. Thus, *r* of wind and solar hybrids is showing a linear decline in general. Figure 2.9 (a), (d) and (f) show the lowest value around 0.8 mixed proportion which implies when wind and solar power are mixing by 0.8 proportion, wind and solar hybrid can achieve the best complementarity. Figure 2.9 (b), (c) and (e) show the lowest *r* occurs when the mixed proportion is 1 which implies when wind

and solar power are equal mixings, wind and solar hybrid can achieve the best complementarity. It provides a useful index to determine the optimal S/W ratio.
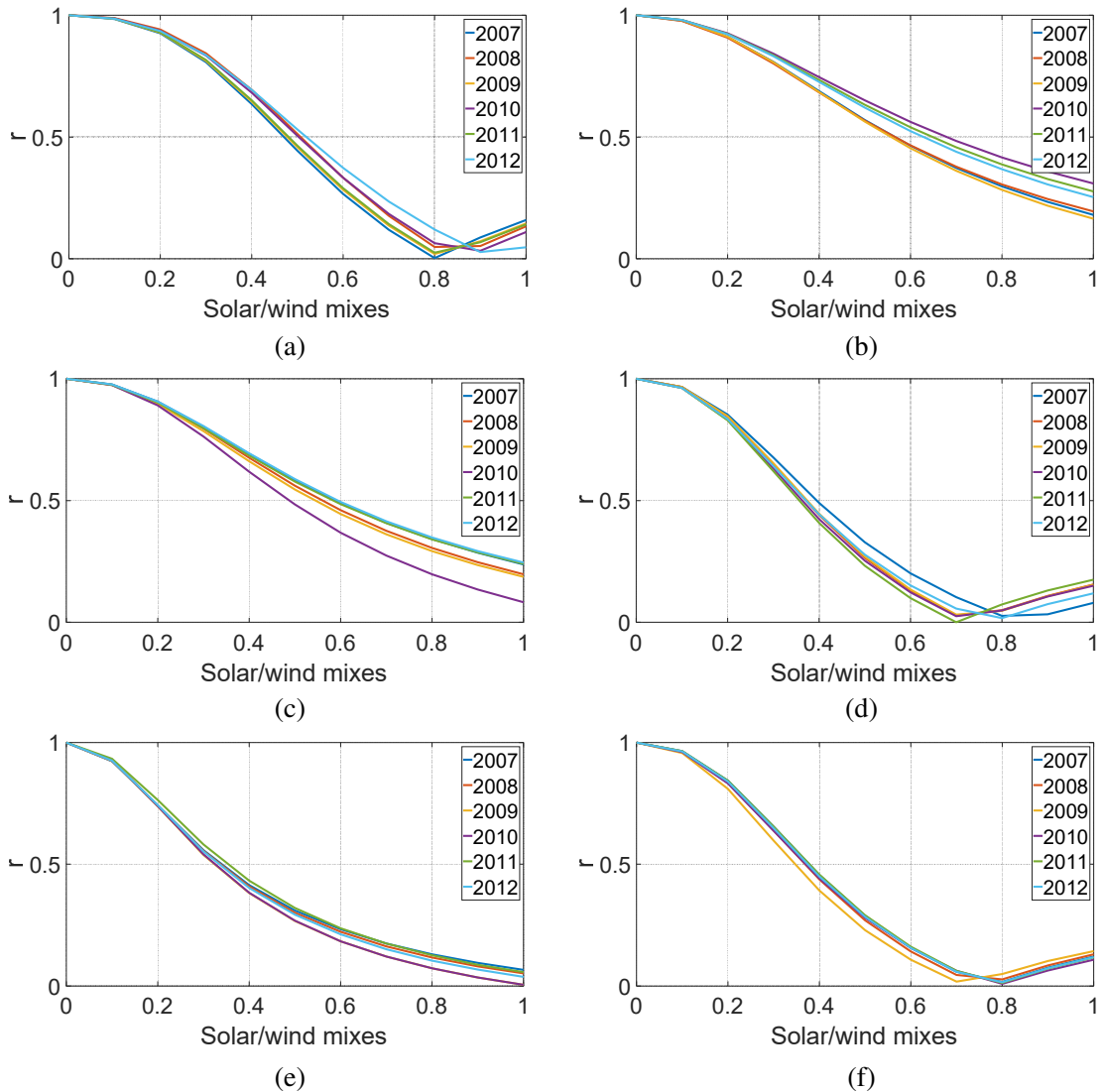
Figure 2.9 Correlation coefficient varies with the mixed proportion of solar/wind power at (a) Quito, (b) Valencia, (c) Mexico City, (d) Houston, (e) Salt Lake City, (f) Vancouver from 2007 to 2012.

2.4 Variability analysis in the frequency domain

It can be seen from Section 2.3 that the variability analysis in the time domain can easily quantify the inter-annual variation of wind and solar power which can help system designers and operators determine the reliability margin of the system operation. However, the smoothness factor and correlation coefficient in the time domain can only be used to

roughly evaluate the fluctuation of interconnected wind and solar power. It is hard to consider their implications for practical power system integration.

Frequency spectrum analysis is widely used in signal processing to analyze signal characteristics [150, 151]. In this section, a set of power spectrum based measure in the frequency domain is developed to quantify the variability of wind and solar power for optimal power system integration.

2.4.1 Frequency spectrum analysis

Based on the power spectrum of wind and solar power, the mitigation of wind and solar power variability can be treated as the filtering of power harmonics in the frequency domain. Thus the variability mitigation capacity of generators, energy storage, and demand response can be easily determined by comparing their power ramping rate and power capacity with the power spectrum of the wind and solar power.

For further analysis, the normalized annual renewable power generation data with sampling time interval T_S at one site can be expressed as

$$P_{N-RE}(i) = \frac{P_{RE}(i)T_S}{\sum_{i=1}^{n} P_{W\&S}(i)T_S} = \frac{P_{RE}(i)}{\sum_{i=1}^{n} P_{RE}(i)} \tag{2.16}$$

where $P_{RE}(i)$ is the annual renewable power generation, and $P_{N-RE}(i)$ represents the corresponding nominalized value. Note that the renewable power mainly refers to wind and solar power so that the normalized annual renewable power generation can be specifically derived as normalized annual wind power generation $P_{N-W}(i)$, normalized annual solar power generation $P_{N-S}(i)$ and normalized annual hybrid wind and solar power generation $P_{N-W\&S}(i)$.

A Fast Fourier Transform (FFT) is a type of algorithm that can rapidly compute the Discrete Fourier transform (DFT) of a sequence. Because computing a sequence of a dataset directly via DFT usually is far too slow, FFT is introduced for practical computation. FFT factorizes DFT matrix into a product of sparse factors, and it reduces calculation times from N^2 to $N\log N$, which makes a massive reduction of computing speed [152]. The FFT is obtained by decomposing a sequence of values into components of different frequencies (i.e. harmonics). Note that Fourier Transform can only be applied to periodic signals. For wind and solar power, in spite of the stochastic intermittence, both $P_{N-W}(i)$ and $P_{N-S}(i)$ show quasi-

periodic features at different timescale. For instance, the peaks of seasonal wind and solar power production regularly occur during a specific season across years for most of the locations. Therefore, an N-point-long equal interval time sample of the normalized renewable power generation $P_{N\text{-}RE}$ is used to construct the value at frequency domain point i. Thus, the DFT of $P_{N\text{-}RE}$ can be described as

$$h_{RE}(i) = \sum_{k=1}^{N-1} P_{N-RE}(k)e^{(i2\pi/N)ki}, \ i = 0, \ 1, \ ..., \ N-1 \tag{2.17}$$

where $h_{RE}(i)$ denotes the harmonic component of $P_{N\text{-}RE}$ at frequency point i, $e^{i2\pi/N}$ is a primitive N-th root of 1. Note that $h_{RE}(i)$ will be written as $h_W(i)$ for wind power harmonics, $h_S(i)$ for solar power harmonics, and $h_{W\&S}(i)$ for hybrid wind and solar power harmonics.

It should be noted that, because the PSD of wind and solar power follows the Kolmogorov spectrum profile, the profile of $|h_{RE}(i)|$ in the frequency domain will also follow a similar curve, and is quasi-periodic. However, the phase angle $\angle h_{RE}(i)$ of each harmonics in Eq. (2.17) is highly time-variant and statistically random, although the profile of annual $P_{N\text{-}RE}(i)$ is quasi-periodic yearly. Hereinafter, only the quasi-periodic $|h_{RE}(i)|$ are employed to facilitate the measurement of wind and solar power variability in the frequency domain, while time-variant $\angle h_{RE}(i)$ of wind and solar power will be neglected.

a. Wind and solar power

Figure 2.10 shows an example frequency spectrum of annual wind and solar power harmonics without the DC component, where $f(i)$ denotes the corresponding frequency of the i-th order harmonics. It can be observed in Figure 2.10 that the profile of $h_W(i)$ and $h_S(i)$ decreases with the increase of frequency in the band of $(4\times10^{-6}, 1.39\times10^{-4})$ Hz or $(2, 69)$ hours that mean the distribution of wind and solar power harmonics is different from white noise (the high-frequency and low-frequency harmonic content of white noise is almost equal). The impact of the variability of wind and solar power on its integration depends more on high-frequency power fluctuations. Figure 2.10 proves that the high-frequency content of wind and solar power fluctuations has a decreasing trend, which implies that the mitigation of high-frequency disturbances of wind power is economically feasible. Moreover, comparing Figure 2.10 (a) and (b), it is clear that the harmonics of wind and solar power have a big difference at 1.16×10^{-5} Hz (24 hours), 2.32×10^{-5} Hz (12 hours) and 4.63×10^{-5} Hz (6 hours). Solar power harmonics have such big spikes that are caused by the diurnal cycle

of solar irradiation: there is only half a day of sunlight per day and solar irradiation in the morning increase from zero to peak value, and the opposite in the afternoon. Therefore, it can be foreseen that solar energy change is very obvious on the time scale of 24 hours, 12 hours and 6 hours. Although the temperature difference produces the wind speed, that is, the sun is indirectly generated, but because the wind speed has been affected by too many environmental factors, the change of wind energy on these time scales is not very significant.
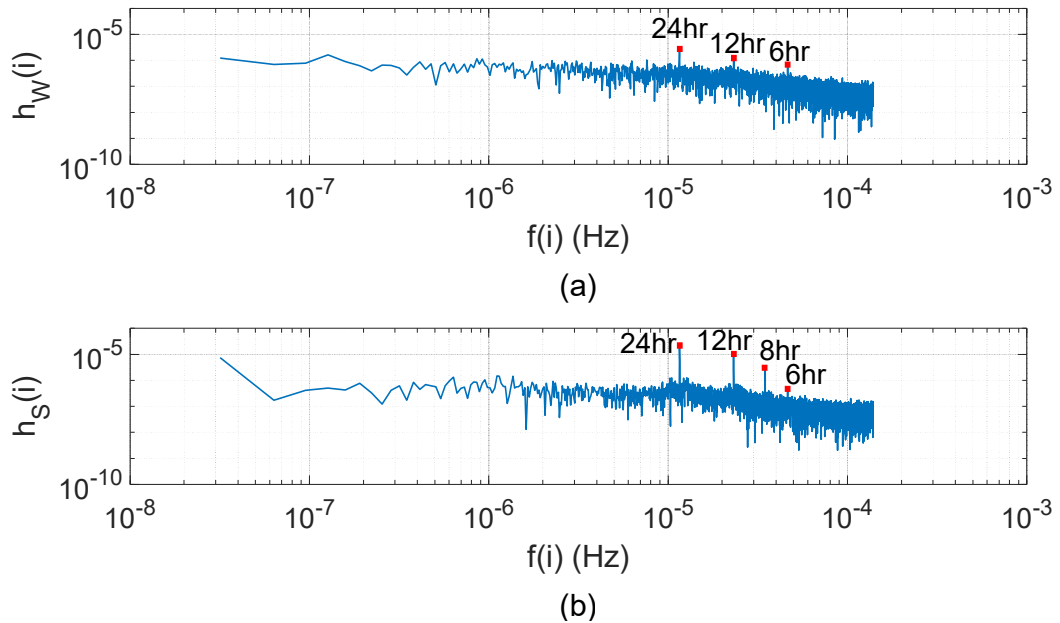
Figure 2.10 Frequency spectrum of (a) wind power and (b) solar power at Houston in 2012.

b. Interconnected wind power

In order to explore the power distribution of interconnected wind power in the frequency domain, FFT is used to transform the output power of the different amount of interconnected wind turbines in 12 selected locations in Colorado State from 2007 to 2012 as shown in Figure 2.3, and the frequency spectrum is shown in the Figure 2.11. It can be seen from Figure 2.11 that the harmonics of wind power within the frequency band higher than 10^{-6} Hz trends to be reduced with the increase of the number of interconnected wind plants. Moreover, this downward trend is becoming saturated as the number of connected fans increases. The results prove that the interconnected wind turbines will significantly mitigate the wind power fluctuations above 10^{-6} Hz, but not affect the wind power fluctuations below 10^{-6} Hz, and this mitigation will weaken as the number of wind turbines increases.
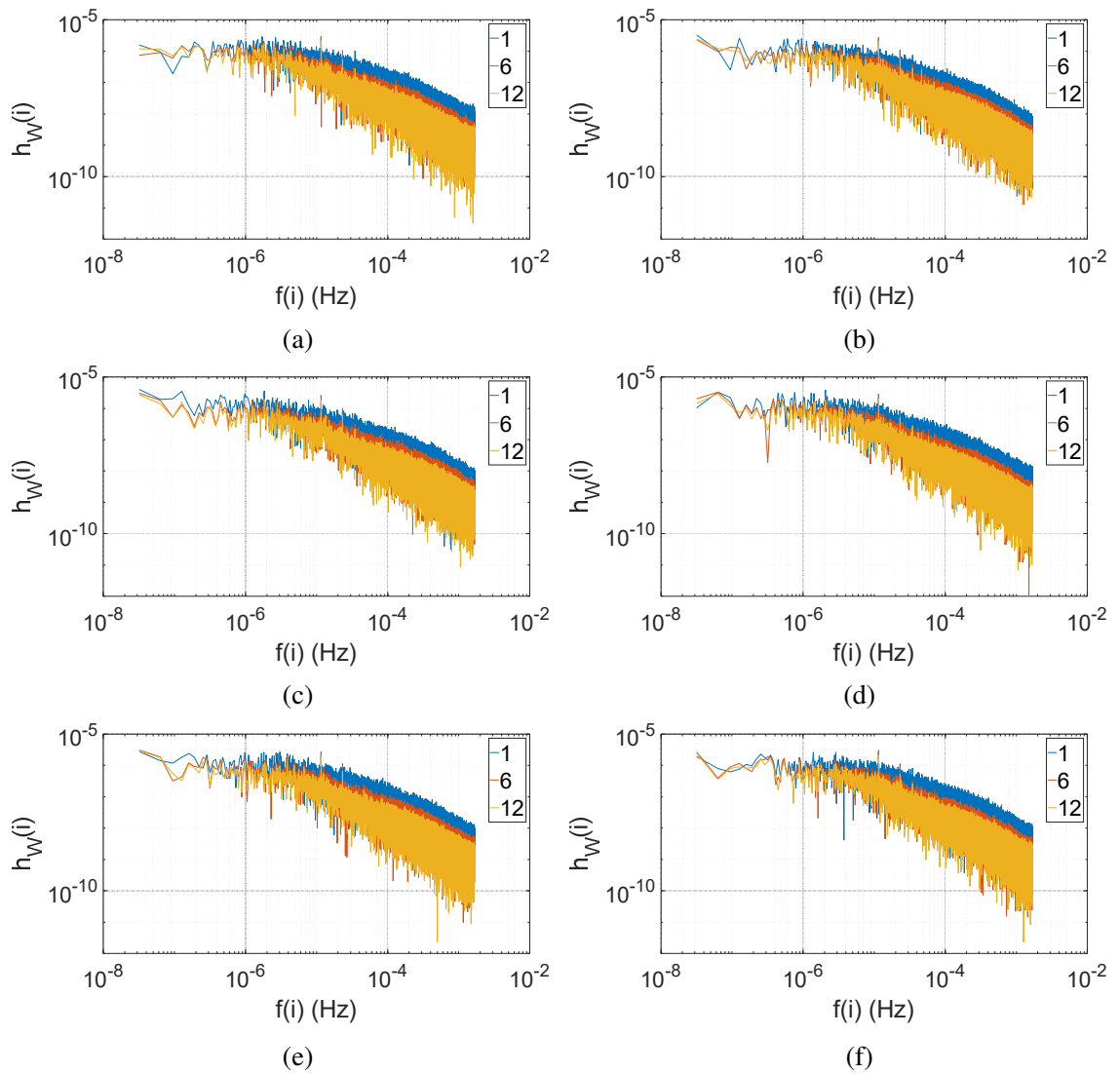
Figure 2.11 Frequency spectrum of different amount of interconnected wind turbines at 12 selected locations in the (a) year of 2007, (b) year of 2008, (c) year of 2009, (d) year of 2010, (e) year of 2011, (f) year of 2012.

By analyzing the frequency spectrum of interconnected wind power, the power system operators and designers can quantify the power fluctuations in each frequency band (also can be easily transformed to time scale by $T=1/f$). Then, they can use the most cost-effective mitigation method of power fluctuation to mitigate the specific power fluctuation according to actual requirements.

c. Interconnected wind and solar power

Figure 2.12 shows the frequency spectrum of different mixed wind/solar proportions for six selected locations across North and South America as shown in Figure 2.5 in 2012. W/S means the mixing ratio of wind and solar power: 100% means pure wind power, and

0% means pure solar power. It can be seen from Figure 2.12 that solar power has more high-frequency harmonics than wind power, and the harmonics of the output power wind and solar hybrid are more like the average of both. Therefore, it is not clear to see from the frequency spectrum that hybrid wind and solar power can effectively improve the mitigation of the variability of wind and solar power.
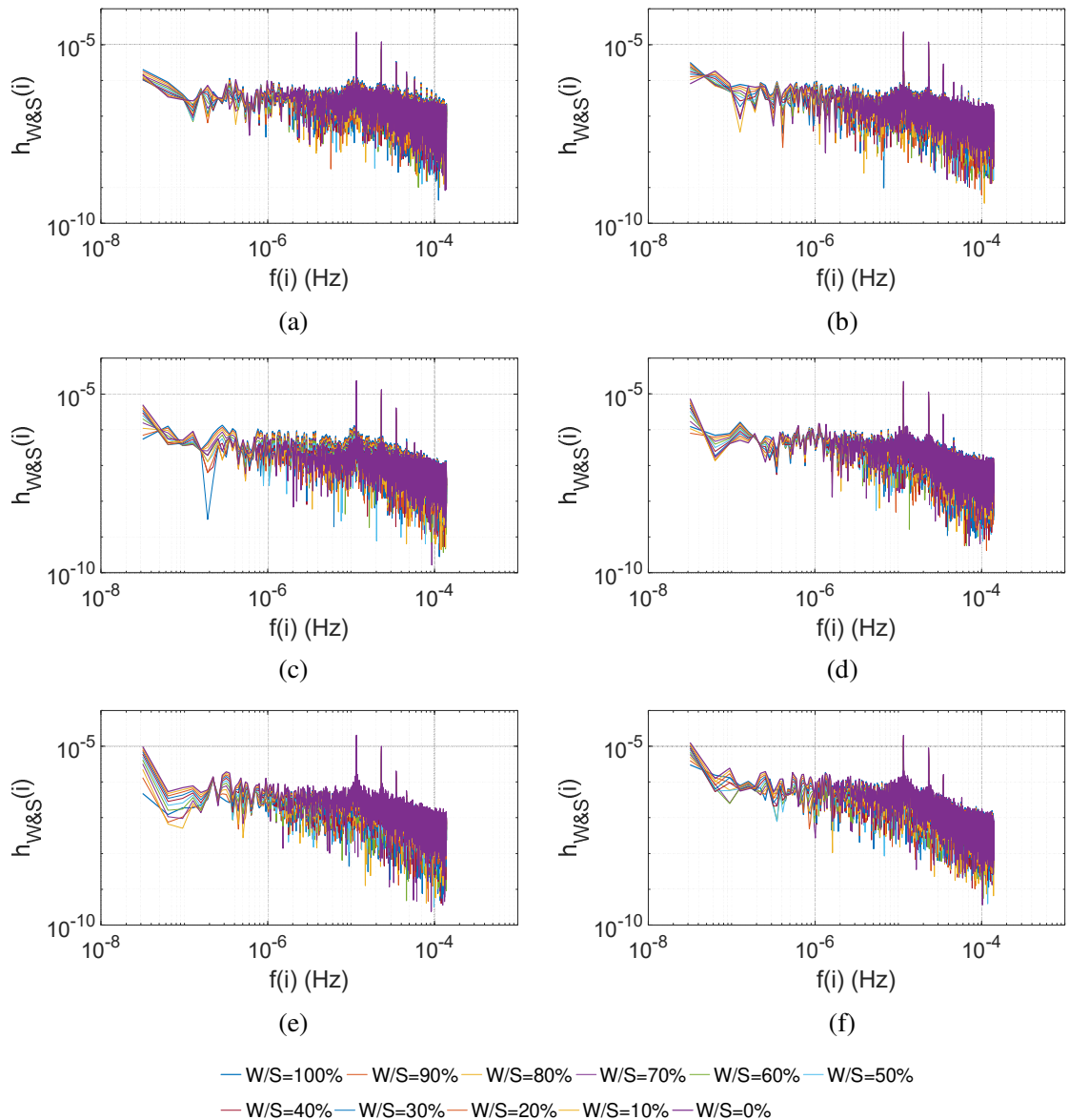
Figure 2.12 Frequency spectrum of different mixed proportions of interconnected wind and solar power in 2012 at (a) Quito, (b) Valencia, (c) Mexico City, (d) Houston, (e) Salt Lake City, (f) Vancouver.

2.4.2 Fluctuation rate

Being considered as a power harmonic source, the fluctuation of annual renewable power generation can be characterized by using the total harmonic distortion of renewable power relative to the constant DC power component. Consequently, a fluctuation rate of annual renewable power generation is defined as

$$
\begin{cases}
F_{RE}(n) = \sqrt{\sum_{i=0}^{N_{RE}-1}\left(h_{RE(y)}(i)/h_{RE(y)}(0)\right)^2} \\
F_{REavg} = \sum_{n=y}^{Y}\left(F_{RE}(y)/(Y-y_0)\right) \\
\delta_{FRE\max} = \left(\max\left(F_{RE}(y)\right)\right)/F_{Wavg} - 1 \\
\delta_{FRE\min} = \left(\min\left(F_{RE}(y)\right)\right)/F_{Wavg} - 1
\end{cases}
\tag{2.18}
$$

where the fluctuation rate of renewable power for the year y is denoted as $F_{RE}(y)$, F_{REavg} is the average value of $F_{RE}(y)$ from the year y_0 to Y, $\delta_{FRE\max}$ and $\delta_{FRE\min}$ are the lower bounds of $F_{RE}(y)$. Note that $F_{RE}(y)$ can also be derived as a fluctuation rate of wind power $F_W(y)$, fluctuation rate of solar power $F_S(y)$, and fluctuation rate of hybrid wind and solar power $F_{W\&S}(y)$. Similarly, F_{REavg} can also be derived as an average fluctuation rate of wind power F_{Wavg}, average fluctuation rate of solar power F_{Savg} and average fluctuation rate of hybrid wind and solar power $F_{W\&Savg}$. Eq. (2.18) is used to calculate the fluctuation rate of wind and solar power. $F_{RE}(y)$ in the frequency domain is somewhat equivalent to the SD in the time domain. Like the inter-annual variation, $\delta_{FRE\max}$ can be used to determine the size (margin) factor of the battery bank. Larger $\delta_{FRE\max}$ indicates that a larger margin for battery bank is needed.

According to Eq. (2.18), for a constant DC power, i.e. $h_{RE(y)}(0) > 0$ and $h_{RE(y)}(i) = 0$ ($i = 1, 2, \ldots, N_{RE}- 1$), $F_{RE}(y) = 1$; otherwise power harmonics with $h_{RE(y)}(i) > 0$ ($i = 1, 2, \ldots, N_{RE}- 1$) would bring a larger $F_{RE}(y) > 1$. That means that an intensive power fluctuation with more incorporated power harmonics will lead to a large $F_{RE}(y)$. Subsequently, the bigger $F_{RE}(y)$ is, the higher the variability of renewable power will be. Therefore, $F_{RE}(y)$ can be used to indicate the renewable power variability in the frequency domain. Since $F_{RE}(y)$ is obtained based on the FFT, its value reflects the actual ratio of annual renewable power fluctuations, that is, $F_{RE}(y)$ is a factor to quantify the variable annual renewable power.

Chapter 2
Variability analysis of wind/solar power

a. Wind power

Table 2.11 lists the values of $F_W(y)$ and F_{Wavg} at the six sites from 2007 to 2012. It can be seen that, the annual wind power variability of six sites can be ranked Los Angeles > Denver > New York ≈ Chicago ≈ Houston ≈ San Francisco. F_{Wavg} at Los Angeles is around two times of those at the other five sites. Moreover, $\delta_{FW\,max}$ and $\delta_{FW\,min}$ further show that Los Angeles and Houston have a larger annual variation of power fluctuation than other sites. That implies that, the most fluctuated wind power might lead to the poorest power supply reliability of SAWP systems at Los Angeles. The SAWP systems at Los Angeles need to cost more on mitigation of wind power variation for reliable operation. Moreover, it can be found that the rankings of the value of $F_{RE}(y)$ at the six sites align with the rankings of corresponding SD.

Table 2.11
Fluctuation rates of wind power at six sites for the years 2007 to 2012.

$F_W(y)$ Year	Location					
	San Francisco	Los Angeles	Denver	Houston	Chicago	New York
2007	1.93	4.37	2.68	2.10	2.00	2.10
2008	1.97	4.21	2.61	2.05	2.01	2.18
2009	1.97	4.31	2.71	1.97	2.03	2.15
2010	1.98	4.18	2.72	1.94	2.05	2.03
2011	2.04	4.16	2.67	1.87	2.02	2.21
2012	1.96	4.66	2.60	2.08	2.03	2.20
F_{Wavg}	1.93	4.37	2.68	2.10	2.00	2.10
δ_{FWmax}	+3.0%	+7.9%	+1.9%	+5.0%	+1.5%	+2.8%
δ_{FWmin}	-2.5%	-3.7%	-2.6%	-6.5%	-1.0%	-5.6%

b. Solar power

Table 2.12 lists the values of $F_S(y)$ and F_{Savg} at the six sites from 1998 to 2017. It can be seen that, the annual solar power variability of six sites can be ranked Quito ≈ Valencia ≈ Mexico City ≈ Houston ≈ Salt Lake City < Vancouver. Note that, with the highest latitude of 50°, the variability of solar power at Vancouver is significantly higher than those at other sites. Moreover, $\delta_{FS\,max}$ and $\delta_{FS\,min}$ further show that Vancouver has a bit larger annual variation of power fluctuation than other sites. That implies that, the most fluctuated solar

power might lead to the poorest power supply reliability of SAPVP systems in Vancouver (high latitude regions). The SAPVP systems at high latitude regions need to cost more on mitigation of solar power variation for reliable operation. Moreover, it can be found that the rankings of the value of $F_{RE}(y)$ at the six sites align with the rankings of the corresponding SD.

Table 2.12

Fluctuation rates of solar power at six sites for the years 1998 to 2017.

$F_S(y)$ Year	Location					
	Quito	Valencia	Mexico City	Houston	Salt Lake City	Vancouver
1998	2.18	2.16	2.16	2.24	2.36	2.62
1999	2.19	2.14	2.16	2.18	2.29	2.62
2000	2.18	2.14	2.15	2.21	2.30	2.54
2001	2.17	2.13	2.17	2.23	2.27	2.50
2002	2.17	2.14	2.16	2.23	2.26	2.44
2003	2.21	2.18	2.19	2.25	2.28	2.49
2004	2.20	2.17	2.19	2.29	2.29	2.51
2005	2.22	2.17	2.18	2.21	2.30	2.52
2006	2.23	2.18	2.19	2.24	2.29	2.53
2007	2.24	2.17	2.19	2.26	2.26	2.57
2008	2.26	2.17	2.20	2.24	2.29	2.53
2009	2.25	2.18	2.21	2.29	2.28	2.47
2010	2.23	2.20	2.18	2.25	2.32	2.53
2011	2.23	2.20	2.16	2.22	2.30	2.56
2012	2.22	2.17	2.20	2.23	2.32	2.64
2013	2.21	2.17	2.19	2.25	2.31	2.57
2014	2.22	2.17	2.21	2.27	2.29	2.48
2015	2.20	2.16	2.21	2.28	2.27	2.49
2016	2.22	2.17	2.19	2.23	2.29	2.49
2017	2.22	2.18	2.17	2.22	2.29	2.45
F_{Savg}	2.21	2.17	2.18	2.24	2.29	2.53
δ_{FSmax}	+2.1%	+1.5%	+1.4%	+2.2%	+2.8%	+3.8%
δ_{FSmin}	-2.0%	-1.7%	-1.3%	-2.8%	-1.1%	-3.4%

c. Hybrid wind and solar power

Table 2.13 lists the values of $F_{W\&Savg}$ at the six sites from 1998 to 2017 and the minimum value for each location has been highlighted in the yellow zone. It can be seen that, Hybrid wind and solar power can effectively reduce power variability. However, it is hard to determine the optimal W/S mixed ratio for all the six locations because the all mixed ration varies from 60% to 20% which is a large range. These imply hybrid wind and solar power can reduce annual power variability but because it is hard to determine the certain mixed ratio, hybrid wind and solar power are not universal for system design.

Table 2.13
Average fluctuation rates of hybrid wind and solar power at six sites from 1998 to 2017.

$F_{W\&Savg}$ / W/S ratio	Location					
	Quito	Valencia	Mexico City	Houston	Salt Lake City	Vancouver
100%	2.42	2.27	3.16	2.17	2.83	2.28
90%	2.33	2.15	2.95	2.06	2.62	2.05
80%	2.26	2.05	2.76	1.97	2.44	1.87
70%	2.21	1.97	2.59	1.92	2.30	1.75
60%	2.18	1.93	2.45	**<u>1.90</u>**	2.19	**<u>1.71</u>**
50%	**<u>2.16</u>**	**<u>1.92</u>**	2.33	1.91	2.13	1.74
40%	2.17	1.94	2.25	1.96	**<u>2.11</u>**	1.85
30%	2.20	1.99	**<u>2.22</u>**	2.04	2.14	2.07
20%	2.24	2.07	**<u>2.22</u>**	2.15	2.23	2.25
10%	2.30	2.18	2.26	2.28	2.35	2.51
0%	2.38	2.31	2.35	2.43	2.51	2.80

2.4.3 Cumulative energy distribution

In Section 2.4.1, the wind and solar power fluctuation are transformed into a combination of sinusoidal harmonics and a DC component via FFT. Thus, wind and solar power harmonics can be treated as a power harmonics source. For wind and solar power, the mitigation of the power fluctuation is a puzzle. The wind and solar power design lack an assessment of the power fluctuation in various frequency bands. Herein, a cumulative energy distribution index $D_{RE}(j)$ for annual renewable energy in the frequency domain is developed to determine the total power fluctuation for continuous frequencies. It can be described as

$$
\begin{cases}
e_{RE(y)}(i) = h_{RE(n)}(i)T(i)/\sqrt{2} \\[2mm]
D_{RE(y)}(j) = \dfrac{\sum_{i=j}^{N-1} e_{RE(n)}(i)}{\sum_{i=1}^{N-1} e_{RE(n)}(i)} \times 100\% \\[4mm]
D_{REavg}(j) = \sum_{n=y_0}^{Y} D_{RE(n)}(j)/(Y-y_0)
\end{cases}
\tag{2.19}
$$

where $e_{RE(y)}(i)$ with $i = 1, 2, \ldots, N-1$ represents the energy of i-th order renewable energy harmonic for the year y; $T(i) = 1/f(i)$ is the period of i-th order renewable power harmonics of frequency $f(j)$; $D_{RE(y)}(j)$ with $j = 1, 2, \ldots, N-1$ denotes the ratio of the total renewable energy harmonics within $[f(j), 1/2T_S]$ Hz to gross annual renewable energy generation; $D_{REavg}(j)$ is the average of $D_{RE(y)}(j)$ for years y_0 to Y. A larger $D_{RE(y)}(j)$ means more gross variability energy in the frequency range of $[f(j), 1/2T_S]$ Hz; and vice versa. Note that $e_{RE(y)}(i)$ can be derived as i-th order wind energy harmonic $e_{W(y)}(i)$, i-th order solar energy harmonic $e_{S(y)}(i)$ and i-th order hybrid wind and solar energy harmonic $e_{W\&S(y)}(i)$. Similarly, $D_{RE(y)}(j)$ and $D_{REavg}(j)$ can be derived as the corresponding factor for wind energy, solar energy and hybrid wind and solar energy as well.

Figure 2.13 shows $D_{Wavg}(j)$ and $D_{Savg}(j)$ at selected 6 locations as shown in Figure 2.2 and selected 6 locations as shown in Figure 2.5 separately. Figure 2.13 (a) shows that, all $D_{Wavg}(j)$ at the six sites are close to each other with noticeable differences among each other in the frequency band of $[1\times10^{-6}, 1.67\times10^{-3}]$ Hz or $[0.167, 278]$ hours, and all $D_{Wavg}(j)$ increases smoothly with the decrease of frequency $f(j)$. Among them, Denver and Houston have higher $D_{Wavg}(j)$ in the high-frequency band that implies wind power in Denver and Houston has more high-frequency power fluctuations. In addition, Los Angeles has less $D_{Wavg}(j)$ in the high-frequency band that implies wind power in Los Angeles are more smooth in small time scales. As shown in Figure 2.13 (b), for six selected locations as shown in Figure 2.1, the higher the latitude is, the lower $D_{Savg}(j)$ in the high-frequency range of $[7.29\times10^{-7}, 2.78\times10^{-4}]$ Hz is. Figure 2.13 (b) also shows that two big energy jumps occur at frequencies of 1.16×10^{-5} Hz (24 hours) and 2.32×10^{-5} Hz (12 hours). This is consistent with cyclic changes in daily solar power.

For both wind and solar power, higher $D_{Wavg}(j)$ and $D_{Savg}(j)$ implies more gross energy fluctuations, which mean higher cost of mitigations for power fluctuations. Therefore, for wind power, sites in Denver and Houston need to spend more money on smoothing power

fluctuations. For solar power, sites in low latitude locations need to cost more on smoothing power fluctuations.
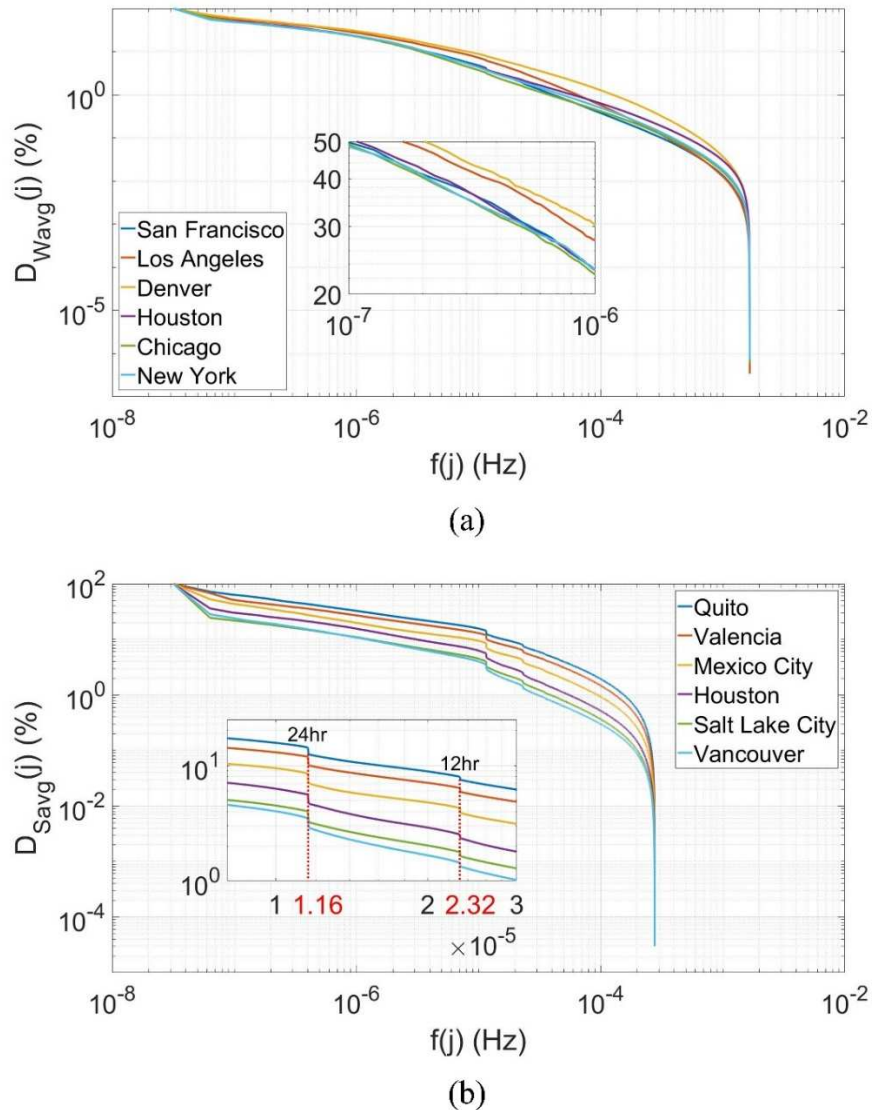
Figure 2.13 $D_{wavg}(j)$ **versus** $f(j)$ **at six selected locations across USA and (b)** $D_{Savg}(j)$ **versus** $f(j)$ **at six selected locations across North and South America.**

Figure 2.14 shows $D_{W(y)}(j)$ from 2007 to 2012 at each location almost overlap each other, but except with small but noticeable variations in the frequency band of $[1 \times 10^{-5}, 1.67 \times 10^{-3}]$, Hz at San Francisco and Los Angeles which is due to there is the uncertainty of annual wind speeds on the west coast of the United States, and sometimes even wind drought. The high degree of similarity among all $D_{W(y)}(j)$ at each location clearly demonstrates that, the energy distribution of annual wind power is QTI. In other words, the wind power variability at each site can be considered to be QTI in the frequency domain. It

should be pointed out that, although the phase angle $\angle h_{RE}(i)$ of renewable power harmonics is time-variant and radom, all $D_{RE(y)}(j)$ at each location almost overlap each other, that is to say, the distribution of annual wind and solar power is QTI. Therefore it is reasonable to neglect $\angle h_{RE}(i)$ in the analysis of wind and solar power variability.
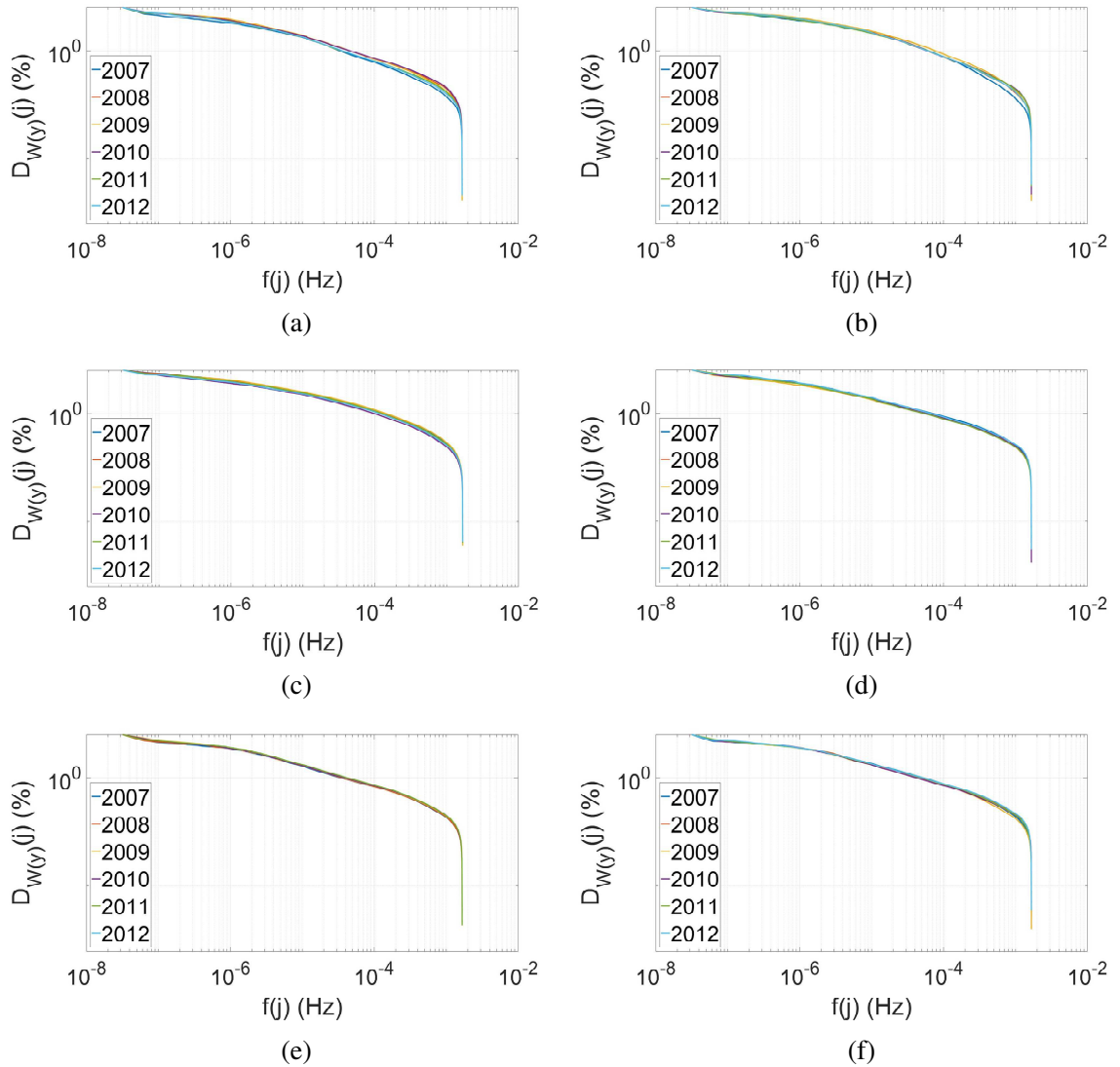
Figure 2.14 $D_{W(y)}(j)$ with frequency $f(j)$ for the years 2007 to 2012 at (a) San Francisco, (b) Los Angeles, (c) Denver, (d) Houston, (e) Chicago, (f) New York.

Figure 2.15 also shows $D_{S(y)}(j)$ from 2007 to 2012 at each location almost overlap each other. Comparing with $D_{W(y)}(j)$, $D_{S(y)}(j)$ for each year is closer, that is because solar power has more obvious daily and seasonal cycles. The high degree of similarity among all $D_{S(y)}(j)$ at each location clearly demonstrates that, the energy distribution of annual solar power is

QTI. In other words, the solar power variability at each site can be considered to be QTI in the frequency domain.
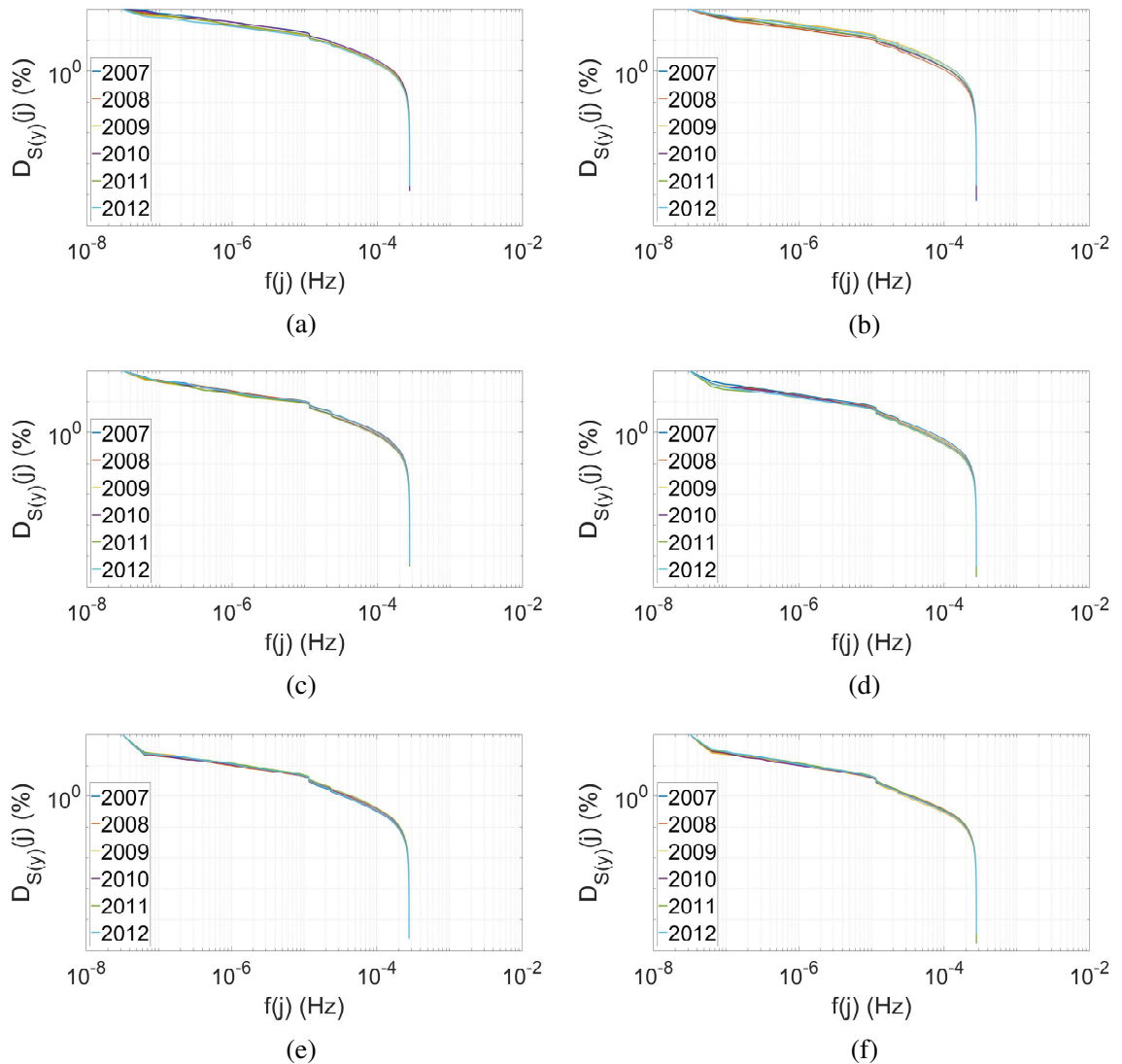
Figure 2.15 $D_{S(y)(j)}$ with frequency $f(j)$ for the years 2007-2012 at (a) Quito, (b) Valencia, (c) Mexico City, (d) Houston, (e) Salt Lake City, (f) Vancouver.

QTI of wind and solar power in the frequency domain implies that the proposed method for quantifying the variability of wind and solar power in the frequency domain is sufficiently reliable and feasible. Thus, proposed wind and solar power variability analysis can be applied to system design and long-term planning and can ensure long-term credibility of decisions.

2.5 Summary

The mitigation of wind and solar power variability has always been a challenge for wind and solar power integration. In this chapter, the variability of wind and solar power has been comprehensively quantified in both the time domain and frequency domain. The proposed measurement parameters for wind and solar power variability include: inter-annual variation, smoothness coefficient, correlation coefficient in the time domain; and frequency spectrum analysis, fluctuation rate and cumulative energy distribution index in the frequency domain. It has been found from the analysis results that:

I. In view of its quasi-periodic characteristics, the intermittent wind/solar power in the time domain can be treated as a QTI source of power harmonics in the frequency domain. The mitigation of wind/solar power fluctuations can be treated as the filtering of power harmonics.

II. The intensity and variability of solar power highly depend on the latitude of its geographic location. Low-latitude regions have intense solar irradiation throughout the year, and solar irradiation in winter and fall at the low-latitude regions is much higher than in spring and winter. The intensity and variability of wind power are irrelevant to the geographic latitude.

III. The interconnection of wind power can effectively improve the smoothness of wind power and reduce wind power variability. However, the smoothness of mixed wind and solar power is not superior to either wind power or solar power at all locations.

IV. The correlation between interconnected wind power will drop rapidly with the increase of the distance between sites. The interconnection of wind and solar power doesn't help reduce the gross correlation.

V. The interconnection of wind power can significantly mitigate high-frequency power fluctuations but this mitigation will trend to saturate with the increase of the number of intercommoned wind turbines. The interconnection of wind and solar power does not show significant effects on power fluctuation mitigation.

The measurement results of wind and solar power provide us insights into the variability of wind and solar power with implications for optimal integration of wind and

solar power into power systems. Chapter 3 and Chapter 4 will demonstrate how to explore the implications of the proposed measures to the wind and solar power variability for the design of off-grid power systems and grid-connected systems, respectively.

Chapter 3

Optimal sizing of standalone wind/solar power systems

3.1 Introduction

A standalone wind/solar power system is widely used in remote areas where mains electricity and/or conventional fuels are unavailable or cost-prohibitive [67, 137, 153, 154]. It can be treated as an electrical power system with 100% penetration level wind/solar power. The variability of intermittent wind/solar power makes it difficult to determine the optimal sizing upon the requirements of system costs and power supply reliability. So far, the optimal sizing of wind and solar power systems is still an open issue.

Based on the variability analysis results in Chapter 2, this chapter investigates the impacts of wind /solar power variability on the optimal sizing of standalone wind/solar power systems. A case study of the SAWP system in Chicago and a case study of the SAPVP system in Houston are carried out to demonstrate the impacts.

3.2 System description

In this thesis, the standalone wind and solar power systems are specific to the standalone residential users. The system load consists of a home's basic household appliances. In addition, this study assumed that the power supply reliability for this kind of standalone power system does not need to be 100%. A more detailed system structure will be introduced in the following text. For most standalone wind/solar power systems, the lead-acid battery bank is usually adopted as the energy storage to mitigate the wind/solar variability and improve the system flexibility.

3.2.1 System structure

(a)

(b)

(c)
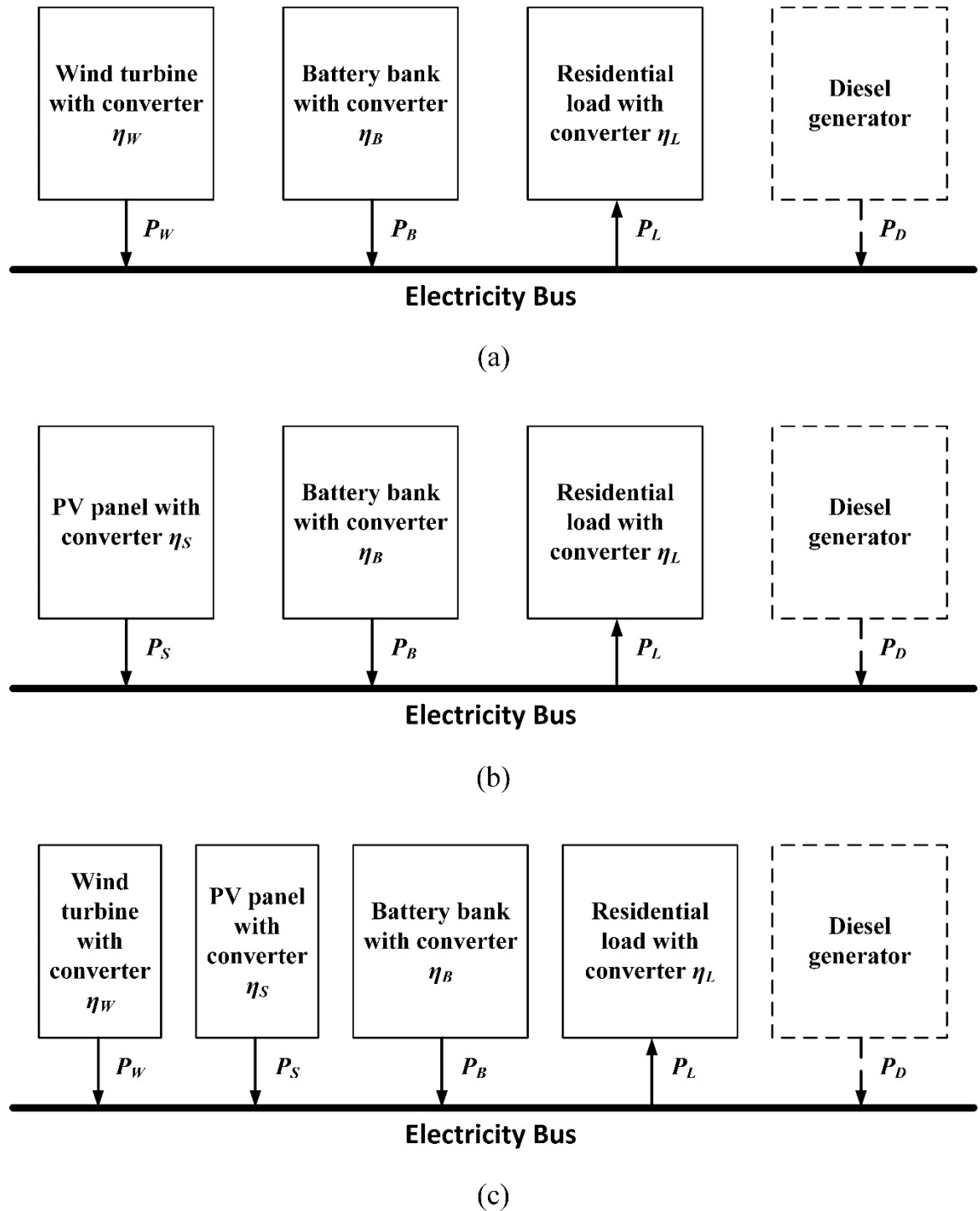
Figure 3.1 The typical standalone (a) wind power, (b) solar power, (c) hybrid wind and solar power systems.

The diagrams of the typical SAWP, SAPVP and standalone hybrid wind and solar power systems are illustrated in Figure 3.1. All these systems consist of wind, solar or wind and solar power generators, a battery bank and a residential load, where power converters

act as the power interfaces of the wind generator/battery/load to the electricity bus with the conversion efficiency of the power generator $\eta_W = \eta_S \leq 95\%$, the conversion efficiency of residential load $\eta_L \leq 95\%$ and the battery round-trip efficiency $\eta_B \leq 81\%$ [35, 155, 156]. For considerations of safety and service life, the battery bank should avoid being overcharged and undercharged. As mentioned above, although the installation of additional diesel engines can improve power supply reliability and reduce the required battery bank capacity, the system cost has increased significantly. Furthermore, some studies have proposed that the energy storage of standalone power systems are divided into long-term energy storage and short-term energy storage. Short-term energy storage usually uses batteries, while long-term energy storage usually uses hydrogen fuel cells. However, due to the low efficiency and high cost of hydrogen fuel cells, long-term energy storage equipment such as hydrogen fuel cells are rarely used in practical standalone power systems. Therefore, the standalone power system discussed in this thesis does not consider diesel generators and long-term energy storage equipment.

3.2.2 Energy management strategy

In the typical SAWP, SAPVP or standalone hybrid wind and solar power systems with energy storage like shown in Figure 3.1, the energy flow is mainly divided into two routes: one is the electric power has been directly delivered to end-user side; another is the electric power will be delivered to the load side after being stored in the battery bank. During the process of energy has been stored into the battery bank, the excess generator power will be stored for future power output deficit. Therefore, the battery bank is employed to smooth the generation-load power mismatch $\Delta P = P_{RE} - P_L$ as shown in Figure 3.2 ('+' means battery bank may charging and '-' means battery bank may discharging). Note that the renewable power generation P_{RE} can be derived as wind power output P_W, solar power output P_S and hybrid wind and solar power output $P_{W\&S}$. The operation of the SAWP, SAPVP or standalone hybrid wind and solar power systems would fall into the following scenarios:

- When $P_{W\&S} \geq P_L$ and the battery is not overcharged, the load demand P_L is met and the battery bank is charged with the excessive power $\Delta P = P_{W\&S} - P_L \geq 0$.

- When $P_{W\&S} \geq P_L$ and the battery is fully charged, the load demand P_L is met and the excessive power $\Delta P = P_{W\&S} - P_L \geq 0$ is discarded as power loss.

- When $P_{W\&S} < P_L$ and the battery is not over-discharged, the battery bank releases power to compensate for the power deficit $\Delta P = P_{W\&S} - P_L \leq 0$.

- When $P_{W\&S} < P_L$ and the battery is over-discharged, the battery bank is charged with $P_{W\&S}$ and the power outage occurs.
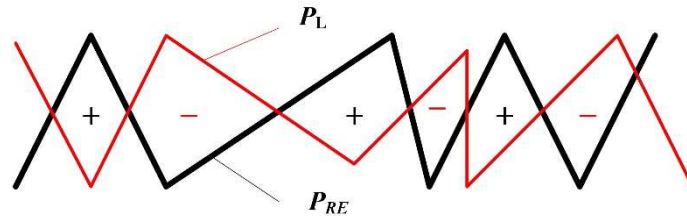
Figure 3.2 The power mismatch between P_{RE} and P_L.

3.3 The mitigation of wind/solar power variability

Since the only sources of generated power for standalone wind and solar power systems are wind and solar, the reliability of standalone wind and solar power systems is directly related to the fluctuation of wind and solar power. In the case of the battery bank is not considered, when the wind and solar power output does not meet the load demand, if the generated power output is greater than the load demand, there will be a waste of power output; or the generated power is less than the load demand, this will cause the power outage. Therefore, investigating the generation-load mismatch power of the standalone wind and solar power systems becomes the key to improve system reliability and reduce system costs.

3.3.1 Generation-load power mismatch

The load profile for standalone power systems in this thesis is based on the research of individual household electricity demand by the University of Oxford and the comprehensive load model in the renewable energy simulation software Trnsys [155, 157]. Due to the standalone wind/solar power system for this study refers to the standalone residential power system (no more additional power generator and cannot connect to the power grid), so that the small amount of power outage is allowed to happen. In fact, for the standalone residential power systems, because the user's electricity habits are different, the load profile can be various. For example, for those who need to go to work during the day, the daily peak electricity consumption is concentrated in the morning and night. For those

who do not need to go to work, the daily peak electricity consumption may last from noon to night. Moreover, for users in warm regions, the annual electricity consumption may exist in the summer for air conditioning. For users in cold regions, the annual electricity consumption may increase in the winter for heating. For the structure of a standalone power system in this thesis, since there is no load shifting, it should ensure that the load mode is fixed to analyze the impact of other variables. Moreover, due to the periodic characteristics of wind and solar power (for example, solar power have the diurnal cycle), so that for the standalone residential power system, generation-load power mismatch or called power imbalance like shown in Figure 3.2 has existed.

(a)

(b)

(c)
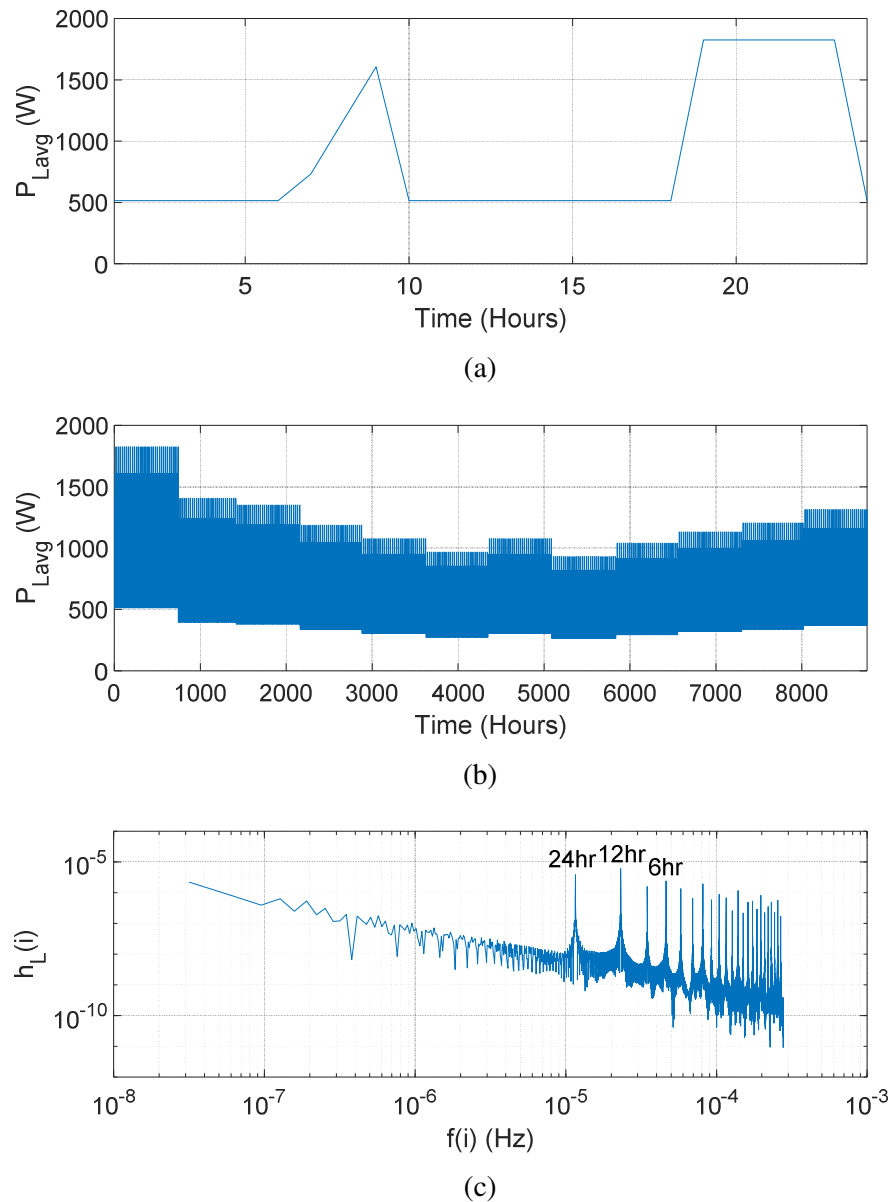
Figure 3.3 A typical average annual residential power consumption (a) 24-hours load data (b) one-year load data, (c) Load harmonic spectrum.

Figure 3.3 illustrates the typical average annual residential load P_{Lavg} employed in the research with $\bar{P}_L = 518.26\text{W}$ and its normalized power harmonics spectrum. Figure 3.3 (a) shows the 24-hours load profile that is called dual-peak profile which means the daily load consumption reaches its peak value in both morning and evening. Figure 3.3 (b) shows the distribution of annual load consumption that winter is a peak in electricity consumption of the year. Figure 3.3 (b) shows the power harmonic spectrum of load consumption. Comparing with the power harmonic spectrum of wind and solar power as shown in Chapter 2, it can be seen that, the power fluctuations of the load are more significant, and the spikes at high frequencies are far more than those of wind and solar power. These imply that, a high degree of the periodicity of the load demand leads to spikes at specific harmonic frequencies above 9×10^{-6} Hz. In comparison, the energy distribution of wind and solar power is of a much higher degree of randomness. In view of the quasi-periodic characteristics of both the wind and solar power and the load demand, the annual generation-load mismatch power $\Delta P = P_{RE} - P_L$ can also be represented as a combined power harmonics and a DC power component.

Since both P_{RE} and P_L are quasi-periodic, the power mismatch $\Delta P = P_{RE} - P_L$ will also be quasi-periodic. By using FFT, annual ΔP can be transformed into normalized mismatch power harmonics data $0 \le h_{M(y)}(i) \le 1$ with $i = 0, 1, 2, \ldots, N - 1$. Subsequently, the energy $e_{M(y)}(i)$ of the i-th order mismatch power harmonics will constitute the energy spectrum of ΔP, which can be calculated as

$$\begin{cases} e_{M(y)}(i) = h_{M(y)}(i)T(i)/\sqrt{2} \\ e_{Mavg}(i) = \sum_{n=y}^{Y} e_{M(y)}(i) \end{cases}, \quad i = 1, 2, \ldots, N-1 \tag{3.1}$$

where $e_{M(y)}(i)$ with $i = 1, 2, \ldots, N - 1$ represents the energy spectrum of i-th order mismatch power for the year y, $e_{Mavg}(i)$ is the energy spectrum of mismatch power for the years y to Y.

For standalone renewable energy systems, due to the specific system structure as shown in Figure 3.1, the transmission efficiency η_T from P_{RE} to P_L can be calculated as [62]:

$$\eta_T = \beta + (1 - \beta) \cdot \eta_B \tag{3.2}$$

where β denotes the ratio of wind and solar power generation directly transferred to the load via electricity bus, and the other (1-β) via the battery. In addition, when the electricity transfer via the local power network, part of the electrical energy will be converted into thermal energy which will cause power loss. Without loss of generality, the correction coefficient γ is introduced to compensate for the power loss on the local power network:

$$\gamma = \frac{1}{\eta_T}$$
(3.3)

For the analysis in this section, for wind/solar power systems, this study assumes that 50% power directly transfers from the power generator to load $\beta = 0.5$ which means that 50% generated power will directly transfer to load, and 50% generated power will charger the battery and battery will power the system when energy deficit happened. Without loss of generality, as mentioned at the beginning of this section, η_B is assumed for 81% in this study, so that via Eq. (3.2) and (3.3), the correction coefficient $\gamma \approx 1.1$ is introduced to compensate for the mismatch transmission loss.

Figure 3.4 gives that the energy spectrums of average annual wind power $e_{Wavg}(i)$, the average annual mismatch power $e_{Mavg}(i)$ and the average annual load consumption power $e_L(i)$ of P_W, P_L and ΔP at six locations for years 2007 to 2012 in the case of:

$$\bar{P}_W = \gamma \cdot \bar{P}_L$$
(3.4)

where $\bar{P}_W$ is the average wind power output and $\bar{P}_L$ is the average load demand.

The power generation of the standalone power systems is set to be slightly larger than the load demand which is because of the loss of energy transmission. It should be noted that average wind power data and average mismatch power for the study period was used to calculate the energy harmonics data in this case. It can be seen from Figure 3.4 that, the mismatch energy harmonics data $e_{Mavg}(i)$ almost overlap with the wind energy harmonics data $e_{Wavg}(i)$ at every location but clearly distinguishable from load consumption energy harmonics $e_L(i)$. That implies that the wind power fluctuation dominates the mismatch power of SAWP systems. Therefore, the mitigation of the mismatch power of SAWP systems can be simply considered as the low-pass filtering of wind power harmonics.
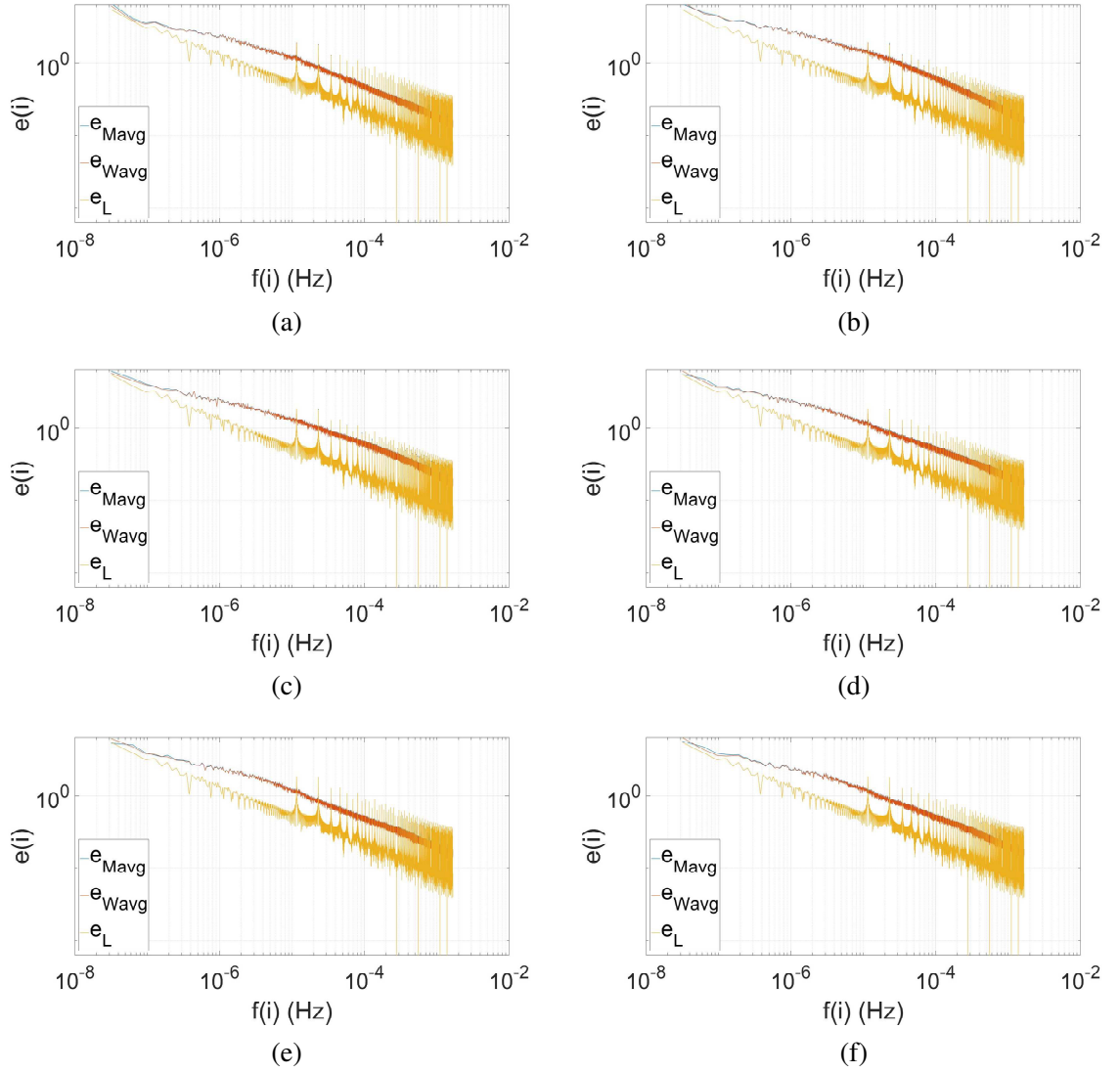
Figure 3.4 Energy spectrum of average annual wind power, average annual generation-load mismatch power and average annual load demand from 2007 to 2012 at (a) San Francisco, (b) Los Angeles, (c) Denver, (d) Houston, (e) Chicago, (f) New York.

Figure 3.5 gives that the energy spectrums of average annual solar power $e_{Savg}(i)$, the average annual mismatch power $e_{Mavg}(i)$ and the average annual load consumption power $e_L(i)$ of P_S, P_L and ΔP at six locations for years 1998 to 2017 in the case of:

$$\bar{P}_S = \gamma \cdot \bar{P}_L \tag{3.5}$$

where $\bar{P}_S$ is the average wind power generation and $\bar{P}_L$ is the average load demand.

As shown in Figure 3.5, because $e_{Mavg}(i)$ and $e_{Savg}(i)$ nearly overlap each other and are well above $e_L(i)$, it implies that the solar power variability dominates ΔP. In addition, both

$e_{M(n)}(i)$ and $e_{Savg}(i)$ drop with the increase of frequency within $[6\times10^{-8}, 2.78\times10^{-4}]$ Hz, while large spikes are occurring at specific harmonic frequencies within $[1\times10^{-5}, 2.78\times10^{-4}]$ Hz. Moreover, the two largest energy spikes at 1.16×10^{-5} Hz (24 hours) and 2.32×10^{-5} Hz (12 hours) which are caused by cyclic changes of daily solar power and load demand. Hence, the mitigation of the power mismatch power of SAPVP systems can be treated as the low-pass filtering of solar power harmonics.
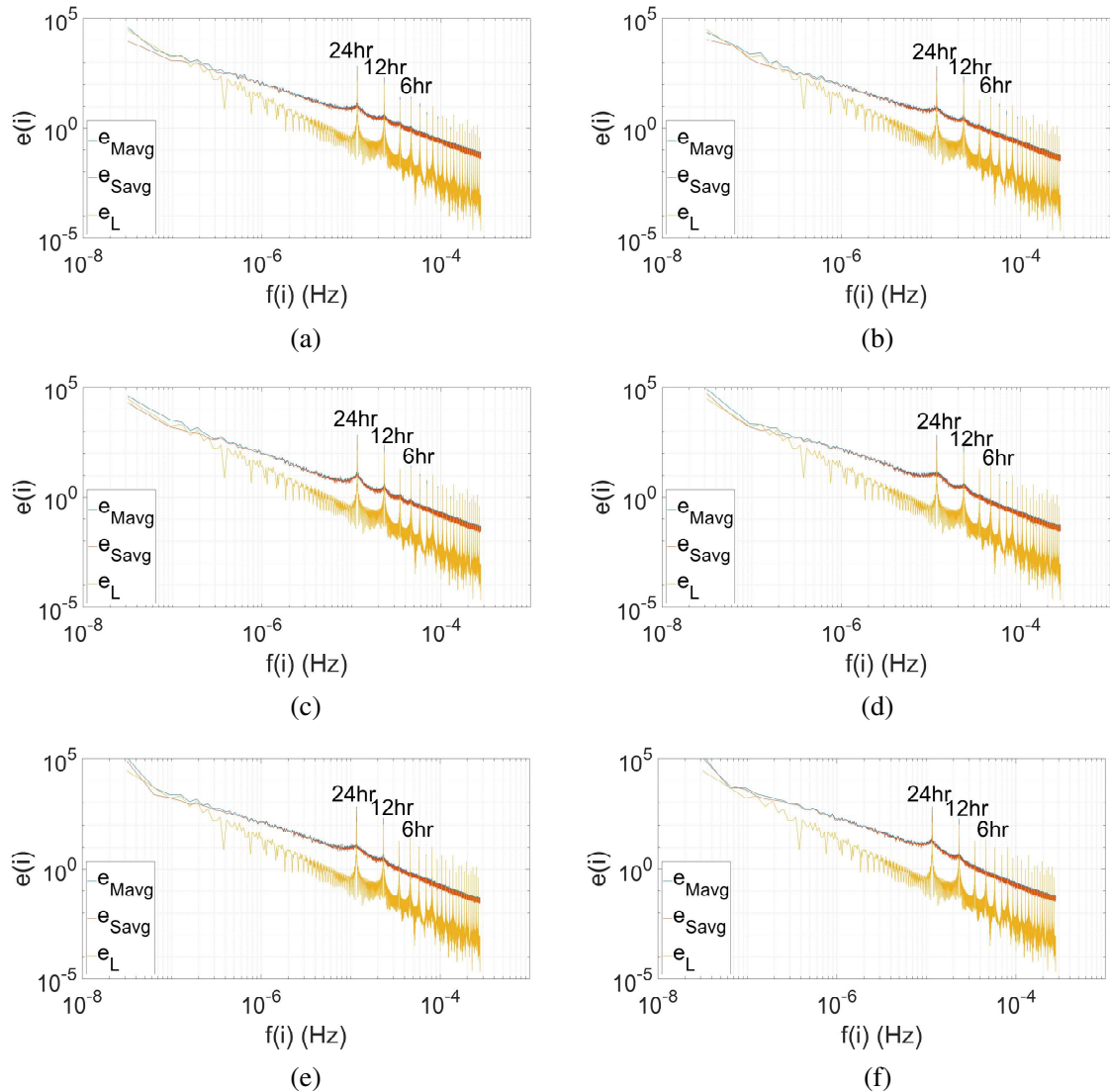
Figure 3.5 Energy spectrum of average annual solar power, average annual generation-load mismatch power and average annual load demand from 1998 to 2017 at (a) Quito, (b) Valencia, (c) Mexico City, (d) Houston, (e) Salt Lake City, (f) Vancouver.

It can be seen from Figures 3.4 and 3.5 that the generation-load mismatch power of standalone wind/solar power systems is dominated by wind and solar power. This is because for standalone wind/solar power systems, the load pattern is relatively fixed, and wind and

solar power is the entire power source, so that the variability of wind or solar power itself directly leads to generation-load power mismatch. Because wind and solar power dominated the generation-load power mismatch, and the power harmonics of the two are almost coincident, the study of generation power mismatch can be directly transformed into the study of wind and solar power fluctuations. According to the QTI of the wind and solar power in the frequency domain confirmed in Chapter 2, exploring the optimization of standalone wind and solar power systems in the frequency domain will have many advantages such as simplicity, fastness, long-term effectiveness, and high credibility.

3.3.2 Energy filter concept
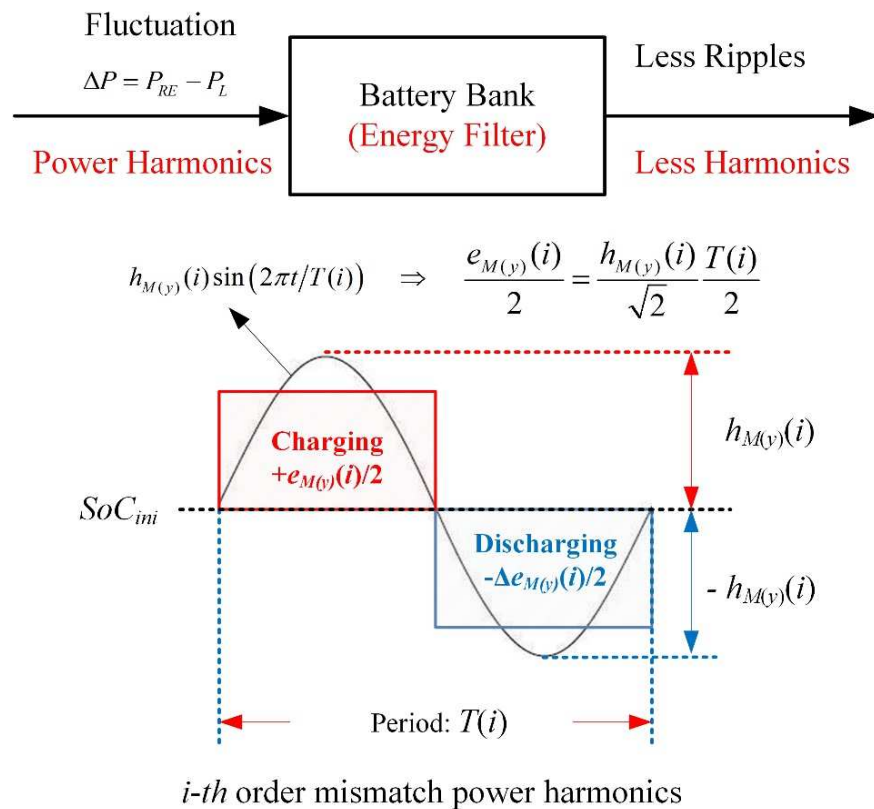
Figure 3.6 A model of low-pass energy filter for the battery bank.

Since the intermittent wind and solar power in the time domain can be treated as a QTI source of power harmonics in the frequency domain. Hence the mitigation of wind/solar power fluctuations can be treated as the filtering of power harmonics. The battery bank which can smooth short-term rapid power fluctuations, can be regarded as a low-pass energy filter. Figure 3.6 shows a model of energy filter for the battery bank. As shown in Figure 3.6,

if the i-th mismatch power harmonics $h_{M(y)}(i)\sin\left(2\pi t/T(i)+\varphi(i)\right)$, with $T(i)$ and $0\le\varphi(i)\le 2\pi$ being the period and phase angle of the harmonics respectively, can be filtered out by the battery bank, the active battery capacity B_{ac} should be large enough to accommodate the energy fluctuation $e_{M(y)}(i)$ caused by i-th order mismatch power harmonics. Moreover, the initial state of charge SoC_{ini} for the battery bank in this thesis is set as:

$$SoC_{ini} = (SoC_{max} + SoC_{min})/2 \tag{3.6}$$

where SoC_{max} is the maximum state of charge for the battery bank and SoC_{min} is the minimum state of charge for the battery bank.
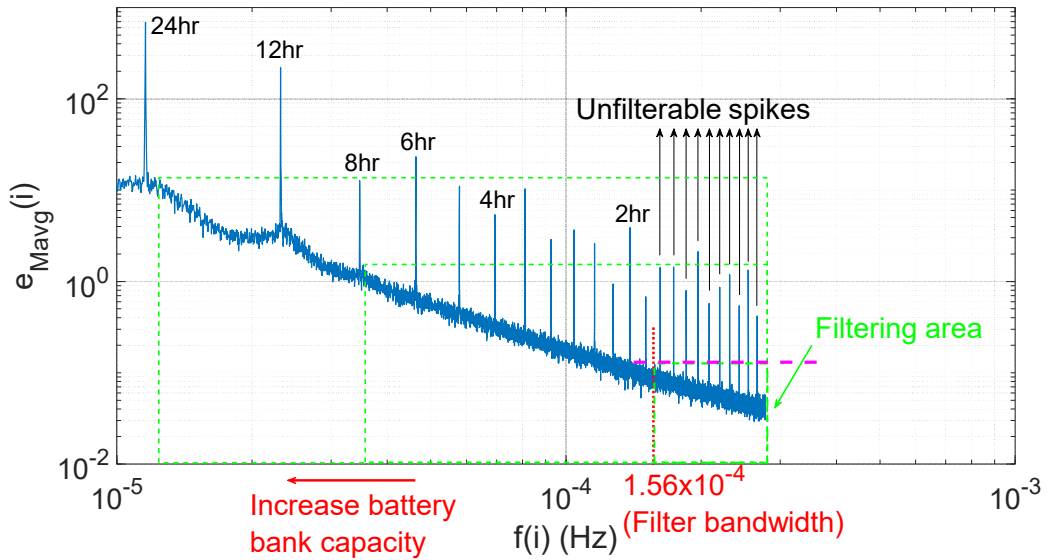
Figure 3.7 Effect of battery capacity on the filtering effect of generation-load mismatch power harmonics.

Figure 3.7 gives a schematic diagram of the average generation-load mismatch energy spectrum of the solar power at Houston. It can be seen that the general trend of e_{Mavg} is increasing with the decreases in frequency. However, because of the strong periodicity of solar power and load demand, e_{Mavg} is not monotonously increasing. There are a few significant spikes within the high-frequency range. This implies when the filter bandwidth is selected in the high-frequency range (battery bank capacity is small), the filtering effect of the battery bank might be worse than the expected or less predictive. For example, if the filter bandwidth is 1.56×10^{-4} Hz, the battery bank is supposed to filter most of the energy

harmonics in the higher frequency range which is pointed out as the filtering area in Figure 3.7. However, due to there are several harmonics spikes beyond the filtering area, the battery bank cannot filter these spikes well. Nevertheless, with the increase of the battery bank capacity (the filter bandwidth is covering more low-frequency range), the filtering area will cover more harmonics spikes which leads to a better filtering effect of the battery. Moreover, for the generation-load mismatch energy spectrum, there are not so many significant spikes so that the battery bank for the wind power system will be more effective.

Due to $e_{M(y)}(i)$ decreases with the increase of frequency. Therefore, if B_{ac} is large enough to filter out i-th order mismatch power harmonics, the battery would be able to filter out higher order mismatch power harmonics. It implies that, B_{ac} actually corresponds to the bandwidth of the low-pass energy filter. Furthermore, because the wind/solar power fluctuation dominates the mismatch power, the mitigation of mismatch power in the standalone wind/solar power systems can be simply considered as the low-pass filtering of only wind/solar power harmonics. Therefore, according to the QTI of wind/solar power, it is reasonable to believe that it is universal to model battery bank through the concept of low-pass energy filters. Moreover, because wind and solar power dominate generation mismatch power so that the variability analysis for wind and solar power in Chapter 2 can be used to determine the battery bank size. In fact, the proposed cumulative energy distribution index $D_{RE}(j)$ for annual renewable power in the frequency domain can more clearly reveal the relationship between energy filter bandwidth and energy fluctuation distribution. Based on the energy distribution analysis results in Chapter 2, a higher $D_{Wavg}(j)$ and $D_{Savg}(j)$ means that, a low-pass energy filter of battery bank with the same active capacity B_{ac} could more efficiently reduce the wind/solar power fluctuations and then more rapidly improve the power supply reliability. For instance, the power supply reliability of the SAWP system at Denver might increase with the fastest rate in the frequency range of $(1 \times 10^{-6}, 1.67 \times 10^{-3})$ Hz because $D_{Wavg}(j)$ there is the highest among all six locations. The power supply reliability of the SAPVP system at Quito might increase with the fastest rate in the frequency range of $(1 \times 10^{-7}, 2.78 \times 10^{-4})$ Hz because $D_{Savg}(j)$ there is the highest among all six locations.

3.4 System parameters

The optimal system sizing is a key factor in the development of reliable, efficient and cost-effective stand/alone wind and solar power systems. The power supply reliability and cost-effectiveness are two primary concerns of most standalone wind/solar system owners.

Chapter 3
Optimal sizing of standalone wind/solar power systems

The most common objective of optimal sizing of standalone wind/solar systems is to minimize the system cost while satisfying the requirement of power supply reliability.

3.4.1 Impacts of wind/solar power variability

a. Size factor

Size factor α is used to determine the size of wind/solar generators. Generally speaking, a larger size factor will lead to higher power supply reliability of standalone wind/solar power systems. Figure 3.8 shows the schematic diagram of generation-load mismatch power changes with the different size factor α for standalone wind/solar power systems. It can be clearly seen that, generation-load power mismatch in SAWP systems fluctuates more randomly, while the mismatch in SAPVP systems fluctuates more regularly due to the daily solar irradiation pattern.

Figure 3.8 (a) shows a diagram of the generation-load power mismatch of a SAWP system without a battery bank, where '-' means that $\Delta P = P_S - P_L < 0$ and will lead to power outages; '+' means that $\Delta P = P_S - P_L > 0$. It can be seen that the high intermittence of wind power makes it difficult for wind power output to meet the load demand properly, so that the generation-load mismatch power of the SAWP systems is large. On the other hand, it can be seen that the wind is continuous and the probability of wind turbines shutdown is relatively small. Therefore, increasing the size of wind turbines, that is, increasing the wind power output can play a greater role in mitigating the energy deficit. As shown in Figure 3.8 (a), as α increases, the area of the '-' in the figure becomes smaller and smaller, but when α is large enough, the wind power output will basically completely cover the load demand. Subsequently, it is difficult to reduce the energy deficit by increasing the size of the wind turbines when α is large enough. Therefore, it can be inferred that increasing the size of wind turbines can effectively reduce the energy deficit, thereby improving the power supply reliability of the SAWP systems, but when the wind turbines are enlarged to a sufficient size, this increase tends to be saturated.

Figure. 3.9 (b) shows a diagram of the generation-load power mismatch of a SAPVP system without a battery bank, where '-' means that $\Delta P = P_S - P_L < 0$ and will lead to power outages; '+' means that $\Delta P = P_S - P_L > 0$. Solar power and wind power are two completely different resources. Solar power has a clear periodicity, that is, the sun rises during the day and falls at night, so that the output power of solar energy at night is zero. The diurnal cycle

of solar power results in that the night energy deficit of SAPVP systems without energy storage devices cannot be mitigated via increasing α. As shown in Figure 3.8 (b), as α increases, the area of the '-' in the figure does not change so much. Thus, the enlargement of the PV panel size cannot reduce the power outages caused by such deficit solar power at nights. It can be inferred that increasing the size of the PV panel cannot effectively reduce the energy deficit, so that the power supply reliability cannot be significantly improved.
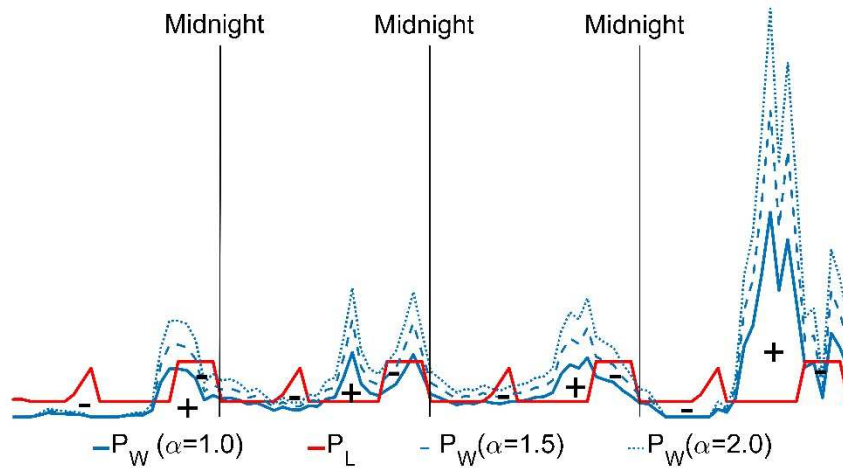
(a)
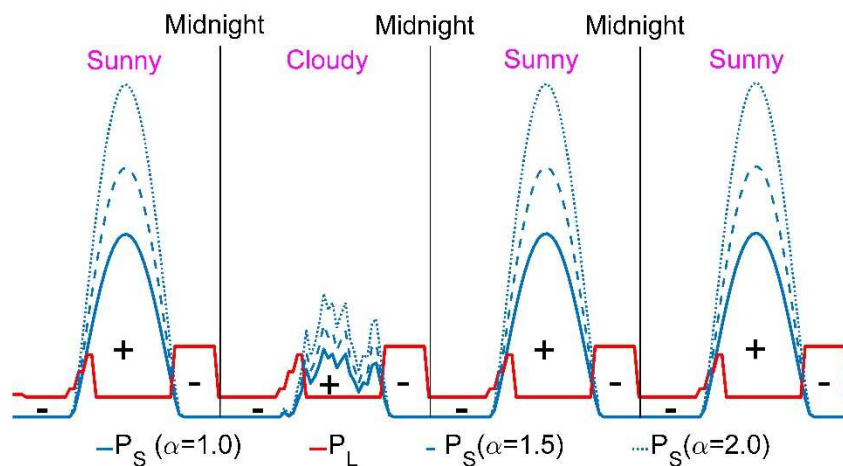
(b)

Figure 3.8 The generation-load mismatch power of (a) SAWP and (b) SAPVP systems with various α.

b. Margin factors of wind turbines and PV panels

The margin factor of wind turbine m_W is used to account for the worst inter-annual variations of wind power in the sizing of the wind turbine. m_W is proposed to ensure that in the worst year of wind resources, the wind turbine can still generate enough power to meet system reliability requirements. In the time domain, the inter-annual variations of wind power for years y_0 to Y at each site can quantify the difference of gross annual wind energy generation. Thus, m_W that used to account for the worst inter-annual variations of wind speed can be calculated as:

$$m_W = 1/(1+\delta_{IW\,min})$$
(3.7)

where $\delta_{IW\,min}$ is the lower bound of $I_W(y)$.

Similarly, in the time domain, inter-annual variations of solar power for years y_0 to Y at each site can quantify the difference of gross annual wind energy generation. Thus, the margin factor of PV panel m_S that used to account for the worst inter-annual variations of solar irradiation can be written as:

$$m_S = 1/(1+\delta_{IS\,min})$$
(3.8)

where $\delta_{IS\,min}$ is the lower bound of $I_S(y)$.

Note that m_W and m_S are margin factors of wind turbines and PV panels for standalone wind/solar power systems. These factors are to ensure that in the worst year of wind or solar resources, the wind turbine or PV panel size is large enough to avoid energy deficit. However, in the grid-connected wind and solar systems, wind and solar power is only a part of the total generated power, so the m_W and m_S are no longer needed. In this case, the margin factor of the overall power generation should be considered.

c. Margin factor of the battery bank

Energy storage is the most important measure to mitigate generation-load mismatch power in the standalone wind/solar power systems. Therefore, the margin factor of the battery bank capacity is needed to ensure the battery bank can mitigate the power fluctuations in the year with maximum annual power variation. As mentioned above, the

fluctuation rate is proposed to quantify the power fluctuation of the annual renewable power output. In addition, because in the standalone wind/solar power systems, wind/solar power variation dominates generated-load mismatch power. Therefore, the margin factor of battery bank capacity m_B can be determined based on the fluctuation rate in the frequency domain. Consequently, m_B that used to cope with the worst annual wind power fluctuation in the sizing of a battery bank of the SAWP systems is defined as:

$$m_B = 1 + \delta_{FW\max} \qquad (3.9)$$

where $\delta_{FW\max}$ is the upper bounds of $F_W(y)$.

Similarly, m_B that used to cope with the worst annual solar power fluctuation in the sizing of the battery bank of the SAPVP systems is defined as:

$$m_B = 1 + \delta_{FS\max} \qquad (3.10)$$

where $\delta_{FS\max}$ is the upper bounds of $F_S(y)$.

3.4.2 Primary sizing principles

The first step of the synthesis of standalone wind/solar power systems is to determine the right sizes of the wind turbines/PV panels and the battery bank to enable standalone wind/solar power systems to provide reliable and cost-effective electricity to meet the load demand. In Chapter 2, formulas for calculating the output power of wind turbines and PV panels have been given. In this section, the proposed size factors and margin factors will be applied to the optimal sizing of standalone wind/solar power systems.

a. Size of wind turbines and PV panels

For a given load demand P_L throughout T, the size of the wind turbines/PV panels for building a self-sustainable and reliable standalone wind/solar power systems should at least satisfy:

$$\begin{cases} \bar{P}_W = \dfrac{1}{T} \int_0^T P_W \, dt = m_W \cdot \alpha \cdot \gamma \cdot \bar{P}_L > \bar{P}_L = \dfrac{1}{T} \int_0^T P_L \, dt \\[2mm] \bar{P}_S = \dfrac{1}{T} \int_0^T P_S \, dt = m_S \cdot \alpha \cdot \gamma \cdot \bar{P}_L > \bar{P}_L = \dfrac{1}{T} \int_0^T P_L \, dt \end{cases} \qquad (3.11)$$

where $\bar{P}_W$, $\bar{P}_S$ and $\bar{P}_L$ are the required average wind power generation, required average solar power generation and the given average load demand, respectively; $\alpha \geq 1$ is the size factor; $\gamma \geq 1$ is the correction coefficient to account for the transmission power losses; and m_W / m_S ≥ 1 is the margin factor of the wind turbines /PV panels to account for the wind speed or solar irradiation variations. Note that for the actual SAWP systems, due to the randomness and uncertainty of the wind power, this study assumed $\beta = 0.5$ and according to Eq. (3.2) and (3.3), $\gamma \approx 1.1$. However, for the actual SAPVP systems, considering the cyclic daily unavailability of solar irradiance at night so that the battery bank will operate more frequently, it is reasonable to assume $\beta = 0.3$ and according to Eq. (3.2) and (3.3), $\gamma \approx 1.14$. Note that the coefficients α, γ, m_W and m_S are not considered in conventional sizing method [67, 158, 159], i.e. $\alpha = \gamma = m_W = m_S = 1$. Because these studies ignore specific annual and inter-annual power variability, many results are only valid for specific situations or locations, while long-term validity and generality are often overlooked.

b. Battery bank capacity

As an energy storage device, the battery bank is utilized to smooth the generation-load mismatch power ΔP. The active battery bank capacity B_{ac} in hours can be expressed as

$$B_{ac} = m_B \cdot B_n \cdot DoD \cdot \eta_B \cdot \left(1/ \bar{P}_L \right) \tag{3.12}$$

where B_n is the nominal battery capacity in kWh, DoD is the depth of discharge of the battery, m_B is the margin factor of the battery capacity, and $\bar{P}_L$ is the average load demand in kW ($\bar{P}_L$ = 518.26 W in this chapter). Considering the inter-annual variations of the generation-load mismatch power, the margin factor $m_B \geq 1$ is utilized to account for the worst power fluctuation.

3.4.3 Power supply reliability

As shown in Figure 3.2, the deficit generation-load mismatch power $\Delta P = P_{RE} - P_L <$ 0 will cause power outages. In standalone wind and solar power systems, power outage time directly reflects power supply reliability. If the power outage time is short, the power supply reliability is high and if the power outage time is long, the power supply reliability is low. To evaluate the power supply reliability of renewable energy systems, the reliability factor R_{RE} is defined as

$$R_{RE} = \left(1 - T_{out}/T_{op}\right) \times 100\% \tag{3.13}$$

where T_{out} is the total power outage time, T_{op} denotes the operating time (usually is a year) and R_{RE} is the power supply reliability of standalone renewable energy systems. A large R_{RE} indicates a high power supply reliability, and vice versa. Note that R_{RE} can be derived as the power supply reliability of SAWP systems R_W, the power supply reliability of SAPVP systems R_S the power supply reliability of standalone hybrid wind and solar power systems $R_{W\&S}$.

3.5 Big data simulation results

In this section, big data simulations will be carried out to provide the dependence of power supply reliability on the size factor and battery capacity. The wind speed data for SAWP systems in the 5-minutes interval is obtained from WIND Toolkit at six locations from 2007 to 2012 shown in Figure 2.2, and wind speed and solar irradiation date for SAPV and standalone hybrid wind-solar systems in the 30-minute interval are obtained from NSRDB at six locations from 1998 to 2017 shown in Figure 2.5. In addition, the load demand will use the typical annual load consumption shown in Figure 3.3 with $\bar{P}_L = 518.26$ W.

3.5.1 SAWP systems

Six SAWP systems having the same residential load demand shown in Figure 3.3 are configured for the six sites. When $\bar{P}_W = m_W \cdot \alpha \cdot \gamma \cdot \bar{P}_L$ with $\alpha = 1$ and $\gamma = 1.1$ and corresponding m_W, the required wind turbine size at the six sites can be calculated using Eqs. (2.1) and (3.11). The battery bank needs to be determined by the required power supply reliability, but the margin factor m_B can be calculated using Eq. (3.10).

a. Margin factor of wind turbines

Table 3.1 gives the margin factor of wind turbines at the six sites for the years 2007-2012. It can be seen that, (i) the wind speed significantly varies from site to site; (ii) m_W significantly varies from site to site. From the data listed in Table 3.1, it is not difficult to know that, Houston has the biggest inter-annual variation which means the SAWP system in Houston need cost more on the wind turbine to ensure that the power supply reliability can meet the requirements within the operating time.

Table 3.1
Margin factor of wind turbines at the six sites for the years 2007-2012.

	Location					
	San Francisco	**Los Angeles**	**Denver**	**Houston**	**Chicago**	**New York**
$\delta_{IW\min}$	-5%	-17%	-9%	-20%	-5%	-7%
m_W	1.05	1.20	1.09	1.25	1.05	1.08

b. Margin factor of the battery bank

Table 3.2 lists the average fluctuation factor F_{Wavg} and margin factor of battery bank at the six sites for the study period. It can be seen that, in terms of F_{Wavg}, the six sites can be ranked Los Angeles > Denver > New York ≈ Chicago ≈ Houston ≈ San Francisco. F_{Wavg} at Los Angeles is around two times of those at the other five sites, and the maximum fluctuation rate $\delta_{WF\max} = 7.9\%$ in Los Angeles is the highest among the six sites. That implies that, the most fluctuated wind power might lead to the poorest power supply reliability of SAWP systems at Los Angeles.

Table 3.2
Margin factor of battery bank of SAWP systems at the six sites for the years 2007-2012.

	Location					
	San Francisco	**Los Angeles**	**Denver**	**Houston**	**Chicago**	**New York**
$\delta_{FW\max}$	+3.0%	+7.9%	+1.9%	+5.0%	+1.5%	+2.8%
F_{Wavg}	1.98	4.32	2.67	2.00	2.02	2.15
m_B	1.03	1.08	1.02	1.05	1.02	1.03

c. Power supply reliability of SAWP systems

Six SAWP systems having the same residential load demand shown in Figure 3.3 are configured for the six sites. When $\overline{P}_W = m_S \cdot \alpha \cdot \gamma \cdot \overline{P}_L$ with $\alpha = 1$ and $\gamma = 1.1$ and corresponding m_W listed in Table 3.1 at the six sites, the required wind turbine size at the six sites listed in Table 3.3.

Figure 3.9 shows the simulation results of the dependence of the power supply reliability of SAWP systems R_W on the active battery capacity B_{ac} and the wind turbine size factor α respectively: (i) with a given α, R_W quasi-linearly increases with the growth of B_{ac},

where the unit of B_{ac} is $\overline{P_L} \cdot hours$, abbreviated Hours; (ii) the lines of R_W against B_{ac} parallelly move up with the growth of α; (iii) compared with Figure 2.13 (a), a higher cumulative energy distribution index $D_{Wavg}(j)$ would lead to a faster ramping rate of R_W against B_{ac}, e.g., R_W at Denver increases with the fastest rate among all six sites when $B_{ac} \leq 100$ hours

Table 3.3
Wind turbine size and average wind speed.

Locations	Swept area of wind turbine A_W (m²)	Average wind speed v_{avg} (m/s)
San Francisco	3.80	7.91
Los Angeles	21.65	4.72
Denver	6.74	6.75
Houston	8.40	6.51
Chicago	3.87	7.71
New York	4.56	7.31

Table 3.4 lists R_{Wavg} of all six SAWP systems with $B_{ac} = 10^0$, 10^1 and 10^2 Hours and α = 1.0, 1.5 and 2.0 respectively, where R_{Wavg} is the average value of R_W for the study period. Table 3.4 indicates that, with the same B_{ac} and α, taking the m_W and m_B into consideration, the ranking of R_{Wavg} at the six sites is Los Angeles < Denver < New York ≈ Chicago ≈ Houston ≈ San Francisco. It can be seen from Table 3.2 that, the six sites are reversely ranked Los Angeles > Denver > New York ≈ Chicago ≈ Houston ≈ San Francisco with respect to the average fluctuation factor F_{Wavg}. The consistency between R_{Wavg} and F_{Wavg} indicates the high degree of dependence between these two indicators – with the same B_{ac} and α, the higher F_{Wavg} is, the lower R_W is. Therefore, the proposed fluctuation factor of wind power provides a useful quality index to the wind resource assessment for the development of the SAWP systems.
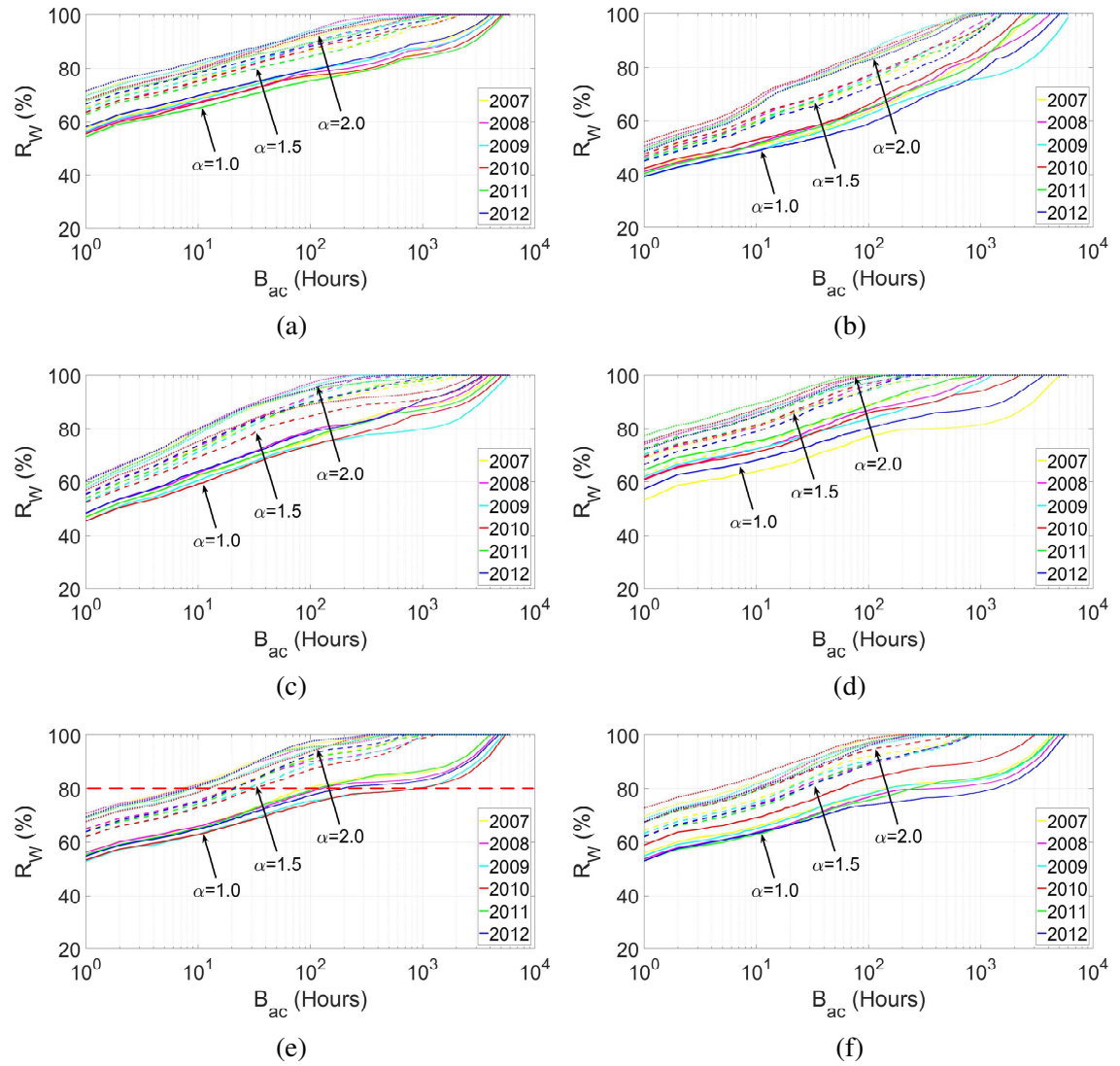
Figure 3.9 Power supply reliability R_W against active battery capacity B_{ac} with α = 1.0, 1.5, 2.0 for the years of 2007 to 2012 at (a) San Francisco, (b) Los Angeles, (c) Denver, (d) Houston, (e) Chicago, (f) New York.

Table 3.4
Average power supply reliability R_{wavg} with B_{ac} = 10^0, 10^1 and 10^2 Hours and α = 1.0, 1.5, and 2.0.

Size factor	$\alpha = 1.0$			$\alpha = 1.5$			$\alpha = 2.0$		
B_{ac}(Hours) R_{Wavg} (%)	10^0	10^1	10^2	10^0	10^1	10^2	10^0	10^1	10^2
San Francisco	56	68	78	64	76	88	69	81	92
Los Angeles	41	51	63	46	60	75	50	67	85
Denver	47	62	76	54	72	90	59	78	94
Houston	60	71	84	69	80	95	74	86	98
Chicago	55	65	78	64	74	90	69	80	96
New York	55	65	78	64	75	91	69	81	97

Generally speaking, the simulation results shown in Figure 3.9 confirm the validity of the new measure of wind power variability. Since the wind power variability at one site can be treated as a QTI power harmonics source in the frequency domain, the dependence of R_W on B_{ac} and α shown in Figure 3.9 can also be treated as QTI, which can be used as datasheet for simplifying the optimal sizing of the battery and the wind turbine.

3.5.2 SAPVP systems

Six SAPVP systems having the same residential load demand shown in Figure 3.3 are configured for the six sites. When $\overline{P_S} = m_S \cdot \alpha \cdot \gamma \cdot \overline{P_L}$ with $\alpha = 1$ and $\gamma = 1.14$ and corresponding m_S, the required PV panel size at the six sites can be calculated using Eqs. (2.6) and (3.11) with $v_i = 2$ m/s, $v_r = 14$ m/s, $v_o = 25$ m/s, $\rho = 1.225$ kg/m^3 and $C_P = 0.593$ [155]. The battery bank needs to be determined by the required power supply reliability but the margin factor m_B can be calculated using Eq. (3.9).

a. Margin factor of PV panels

Table 3.5 lists the margin factor of PV panels at all six sites during 1998-2007. It can be observed that m_S slightly varies from 1.04 to 1.08 for all six sites. That implies that the inter-annual variations of solar power do not change very much from year to year and from site to site. Because of the relatively small m_S of the SAPVP system, the cost of PV panels is relatively low as well.

Table 3.5
Margin factor of PV panels at the six sites for the years 1998-2017.

	Location					
	Quito	Valencia	Mexico City	Houston	Salt Lake City	Vancouver
Latitude	$\approx 0°$	$\approx 10°$	$\approx 20°$	$\approx 30°$	$\approx 40°$	$\approx 50°$
δ_{ISmin}	-5.09%	-5.48%	-4.04%	-5.49%	-4.61%	-8.04%
m_S	1.05	1.06	1.04	1.06	1.05	1.08

b. Margin factor of the battery bank

As given in Table 3.6, m_B slightly varies from 1.01 to 1.04 for all six sites. Taking the maximum fluctuation rate δ_{SFmax} into consideration, in terms of F_{Savg}, the six sites can be

ranked Quito ≈ Valencia ≈ Mexico City ≈ Houston ≈ Salt Lake City < Vancouver. Note that, with the highest latitude of 50°, the variability of solar power at Vancouver is significantly higher than those at other sites.

Table 3.6
Margin factor of battery bank of SAPVP systems at the six sites for the years 1998-2017.

	Location					
	Quito	**Valencia**	**Mexico City**	**Houston**	**Salt Lake City**	**Vancouver**
δ_{FSmax}	+2.13%	+1.45%	+1.36%	+2.17%	+2.82%	+3.78%
F_{Savg}	2.21	2.17	2.18	2.24	2.29	2.53
m_B	1.02	1.01	1.01	1.02	1.03	1.04

c. Power supply reliability of SAPVP systems

Six SAPVP systems with the same residential load demand shown in Figure 3.3, are settled in the six sites. When $\overline{P}_S = m_S \cdot \alpha \cdot \gamma \cdot \overline{P}_L$ with $\alpha = 1$ and $\gamma = 1.14$ and corresponding m_S listed in Table 3.5 at the six sites. The required solar panel sizes at the six sites are calculated and listed in Table 3.7. It can be seen from Table 3.7 that the solar irradiation on Earth's surface drops with the increase of the latitude, but variations in atmospheric transmissivity due to meteorological events (e.g., cloud cover) could weaken the solar irradiation. For instance, the solar irradiation at Mexico City of latitude 20° is the highest instead of those at Quito and Valencia.

Table 3.7
PV panel size and average solar irradiation.

Location	Latitude	PV panel area A (m²)	Average solar irradiation I_{avg} (W·m⁻²)
Quito	≈ 0°	9.84	447.64
Valencia	≈ 10°	9.66	455.90
Mexico city	≈ 20°	8.90	494.60
Houston	≈ 30°	10.87	405.22
Salt Lake City	≈ 40°	11.23	392.31
Vancouver	≈ 50°	16.07	274.58

Figure 3.10 gives the simulation results of the responses of R_{Savg} versus B_{ac} for the SAPVP systems with $\alpha = 1.0$, 1.5 and 2 at six sites respectively. It can be seen from Figure

3.10 that: (i) if B_{ac} < 12 hours, R_{Savg} increases with the growth of B_{ac}, while the enlargement of the PV panel size has a slight impact on the R_{Savg}; (ii) if B_{ac}>24 hours, the increment of either PV panel size or battery capacity can improve the power supply reliability; (i) the power supply reliability of the SAPV system generally decreases with the growth of the latitude.

Generally speaking, Figure 3.10 shows the QTI impacts of solar power variability on the sizing of the battery bank and PV panel. The QTI responses of R_{Savg} versus B_{ac} and α shown in Figure 3.10 can be used as a look-up datasheet for simplifying the optimal sizing of SAPV systems.
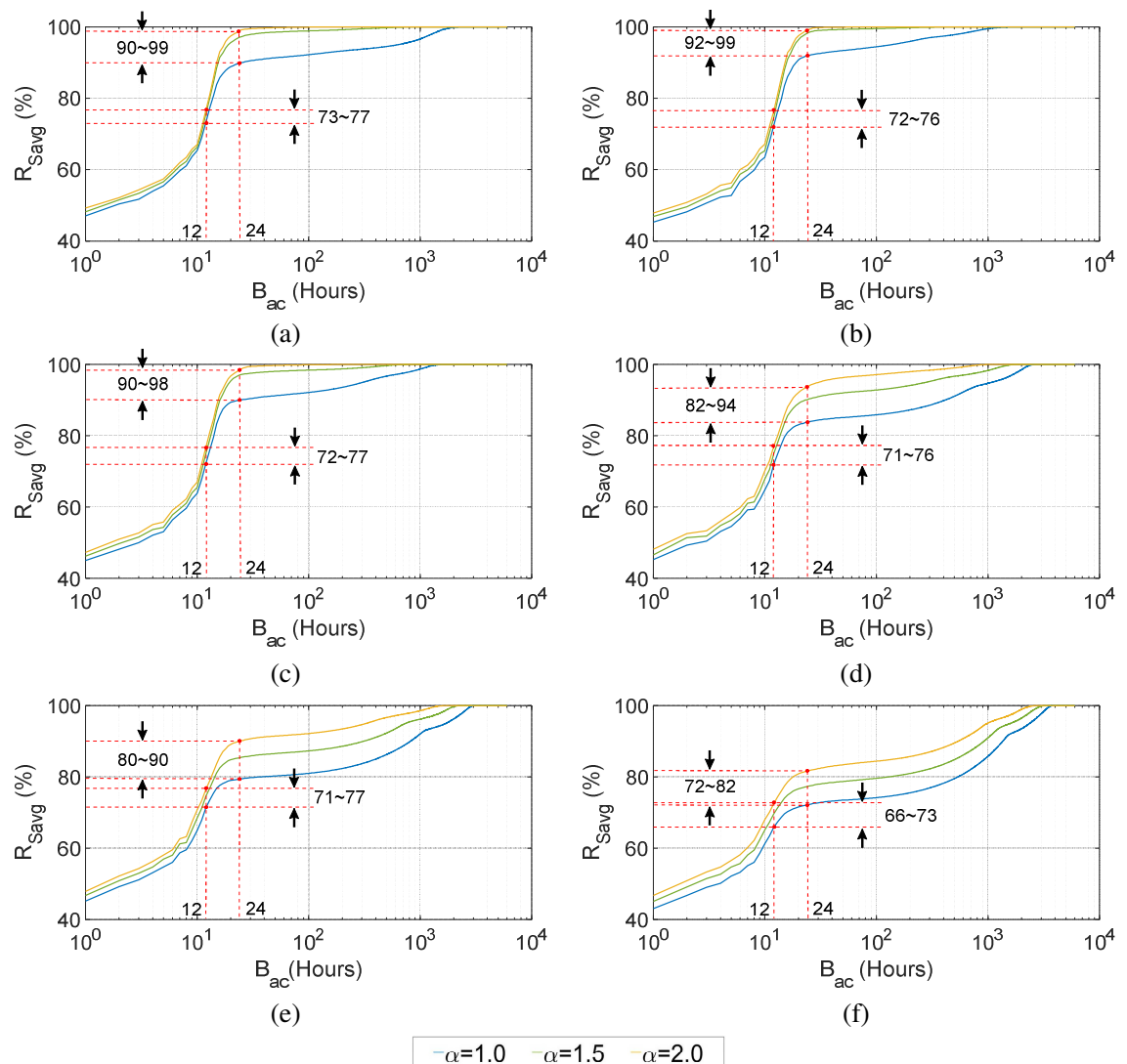
Figure 3.10 Average power supply reliability R_{Savg} versus active battery capacity B_{ac} with = 1.0, 1.5, 2.0 for the years of 1998 to 2017 at (a) Quito, (b) Valencia, (c) Mexico City, (d) Houston, (e) Salt Lake City, (f) Vancouver.

3.5.3 Standalone hybrid wind and solar power systems

Six standalone hybrid wind and solar power systems with the same residential load demand shown in Figure 3.3, are settled in the six sites. When $\overline{P}_S = m_S \cdot \alpha \cdot \gamma \cdot \overline{P}_L$ with $\alpha = 1$ and $\gamma = 1.1$. $m_{W\&S}$ and m_B are assumed to 1 in order to achieve the unbiased study of wind and solar mixed power.

Table 3.8 gives the simulation results of the responses of $R_{W\&Savg}$ versus B_{ac} for the standalone hybrid wind and solar power systems with W/S mixed ratio from 100% (pure wind) to 0% (pure solar) at Quito. The minimum value of $R_{W\&Savg}$ for different B_{ac} has been highlighted in the yellow zone. It can be seen from Table 3.8 that: (i) if $B_{ac} < 14$ hours, more wind power in the hybrid systems will bring smaller power supply reliability; (ii) if $B_{ac} > 17$ hours, 40% solar power in the hybrid systems can improve the power supply reliability. However. With the increase of B_{ac}, the improvement of power supply reliability trend to depend on more wind power participation. Table B1 to Table B5 (in Appendix B) is the simulation results of the responses of $R_{W\&Savg}$ versus B_{ac} for the standalone hybrid wind and solar power systems at Valencia, Mexico, Houston, Salt Lake City and Vancouver. All of the results show that it is hard to find the optimal mixed ratio for standalone hybrid wind and solar power systems.

Table 3.8
The average power supply reliability $R_{W\&Savg}$ versus active battery capacity B_{ac} with wind and solar mixed ratio varies from 100% to 0% for the years of 1998 to 2017 at Quito.

$R_{W\&Savg}$ B_{ac}	W/S mixed ratio										
	100%	90%	80%	70%	60%	50%	40%	30%	20%	10%	0%
1	**47.78**	47.86	47.39	47.03	46.86	46.68	46.30	45.95	45.63	45.40	44.03
2	52.20	**52.27**	51.74	51.25	51.02	50.75	50.29	49.85	49.45	49.53	48.96
3	54.55	**54.70**	54.15	53.75	53.47	53.19	52.78	52.11	51.40	50.14	48.67
4	56.11	**56.17**	55.73	55.32	55.04	54.76	54.36	53.83	53.25	52.97	51.54
5	58.09	**58.22**	57.79	57.37	57.09	56.83	56.41	55.81	55.03	54.07	53.28
6	59.80	**59.91**	59.46	59.10	58.84	58.48	58.04	57.43	56.83	56.17	54.25
7	61.86	**62.01**	61.57	61.14	60.75	60.44	59.96	59.30	58.59	57.76	56.81
8	63.85	**63.96**	63.53	63.06	62.67	62.26	61.60	60.94	60.18	59.42	58.22
9	66.29	**66.41**	65.85	65.27	64.81	64.32	63.60	62.78	61.85	60.97	59.40
10	69.02	**69.04**	68.56	67.99	67.47	66.79	65.94	65.04	64.07	63.20	61.26
11	71.88	**71.85**	71.37	70.73	70.07	69.32	68.19	66.83	65.58	64.43	63.36
12	75.33	**75.49**	75.15	74.73	74.25	73.57	72.53	71.11	69.48	67.65	65.37
13	78.63	**79.01**	78.88	78.69	78.49	78.04	77.15	75.93	74.32	72.33	69.09
14	81.40	81.91	**81.99**	81.96	81.97	81.80	81.16	80.07	78.51	76.33	72.75
15	83.92	84.61	84.86	85.07	85.26	**85.29**	84.96	84.11	82.58	80.07	75.80
16	86.04	86.81	87.25	87.62	87.95	**88.19**	88.07	87.50	86.30	83.78	78.78
17	87.72	88.58	89.12	89.59	90.01	90.34	**90.38**	90.01	89.01	86.43	81.25
18	89.00	89.9	90.50	91.03	91.52	91.93	**91.97**	91.65	90.72	88.17	82.97
19	90.07	91.01	91.67	92.25	92.76	93.16	**93.31**	93.01	92.10	89.34	84.05
20	90.92	91.86	92.58	93.19	93.79	94.21	**94.37**	94.15	93.22	90.39	84.93
21	91.62	92.61	93.32	93.98	94.59	95.05	**95.22**	94.98	94.05	91.17	85.72
22	92.20	93.16	93.93	94.61	95.23	95.71	**95.89**	95.71	94.74	91.77	86.33
23	92.70	93.70	94.44	95.15	95.79	96.25	**96.46**	96.27	95.27	92.29	86.79
24	93.08	94.13	94.91	95.61	96.25	96.70	**96.92**	96.74	95.70	92.74	87.20
25	93.46	94.48	95.28	95.96	96.58	97.07	**97.27**	97.12	96.08	93.11	87.53
26	93.76	94.79	95.55	96.26	96.88	97.37	**97.59**	97.43	96.38	93.45	87.83
27	94.01	95.06	95.86	96.52	97.14	97.64	**97.85**	97.68	96.64	93.72	88.06
28	94.26	95.26	96.06	96.73	97.37	97.82	**98.03**	97.87	96.85	93.94	88.30
29	94.47	95.49	96.27	96.93	97.55	98.02	**98.20**	98.02	97.01	94.11	88.49
30	94.67	95.68	96.44	97.10	97.70	98.15	**98.35**	98.15	97.15	94.30	88.69
31	94.83	95.83	96.59	97.26	97.85	98.29	**98.46**	98.27	97.27	94.43	88.84
32	95.00	95.99	96.72	97.38	97.97	98.40	**98.55**	98.33	97.36	94.55	88.95
33	95.13	96.11	96.86	97.50	98.06	98.48	**98.64**	98.42	97.43	94.63	89.08
34	95.26	96.24	96.97	97.60	98.16	98.57	**98.70**	98.50	97.52	94.73	89.14
35	95.38	96.33	97.08	97.70	98.25	98.65	**98.78**	98.57	97.59	94.83	89.27
36	95.50	96.44	97.17	97.79	98.33	98.72	**98.83**	98.63	97.66	94.89	89.35
37	95.60	96.55	97.26	97.86	98.38	98.78	**98.89**	98.68	97.73	94.97	89.42
38	95.70	96.64	97.35	97.96	98.47	98.84	**98.96**	98.73	97.78	95.03	89.51
39	95.80	96.72	97.44	98.02	98.54	98.89	**98.99**	98.77	97.83	95.09	89.58
40	95.90	96.83	97.53	98.09	98.60	98.95	**99.04**	98.82	97.87	95.16	89.68
41	95.99	96.92	97.59	98.15	98.65	99.00	**99.10**	98.86	97.91	95.22	89.74
42	96.08	96.99	97.64	98.22	98.70	99.05	**99.13**	98.89	97.95	95.27	89.80
43	96.16	97.08	97.72	98.27	98.75	99.10	**99.17**	98.93	97.97	95.32	89.88
44	96.25	97.14	97.77	98.32	98.79	99.14	**99.21**	98.96	98.02	95.37	89.92
45	96.33	97.21	97.83	98.36	98.84	99.17	**99.24**	98.99	98.04	95.38	89.97
46	96.40	97.26	97.89	98.42	98.88	99.20	**99.26**	99.01	98.07	95.42	90.03

47	96.47	97.31	97.94	98.45	98.93	99.22	**99.29**	99.04	98.09	95.46	90.09
48	96.54	97.36	97.98	98.50	98.96	99.25	**99.31**	99.06	98.11	95.48	90.12
49	96.60	97.43	98.03	98.54	99.00	99.28	**99.33**	99.09	98.14	95.50	90.16
50	96.67	97.47	98.07	98.59	99.03	99.30	**99.37**	99.12	98.16	95.54	90.23
51	96.71	97.51	98.12	98.61	99.07	99.33	**99.39**	99.13	98.17	95.56	90.28
52	96.77	97.56	98.16	98.65	99.09	99.35	**99.40**	99.15	98.20	95.58	90.29
53	96.83	97.62	98.19	98.68	99.14	99.39	**99.43**	99.16	98.20	95.62	90.32
54	96.88	97.67	98.25	98.73	99.15	99.40	**99.45**	99.18	98.22	95.64	90.37
55	96.93	97.71	98.28	98.76	99.18	99.43	**99.46**	99.20	98.23	95.67	90.43
56	97.00	97.74	98.31	98.78	99.20	99.44	**99.48**	99.21	98.25	95.65	90.45
57	97.03	97.77	98.35	98.81	99.23	99.46	**99.50**	99.23	98.27	95.69	90.48
58	97.08	97.81	98.37	98.83	99.25	99.48	**99.51**	99.25	98.28	95.70	90.51
59	97.12	97.85	98.40	98.87	99.27	99.50	**99.53**	99.26	98.29	95.74	90.53
60	97.15	97.88	98.44	98.89	99.30	99.51	**99.53**	99.27	98.30	95.74	90.59
61	97.20	97.93	98.47	98.91	99.31	99.52	**99.55**	99.29	98.31	95.77	90.60
62	97.24	97.95	98.49	98.94	99.34	99.54	**99.56**	99.30	98.32	95.77	90.62
63	97.29	98.00	98.53	98.96	99.36	99.55	**99.58**	99.31	98.33	95.80	90.66
64	97.32	98.01	98.55	98.98	99.38	99.56	**99.59**	99.33	98.34	95.80	90.67
65	97.35	98.05	98.57	99.01	99.40	99.59	**99.60**	99.34	98.35	95.82	90.73
66	97.37	98.08	98.60	99.02	99.41	99.60	**99.61**	99.34	98.35	95.84	90.73
67	97.41	98.11	98.62	99.05	99.43	99.61	**99.62**	99.36	98.36	95.85	90.76
68	97.44	98.13	98.65	99.07	99.44	99.62	**99.63**	99.36	98.39	95.86	90.79
69	97.46	98.17	98.67	99.10	99.45	99.63	**99.64**	99.38	98.38	95.86	90.81
70	97.50	98.19	98.69	99.12	99.46	99.64	**99.65**	99.39	98.40	95.87	90.85
71	97.53	98.22	98.72	99.14	99.48	99.64	**99.66**	99.39	98.40	95.9	90.86
72	97.56	98.24	98.74	99.16	99.49	99.66	**99.68**	99.40	98.41	95.9	90.88
73	97.60	98.27	98.75	99.17	99.50	99.67	**99.68**	99.41	98.41	95.91	90.92
74	97.63	98.28	98.77	99.19	99.52	99.67	**99.69**	99.42	98.42	95.93	90.91
75	97.67	98.31	98.79	99.21	99.53	99.68	**99.70**	99.43	98.42	95.94	90.94
76	97.69	98.33	98.82	99.23	99.54	99.69	**99.70**	99.44	98.43	95.95	90.96
77	97.73	98.35	98.84	99.25	99.55	**99.71**	**99.71**	99.44	98.44	95.95	90.96
78	97.75	98.38	98.85	99.27	99.56	**99.72**	**99.72**	99.45	98.45	95.96	90.99
79	97.78	98.39	98.88	99.28	99.57	**99.73**	99.72	99.46	98.46	95.97	91.00
80	97.81	98.41	98.89	99.30	99.58	**99.73**	99.73	99.47	98.47	95.99	91.02
81	97.84	98.43	98.91	99.31	99.59	**99.74**	99.74	99.47	98.48	96.00	91.06
82	97.86	98.45	98.93	99.34	99.60	**99.75**	99.74	99.48	98.47	95.99	91.06
83	97.88	98.47	98.95	99.35	99.61	**99.76**	99.75	99.48	98.48	96.00	91.06
84	97.91	98.50	98.97	99.36	99.62	**99.76**	99.75	99.49	98.48	96.02	91.12
85	97.94	98.51	98.98	99.37	99.63	**99.77**	99.76	99.49	98.50	96.01	91.09
86	97.94	98.54	99.00	99.38	99.64	**99.78**	99.77	99.50	98.50	96.04	91.14
87	97.97	98.55	99.01	99.39	99.65	**99.78**	99.77	99.50	98.51	96.05	91.13
88	97.99	98.58	99.03	99.41	99.66	**99.79**	99.77	99.51	98.51	96.05	91.17
89	98.01	98.61	99.04	99.42	99.68	**99.79**	99.77	99.52	98.51	96.05	91.17
90	98.03	98.63	99.06	99.43	99.69	**99.80**	99.78	99.52	98.52	96.05	91.19
91	98.06	98.65	99.08	99.44	99.70	**99.81**	99.78	99.52	98.53	96.07	91.19
92	98.08	98.66	99.09	99.45	99.71	**99.81**	99.78	99.53	98.52	96.08	91.21
93	98.09	98.68	99.11	99.46	99.72	**99.82**	99.79	99.53	98.53	96.08	91.23
94	98.12	98.69	99.12	99.47	99.72	**99.82**	99.79	99.53	98.53	96.09	91.24
95	98.14	98.70	99.14	99.49	99.73	**99.82**	99.80	99.53	98.53	96.09	91.26
96	98.16	98.73	99.16	99.50	99.74	**99.83**	99.80	99.54	98.53	96.09	91.26
97	98.18	98.74	99.17	99.50	99.75	**99.83**	99.80	99.54	98.54	96.12	91.28
98	98.20	98.76	99.18	99.52	99.75	**99.84**	99.80	99.55	98.55	96.13	91.28

| 99 | 98.21 | 98.77 | 99.19 | 99.53 | 99.76 | **99.84** | 99.81 | 99.55 | 98.55 | 96.12 | 91.31 |
| 100 | 98.23 | 98.79 | 99.21 | 99.54 | 99.76 | **99.85** | 99.81 | 99.56 | 98.55 | 96.11 | 91.32 |

Generally speaking, hybrid two variable renewable energy sources (wind and solar power) can indeed reduce the overall power variability, but it is difficult to determine the optimal mixing ratio. For standalone wind and solar power systems, the size of the system is critical but the uncertain mixing ratio of the wind and solar makes it difficult to determine the size of the standalone hybrid system. Therefore, this study will not continue to discuss hybrid wind and solar systems in the study of standalone wind and solar power systems.

3.6 Optimal sizing process

The optimal sizing of standalone wind and solar power system aims to a reliable system operation with minimum system costs. Figure 3.10 generally describes the proposed sizing approach. γ is the correction coefficient; A_W and A_S are the size of wind turbine and PV panel; m_B is the margin factor of the battery bank; m_W and m_S are the margin factors of wind turbine and PV panel; α is the size factor of wind and solar generators; B_{ac} is the active battery bank capacity and B_n is the nominal battery bank capacity; R_W and R_S are the power supply reliability of the wind and solar power, and R_{set} is the set power supply reliability; COE_W and COE_S are the Cost of Energy of wind and solar power. The proposed optimal sizing method is to determine the margin coefficient of the wind turbine/PV panel and the battery bank through inter-annual variation of the wind and solar power. Then, this approach quantifies wind and solar power fluctuations to determine the relationship between size factor and power supply reliability. Subsequently, the minimum Cost of Energy with acceptable power supply reliability can be figure out. The specific calculation method and function of each coefficient will be elaborated in the following sections.
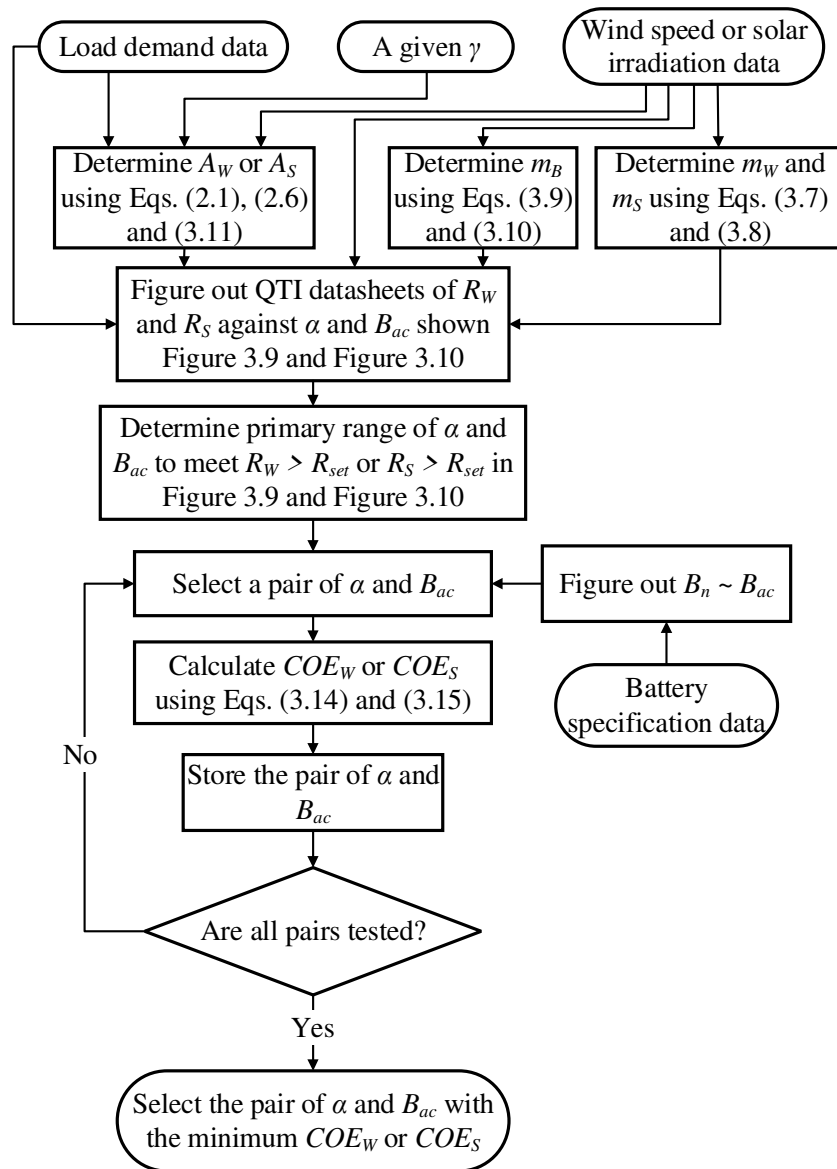
Figure 3.11 The process of optimal sizing of SAWP and SAPVP systems using the proposed approach.

3.7 Case studies

For standalone wind/solar power systems, end-load users are concerned about power supply reliability and system costs. One typical design scenario for the optimal sizing of standalone wind/solar power systems is to build the most cost-effective system subject to various constraints, especially the constraints on the power supply reliability. Thus, the optimization of standalone wind/solar power systems should aim to achieve the required power supply reliability at the lowest systems costs.

3.7.1 System costs

For the standalone wind and solar power systems mentioned in Chapters 2 and 3, the system costs include the cost of wind turbines or PV panels and the cost of the battery bank. The costs of each component are mainly divided into installation costs and maintenance costs. Usually, when calculating the system costs of power systems, in order to make the costs of different power resources comparable, Cost of Energy (COE) is introduced to represent the cost of unit energy output ($/kWh) [68, 154]. Higher COE means higher system costs and vice versa. The COE of SAWP systems COE_W can be described as:

$$COE_W = \frac{\overbrace{C_{Wi} \cdot A_W \cdot \alpha \cdot \gamma \cdot m_W + C_{Wm} \cdot (Y-y)}^{\text{cost of wind turbine}}}{R_W \cdot \int P_L dt} + \frac{\overbrace{(C_{Bi} + C_{Bm}) \cdot B_n \cdot m_B}^{\text{cost of battery bank}}}{R_W \cdot \int P_L dt} \quad (3.14)$$

where C_{Wi} and C_{Bi} denote the initial cost coefficients of wind turbines in $\cdot$m^{-2}, and battery bank in $\cdot$kWh^{-1} respectively; C_{Wm} and C_{Bm} denote the maintenance and replacement cost of wind turbines in $\cdot$m^{-2} and battery bank in $\cdot$kWh^{-1} respectively.

The COE of SAPVP systems COE_S can be described as:

$$COE_S = \frac{\overbrace{C_{Pi} \cdot A_S \cdot \alpha \cdot m_S + C_{Pm} \cdot A_S \cdot \alpha \cdot m_S}^{\text{cost of PV panel}}}{R_S \cdot \int P_L dt} + \frac{\overbrace{(C_{Bi} + C_{Bm}) \cdot B_n \cdot m_B}^{\text{cost of battery bank}}}{R_S \cdot \int P_L dt} \quad (3.15)$$

where C_{Pi} denotes the initial cost coefficients of PV panels in $\cdot$m^{-2}, C_{Pm} denotes the maintenance of the PV panels in $\cdot$m^{-2}.

3.7.2 Optimization objective and constraints

Based on Eqs. (3.14) and (3.15), the optimal sizing objective of standalone wind/solar power systems is finding the minimum COE:

$$\text{Optimization objective} \rightarrow \min\{COE\} \quad (3.16)$$

and the constraints of this optimization is

$$\begin{cases} R_W \geq R_{set} \\ R_S \geq R_{set} \end{cases} \qquad (3.17)$$

where R_{set} is the specified minimum required power supply reliability. Noted that using Eq. (3.14), (3.15) and (3.16) to optimize wind and solar power systems are actually determining the minimum cost set of the wind turbine and PV panel size and the battery capacity (A_W, A_S and B_n) subject to the constraint of Eq. (3.17).

3.7.3 SAWP system in Chicago

A case study of the optimal sizing of a SAWP system in Chicago with a typical residential load demand shown in Figure 3.3 with $\bar{P}_L = 518.26$ W is presented. The wind speed data of Chicago from 2007 to 2012 are extracted from the WIND Toolkit. The case study is following the proposed sizing process shown in Figure 3.2. The sizing constraints for the minimization of the COE_W can be specified as:

$$R_{W\min} \leq R_{set} \leq R_{Wavg} < 100\% \qquad (3.18)$$

where $R_{W\min}$ represents the minimum system reliability of the SAWP system ($R_{W\min} = 55\%$ at Chicago, as shown in Figure 3.9 (e)). Note that, based on the dependence relationships of R_W vs. B_{ac} and R_W vs. α as shown in Figure 3.9 (e), the sizing constraint zone is enclosed by a convex combination of quasi-linear lines, which might help simplify the sizing optimization of the SAWP systems. For this case study, the specification objective of the SAWP system is set as $R_{set} = 80\%$ and the life cycle is six years.

From Figure 3.10 (e), it can be seen that, if $R_W \geq R_{set} = 80\%$, the constraint of active battery capacity for the minimization of the cost function in Eq. (3.14) can be explicitly specified as 10 hours $< B_{ac} < 1500$ hours. Obviously, the explicit constraint of B_{ac} could lead to a significant reduction of computation in the optimal sizing.

Details of the wind turbine and lead-acid battery [160] are listed in Table 3.9. Noted that, the price of commercial wind turbines has a big difference because of the difference in a specific configuration. The values of C_{Wi} and C_{Wm} in Table 3.9 are according to the wind turbine price of Bergey, Jacobs, and Endurance's product [161, 162]. Moreover, the cycle life of the lead-acid battery bank nonlinearly depends on the depth of discharge DoD in

practice (*DoD* indicates the percentage of the discharged battery relative to the total battery capacity). For instance, as shown in Table 3.9, if *DoD* = 10%, the battery capacity will fall under 80% of the original capacity after 6200 times complete charge/discharge cycles, while *DoD* = 20%, the cycle life will drop to 5700 times.

Table 3.9
Details of wind turbines and lead-acid battery bank.

Wind turbines		Lead-acid battery bank		*DoD* (%)	Cycle life
C_{Wi}	1000 \$/m^2	C_{Bi}	225 \$/kWh	10	6200
C_{Wm}	100 \$/years	C_{Bm}	0 \$/m^2	20	5700
Life	20 years	Life	*DoD*-dependent	50	1800
η_W	90%	η_B	81%	80	600
				100	425

Figure 3.12 shows the average Number of annual complete charge/discharge Cycles (*NoC*) of battery bank NoC_{avg} decreases with the growth of B_{ac}, while it doesn't change very much with $\alpha = 1 \sim 2$. Note that, this study assumes that a complete charge/discharge cycle of the battery bank means the SoC of the battery bank is charged from 0% to 100% and discharged from 100% to 0% no matter how many times of the charging/discharging process the battery bank really underwent. If the battery capacity is allowed to fall under 80% of the original capacity, the life cycle of the battery would be prolonged. In addition, since the battery capacity will fall under 80% of its original capacity after the cycle life of the battery, the final battery capacity can be chosen as $B^* = B_n/80\% = 1.25B_n$ to guarantee the system reliability always meet the specific required reliability R_{set} over the study period, where B_n is calculated by using Eq. (3.12). From Table 3.9 it can be seen that, if a large *DoD* is taken, the life cycle of the battery bank might be shorter than 6 years, that is to say, the SAWP system needs several sets of the battery bank for sustaining its regular operation over 6 years. Based on Table 5 and Fig. 12, the most cost-effective final battery capacity B^* in our case study is figured out by

$$B^* = 1.25 N_B B_n = 1.25 N_B B_{ac} \overline{P}_L / (DoD \cdot \eta_B \cdot m_B)$$ (3.19)

where N_B is the required number of the battery bank. The results of most cost-effective final battery capacity B^* is listed in Table 3.10
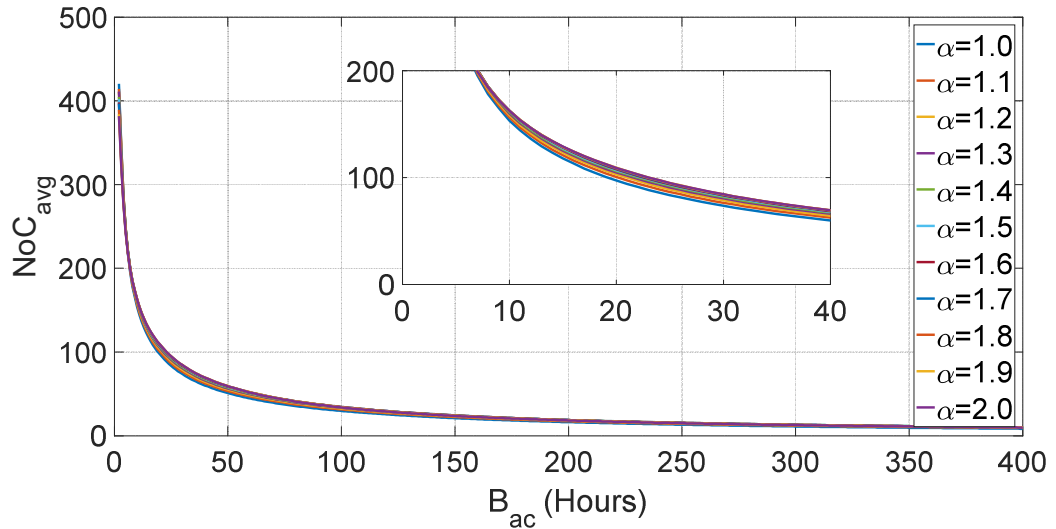
Figure 3.12 *NoC$_{avg}$* of the battery bank of the SAWP system in Chicago with *α* from 1 to 2 for the years 2007-2012.

Based on Figure 3.9 (e) and Table 3.3, 3.9 and 3.10, the results of the optimal sizing of the SAWP system in Chicago are listed in Table 3.11. The minimum *COE$_W$* of 0.026 \$·kWh^{-1} occurs at B_{ac} = 20 hours, *DoD* = 80%, and α = 1.6. Therefore, taking the QTI impacts of wind power variability into consideration, (i) according to Table 3.10, the final battery capacity would be chosen as $B^* = 1.89 B_{ac}\bar{P}_L \approx 19.60$ kWh; (ii) according to Table 3.3, the selected wind turbine swept area is $\alpha \times A_W = 1.6 \times 3.87 \approx 6.19$ m^2.

Table 3.10
Most cost-effective final battery capacity *B**.

B_{ac} (hours)	*DoD* (%)	N_B	B^* (kWh)
1 ~11	50	1	$3.03 B_{ac}\bar{P}_L$
12 ~ 19	100	2	$3.03 B_{ac}\bar{P}_L$
20 ~ 32	80	1	$1.89 B_{ac}\bar{P}_L$
≥ 33	100	1	$1.51 B_{ac}\bar{P}_L$

Table 3.11
COEw **with different wind turbine size factor and active battery capacity.**

Battery bank Capacity		COE_W ($/kWh)										
DoD (%)	B_{ac} (Hours)	α=1.0	α=1.1	α=1.2	α=1.3	α=1.4	α=1.5	α=1.6	α=1.7	α=1.8	α=1.9	α=2.0
50	≤10	n/a	n/a	n/a	n/a	n/a	n/a	n/a	n/a	n/a	n/a	0.027
50	11	n/a	n/a	n/a	n/a	n/a	n/a	n/a	n/a	n/a	n/a	0.028
100	12	n/a	n/a	n/a	n/a	n/a	n/a	n/a	n/a	n/a	0.028	0.028
100	13	n/a	n/a	n/a	n/a	n/a	n/a	n/a	n/a	n/a	0.029	0.029
100	14	n/a	n/a	n/a	n/a	n/a	n/a	n/a	n/a	0.029	0.029	0.030
100	15	n/a	n/a	n/a	n/a	n/a	n/a	n/a	n/a	0.030	0.030	0.030
100	16	n/a	n/a	n/a	n/a	n/a	n/a	n/a	0.030	0.030	0.031	0.031
100	17	n/a	n/a	n/a	n/a	n/a	n/a	n/a	0.031	0.031	0.031	0.032
100	18	n/a	n/a	n/a	n/a	n/a	n/a	n/a	0.031	0.032	0.032	0.033
100	19	n/a	n/a	n/a	n/a	n/a	n/a	n/a	0.032	0.033	0.033	0.033
80	20	n/a	n/a	n/a	n/a	n/a	n/a	**0.026**	0.027	0.027	0.027	0.028
80	21	n/a	n/a	n/a	n/a	n/a	n/a	0.027	0.027	0.027	0.028	0.028
80	22	n/a	n/a	n/a	n/a	n/a	n/a	0.027	0.027	0.028	0.028	0.028
80	23	n/a	n/a	n/a	n/a	n/a	n/a	0.027	0.028	0.028	0.028	0.029
80	24	n/a	n/a	n/a	n/a	n/a	0.027	0.028	0.028	0.028	0.029	0.029
80	25	n/a	n/a	n/a	n/a	n/a	0.028	0.028	0.028	0.029	0.029	0.030
80	26	n/a	n/a	n/a	n/a	n/a	0.028	0.029	0.029	0.029	0.030	0.030
80	27	n/a	n/a	n/a	n/a	n/a	0.029	0.029	0.029	0.030	0.030	0.030
80	28	n/a	n/a	n/a	n/a	n/a	0.029	0.029	0.030	0.030	0.031	0.031
80	29	n/a	n/a	n/a	n/a	n/a	0.030	0.030	0.030	0.031	0.031	0.031
80	30	n/a	n/a	n/a	n/a	0.030	0.030	0.030	0.031	0.031	0.031	0.032
≥ 80	≥ 31	≥ 0.105	≥ 0.048	≥ 0.036	≥ 0.030	≥ 0.030	≥ 0.031	≥ 0.031	≥ 0.031	≥ 0.031	≥ 0.032	≥ 0.032

This case study shows that, the QTI impacts of wind power variability shown in Figure 3.9 allows the designer to locate the explicit constraint of battery capacity rapidly and then significantly reduce the search computation burden in the optimal sizing of SAWP systems.

3.7.4 SAPVP system in Houston

A case study of the optimal sizing of a SAPVP system in Houston with a typical residential load demand shown in Figure 3.3 with $\bar{P}_L$ = 518.26 W is presented. The wind speed data of Houston from 1998 to 2017 is extracted from NSRDB. The case study is following the proposed sizing process shown in Figure 3.11. Based on the QTI responses of R_{savg} versus B_{ac} shown in Figure 3.10 (d), there are two scenarios with different constraints of power supply reliability for the optimal sizing of the SAPVP system in Houston.

Chapter 3
Optimal sizing of standalone wind/solar power systems

1) Scenario 1: $R_{S\,min} < R_{set} < R_{savg} < 82\%$

From Figure 3.10 (d), it can be found that the minimum active battery capacity is B_{ac} ≥ 14 hours with $\alpha = 2$ in this scenario. Hence the design constraints for the minimization of COE_S in Eq. (3.16) can be explicitly specified as $R_{set} < R_{Savg} \leq 1$, $1 \leq \alpha \leq 2$, and $B_{ac} \geq 14$ hours. Moreover, as shown in Figure 3.10 (d), R_{savg} monotonously increases with the growth of either B_{ac} or α. Thus, the design constraints form a convex zone, which would help simplify the sizing optimization

2) Scenario 2: $82\% < R_{set} \leq R_{savg} \leq 1$

From Figure 3.10 (d), it can be found that the minimum active battery capacity is B_{ac} ≥ 14 hours with $\alpha = 2$ in this scenario. Hence the design constraints for the minimization of COE_S in Eq. (3.16) can be explicitly specified as $R_{set} < R_{Savg} \leq 1$, $1 \leq \alpha \leq 2$, and $B_{ac} \geq 14$ hours. Moreover, as shown in Figure 3.10 (d), R_{savg} monotonously increases with the growth of either B_{ac} or α. Thus, the design constraints form a convex zone, which would help simplify the sizing optimization.

Table 3.12
Details of PV panels and lead-acid battery bank.

PV panels		Lead-acid battery bank		*DoD* (%)	Cycle life
C_{Pi}	830 \$/m^2	C_{Bi}	225 \$/kWh	10	6200
C_{Pm}	0 \$/m^2	C_{Bm}	0 \$/m^2	20	5700
Life	25 years	Life	*DoD*-dependent	50	1800
η_{PV}	15%	η_B	81%	80	600
				100	425

For this case study, the specification objectives of the SAPVP systems are set as $R_{set} = 83\%$ and the life cycle is 20 years. It is clear that our case study is in Scenario 2. Details of the chosen PV panel [163] and lead-acid battery are listed in Table 3.12. Note that, the cycle life of the lead-acid battery nonlinearly depends on *DoD* in practice. For instance, as shown in Table 3.12, if *DoD* = 10%, the battery capacity will fall under 80% of the original capacity

after 6200 times complete charge/discharge cycles, while $DoD = 20\%$, the cycle life will drop to 5700 times.
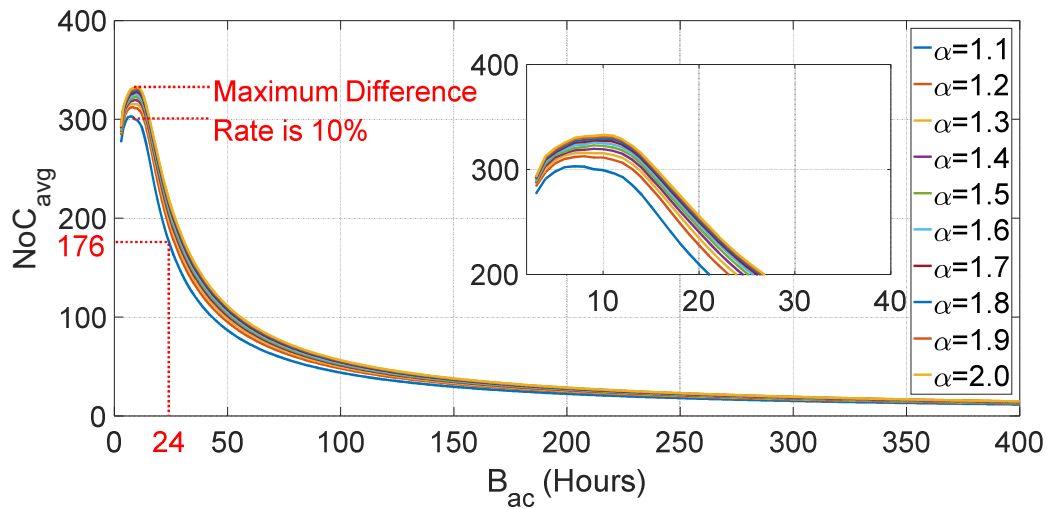
Figure 3.13 *NoC$_{avg}$* of the battery bank of the SAPVP system in Houston with *α* from 1 to 2 for the years 1998-2017.

Figure 3.12 gives the *NoCavg* of battery bank versus B_{ac} and α. Note that, because the battery capacity will be below 80% of its original value after the cycle life of the battery, the final battery capacity can be chosen as $B^* = B_n/0.8 = 1.25B_n$ to guarantee $R_{set} < R_{Savg}$ over the specified life cycle of 20 years (study period according to the data availability), where B_n can be calculated by using Eq. (3.12). From Table 3.12, it can be observed that, if $DoD \geq 50\%$ is taken, the life cycle of battery bank might be much shorter than 20 years, that is to say, the SAPV system needs several sets of the battery bank for regular operation over 20 years. For example, if a set of battery bank with $B_{ac} = 12$ hours and $DoD = 50\%$ is employed in the SAPVP systems, the cycle life of the battery bank is 1800 times and *NoC$_S$* of the battery bank is above 300 times, then the life cycle of one set of battery bank will be less than 6 years. Therefore at least 4 sets of battery banks are needed. According to Table 3.12 and Figure 3.11, the most cost-effective final battery capacity B^* in our case study is figured out using Eq. (3.19) and the results of most cost-effective final battery capacity B^* is listed in Table 3.13,

According to Figure 3.10 (d) and Table 3.7, 3.12 and 3.13, the results of the optimal sizing of the SAPVP systems at Houston are given in Table 3.14. It can be found from Table 3.14 that, the minimum COE of 0.059 $\$\cdot kWh^{-1}$ occurs at $B_{ac} = 17$ Hours, $DoD = 20\%$, and α

= 1.2. Therefore, taking the QTI impacts of solar power variability into consideration, the results of optimal sizing of the SAPVP system at Houston are: (i) according to Table 3.13, the final battery capacity would be chosen as $B^* = 7.72B_{ac}\bar{P}_L \approx 67.7$ kWh; (ii) according to Table 3.7, the area of PV panel is $\alpha \times 10.87 \approx 13.04 \text{m}^2$.

Table 3.13
Most cost-effective final battery capacity B^*.

B_{ac} (hours)	DoD (%)	N_B	B^* (kWh)
1 ~11	50	1	$3.03B_{ac}\bar{P}_L$
12 ~ 19	100	2	$3.03B_{ac}\bar{P}_L$
20 ~ 32	80	1	$1.89B_{ac}\bar{P}_L$
≥ 33	100	1	$1.51B_{ac}\bar{P}_L$

Table 3.14
***COE_S* with different PV panel size factor and active battery capacity.**

Battery bank Capacity		COE_S ($/kWh)										
DoD (%)	B_{ac} (Hours)	α=1.0	α=1.1	α=1.2	α=1.3	α=1.4	α=1.5	α=1.6	α=1.7	α=1.8	α=1.9	α=2.0
50	≤13	n/a	n/a	n/a	n/a	n/a	n/a	n/a	n/a	n/a	n/a	n/a
50	14	n/a	n/a	n/a	n/a	n/a	n/a	n/a	n/a	n/a	n/a	0.087
50	15	n/a	n/a	n/a	n/a	n/a	0.080	0.082	0.083	0.085	0.086	0.088
50	16	n/a	n/a	n/a	0.080	0.081	0.082	0.083	0.084	0.086	0.087	0.089
20	17	n/a	n/a	**0.059**	0.060	0.062	0.063	0.064	0.066	0.067	0.069	0.070
20	18	n/a	n/a	0.061	0.062	0.063	0.064	0.066	0.067	0.068	0.070	0.071
20	19	n/a	n/a	0.063	0.064	0.065	0.066	0.067	0.068	0.070	0.071	0.072
20	20	n/a	0.064	0.065	0.065	0.066	0.067	0.069	0.070	0.071	0.072	0.074
20	21	n/a	0.066	0.067	0.067	0.068	0.069	0.070	0.071	0.073	0.074	0.075
≥ 20	≥ 22	$\geq$ 0.088	$\geq$ 0.068	$\geq$ 0.069	$\geq$ 0.069	$\geq$ 0.070	$\geq$ 0.071	$\geq$ 0.072	$\geq$ 0.073	$\geq$ 0.074	$\geq$ 0.076	$\geq$ 0.077

This case study shows that, the QTI impacts of solar power variability shown in Figure 3.10 allow us to rapidly locate the explicit constraint of battery capacity and then significantly reduce the search computation burden in the optimal sizing of SAPVP systems.

3.8 Summary

The variability of intermittent wind and solar power has significant impacts on the power supply reliability and system costs of standalone wind/solar power systems. In this

chapter, this study investigates the impacts of the wind and solar power variation on the optimal sizing of the standalone wind/solar power systems based on the proposed variability quantification measures in Chapter 2. Taking the impacts of wind and solar power variability into consideration, big data simulations of the six SAWP and six SAPVP systems with the same residential load demand at the six sites were carried out to reveal the dependency between the sizing of the system components (i.e., the battery and the wind turbines/PV panels) and the power supply reliability. The case studies of optimal sizing of the SAWP system at Chicago and optimal sizing of the SAPVP system at Houston were carried out to demonstrate the feasibility of the proposed methods, which aims is to minimize the system cost while satisfying the requirement of power supply reliability. It has been found from the study that:

I.   The variability parameters for wind/solar power, such as interannual variations, fluctuation rate, and cumulative energy distribution index, are applied to the optimal sizing of standalone wind/solar power systems.

II.   Big data based spectrum analysis of wind power and load power indicates that the wind/solar power variation dominates the mismatch power of standalone wind/solar power systems in the case of $P_{Wavg}/P_{Savg} > \bar{P}_L$. Thus, the power fluctuation mitigation of standalone wind/solar power systems can be simply treated as the filtering of wind/solar power harmonics.

III. Mixing wind and solar power can improve the power supply reliability of standalone hybrid wind and solar power systems. However, the optimal mixed wind and solar ratio vary with the increase of battery capacity and the site location so that it is hard to size it.

IV.   The power supply reliability of the SAPVP system generally decreases with the increase of latitude. A higher cumulative energy distribution index $D_{Savg}(j)$ is corresponding to a faster ramping rate of R_S versus B_{ac}.

V.   A higher cumulative energy distribution index $D_{REavg}(j)$ is corresponding to a faster ramping rate of the power supply reliability R_{RE} against active battery capacity B_{ac}.

VI.   The rank of R_{REavg} is reversely consistent with the rank of F_{REmean}. With the same B_{ac} and α, the higher F_{REavg} is, the lower R_{RE} is. The fluctuation rate can provide a useful

quality indicator to the renewable energy resources assessment for the development of standalone wind/solar power systems.

VII.   The dependence of R_W/R_S on B_{ac} and α of SAWP/SAPVP systems can be considered as QTI responses, which can be used to quickly determine the explicit constraints of the minimization of the cost function and significantly reduce the computation in the optimal sizing of SAWP/SAPVP systems.

Chapter 4

Implications of variability on grid integration of wind and solar power

4.1 Introduction

Integration costs that consist of variability costs and uncertainty costs is an important part of the total economic costs of wind and solar power. The growth of wind and solar energy penetration has led to variability costs play a bigger role in integration costs, especially the large time scale variability costs become non-negligible when energy penetration is high ($\geq 30\%$).

This chapter attemptS to employ the cumulative energy distribution index to evaluate the variability costs for the integration of high penetration level wind/solar power into power grids. Different from standalone wind/solar power systems, flexible resources which include energy storage facilities, dispatchable power generators, and demand side management, are used to mitigate wind/solar power variability and improve the power grid flexibility for the power system integration. Big data simulations of the Electric Reliability Council of Texas power system (ERCOT) in 2018 reveal the impacts of grid flexibility on wind/solar energy curtailment rate and capacity factor at different penetrations. The maximum wind/solar energy penetration can be roughly determined according to the requirements of the wind/solar power capacity factor and energy curtailment of the power systems with specific flexibility. A case study of 70% grid flexibility with 20 wind farms and 10 solar plants interconnected ERCOT power system shows that the developed large time scale variability costs index can be used to estimate the variability cost when wind and solar energy penetration is between 30% to the maximum penetration.

4.2 Grid-connected wind and solar power systems

4.2.1 ERCOT power grid

Electricity generated from power plants transfers through a complex network of electricity substations, transmission lines, and distribution transformers before it powers the end-load users. In the United States, the power system consists of more than 7,300 power plants, nearly 160,000 miles of high-voltage transmission lines and millions of transformers,

which connect 145 million customers. The electrical power grid that powers North America is composed of multiple local synchronous grids as shown in Figure 4.1 [164]. Each area is specified to use 60 Hz power [165]. Local power grids are interconnected to form larger networks for reliability and commercial purposes. The United States power system in the lower 48 states is made up of three main interconnections that are Eastern Interconnection, Western Interconnection and Texas Interconnection. Basically, these three main power interconnections are quite independent and do not directly transfer electrical power to each other frequently [166]. Eastern Interconnection consists of the Northwest power grid, Southwest power grid and California power grid with the peak load is about 470,000 GW in 2011 [167]. Western Interconnection consists of Southwest Power Pool (SPP), Midcontinent Independent System Operator (MISO), SERC Reliability Corporation (SERC), Florida Reliability Coordinating Council (FRCC), PJM Interconnection (PJM), New York energy law (NYISO) and ISO New England (ISO-NE) with the peak load is about 130,000 GW in 2011 [167]. Texas Interconnection consists of the Electric Reliability Council of Texas (ERCOT) with the peak load is about 64,000 GW in 2011 [167]. Note that because Texas Interconnection only consists of ERCOT, ERCOT can directly refer to Texas Interconnection.
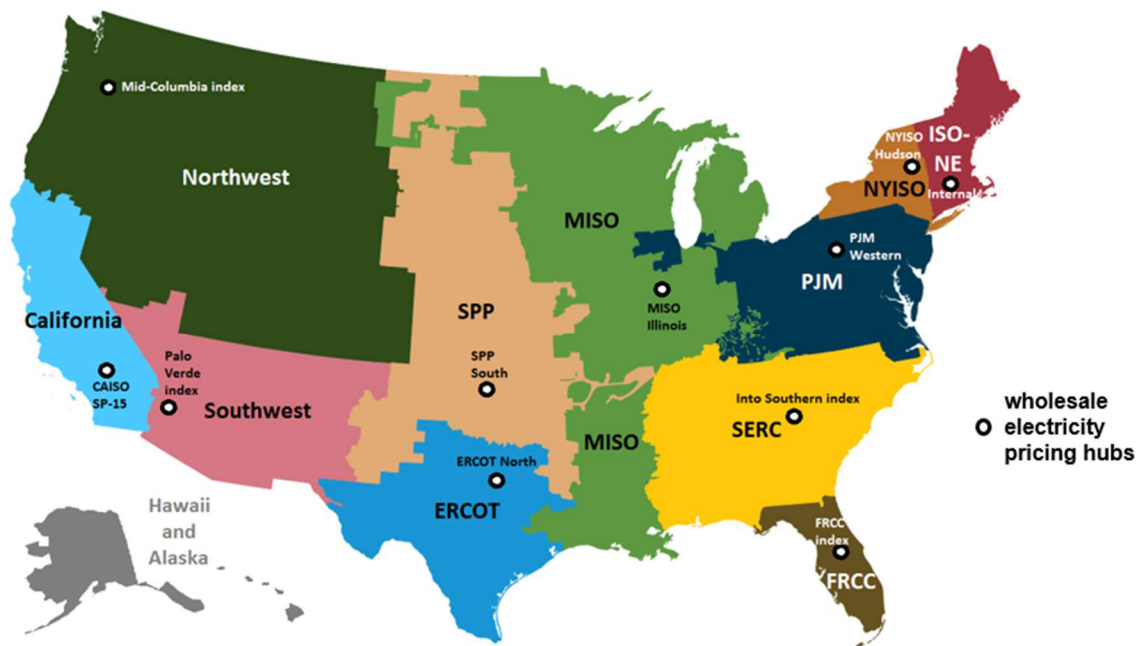
Figure 4.1 Map of North America electric power grid [164].

The actual operation of the electric system in the USA is managed by entities called balancing authorities. Most, but not all, balancing authorities are electric utilities that have taken on the balancing responsibilities for a specific portion of the power system. All of the regional transmission organizations in the United States also function as balancing authorities. ERCOT is unique in that the balancing authority, interconnection, and the regional transmission organization are all the same entity and physical system. In addition, ERCOT provides publicly available data that can cover the year of 2018. Since the power grid structure and load requirements of ERCOT have not changed much during a long period, ERCOT is a good research object for grid-connected wind and solar power.
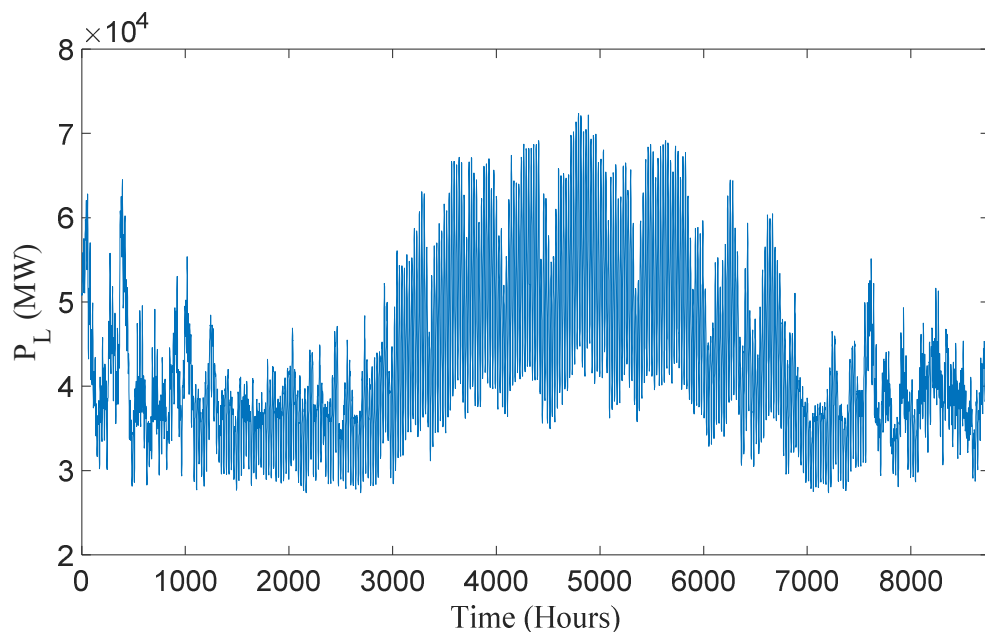
Figure 4.2 Hourly load demand of ERCOT in 2018.

A reliable electric power system needs to ensure the generation-demand balance during the operation. Figure 4.2 illustrates the hourly load demand P_L of the ERCOT in 2018 [168]. ERCOT services about 20 million customers and the total annual electricity consumption and demand profile have been relatively stable for many years. Meanwhile, Texas has great wind/solar resources and the ERCOT has a very small import-export capacity (less than 1 GW) [99] to the other power system in the United States which means nearly all of the electricity generated in ERCOT requires to be self-consumption. In addition, the electricity market of the ERCOT has a dynamic energy balancing price which means the variability of wind and solar power will further affect the system economics.

In order to meet the load demand likes Figure 4.2, three types of power plants are introduced to form a relatively complete grid structure, which are baseload power plants, intermediate power plants and peaking power plants [169]. These three types of power plants are required to meet the constant load demand, power fluctuations on different time scales, and seasonal demand peaks separately. In addition, utilities need to keep some operating reserves for contingencies and frequency regulation. Therefore, there are some power plants required to maintain operating throughout the year in order to ensure that the power grid has sufficient operating flexibility.

4.2.2 Wind and solar data

For the analysis and estimation of wind/solar variability, the actual wind speed data and solar irradiation with a sampling time interval $T_S = 1$ hour are obtained from the WIND Toolkit and the NSRDB. This study employs wind and solar resources data of ERCOT for the year 2008, and all the selected power plant locations are generally the locations of the actual power plant that are operating or under construction. Moreover, because this study focuses on the impacts of wind and solar power variability, this study assumes that sufficient transmission capacity is constructed, and transmission and distribution losses are zero. Meanwhile, the dispatchable generators are able to follow the power ramp rate of wind and solar power in the simulations.

a. Wind farm locations

Figure 4.3 shows 20 selected onshore wind farm locations in ERCOT for further simulations. Moreover, in general, wind energy penetration is larger than other variable renewable energy which makes wind power becoming the main trend of variable renewable energy. Thus, in most power grids, the installed capacity of wind power is much larger than the installed capacity of other renewable energy sources. In this case, this study specifically explores the impacts of the interconnection of wind power. Five, ten, fifteen wind farms distribute in three areas surrounded by dotted lines of red, green and purple respectively as shown in Figure 4.3. The impact of different scales of interconnected wind farms (5, 10, 15, 20 interconnected wind farms) will be explored. The output power of all these wind farms is modeled from the 3TIER model which belongs to WIND Toolkit. 3TIER model is developed based on Vestas V90 3MW turbines, which have auxiliary equipment that guarantees the power ramp rate of the wind power will be controlled within the acceptable range of the power system. Note that because this chapter explores the impact of variability

on grid-connected wind power, this study assumes that all wind farms have the same amount
of wind turbines.
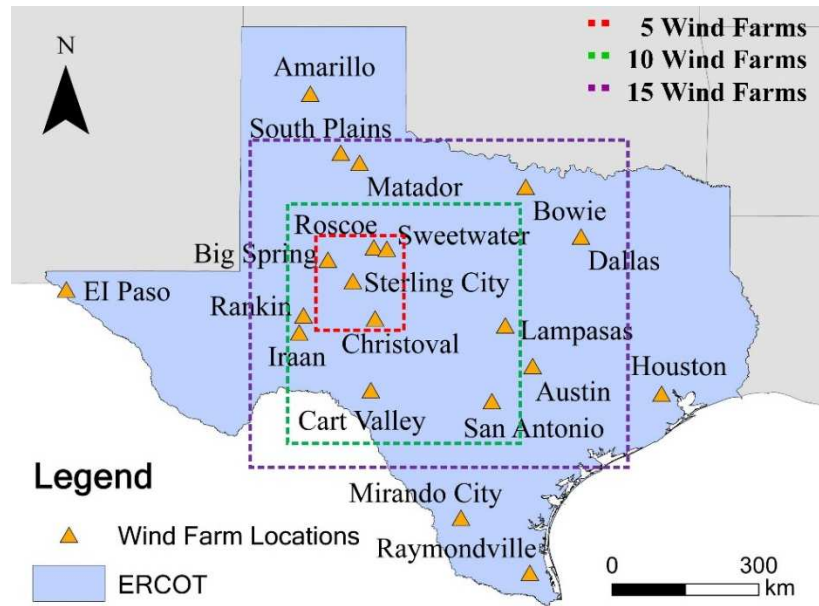
**Figure 4.3 Geographical locations of 20 selected wind farms in ERCOT and selected groups
of different scales of interconnected wind farms.**

b. Solar plant locations
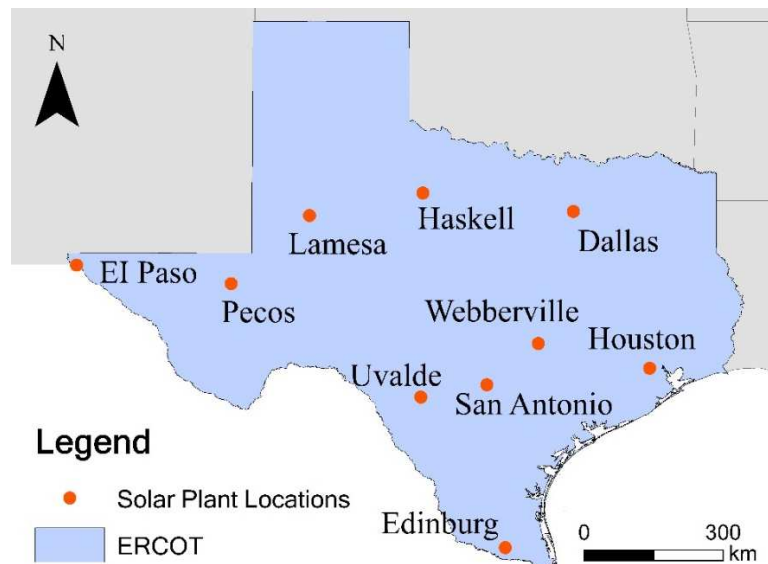
Figure 4.4 Geographical locations of 10 selected solar plants in ERCOT.

Figure 4.4 shows 10 selected solar plant locations in ERCOT for further simulations. The output power of these solar plants is modeled by 100-kW Grid-Connected PV Array model in Matlab. Same as 3TIER model, the solar power model guarantees the power ramp rate of solar power will be controlled. Note that because this chapter explores the impact of variability on grid-connected solar power, this study assumes that all solar plants have the same size.

4.2.3 System parameters

Reliable electric power system operation requires a mix of power plants that can respond to the continually varying demand for electricity as well as provide operating reserves for contingencies. Generally, power plants of the power grid can be divided into three types: baseload generator (meeting the constant demand), intermediate load generator (meeting the daily variation in demand), and peaking generator (meeting the peak summertime demand).

Moreover, in order to meet daily, weekly, and seasonal variations in load demand, utilities must keep additional power plants available (generally about 3% to 10% of system load [170]) to meet unforeseen increases in load demand and other contingencies. These additional power plants are often referred to as operating reserves, which can deal with frequency regulation (the ability to respond to small, random fluctuations around normal load), load-forecasting errors and so on [171].

a. Grid flexibility

Grid flexibility can be defined as the ability of the power system to respond to the variation and uncertainty of net load. The minimum output power of baseload generators, intermediate load generators, peaking generators and operating reserves determine the grid flexibility. Hence, if the minimum power generation of a power system can be reduced to a reasonably low level while ensuring system reliability, then this power system will be considered to have high grid flexibility. In practice, the minimum power generation of the power system is subject to various restrictions and it is difficult to reach a particularly low level. For instance, many thermal plants are responsible for district heating which means many units have to operate at a high output level no matter how much the load demand is. In some regions that have good freshwater resources, during the rainy season, many hydro units need to operate in full output power to reduce system cost and flood pressure. In

addition, transmission constraints in the power system can affect grid flexibility. For some grids with small transmission capacity, renewable energy curtailment is relatively higher than others, and such a power grid has relatively low grid flexibility as well. In this thesis, in order to focus on the impact of renewable energy variability on the power system, this study assumes that there is enough transmission capacity to avoid transmission-related curtailment. Therefore, grid flexibility can be described as

$$\begin{cases} G_{\min} = \dfrac{P_{G\min}}{P_{L\text{peak}}} \times 100\% \\ F_G = 100\% - G_{\min} \end{cases} \tag{4.1}$$

where G_{min} is the minimum generation level of the power system, $P_{G\,\min}$ is the minimum power output from all the generators in the power systems, $P_{L\,\text{peak}}$ is the approximate peak load demand within a year, F_G is the grid flexibility. Note that this study assumes that the composition of power generation in the power system does not change during the experiment and $P_{G\,\min}$ keeps constant throughout the year. From Figure 4.2 it can be seen that the peak load demand of ERCOT occurs in summer, accounting for 7×10^4 MW, i.e., $P_{L\,\text{peak}}$ is 7×10^4 MW.

b. Renewable energy penetration

To evaluate the proportion of the wind and solar power in the power grid, wind/solar energy penetration has been introduced. Because wind and solar power are zero or very low carbon emission energy resources and have no raw material cost, most utilities expect that wind/solar energy penetration can be increased as large as possible. However, due to grid flexibility and market price constraints, for a reliable and economic power system, there is an upper limit for the penetration of variable wind/solar energy penetration generally. Meanwhile, wind/solar energy penetration can be described for different duration of time (monthly, quarterly, annually) but normally, it is specified annually. In this thesis, the annual renewable energy penetration is defined as:

$$p_{RE} = \frac{\sum_{i=1}^{8760} P_{REgen}(i)}{\sum_{i=1}^{8760} P_G(i)} \times 100\% \tag{4.2}$$

where p_{RE} is renewable energy penetration and it can be specifically divided into wind energy penetration p_W, solar energy penetration p_S or hybrid wind and solar energy penetration $p_{W\&S}$,

P_{REgen}(i) represents the generated power from renewable power and it can be specifically divided into generated wind power $P_{Wgen}(i)$, generated solar power $P_{sgen}(i)$, and generated hybrid wind and solar power $P_{W\&sgen}(i)$, $P_G(i)$ is gross power generation of the power system.

Note that for a reliable power system, the power supply should always be able to meet the load demand, and the generation-load mismatch within the permissible range can be accepted. In order to facilitate the calculation, the hourly power supply is specified to meet the hourly load demand completely. Therefore, for the load demand like ERCOT, the annual total power generation is equal to the annual total load demand:

$$\sum_{i=1}^{8760} P_G(i) = \sum_{i=1}^{8760} P_L(i) \tag{4.3}$$

where $P_L(i)$ is the gross load demand.

4.2.4 Economic parameters

The system economy is the most concerning issue for utilities. Wind and solar power can save fuel costs and carbon emissions costs for utilities. However, due to the variability of wind/solar power, the wind/solar power output cannot guarantee to meet the load demand at any time. Generally, utilities use curtailment rate and capacity factor to evaluate the economics of wind and solar power.

a. Curtailment Rate

Due to the variability and uncertainty of wind and solar power, sometimes in order to respond to the load demand, wind farms and solar plants are forced to generate electricity below their full potential in a process known as wind and solar energy curtailment. High wind and solar energy curtailment can decrease the economics of wind and solar power so that utilities and wind farms/solar plants will set an upper limit for the curtailment. Different grid characteristics will affect wind are solar energy curtailment differently. For instance, due to the very small import-export capacity of ERCOT, excess wind and solar energy cannot be effectively transmitted to the neighboring power grid, so nearly all available wind and solar energy that exceeds demand must be curtailed. Therefore, this study defines the renewable energy curtailment rate as

$$CR_{RE} = \frac{\sum_{i=1}^{8760} P_{cur\ RE}(i)}{\sum_{i=1}^{8760} P_{ava\ RE}(i)} \times 100\%$$

(4.4)

where CR_{RE} is the renewable energy curtailment rate and it can be divide into wind energy curtailment rate CR_W, solar energy curtailment rate CR_S and hybrid wind and solar energy curtailment rate $CR_{W\&S}$, $P_{cur\ RE}(i)$ represents the curtailed potential power from renewable energy and it can be divided into the curtailed potential power from wind power $P_{cur\ W}(i)$, solar power $P_{cur\ S}(i)$, or hybrid wind and solar power $P_{cur\ W\&S}(i)$, $P_{ava\ RE}(i)$ is available renewable power and it can be divided into available wind power $P_{ava\ W}(i)$, available solar power $P_{ava\ S}(i)$, or available hybrid wind and solar power $P_{ava\ W\&S}(i)$. Generally, when the penetration of wind/solar power is low, wind/solar energy curtailment rate is usually below 6% [172]. However, in some regions just like ERCOT, because excess energy cannot be shared with other power grid and the wind and solar energy penetration are planned to a high level so that the wind/solar energy curtailment rate will be higher than others (usually below 20%) [173].

b. Capacity Factor

As wind speed and solar radiation fluctuate over time, it is impossible for wind power plants and solar power plants to maintain output power at rated power throughout the whole year. Therefore, the capacity factor is proposed to evaluate the ratio of wind and solar power generation to their rated output power during a year. The renewable energy capacity factor can be described as:

$$CF_{RE} = \frac{\sum_{i=1}^{8760} P_{REgen}(i)}{P_{rat\ RE} \cdot 8760} \times 100\%$$

(4.5)

where CF_{RE} is the capacity factor of renewable energy and it can be divided into wind power capacity factor CF_W, solar power capacity factor CF_S or hybrid wind and solar power capacity factor $CF_{W\&S}$, $P_{rat\ RE}(i)$ is rated renewable power output and it can be divided into rated wind power output $P_{rat\ W}(i)$, rated solar power output $P_{rat\ S}(i)$, and rated hybrid wind and solar power output $P_{rat\ W\&S}(i)$. In this study, the rated power output for a single wind turbine and a unit of the PV array is the nameplate capacity of the simulation models that are 3MW for wind turbines and 0.1MW for PV arrays. Furthermore, capacity factor also has a great impact on the economics of wind/solar power. [100, 174] pointed out that the

Levelized cost of energy from wind/solar power is proportional to 1/capacity factor. Therefore, the larger the capacity factor, the higher the system cost, and vice versa.

4.3 Variability of wind and solar power

4.3.1 Impact of variable renewable generation

Variable renewable generators (primarily wind and solar power generators) are unlike conventional generators. They cannot be dispatched (except by curtailing output) and their output varies depending on local weather conditions. Different from standalone wind and power systems whose operation is completely running by wind and solar power generation, grid-connected wind and solar power are normally hard to reach 50% of the gross power generation [175]. Thus, the power variation of the power system mismatch power is not dominated by wind and solar power. In fact, the conventional power grid does not have big power variation basically because all the conventional generators can follow the variation of load demand. However, when intermittent wind and solar power are connected into the power grid, conventional generators used to meet the load demand must be able to reduce output and accommodate wind and solar generation. Therefore, this study can say that wind and solar power are the fluctuation sources of grid power variation.
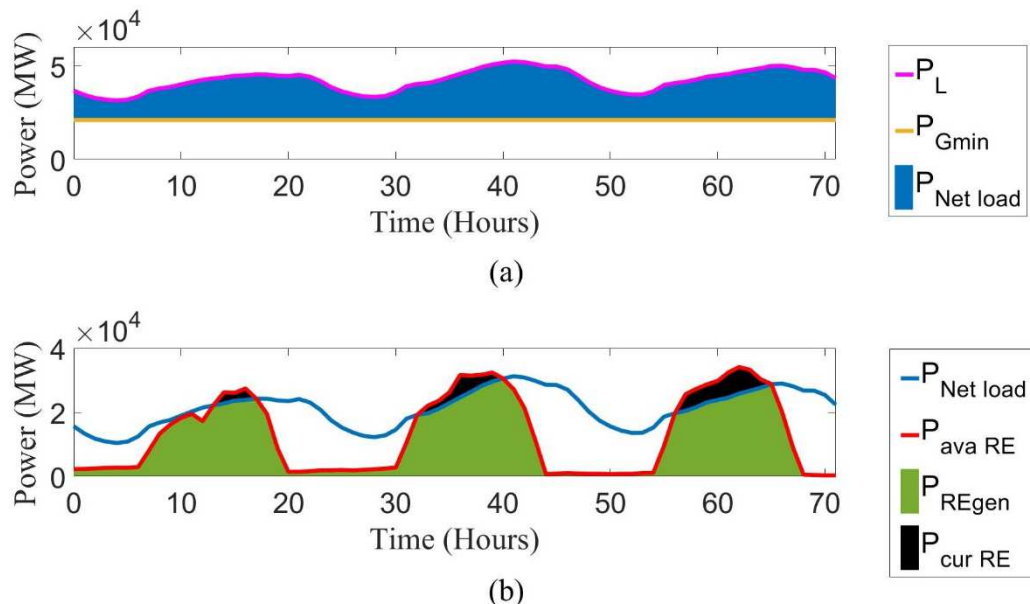
Figure 4.5 Illustration of the impact of grid flexibility on wind and solar power for (a) load configuration, (b) curtailed energy.

Figure 4.5(a) shows that for three consecutive days of ERCOT in April 2008, when F_G is 70% ($P_{G\,min}$ = 30% × 70000 MW = 21000 MW) the power generators need to meet the net load $P_{Net\,load}$ which is the blue area. It is not difficult to infer that the higher the F_G, the greater the annual $P_{Net\,load}$. Subsequently, from Figure 4.5(b) it can be seen that, net load will directly affect the integration of variable renewable power. Excessive variable renewable power generation (the power ramp rate of variable renewable output meet the grid standard) and small net load may cause a large amount of the curtailed renewable power $P_{cur\,RE}$. Therefore, if the power system has insufficient F_G, the large amount of available renewable power $P_{ava\,RE}$ may only result in a small generated renewable power P_{REgen} which is uneconomical.

4.3.2 Quantification of generated wind and solar power variations

For a reliable power system, intermittent and uncertain wind and solar power are equivalent to a noise source that needs to be filtered. Although the stochastic intermittence, annual wind and solar power is quasi-periodic at different timescales as mentioned in Chapter 2. Thus, quantifying the power harmonics of wind and solar power in the frequency domain is quantifying the power variation of the power grid (the DC component does not cause power variation). For further analysis, the normalized annual wind and solar power generation data with sampling interval T_S = 1 hour is defined as

$$P_{N-REgen}(i) = \frac{P_{REgen}(i)T_S}{\sum_{i=1}^{8760} P_{REgen}(i)T_S} = \frac{P_{REgen}(i)}{\sum_{i=1}^{8760} P_{REgen}(i)} \tag{4.6}$$

where $P_{N\text{-}REgen}(i)$ denotes normalized renewable power generation and it can be divided into normalized wind power generation $P_{N\text{-}Wgen}$, normalized wind power generation $P_{N\text{-}Sgen}$ and normalized hybrid wind and solar power generation $P_{N\text{-}W\&Sgen}$.

As mentioned in Chapter 2, using FFT, $P_{N\text{-}REgen}(i)$ in the time domain can be transformed into a set of power harmonics data $h_{REgen}(i)$ with i=1, 2, …, 4379 in the frequency domain and the DC component $h_{REgen}(0)$ =1/8760 at 0 Hz:

$$h_{REgen}(i) = \sum_{k=1}^{N-1} P_{N-REgen}(k)e^{(i2\pi/N)ki}, \; i = 0, \; 1, \; ..., \; N-1 \tag{4.7}$$

This implies that the wind and solar power output can be treated as a power harmonics source so that the energy fluctuations of wind and solar power at various time scales can be

quantified. Thus, a proposed cumulative energy distribution index D_{REgen} (j) for annual generated wind and solar power can be used to quantify the variability of grid-connected wind and solar power on different time scales which is defined as below

$$
\begin{cases}
e_{REgen}(i) = h_{REgen}(i)T(i)/\sqrt{2} \\
\\
D_{REgen}(j) = \dfrac{\sum_{i=j}^{4379} e_{REgen}(i)}{\sum_{i=1}^{4379} e_{REgen}(i)} \times 100\%
\end{cases}
\tag{4.8}
$$

where $e_{REgen}(i)$ with i=1, 2, …, 4379 is the energy of i-th order generated renewable power harmonic; $D_{REgen}(j)$ with j=1, 2, …, 4379 denotes cumulative energy distribution index within [$f(j)$, 1.39×10^{-4}] Hz. The time scale of cumulative wind/solar power harmonics that have a higher frequency than of i-th order renewable power harmonics can be defined as $T(i)$ = $1/f(i)$. Due to the ancillary services in different power systems have their own power ramp rate and capacity, the variability of renewable power in what time scale should be mitigated with high priority should be determined by the characteristics and structure of the specific power grid.
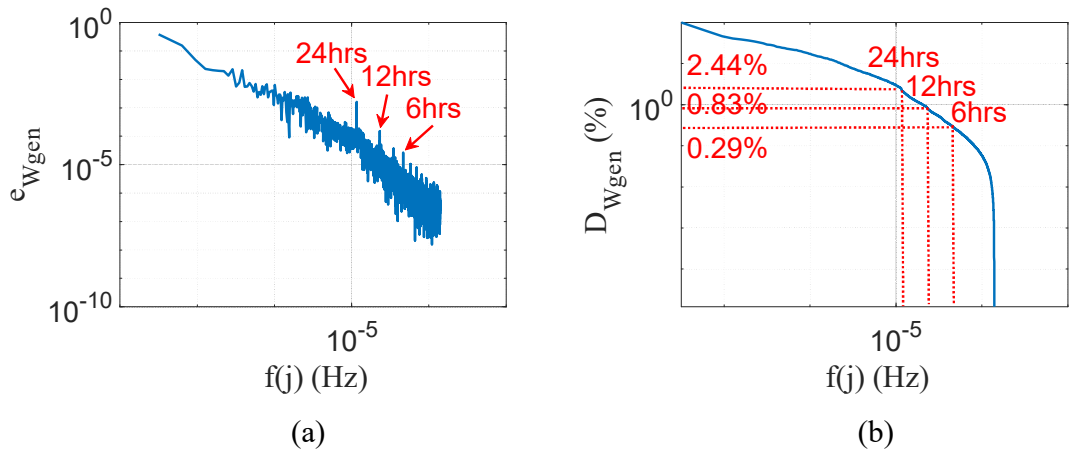
Figure 4.6 Schematic diagram of cumulative energy distribution index of 70% grid flexibility, 20% wind energy penetration 20 interconnected wind farms in 2008 ERCOT power system. (a) The power spectrum of generated wind power and (b) D_{Wgen} varies with the change of the frequency.

The developed cumulative energy distribution index $D_{REgen}(j)$ is transforming the annual renewable energy generation for each frequency band into the frequency domain and accumulate energy fluctuations from high frequencies to low frequencies. Figure 4.6(b) shows an accumulation result of wind energy fluctuations in the frequency domain. System

operators and designers can quickly find the amount of total wind energy fluctuations for a specific frequency band via $D_{Wgen}(j)$. Figure 4.6(a) also shows that some obvious spikes occur at frequencies of 1.16×10^{-5} Hz (24 hours), 2.32×10^{-5} Hz (12 hours) and 4.63×10^{-5} Hz (6 hours). This implies that generated wind energy will be affected by the 24-hour cycle of load demand. Moreover, Figure 4.6(b) revealed the total energy the ratio of fluctuation within 24 hours, 12 hours and 6 hours to the gross energy fluctuations.

4.3.3 Impact of wind and solar power penetration

The load demand in the power grid can be roughly divided into two categories: residential demand and industrial demand. Resident demand has a significant 24-hour pattern and takes a non-negligible weight in the total load demand. In order to ensure that the generator output power of the power grid is relatively smooth to reduce voltage and frequency oscillations, the industrial load usually also presents a 24-hour pattern to fill the valley of the total load demand [176-178]. Thus, the total load demand of the power grid also shows the profile of the 24-hour pattern which can be seen from the harmonic spikes in Figure 4.6(a) as well. In this section, this study will evaluate the cumulative energy distribution index $D_{REgen}(j)$ at frequencies of 1.16×10^{-5} Hz (24 hours) in different scenarios.

a. Wind power interconnection

Figure 4.7 shows D_{Wgen} at frequencies of 1.16×10^{-5} Hz (24 hours) against various wind energy penetration for 5, 10, 15, 20 interconnected wind farms under different grid flexibility. Basically, energy fluctuation within a day requires operating reserves to mitigate, which brings higher dispatch costs, and fluctuations on a larger time scale are easily balanced by the power grid. It can be seen from Figure 4.7 that for different grid flexibility wind power systems, the limits of maximum wind energy penetration is quite different. Higher grid flexibility can lead to higher maximum wind energy penetration. Figure 4.7(a)-(d) show that when the grid flexibility is between 100% to 70%, D_{Wgen} can maintain almost constant before a certain wind energy penetration, that are 39% under 100% F_G, 31% under 90% F_G, 20% under 80% F_G, 11% under 70% F_G separately. However, when grid flexibility is low ($F_G =$ 50%, $F_G =$ 60%), D_{Wgen} will become larger and no more constant interval of D_{Wgen} remain for different wind energy penetration. This implies that when the system has sufficient F_G, the D_{Wgen} within a 24-hour time scale has a constant interval with the increase of wind energy penetration. Increasing the wind energy penetration within this interval will not bring additional D_{Wgen}.
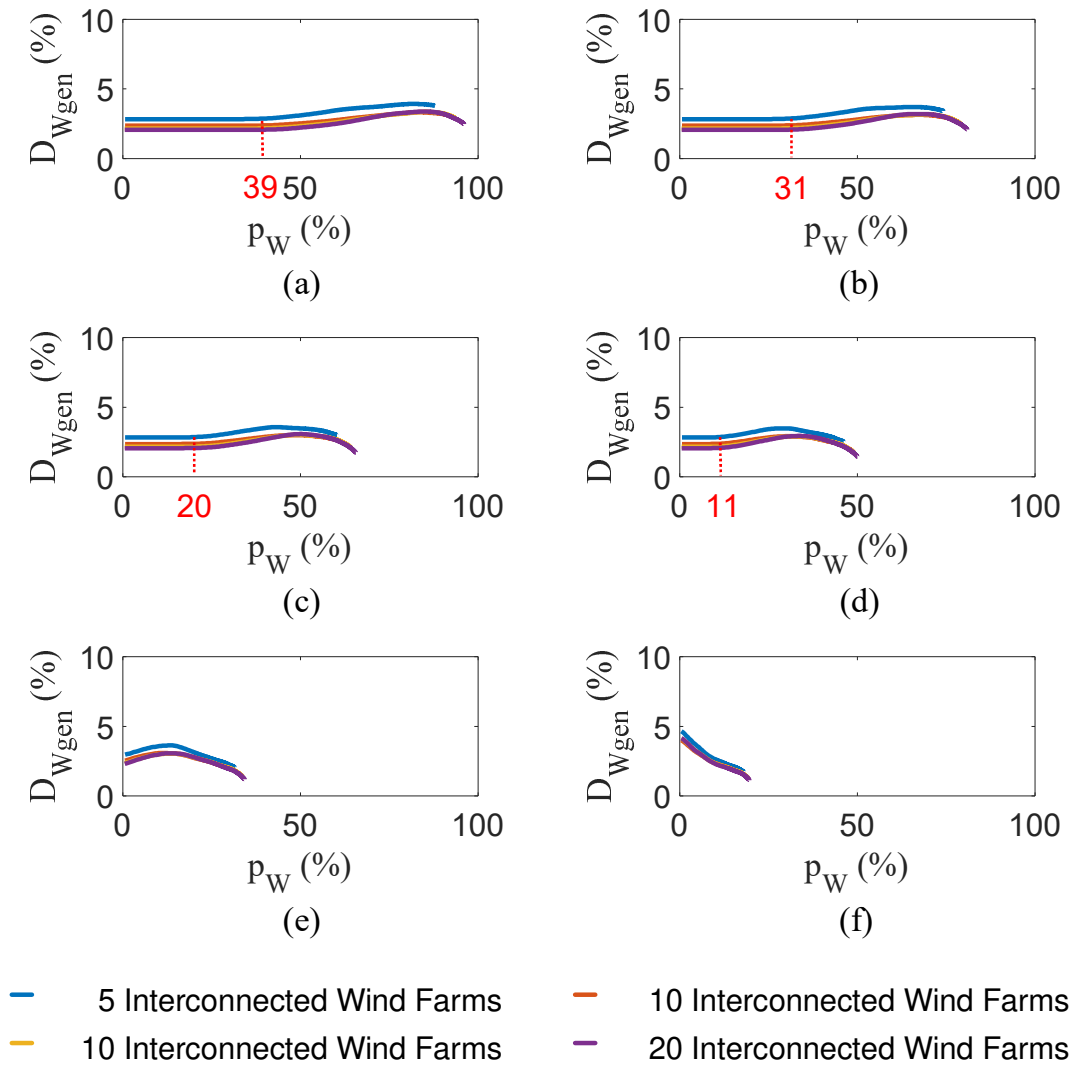
Figure 4.7 D_{Wgen} **against various wind energy penetration for 5, 10, 15, 20 interconnected wind farms at 1.16×10⁻⁵ Hz (24 hours) under (a) 100%, (b) 90%, (c) 80%, (d) 70%, (e) 60%, (f) 50% grid flexibility.**

In addition, it can be seen that, the increase in the number of interconnected wind farms can help the power grid improve the maximum wind energy penetration. Moreover, this study can find that, as the number of interconnected wind farms increases, D_{Wgen} decreases slightly under different grid flexibility. However, with the scale of interconnected wind farms becomes increasing, the decrease of D_{Wgen} tends to coincide. These imply that, the increase in the interconnection scale of wind farms can improve the maximum wind energy penetration in the power grid, and reduce the D_{Wgen} properly but as the number of interconnected wind farms increase, this reduction tends to saturate.

b. Wind and solar interconnection
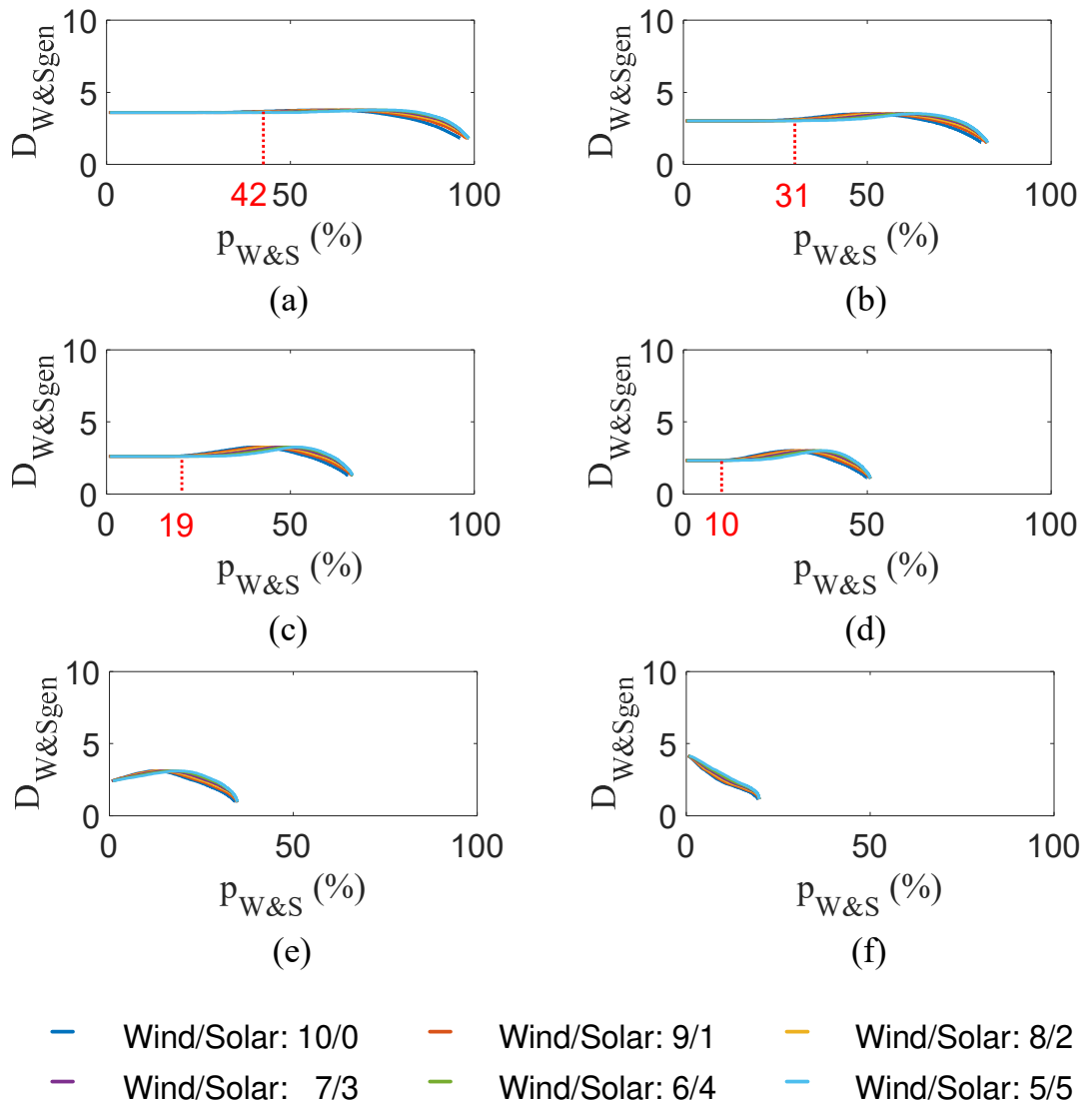
Figure 4.8 $D_{W\&Sgen}$ against 10/0, 9/1, 8/2, 7/3, 6/4, 5/5 Wind/Solar mixed proportion in 24 hours' time scale under (a) 100%, (b) 90%, (c) 80%, (d) 70%, (e) 60%, (f) 50% grid flexibility.

Fig. 4.8 show $D_{W\&Sgen}$ at 24 hours' time scale against various wind and solar energy penetration for different wind/solar mixed proportion under different grid flexibility. It can be seen from Figure 4.8(a)-(e) that, comparing with the pure wind power system, hybrid wind and solar power cannot reduce the $D_{W\&Sgen}$ properly at all wind and solar energy penetration. When wind and solar energy penetration is low, mixed wind and solar power can slightly improve the reduction of $D_{W\&Sgen}$, but when wind and solar energy penetration is high, pure wind power systems have fewer power fluctuations. Figure 4.8(f) shows that when grid flexibility is insufficient, pure wind power systems always have smaller $D_{W\&Sgen}$ than hybrid systems. Moreover, the constant interval of $D_{W\&Sgen}$ still exists for hybrid wind

and solar power systems, which are that are 42% under 100% F_G, 31% under 90% F_G, 19% under 80% F_G, 10% under 70% F_G separately

c. Additional energy storage
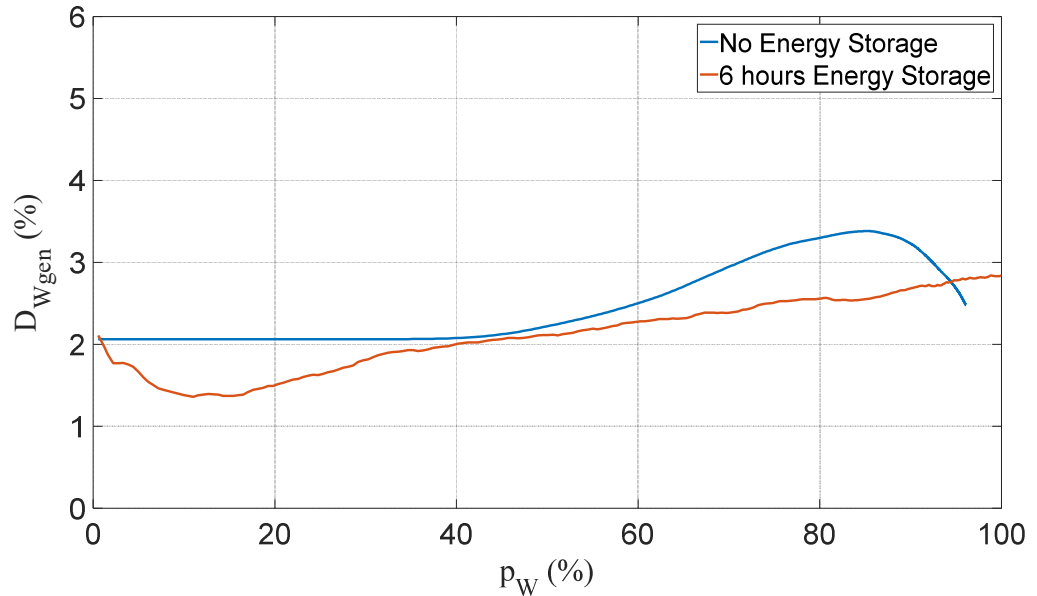
Figure 4.9 D_{Wgen} against various wind energy penetration under 100% grid flexibility with or without 6 hours energy storage.

The previous results show that improve grid flexibility can effectively improve wind and solar energy penetration. However, if the system operators and planners expect to achieve a very high wind/solar energy penetration, energy storage is widely recognized as the ideal solution. There are so many energy storage technologies available or under development, but cost constraints have prevented energy storage from being used on a conventional utilization so far. Therefore, how to assemble energy storage can effectively improve the penetration of wind and solar power has become a challenging issue.

Figure 4.9 shows D_{Wgen} (20 interconnected wind farms) against various wind energy penetration under 100% grid flexibility with or without 6 hours energy storage. Note that, herein, the 6 hours energy storage is the energy storage capacity equivalent to 6 hours times actual wind power installed capacity. For instance, if the actual wind power installed capacity is 30 GW, the capacity 6 hours energy storage will be 180 GWh. The results show that, energy storage can effectively reduce power fluctuations which lead D_W to decrease. In addition, the maximum wind energy penetration can be improved.

4.4 Simulation results and decisions

Big data simulations for the ERCOT system in 2008 explore the impacts of grid flexibility, the different number of interconnected wind farms and hybrid wind/solar power on wind/solar energy penetration, curtailment rate, capacity factor and variability distribution index. All the wind and solar power data have been introduced in Section 3. The grid flexibility has been selected from 50% to 100% to cover the actual system situations and high-level grid flexibility situations. Four groups of the different numbers of interconnected wind farms have been selected as shown in Figure 4.3. Moreover, for ERCOT and most of the power systems, the energy penetration of solar power is still relatively small comparing to wind power. Thus, the wind/solar mixed proportion for the hybrid system in this study has been limited between 10/0 to 5/5.

4.4.1 Wind power interconnection

Figure 4.10 shows the wind energy curtailment rate varies with the increase of wind energy penetration in four interconnected wind farms scenarios (5, 10, 15, 20 interconnected wind farms) in different grid flexibility. The total maximum installed capacity of 20 selected interconnected wind farms has been set to 600GW (Texas has more than 1000GW actual wind energy resource [99]). It can be seen that, when grid flexibility is low ($F_G = 50\%$, $F_G = 60\%$), before the wind energy penetration rate beyond 20%, the wind energy curtailment rate exceeds 20%, and it maintains a very rapid growth with the increase of the wind energy penetration. On the other hand, when grid flexibility is high ($F_G = 90\%$, $F_G = 100\%$), the wind energy curtailment rate exceeds 20% when wind energy penetration larger than 50%, the growth of it is much smoother comparing with low grid flexibility scenario. Thus, for the interconnected wind farms in this paper, the increase in grid flexibility can significantly reduce the wind energy curtailment rate, and can help utilities increase the upper limit of wind energy penetration.

In addition, it can be seen that, for four interconnected wind farms scenarios, the higher the grid flexibility, the smoother the growth of wind energy curtailment rate. Meanwhile, when grid flexibilities are 100%, 90%, 80%, 70%, wind energy curtailment can maintain about zero before the wind energy penetration increase to 39%, 31%, 19%, 10%. Moreover, higher grid flexibility will mitigate wind energy curtailment at the same wind energy penetration which leads to improvement of the high penetration wind energy integration. Figure 4.10 also implies that multi-location, long-distance wind farm interconnection can

reduce wind energy curtailment rate, but with the increase of the number of interconnected wind farms, this reduction tends to saturate.
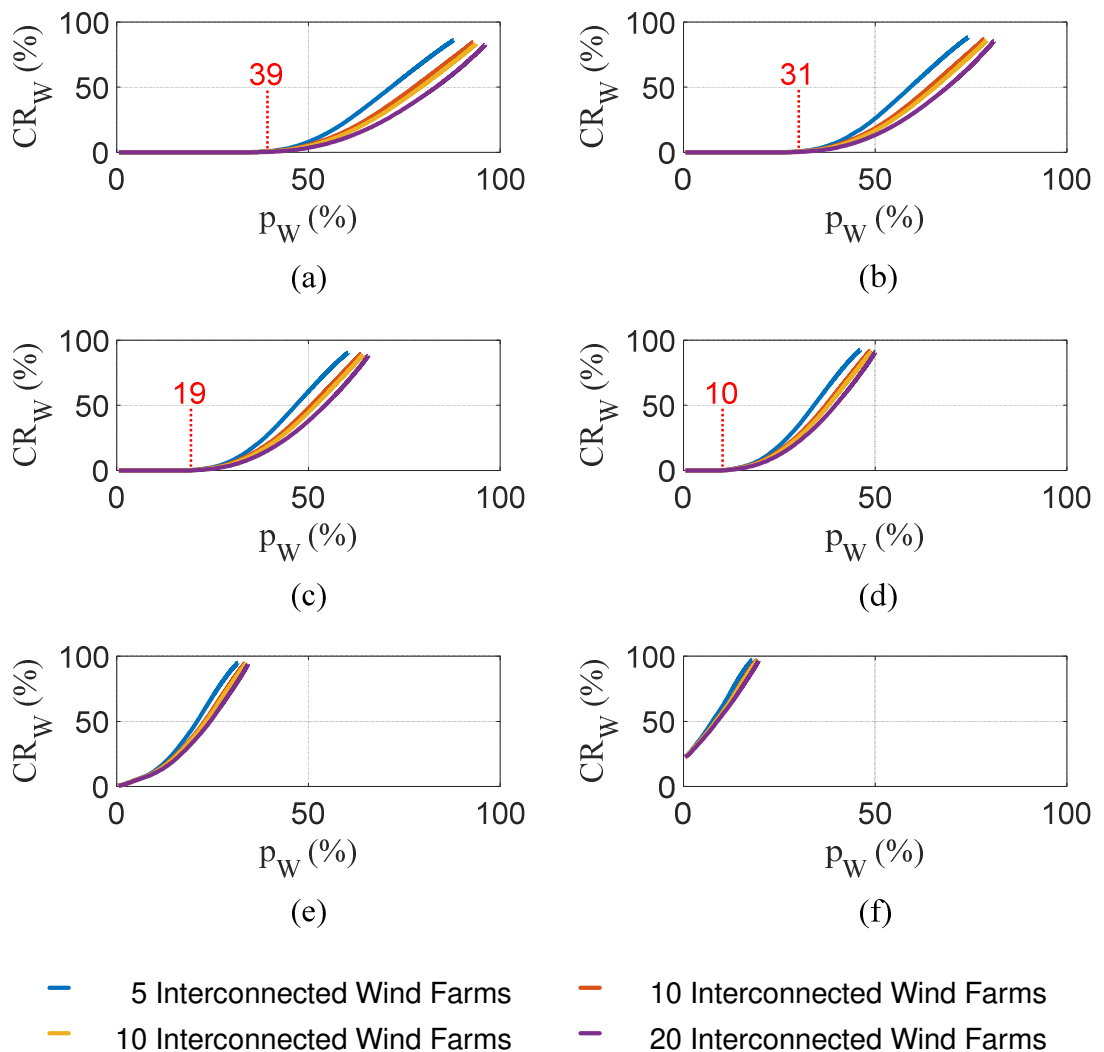
Figure 4.10 Wind energy curtailment rate against various wind energy penetration for 5, 10, 15, 20 interconnected wind farms under (a) 100%, (b) 90%, (c) 80%, (d) 70%, (e) 60%, (f) 50% grid flexibility.

Figure 4.11 shows the wind power capacity factor varies with the increase of wind energy penetration in four interconnected wind farms scenarios (5, 10, 15, 20 interconnected wind farms) in different grid flexibility. It can be seen that, when grid flexibility is low (F_G = 60%), the maximum value of the wind energy capacity factor is only about 30%, and it reaches a minimum value which is about 1.5% when the wind energy penetration is about 20%. And it maintains a very rapid growth with the increase of wind energy penetration. However, when grid flexibility is high (F_G = 90%, F_G = 100%), the wind energy capacity factor can maintain a maximum value of 40% when the wind energy penetration does not

exceed 30%. In addition, the wind energy capacity factors of these two high flexibility power systems only fell to the trough of 6% and 7% when wind energy penetration reaches 80% and 96% respectively. Moreover, with the increase of grid flexibility, the reduction of wind energy capacity factor caused by the increase of wind energy penetration becomes smoother. Thus, for the interconnected wind farms, the increase of grid flexibility can improve the wind energy capacity factor only when wind energy penetration exceeds a certain value.
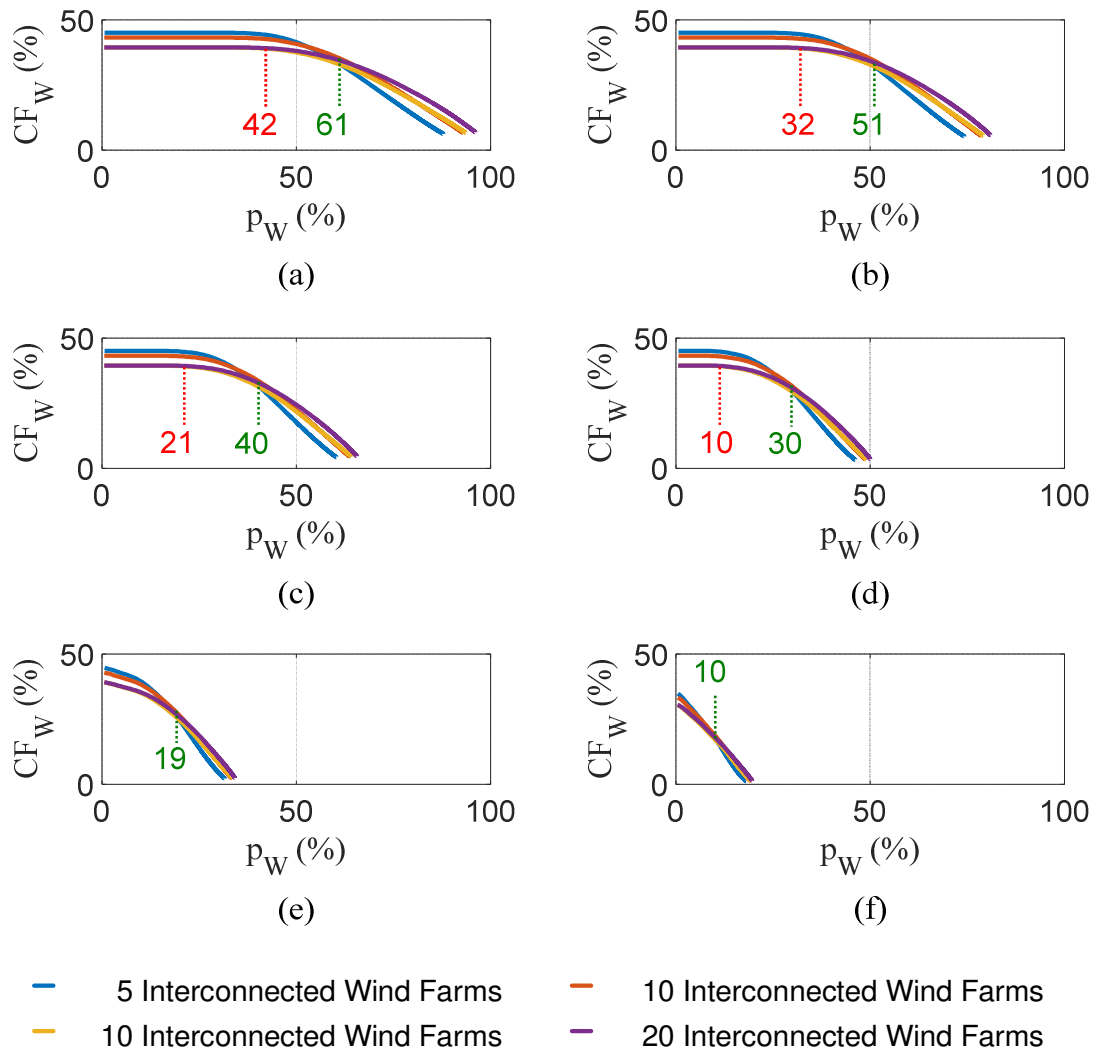
Figure 4.11 Wind energy capacity factor against various wind energy penetration for 5, 10, 15, 20 interconnected wind farms under (a) 100%, (b) 90%, (c) 80%, (d) 70%, (e) 60%, (f) 50% grid flexibility.

In addition, it can be seen that, for four interconnected wind farms scenarios, the higher the grid flexibility, the smoother the decline of wind power capacity factor. Similar to wind energy curtailment rate, when grid flexibilities are 100%, 90%, 80%, 70%, wind power capacity factor can maintain constants before the wind energy penetration increase to 42%,

33%, 21%, 10%. Moreover, Figure 4.11 also shows for 100%, 90%, 80%, 70%, 60%, 50% grid flexibility, the wind power capacity factor of 20 interconnected wind farms is lower than less interconnected wind farms scenarios when the wind energy penetration is low. However, when the wind energy penetration beyond 61%, 51%, 40%, 30%, 19%, 10% in each case, 20 interconnected wind farms have a better capacity factor. This implies, increasing the number of interconnected wind farms will only improve the wind power capacity factor when wind energy penetration beyond a specific value, and the more flexible the system is, the higher the wind energy penetration allowed.

4.4.2 Wind and solar power interconnection
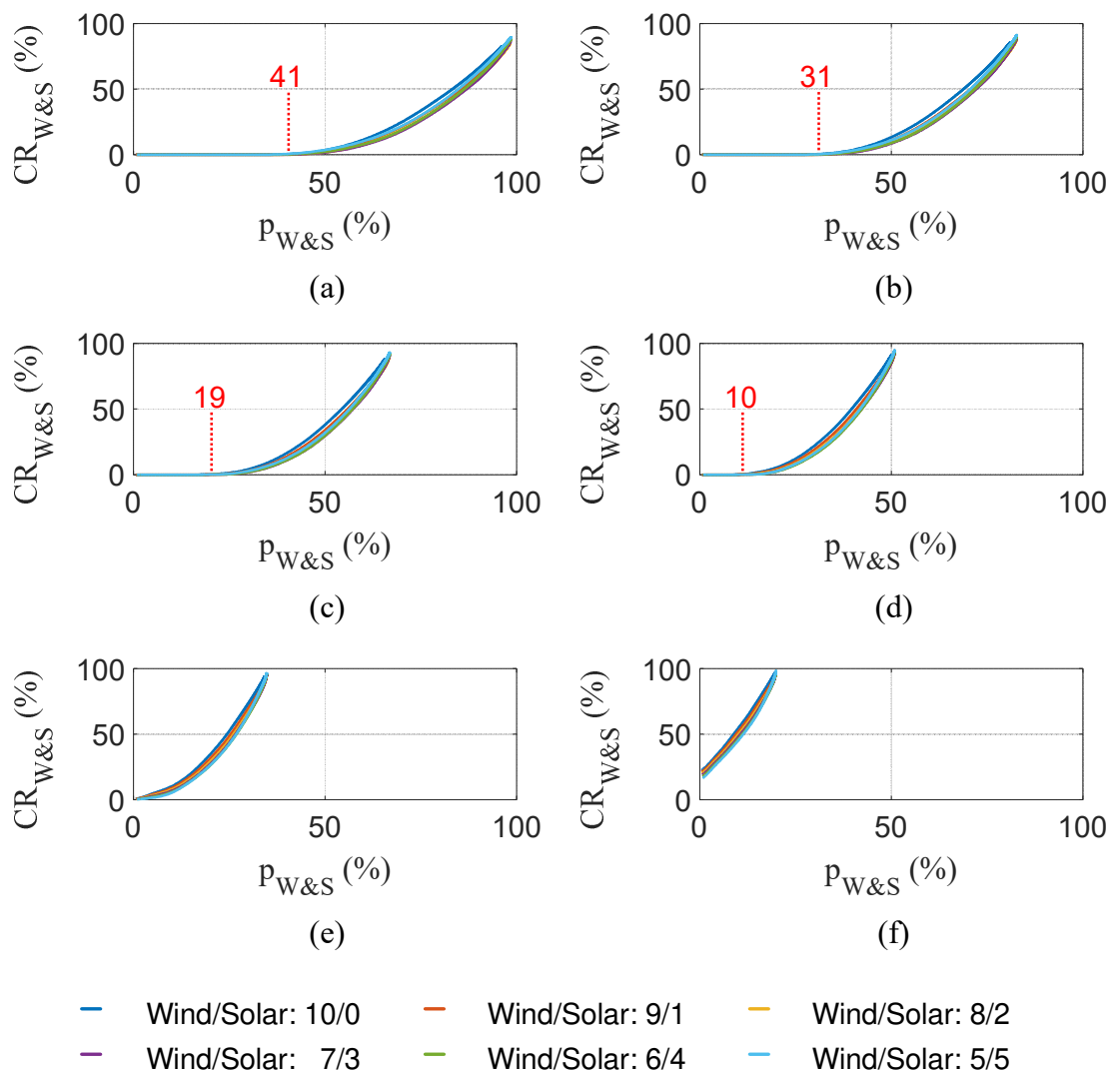
Figure 4.12 Wind and solar energy curtailment rate against various wind and solar energy penetration in different Wind/Solar combinations under (a) 100%, (b) 90%, (c) 80%, (d) 70%, (e) 60%, (f) 50% grid flexibility.

Figure 4.12 shows how wind and solar energy curtailment rate changes with different proportions of additional solar power against the increase of wind and solar energy penetration under different grid flexibility. Note that in this thesis, the combination ratio of wind/solar refers to the ratio of wind/solar installed capacity. It can be seen that, for different grid flexibility, wind-solar hybrid power systems always have lower energy curtailment than wind-only power systems. Among Figure 4.12, Figure 4.12(a)-(c) show that when the grid flexibility is selected from 100% to 80%, the 7/3 wind-solar combination can bring the lowest energy curtailment rate. Figure 4.12(d)-(f) show that when the grid flexibility is selected from 70% to 50%, the 6/4 wind-solar combination can bring the lowest energy curtailment rate. Furthermore, Figure 4.12(a)-(b) show that for optimal mixed wind/solar hybrid systems, the constant interval of curtailment rate in high grid flexibility power system ($F_G = 100\%$, $F_G = 90\%$) is slightly larger than pure wind power system.
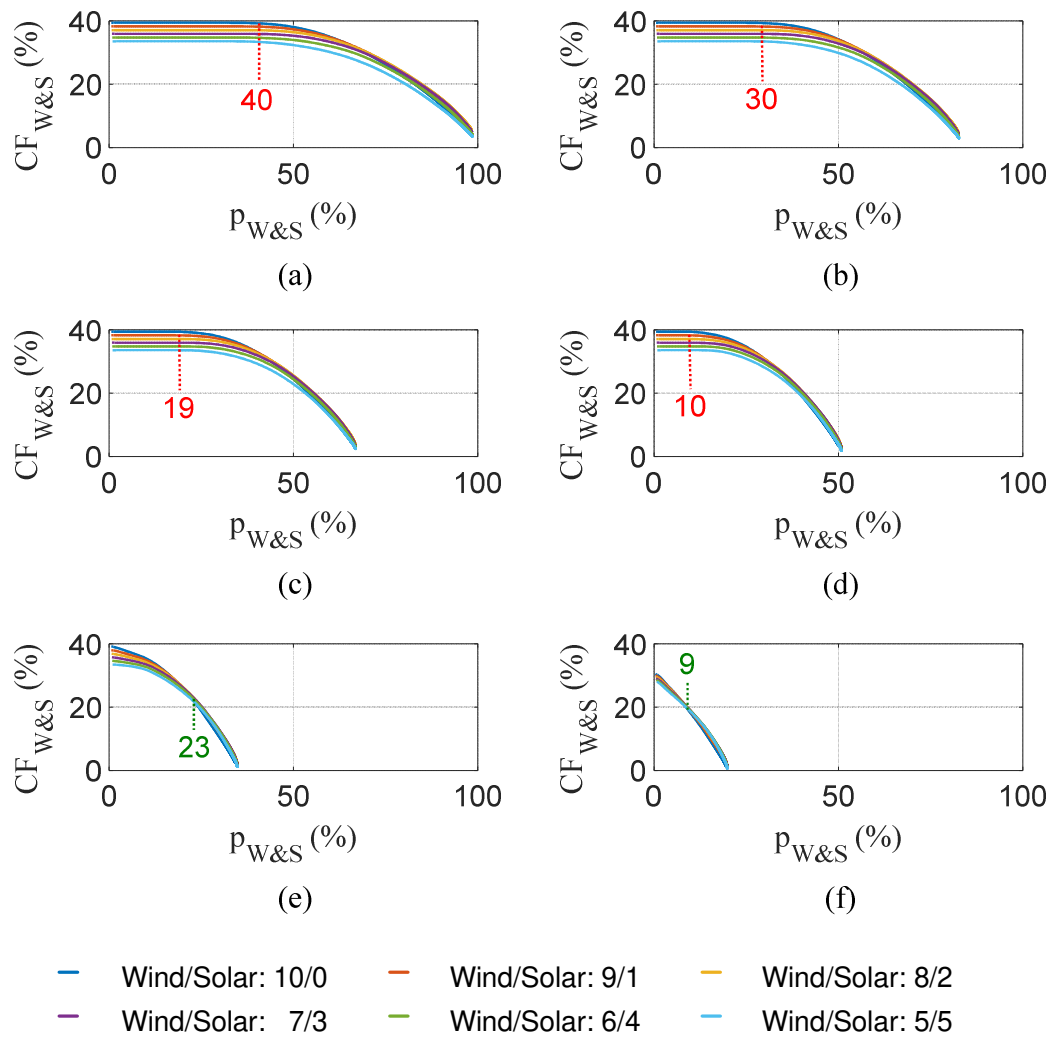
Figure 4.13 Wind and solar energy capacity factor against various wind and solar energy penetration in different Wind/Solar combinations under (a) 100%, (b) 90%, (c) 80%, (d) 70%, (e) 60%, (f) 50% grid flexibility.

Figure 4.13 shows how wind and solar energy curtailment rate changes with different proportions of additional solar power against the increase of wind and solar energy penetration in different grid flexibility. Figure 4.13(a)-(d) show that, 100% - 770% grid flexibility, pure wind power systems always have a high capacity factor, and even when the wind/solar energy penetration reach to a high level it still has a good capacity factor which is very closed to hybrid systems. Moreover, As the proportion of additional solar power increases, wind/solar power capacity factor keep decrease, 5/5 mixed wind/solar power system have the worst capacity factor all the time. This is because the capacity factor of solar power is generally much small than the wind power capacity factor due to the solar diurnal cycle. However, Figure 4.13(e)-(f) show that, if grid flexibility is 60% and 50%, when wind and solar energy penetration beyond 23% and 9%, hybrid wind/solar power systems have a better capacity factor than pure wind systems. In general, hybrid wind/solar power cannot effectively improve the capacity factor in all situations.

4.4.3 Additional energy storage

Figure 4.14 shows wind energy curtailment rate and wind power capacity factor against various wind energy penetration under 100% grid flexibility with or without 6 hours energy storage. It can be seen that, for both wind energy curtailment rate and wind power capacity factor, install energy storage cannot make any improvement before the wind energy penetration reaches 40%. This implies that, energy storage cannot bring any technical-economics brief when the wind energy penetration is not enough (still in the constant interval). However, energy storage can indeed improve wind energy curtailment rate and wind power capacity factor in high penetration situation and the maximum energy penetration can be improved as well.
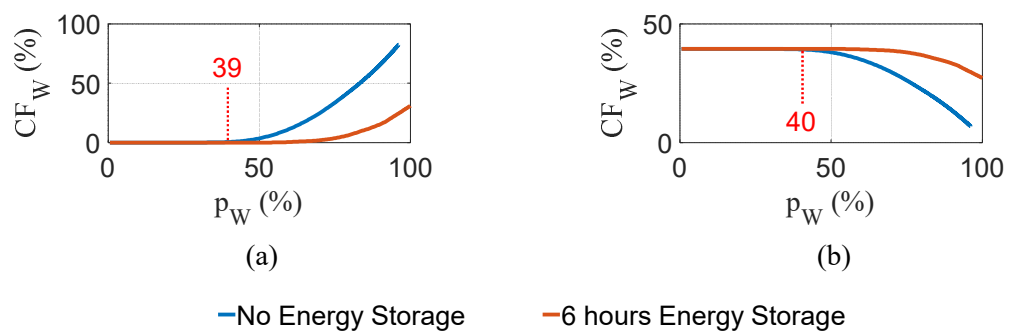
Figure 4.14 (a) Wind energy curtailment rate and (b) wind power capacity factor against various wind energy penetration under 100% grid flexibility with or without 6 hours energy storage.

4.5 Cumulative energy distribution index for optimal penetration estimation
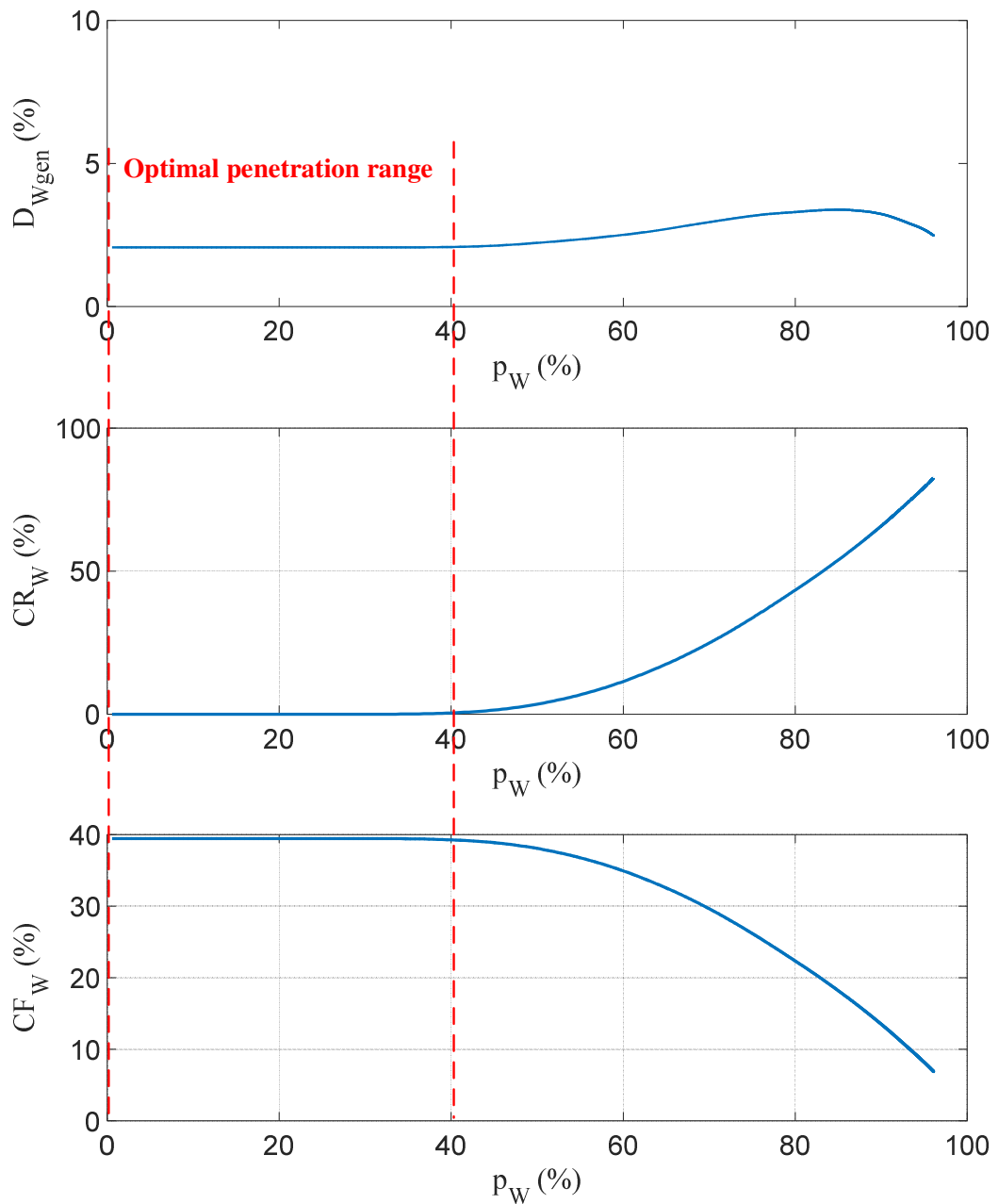
Figure 4.15 An example of an optimal penetration range (constant interval) for 20 interconnected wind farms with 100% grid flexibility.

Comparing the cumulative energy distribution index and the two economic parameters (curtailment rate and capacity factor) this study can find a similar constant interval with the increase of renewable energy penetration for interconnected wind or interconnected wind and solar power. However, with additional energy storage, the cumulative energy

distribution index will be reduced at any wind/solar energy penetration level, but the improvement of two economic parameters is observed only when the energy penetration level beyond the constant interval. Thus, the cumulative energy distribution index can be used to simplify the optimization of wind and solar energy penetration. Figure 4.15 shows an example of 20 interconnected wind farms with 100% grid flexibility. Generally, with the increase of wind energy penetration in the constant interval, system cost will increase quasi-linearly, because the wind energy curtailment and capacity factor keep constant within this penetration range. Furthermore, in this constant interval, adding energy storage will not reduce the system cost.

4.6 Novel calculation of variability costs

Figure 4.16 describes the process of the calculation of the variability costs for grid-connected wind and solar power systems. Note that the economic constraints of the variability cost have been assumed to the capacity factor and the curtailment rate of the wind and solar power. If the system can meet the economic requirements, the variability costs of the wind and solar power can be easily calculated via Eq. (4.9).
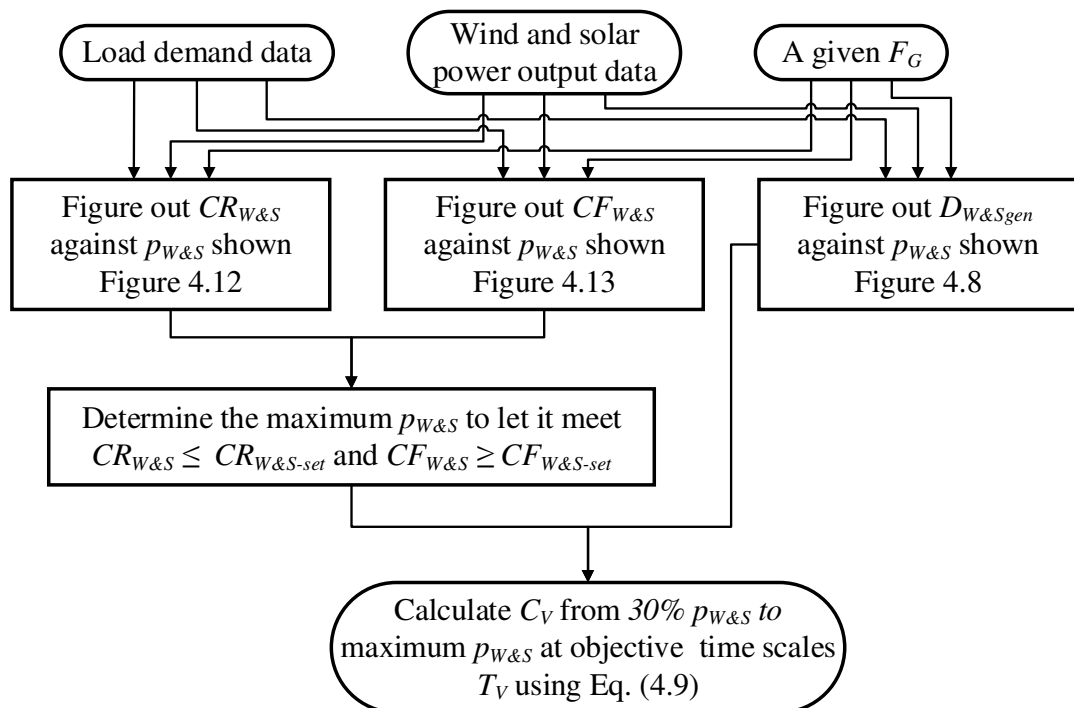
Figure 4.16 Calculating variability costs using the proposed approach.

The total economic costs are a primary concern of wind and solar power system operators. With variability costs of wind and solar power shifting from the end-user side to power generation and transmission side, exploring the variability cost caused by intermittent wind and solar power becomes particularly important. Due to proposed cumulative energy distribution index for renewable power can directly quantify power variations, so that the variability costs of renewable power can be described as

$$C_V = \frac{P_{BES} \cdot D_{REgen}(j) \cdot \sum_{i=1}^{8760} P_{REgen}(i)}{\sum_{i=1}^{8760} P_{REgen}(i)} = P_{BES} \cdot D_{REgen}(j) \tag{4.9}$$

where C_V is the variability costs, P_{BES} is the balancing energy services prices.

Generally, for economic considerations, for a renewable power system with determined grid flexibility, there are economic constraints for renewable energy curtailment rate and capacity factor:

$$CR_{RE} \leq CR_{RE-set}$$
$$CF_{RE} \geq CF_{RE-set} \tag{4.10}$$

where CR_{RE-set} is the specified maximum renewable energy curtailment, CF_{RE-set} is the specified minimum renewable power capacity factor.

A case study for 20 interconnected wind farms and 10 additional interconnected solar plants with 6/4 mixed proportion in assumed 70% grid flexibility ERCOT in 2008 demonstrate the calculation of variability costs. The process of the calculation is drawn as a flow chart in Figure 4.16. CR_{RE-set} and CF_{RE-set} have been reasonably set to 20% and 30% separately. According to Figure 4.12(d) and Figure 4.13(d), the maximum wind and solar energy penetration are limited to about 30% to meet these constraints. In addition, according to [102], P_{BES} of the ERCOT in 2008 is 53.54$/MWh. The results are listed in Table 1. It can be seen that, with the increase of selected time scale T_V for C_V, C_V increase significantly from average cost of 4.36$/MWh to the average cost of 11.6$/MWh. Meanwhile, with the increase of wind and solar power penetration, the C_V rises monotonously. Note that in this case study, this study assumes that only the power variation that below 6 hours will be charged. Due to the availability of the renewable energy source and load data, the highest resolution can only be 3-hour.

Table 4.1
3-hour to 6-hour variability costs with grid flexibility= 70%, 6/4 mixed wind/solar power system, and penetration level from 30% to maximum.

C_V (\$/MWh)	$p_{W\&S} = 30\%$	$p_{W\&S} = 35\%$	$p_{W\&S} = 40\%$	$p_{W\&S} = 45\%$	$p_{W\&S} = 50\%$
T_V = 3 hours	4.1	4.1	4.3	4.5	4.8
T_V = 4 hours	6.9	6.9	7.2	7.4	7.9
T_V = 5 hours	9.2	9.6	9.9	10.0	10.5
T_V = 6 hours	11.1	11.1	11.3	11.9	12.6

4.7 Summary

This chapter uses the proposed cumulative energy distribution index to measure the variability of wind and solar power in ERCOT. The cumulative energy distribution index is proved to have a similar constant interval of energy penetration to energy curtailment and capacity factor for wind and solar power. Within this constant interval, the increase in the wind and solar energy penetration will lead to quasi-linear growth of system costs. Therefore the cumulative energy distribution index can be used to determine the optimal wind and solar energy penetration range quickly. It found that adding energy storage can only effectively improve the wind and solar energy penetration when energy penetration beyond the constant interval. On the other hand, within the constant interval, increasing grid flexibility is an effective way to improve wind and solar penetration. Therefore, the cumulative energy distribution index can also provide a benchmark for the planning of energy storage or grid flexibility. Meanwhile, the impacts of grid flexibility and energy storage on wind and solar energy curtailment rate and wind and solar power capacity factor is revealed. It has been found from the study that

I.   Increasing grid flexibility can significantly reduce wind and solar energy curtailment rate and improve wind and solar power capacity factor. Subsequently, the maximum penetration of wind and solar energy can be improved. In addition, energy storage can only be an effective method to improve wind and solar energy penetration when the wind and solar energy penetration beyond the constant interval that determined via the proposed cumulative energy distribution index.

II.   Large scale interconnection of wind power can reduce wind energy curtailment rate, but only can improve wind power capacity factor when wind energy penetration exceeds a specific value.

III.   Interconnecting additional solar power plants will not bring much change to the wind and solar energy curtailment rate. Additional solar power plants only could reduce wind and solar power capacity factor at the low wind and solar energy penetration, and only could improve wind and solar power capacity factor when wind and solar energy penetration exceeds a certain value. Moreover, only with a specific mixed proportion of wind and solar power, the wind and solar power variations can be mitigated. For a hybrid system with a grid flexibility of 70%, the optimal wind/solar mixed proportion is 9/1.

IV.   The proposed cumulative energy distribution index can be used to simplify the variability cost for grid-connected wind and solar power.

Chapter 5

Conclusions and Future Work

5.1 Conclusions

This thesis explores the wind and/or solar power variability for optimal integration of wind and/or solar into power systems. The main contributions of this thesis include:

- In Chapter 2, a new measure is proposed to comprehensively analyze the variability of wind and/or solar power in both the time domain and frequency domain with implications for the optimal power system integration. In the time domain, the measure mainly includes inter-annual variation, smoothness coefficient and correlation coefficient; while in the frequency domain, it mainly includes frequency spectrum analysis, fluctuation rate, and cumulative energy distribution. Big-data variability analysis results of wind and/or solar power data are taken from two NREL databases indicate the dependence of wind and/or solar power variability on the geographic location latitude, the interconnection, the mixture, and the frequency distribution.

- In Chapter 3, this study explores the impacts of wind and/or solar variability on the optimal sizing of standalone wind and solar power systems. Based on the variability analysis of wind and/or solar power, the low-pass energy filtering capability of the battery and the power gap filling capability of the wind/solar power generators are investigated in the mitigation of wind/solar power variability. The proposed measurement parameters for wind/solar power variability are applied to the system sizing of standalone wind/solar power systems. Furthermore, big data simulations of six SAWP systems at six far apart sites across the USA and six SAPVP systems at six sites from latitude 0° to 50° across North and South America, provide QTI dependence of power supply reliability against the battery capacity and the PV panel/wind turbine size to quantify the impacts of wind/solar power variability on the system sizing. Case studies of optimal sizing of a SAWP system at Chicago and a SAPV system at Houston, are carried out to demonstrate the feasibility of the proposed approach.

- In Chapter 4, It explores the impacts of wind and/or solar variability on the penetration and integration costs of grid-connected wind and solar power. Big data simulations of the Electric Reliability Council of Texas power system (ERCOT) in 2018 reveal the proposed cumulative energy distribution index can be used to find the optimal range of wind and solar energy penetration for the cost-effective wind and solar power installation. In addition, the cumulative energy distribution index is used to quantify the impacts of wind and/or solar power variability on optimizing the variability costs for wind and/or solar power into the power grid.

Note that in this thesis, for the standalone wind/solar power system, this study only focuses on the typical residential load and for the grid-connected power system, due to the limit of data availability, the power grid used in this study is Electric Reliability Council of Texas power system (ERCOT). Thus, if the sizing method proposed in this thesis is used in a large-scale standalone network, such as an off-grid power system on an island with complex loads, the simulation results may be slightly different. However, due to the proposed sizing method is based on the variability of the wind and solar power, it can be expected that the proposed method is feasible for different standalone power systems. In addition, for some electricity markets that do not have short-term dynamic energy balancing prices, the proposed variability costs are not applicable.

5.2 Future work

Following research topics are expected to be done to advance the investigation in the future:

- Large historical wind datasets with high time resolution from a more extensive geographic context need to be analyzed to reaffirm the validity of current research outcomes.
- With more and more electric vehicles being plugged into the power grid as flexible loads, electric vehicles impose higher and higher impacts on the grid flexibility, which need to be considered for optimal grid integration of wind/solar power.
- Dynamic financial models are needed for the evaluation of grid integration costs of wind and/or solar power. For example, the interest rate and inflation rate should be considered in the calculation of system costs.

- The relationship between the variability of variable renewable energy and real risk rate need to be explored for evaluating the net present value and the payback period of variable renewable energy.

Appendix A

Table A.1
Inter-annual hybrid wind and solar power variations at the six sites for the year 1998.

$I_{W\&S}(y)$ / S/W ratio	Location					
	Quito	Valencia	Mexico City	Houston	Salt Lake City	Vancouver
0%	0.88	0.81	1.39	1.2	0.95	1.09
10%	0.90	0.83	1.36	1.18	0.95	1.08
20%	0.91	0.85	1.32	1.16	0.95	1.06
30%	0.92	0.87	1.29	1.14	0.95	1.05
40%	0.94	0.89	1.26	1.13	0.95	1.04
50%	0.95	0.91	1.22	1.11	0.95	1.02
60%	0.96	0.93	1.19	1.09	0.95	1.01
70%	0.97	0.95	1.15	1.08	0.95	0.99
80%	0.99	0.97	1.12	1.06	0.95	0.98
90%	1.00	0.99	1.08	1.04	0.95	0.96
100%	1.01	1.01	1.05	1.02	0.95	0.95

Table A.2
Inter-annual hybrid wind and solar power variations at the six sites for the year 1999.

$I_{W\&S}(y)$ / S/W ratio	Location					
	Quito	Valencia	Mexico City	Houston	Salt Lake City	Vancouver
0%	1.00	0.91	1.25	1.03	1.07	1.20
10%	1.00	0.92	1.23	1.04	1.07	1.17
20%	1.00	0.93	1.21	1.04	1.06	1.14
30%	1.00	0.94	1.18	1.04	1.06	1.11
40%	1.00	0.95	1.16	1.04	1.05	1.09
50%	1.00	0.97	1.14	1.05	1.05	1.06
60%	0.99	0.98	1.12	1.05	1.04	1.03
70%	0.99	0.99	1.10	1.05	1.04	1.00
80%	0.99	1.00	1.08	1.05	1.03	0.97
90%	0.99	1.01	1.05	1.06	1.03	0.95
100%	0.99	1.03	1.03	1.06	1.02	0.92

Table A.3
Inter-annual hybrid wind and solar power variations at the six sites for the year 2000.

$I_{W\&S}(y)$ / S/W ratio	Location					
	Quito	Valencia	Mexico City	Houston	Salt Lake City	Vancouver
0%	0.96	0.9	1.05	1.14	1.03	1.00
10%	0.97	0.92	1.05	1.13	1.03	1.00
20%	0.98	0.93	1.05	1.12	1.03	0.99
30%	0.98	0.95	1.04	1.11	1.03	0.99
40%	0.99	0.96	1.04	1.10	1.02	0.98
50%	0.99	0.97	1.04	1.09	1.02	0.98
60%	1.00	0.99	1.04	1.09	1.02	0.97
70%	1.01	1.00	1.04	1.08	1.02	0.97
80%	1.01	1.02	1.04	1.07	1.02	0.96
90%	1.02	1.03	1.03	1.06	1.02	0.96
100%	1.02	1.04	1.03	1.05	1.02	0.95

Table A.4
Inter-annual hybrid wind and solar power variations at the six sites for the year 2001.

$I_{W\&S}(y)$ / S/W ratio	Location					
	Quito	Valencia	Mexico City	Houston	Salt Lake City	Vancouver
0%	0.91	1.07	1.06	0.89	0.98	1.04
10%	0.92	1.07	1.05	0.90	0.98	1.04
20%	0.94	1.07	1.05	0.91	0.99	1.03
30%	0.96	1.07	1.04	0.92	1.00	1.03
40%	0.97	1.07	1.04	0.93	1.00	1.02
50%	0.99	1.07	1.04	0.94	1.01	1.02
60%	1.01	1.07	1.03	0.94	1.02	1.01
70%	1.03	1.07	1.03	0.95	1.03	1.00
80%	1.04	1.07	1.02	0.96	1.03	1.00
90%	1.06	1.07	1.02	0.97	1.04	0.99
100%	1.08	1.07	1.02	0.98	1.05	0.99

Table A.5
Inter-annual hybrid wind and solar power variations at the six sites for the year 2002.

$I_{W\&S}(y)$ / S/W ratio	Location					
	Quito	Valencia	Mexico City	Houston	Salt Lake City	Vancouver
0%	0.91	1.05	0.95	1.09	0.93	0.93
10%	0.93	1.05	0.96	1.08	0.94	0.95
20%	0.94	1.05	0.97	1.07	0.95	0.96
30%	0.96	1.05	0.97	1.06	0.97	0.98
40%	0.98	1.05	0.98	1.05	0.98	1.00
50%	1.00	1.05	0.99	1.04	1.00	1.02
60%	1.01	1.05	0.99	1.03	1.01	1.04
70%	1.03	1.06	1.00	1.02	1.02	1.06
80%	1.05	1.06	1.01	1.01	1.04	1.07
90%	1.07	1.06	1.02	0.99	1.05	1.09
100%	1.09	1.06	1.02	0.98	1.07	1.11

Table A.6
Inter-annual hybrid wind and solar power variations at the six sites for the year 2003.

$I_{W\&S}(y)$ / S/W ratio	Location					
	Quito	Valencia	Mexico City	Houston	Salt Lake City	Vancouver
0%	0.96	0.93	0.97	0.90	0.98	0.98
10%	0.97	0.94	0.98	0.90	0.98	0.99
20%	0.97	0.95	0.98	0.91	0.98	0.99
30%	0.98	0.95	0.98	0.92	0.99	1.00
40%	0.99	0.96	0.98	0.92	0.99	1.01
50%	0.99	0.96	0.99	0.93	1.00	1.01
60%	1.00	0.97	0.99	0.94	1.00	1.02
70%	1.00	0.98	0.99	0.94	1.00	1.02
80%	1.01	0.98	1.00	0.95	1.01	1.03
90%	1.02	0.99	1.00	0.95	1.01	1.04
100%	1.02	1.00	1.00	0.96	1.02	1.04

Table A.7
Inter-annual hybrid wind and solar power variations at the six sites for the year 2004.

$I_{W\&S}(y)$ / S/W ratio	Location					
	Quito	Valencia	Mexico City	Houston	Salt Lake City	Vancouver
0%	1.00	1.09	1.05	0.93	0.91	0.83
10%	1.00	1.08	1.04	0.93	0.92	0.85
20%	1.01	1.07	1.03	0.93	0.93	0.88
30%	1.01	1.06	1.03	0.93	0.94	0.90
40%	1.01	1.05	1.02	0.93	0.95	0.92
50%	1.02	1.05	1.01	0.93	0.96	0.94
60%	1.02	1.04	1.01	0.93	0.97	0.96
70%	1.03	1.03	1.00	0.93	0.98	0.98
80%	1.03	1.02	0.99	0.93	0.99	1.01
90%	1.03	1.01	0.99	0.94	1.00	1.03
100%	1.04	1.00	0.98	0.94	1.01	1.05

Table A.8
Inter-annual hybrid wind and solar power variations at the six sites for the year 2005.

$I_{W\&S}(y)$ / S/W ratio	Location					
	Quito	Valencia	Mexico City	Houston	Salt Lake City	Vancouver
0%	1.10	0.94	1.14	0.85	0.98	0.90
10%	1.09	0.95	1.12	0.87	0.98	0.91
20%	1.08	0.95	1.11	0.89	0.98	0.92
30%	1.07	0.96	1.09	0.91	0.98	0.92
40%	1.06	0.96	1.08	0.93	0.99	0.93
50%	1.05	0.97	1.06	0.94	0.99	0.94
60%	1.04	0.97	1.05	0.96	0.99	0.95
70%	1.03	0.98	1.03	0.98	0.99	0.95
80%	1.02	0.98	1.02	1.00	0.99	0.96
90%	1.01	0.99	1.00	1.02	0.99	0.97
100%	1.00	1.00	0.99	1.04	1.00	0.98

Table A.9
Inter-annual hybrid wind and solar power variations at the six sites for the year 2006.

$I_{W\&S}(y)$ / S/W ratio	Location					
	Quito	Valencia	Mexico City	Houston	Salt Lake City	Vancouver
0%	1.04	0.97	0.96	0.95	1.03	1.18
10%	1.03	0.97	0.97	0.95	1.03	1.17
20%	1.02	0.98	0.97	0.96	1.03	1.15
30%	1.02	0.98	0.97	0.96	1.03	1.14
40%	1.01	0.98	0.97	0.97	1.02	1.12
50%	1.01	0.98	0.98	0.97	1.02	1.11
60%	1.00	0.98	0.98	0.98	1.02	1.09
70%	1.00	0.98	0.98	0.99	1.02	1.08
80%	0.99	0.98	0.99	0.99	1.02	1.06
90%	0.98	0.98	0.99	1.00	1.01	1.05
100%	0.98	0.98	0.99	1.00	1.01	1.03

Table A.10
Inter-annual hybrid wind and solar power variations at the six sites for the year 2007.

$I_{W\&S}(y)$ / S/W ratio	Location					
	Quito	Valencia	Mexico City	Houston	Salt Lake City	Vancouver
0%	1.07	1.02	0.82	0.75	0.97	0.95
10%	1.06	1.02	0.83	0.77	0.97	0.95
20%	1.05	1.02	0.85	0.79	0.98	0.95
30%	1.04	1.02	0.87	0.81	0.99	0.94
40%	1.04	1.01	0.88	0.82	1.00	0.94
50%	1.03	1.01	0.90	0.84	1.00	0.94
60%	1.02	1.01	0.92	0.86	1.01	0.93
70%	1.02	1.00	0.94	0.88	1.02	0.93
80%	1.01	1.00	0.95	0.9	1.03	0.93
90%	1.00	1.00	0.97	0.92	1.03	0.92
100%	1.00	0.99	0.99	0.93	1.04	0.92

Table A.11
Inter-annual hybrid wind and solar power variations at the six sites for the year 2008.

$I_{W\&S}(y)$ S/W ratio	Location					
	Quito	Valencia	Mexico City	Houston	Salt Lake City	Vancouver
0%	1.09	1.12	0.94	1.18	1.10	0.98
10%	1.07	1.11	0.94	1.17	1.09	0.98
20%	1.05	1.10	0.95	1.15	1.08	0.98
30%	1.03	1.09	0.95	1.13	1.07	0.98
40%	1.01	1.08	0.96	1.12	1.06	0.97
50%	0.99	1.08	0.96	1.10	1.06	0.97
60%	0.97	1.07	0.96	1.08	1.05	0.97
70%	0.95	1.06	0.97	1.07	1.04	0.97
80%	0.93	1.05	0.97	1.05	1.03	0.97
90%	0.91	1.04	0.97	1.03	1.02	0.96
100%	0.89	1.03	0.98	1.02	1.01	0.96

Table A.12
Inter-annual hybrid wind and solar power variations at the six sites for the year 2009.

$I_{W\&S}(y)$ S/W ratio	Location					
	Quito	Valencia	Mexico City	Houston	Salt Lake City	Vancouver
0%	1.09	1.16	0.95	1.09	0.93	0.98
10%	1.08	1.14	0.95	1.08	0.93	0.99
20%	1.07	1.13	0.96	1.07	0.94	1.00
30%	1.06	1.11	0.97	1.06	0.94	1.01
40%	1.05	1.09	0.97	1.05	0.95	1.02
50%	1.04	1.08	0.98	1.03	0.95	1.03
60%	1.03	1.06	0.98	1.02	0.96	1.04
70%	1.01	1.04	0.99	1.01	0.96	1.05
80%	1.00	1.02	1.00	1.00	0.97	1.06
90%	0.99	1.01	1.00	0.99	0.97	1.07
100%	0.98	0.99	1.01	0.97	0.98	1.08

Table A.13
Inter-annual hybrid wind and solar power variations at the six sites for the year 2010.

$I_{W\&S}(y)$ / S/W ratio	Location					
	Quito	Valencia	Mexico City	Houston	Salt Lake City	Vancouver
0%	1.00	0.69	1.34	1.01	1.09	1.11
10%	1.00	0.71	1.31	1.01	1.07	1.09
20%	0.99	0.74	1.27	1.01	1.06	1.08
30%	0.98	0.76	1.24	1.01	1.05	1.07
40%	0.98	0.79	1.21	1.01	1.03	1.06
50%	0.97	0.81	1.17	1.02	1.02	1.05
60%	0.97	0.84	1.14	1.02	1.01	1.04
70%	0.96	0.86	1.1	1.02	0.99	1.03
80%	0.96	0.89	1.07	1.02	0.98	1.02
90%	0.95	0.91	1.03	1.03	0.97	1.01
100%	0.95	0.94	1.00	1.03	0.95	1.00

Table A.14
Inter-annual hybrid wind and solar power variations at the six sites for the year 2011.

$I_{W\&S}(y)$ / S/W ratio	Location					
	Quito	Valencia	Mexico City	Houston	Salt Lake City	Vancouver
0%	1.12	0.84	0.96	1.38	0.98	0.98
10%	1.11	0.85	0.97	1.35	0.98	0.98
20%	1.1	0.86	0.98	1.32	0.98	0.97
30%	1.08	0.87	0.99	1.29	0.97	0.96
40%	1.07	0.88	1.00	1.26	0.97	0.96
50%	1.06	0.88	1.01	1.24	0.96	0.95
60%	1.05	0.89	1.02	1.21	0.96	0.95
70%	1.04	0.90	1.03	1.18	0.95	0.94
80%	1.03	0.91	1.04	1.15	0.95	0.93
90%	1.02	0.92	1.05	1.12	0.95	0.93
100%	1.00	0.93	1.06	1.10	0.94	0.92

Table A.15
Inter-annual hybrid wind and solar power variations at the six sites for the year 2012.

$I_{W\&S}(y)$ / S/W ratio	Location					
	Quito	Valencia	Mexico City	Houston	Salt Lake City	Vancouver
0%	0.96	0.75	0.86	0.88	1.17	1.03
10%	0.96	0.77	0.87	0.89	1.15	1.02
20%	0.96	0.79	0.88	0.91	1.13	1.01
30%	0.97	0.81	0.89	0.92	1.12	1.00
40%	0.97	0.83	0.91	0.93	1.10	0.99
50%	0.97	0.85	0.92	0.95	1.08	0.97
60%	0.98	0.87	0.93	0.96	1.06	0.96
70%	0.98	0.89	0.94	0.98	1.05	0.95
80%	0.98	0.91	0.96	0.99	1.03	0.94
90%	0.99	0.93	0.97	1.01	1.01	0.93
100%	0.99	0.95	0.98	1.02	1.00	0.91

Table A.16
Inter-annual hybrid wind and solar power variations at the six sites for the year 2013.

$I_{W\&S}(y)$ / S/W ratio	Location					
	Quito	Valencia	Mexico City	Houston	Salt Lake City	Vancouver
0%	1.01	0.94	0.94	1.08	0.89	0.76
10%	1.01	0.95	0.95	1.07	0.90	0.78
20%	1.01	0.95	0.95	1.07	0.90	0.81
30%	1.01	0.96	0.96	1.06	0.91	0.83
40%	1.01	0.97	0.96	1.05	0.92	0.85
50%	1.02	0.97	0.97	1.05	0.93	0.88
60%	1.02	0.98	0.97	1.04	0.94	0.90
70%	1.02	0.99	0.98	1.03	0.95	0.92
80%	1.02	0.99	0.98	1.02	0.96	0.94
90%	1.02	1.00	0.99	1.02	0.96	0.97
100%	1.03	1.01	0.99	1.01	0.97	0.99

Table A.17
Inter-annual hybrid wind and solar power variations at the six sites for the year 2014.

$I_{W\&S}(y)$ S/W ratio	Location					
	Quito	Valencia	Mexico City	Houston	Salt Lake City	Vancouver
0%	1.00	1.12	0.73	1.00	1.00	0.98
10%	1.00	1.11	0.75	1.00	1.00	0.98
20%	1.00	1.10	0.78	1.00	1.00	0.99
30%	0.99	1.09	0.80	0.99	1.00	1.00
40%	0.99	1.08	0.82	0.99	0.99	1.00
50%	0.99	1.07	0.84	0.98	0.99	1.01
60%	0.99	1.06	0.86	0.98	0.99	1.01
70%	0.98	1.05	0.89	0.97	0.99	1.02
80%	0.98	1.04	0.91	0.97	0.98	1.02
90%	0.98	1.03	0.93	0.96	0.98	1.03
100%	0.98	1.02	0.95	0.96	0.98	1.03

Table A.18
Inter-annual hybrid wind and solar power variations at the six sites for the year 2015.

$I_{W\&S}(y)$ S/W ratio	Location					
	Quito	Valencia	Mexico City	Houston	Salt Lake City	Vancouver
0%	0.84	1.24	0.73	0.80	0.88	0.80
10%	0.86	1.22	0.75	0.82	0.89	0.82
20%	0.88	1.20	0.77	0.83	0.90	0.85
30%	0.90	1.17	0.80	0.85	0.91	0.88
40%	0.92	1.15	0.82	0.86	0.92	0.91
50%	0.94	1.13	0.84	0.88	0.93	0.94
60%	0.96	1.10	0.86	0.89	0.94	0.97
70%	0.98	1.08	0.88	0.91	0.96	1.00
80%	1.00	1.06	0.91	0.92	0.97	1.02
90%	1.02	1.03	0.93	0.93	0.98	1.05
100%	1.04	1.01	0.95	0.95	0.99	1.08

Table A.19
Inter-annual hybrid wind and solar power variations at the six sites for the year 2016.

$I_{W\&S}(y)$ / S/W ratio	Location					
	Quito	Valencia	Mexico City	Houston	Salt Lake City	Vancouver
0%	1.09	1.27	1.02	0.82	1.03	1.12
10%	1.08	1.25	1.01	0.84	1.03	1.11
20%	1.07	1.22	1.01	0.85	1.02	1.10
30%	1.05	1.19	1.00	0.87	1.02	1.09
40%	1.04	1.16	1.00	0.88	1.02	1.08
50%	1.03	1.13	0.99	0.90	1.01	1.07
60%	1.02	1.10	0.99	0.91	1.01	1.07
70%	1.01	1.07	0.98	0.93	1.01	1.06
80%	1.00	1.04	0.98	0.94	1.01	1.05
90%	0.99	1.01	0.97	0.96	1.00	1.04
100%	0.98	0.98	0.97	0.97	1.00	1.03

Table A.20
S **varies with the different mixed proportions of solar/wind power at Quito from 2007 to 2012.**

S / Year	Mixed proportions of solar/wind power									
	0.1	0.2	0.3	0.4	0.5	0.6	0.7	0.8	0.9	1.0
2007	0.11	0.19	0.23	0.21	0.15	0.05	-0.07	-0.22	-0.38	-0.54
2008	0.11	0.19	0.24	0.24	0.20	0.13	0.03	-0.10	-0.23	-0.38
2009	0.11	0.19	0.22	0.21	0.15	0.05	-0.07	-0.21	-0.36	-0.53
2010	0.10	0.18	0.22	0.21	0.17	0.09	-0.02	-0.15	-0.29	-0.45
2011	0	0.11	0.19	0.23	0.21	0.15	0.06	-0.06	-0.20	-0.35
2012	0	0.10	0.16	0.19	0.18	0.12	0.04	-0.07	-0.20	-0.34

Table A.21
S **varies with the different mixed proportions of solar/wind power at Valencia from 2007 to 2012.**

S \ Year	Mixed proportions of solar/wind power									
	0.1	0.2	0.3	0.4	0.5	0.6	0.7	0.8	0.9	1.0
2007	0.04	0.04	0.00	-0.08	-0.19	-0.33	-0.48	-0.64	-0.81	-0.99
2008	0.04	0.03	-0.02	-0.11	-0.24	-0.38	-0.54	-0.71	-0.89	-1.07
2009	0.05	0.05	0.01	-0.07	-0.18	-0.31	-0.46	-0.62	-0.79	-0.97
2010	0.02	0.00	-0.05	-0.13	-0.24	-0.37	-0.51	-0.66	-0.81	-0.98
2011	0.03	0.02	-0.03	-0.11	-0.22	-0.35	-0.49	-0.64	-0.80	-0.97
2012	0.03	0.03	-0.02	-0.10	-0.20	-0.33	-0.47	-0.62	-0.78	-0.95

Table A.22
S **varies with the different mixed proportions of solar/wind power at Mexico City from 2007 to 2012.**

S \ Year	Mixed proportions of solar/wind power									
	0.1	0.2	0.3	0.4	0.5	0.6	0.7	0.8	0.9	1.0
2007	0.03	0.00	-0.06	-0.17	-0.30	-0.45	-0.62	-0.80	-0.98	-1.17
2008	0.03	0.02	-0.04	-0.14	-0.27	-0.42	-0.59	-0.77	-0.95	-1.15
2009	0.03	0.02	-0.05	-0.16	-0.29	-0.45	-0.63	-0.82	-1.01	-1.21
2010	0.06	0.06	0.01	-0.08	-0.22	-0.37	-0.55	-0.74	-0.93	-1.14
2011	0.02	-0.01	-0.08	-0.19	-0.33	-0.49	-0.67	-0.85	-1.04	-1.24
2012	0.02	0.00	-0.07	-0.17	-0.30	-0.46	-0.62	-0.80	-0.98	-1.17

Table A.23

S varies with the different mixed proportions of solar/wind power at Salt Lake City from 2007 to 2012.

Year \ S	Mixed proportions of solar/wind power									
	0.1	0.2	0.3	0.4	0.5	0.6	0.7	0.8	0.9	1.0
2007	0.00	-0.15	-0.39	-0.69	-1.03	-1.38	-1.74	-2.11	-2.48	-2.86
2008	0.01	-0.13	-0.37	-0.66	-0.99	-1.33	-1.69	-2.05	-2.42	-2.80
2009	0.03	-0.09	-0.31	-0.59	-0.91	-1.25	-1.60	-1.95	-2.32	-2.68
2010	0.03	-0.09	-0.30	-0.58	-0.90	-1.23	-1.58	-1.93	-2.29	-2.65
2011	0.01	-0.10	-0.31	-0.57	-0.87	-1.19	-1.52	-1.86	-2.21	-2.55
2012	0.01	-0.12	-0.34	-0.63	-0.95	-1.29	-1.64	-2.00	-2.37	-2.74

Table A.24
S varies with the different mixed proportions of solar/wind power at Vancouver from 2007 to 2012.

Year \ S	Mixed proportions of solar/wind power									
	0.1	0.2	0.3	0.4	0.5	0.6	0.7	0.8	0.9	1.0
2007	0.10	0.12	0.06	-0.06	-0.23	-0.44	-0.66	-0.89	-1.13	-1.38
2008	0.10	0.12	0.05	-0.08	-0.26	-0.47	-0.70	-0.94	-1.19	-1.45
2009	0.10	0.11	0.02	-0.14	-0.35	-0.58	-0.84	-1.10	-1.37	-1.65
2010	0.09	0.10	0.03	-0.11	-0.30	-0.52	-0.75	-1.00	-1.25	-1.51
2011	0.10	0.12	0.06	-0.07	-0.24	-0.44	-0.66	-0.90	-1.14	-1.39
2012	0.10	0.12	0.05	-0.08	-0.26	-0.46	-0.69	-0.93	-1.17	-1.42

Appendix B

Table B.1
Average power supply reliability $R_{W\&Savg}$ versus active battery capacity B_{ac} with wind and solar mixed ratio varies from 100% to 0% for the years of 1998 to 2017 at Valencia.

$R_{W\&Savg}$ / B_{ac}	W/S mixed ratio										
	100%	**90%**	**80%**	**70%**	**60%**	**50%**	**40%**	**30%**	**20%**	**10%**	**0%**
1	63.06	**64.18**	63.98	63.30	62.36	61.23	59.64	57.42	54.16	48.85	42.71
2	66.75	**67.92**	67.91	67.27	66.42	65.32	63.73	61.75	58.73	53.56	46.57
3	68.00	69.12	**69.17**	68.62	67.84	66.76	65.39	63.48	60.49	55.26	46.91
4	69.66	70.80	**70.98**	70.53	69.80	68.81	67.52	65.71	62.84	57.77	50.15
5	70.56	71.71	**71.95**	71.67	71.01	70.02	68.74	66.94	64.12	59.03	51.99
6	71.79	72.98	**73.29**	73.04	72.43	71.61	70.41	68.69	66.09	61.22	53.14
7	72.75	73.98	**74.38**	74.32	73.78	73.08	71.92	70.24	67.64	62.80	55.94
8	73.76	75.00	**75.48**	75.39	75.01	74.30	73.25	71.62	69.13	64.38	56.96
9	74.71	75.98	76.52	**76.56**	76.30	75.71	74.77	73.29	70.99	66.48	58.18
10	75.58	76.93	77.54	**77.68**	77.56	77.07	76.17	74.74	72.38	67.94	60.26
11	76.70	78.04	78.68	**78.88**	78.81	78.47	77.65	76.26	74.01	69.76	61.70
12	78.31	79.76	80.52	80.92	**81.06**	80.95	80.41	79.24	77.23	73.22	63.94
13	80.11	81.65	82.54	83.10	83.44	**83.62**	83.34	82.46	80.66	76.99	68.48
14	81.71	83.32	84.32	85.00	85.53	85.94	**85.99**	85.46	83.98	80.63	71.74
15	82.99	84.66	85.73	86.53	87.19	87.81	**88.12**	87.96	86.88	84.00	74.92
16	83.97	85.66	86.76	87.56	88.32	89.08	89.57	**89.65**	88.96	86.51	78.35
17	84.59	86.30	87.43	88.30	89.10	89.88	90.50	**90.75**	90.30	88.25	81.07
18	85.06	86.76	87.88	88.77	89.63	90.45	91.09	**91.45**	91.17	89.42	83.38
19	85.45	87.17	88.27	89.17	90.04	90.86	91.56	**91.97**	91.78	90.33	84.82
20	85.77	87.49	88.65	89.54	90.40	91.23	91.95	**92.39**	92.3	91.06	86.24
21	86.11	87.75	88.96	89.84	90.72	91.58	92.29	**92.74**	92.73	91.6	87.41
22	86.41	88.06	89.22	90.10	91.00	91.85	92.56	93.00	**93.05**	92.08	88.26
23	86.66	88.30	89.47	90.38	91.24	92.13	92.84	93.28	**93.29**	92.41	88.98
24	86.91	88.56	89.70	90.62	91.50	92.32	93.05	93.46	**93.51**	92.67	89.54
25	87.16	88.80	89.95	90.84	91.70	92.54	93.23	93.67	**93.72**	92.90	89.86
26	87.42	89.02	90.18	91.04	91.88	92.71	93.39	93.82	**93.88**	93.06	90.09
27	87.65	89.26	90.38	91.23	92.09	92.89	93.55	93.96	**94.02**	93.23	90.30
28	87.86	89.45	90.58	91.44	92.27	93.05	93.68	94.11	**94.15**	93.38	90.48
29	88.05	89.65	90.75	91.61	92.41	93.19	93.82	94.20	**94.27**	93.51	90.66
30	88.27	89.85	90.91	91.75	92.56	93.32	93.95	94.31	**94.38**	93.62	90.77
31	88.43	89.97	91.10	91.92	92.68	93.43	94.09	94.44	**94.49**	93.72	90.92
32	88.62	90.14	91.24	92.07	92.84	93.58	94.19	94.53	**94.61**	93.82	91.01
33	88.77	90.31	91.40	92.22	92.98	93.71	94.28	94.65	**94.68**	93.90	91.12
34	88.94	90.44	91.53	92.35	93.10	93.81	94.38	94.74	**94.75**	93.99	91.21
35	89.11	90.58	91.67	92.47	93.23	93.89	94.46	94.81	**94.85**	94.08	91.28
36	89.26	90.72	91.83	92.62	93.36	94.01	94.54	94.88	**94.93**	94.15	91.38
37	89.41	90.88	91.95	92.74	93.46	94.12	94.62	94.96	**95.00**	94.21	91.45
38	89.51	91.00	92.08	92.84	93.56	94.20	94.69	95.05	**95.08**	94.29	91.53
39	89.67	91.13	92.18	92.96	93.62	94.27	94.77	95.12	**95.12**	94.34	91.60
40	89.78	91.29	92.31	93.06	93.72	94.34	94.85	95.16	**95.18**	94.41	91.65
41	89.93	91.39	92.41	93.14	93.81	94.42	94.92	95.24	**95.26**	94.46	91.72
42	90.05	91.49	92.49	93.20	93.88	94.51	94.99	95.29	**95.30**	94.51	91.77
43	90.17	91.61	92.59	93.30	93.96	94.57	95.06	95.36	**95.37**	94.56	91.84

44	90.30	91.73	92.66	93.39	94.02	94.64	95.10	95.41	**95.41**	94.60	91.90
45	90.40	91.81	92.76	93.47	94.10	94.69	95.18	95.46	**95.48**	94.65	91.95
46	90.54	91.93	92.84	93.55	94.20	94.77	95.22	95.49	**95.52**	94.71	91.99
47	90.63	91.99	92.94	93.62	94.25	94.84	95.30	95.55	**95.57**	94.74	92.05
48	90.72	92.09	93.01	93.70	94.31	94.90	95.31	95.60	**95.61**	94.77	92.09
49	90.84	92.18	93.09	93.78	94.39	94.97	95.37	95.65	**95.66**	94.83	92.16
50	90.94	92.25	93.18	93.82	94.45	95.00	95.42	95.69	**95.72**	94.85	92.19
51	91.04	92.33	93.24	93.92	94.49	95.05	95.47	95.74	**95.74**	94.90	92.24
52	91.10	92.40	93.33	93.97	94.57	95.09	95.52	95.77	**95.77**	94.94	92.27
53	91.21	92.51	93.39	94.03	94.64	95.16	95.55	95.83	**95.82**	94.97	92.32
54	91.29	92.56	93.46	94.10	94.67	95.20	95.59	95.86	**95.87**	95.00	92.36
55	91.36	92.66	93.55	94.18	94.71	95.25	95.65	**95.91**	95.88	95.03	92.40
56	91.44	92.72	93.60	94.21	94.78	95.29	95.70	**95.94**	95.92	95.06	92.44
57	91.51	92.79	93.65	94.26	94.81	95.33	95.71	**95.97**	95.94	95.12	92.49
58	91.60	92.86	93.70	94.30	94.85	95.37	95.76	**96.00**	95.98	95.15	92.52
59	91.68	92.93	93.77	94.36	94.89	95.39	95.80	**96.04**	96.02	95.19	92.55
60	91.74	92.97	93.82	94.42	94.95	95.47	95.82	**96.07**	96.05	95.20	92.59
61	91.81	93.03	93.85	94.47	94.97	95.46	95.85	**96.11**	96.10	95.24	92.63
62	91.88	93.09	93.91	94.50	95.01	95.53	95.89	**96.13**	96.14	95.27	92.65
63	91.95	93.15	93.96	94.57	95.06	95.56	95.92	**96.17**	96.16	95.30	92.69
64	92.00	93.21	94.02	94.57	95.11	95.57	95.95	**96.21**	96.19	95.32	92.74
65	92.07	93.26	94.06	94.64	95.15	95.60	95.98	**96.22**	96.20	95.33	92.75
66	92.12	93.29	94.10	94.68	95.18	95.64	96.02	**96.26**	96.23	95.36	92.78
67	92.17	93.34	94.13	94.68	95.20	95.66	96.04	**96.30**	96.26	95.38	92.78
68	92.25	93.38	94.18	94.74	95.24	95.71	96.07	**96.33**	96.30	95.41	92.85
69	92.30	93.43	94.19	94.78	95.27	95.73	96.09	**96.35**	96.31	95.44	92.87
70	92.34	93.47	94.25	94.81	95.27	95.75	96.13	**96.39**	96.33	95.47	92.91
71	92.39	93.53	94.29	94.82	95.31	95.79	96.16	**96.40**	96.36	95.50	92.92
72	92.45	93.56	94.32	94.86	95.34	95.82	96.18	**96.42**	96.39	95.51	92.95
73	92.51	93.60	94.36	94.91	95.38	95.85	96.20	**96.43**	96.41	95.53	92.98
74	92.56	93.65	94.39	94.92	95.40	95.86	96.23	**96.47**	96.44	95.57	93.00
75	92.59	93.69	94.43	94.98	95.44	95.90	96.23	**96.49**	96.46	95.59	93.04
76	92.64	93.73	94.48	95.02	95.46	95.92	96.27	**96.53**	96.48	95.62	93.06
77	92.68	93.74	94.52	95.03	95.49	95.95	96.29	**96.53**	96.52	95.63	93.10
78	92.73	93.79	94.54	95.06	95.52	95.96	96.32	**96.56**	96.53	95.65	93.14
79	92.77	93.84	94.58	95.10	95.53	95.97	96.34	**96.60**	96.55	95.67	93.14
80	92.81	93.87	94.61	95.12	95.57	96.01	96.37	**96.61**	96.59	95.70	93.16
81	92.85	93.90	94.64	95.13	95.60	96.03	96.40	**96.63**	96.62	95.72	93.19
82	92.88	93.94	94.65	95.16	95.61	96.04	96.40	**96.65**	96.62	95.76	93.19
83	92.90	93.96	94.67	95.20	95.65	96.08	96.42	**96.67**	96.67	95.78	93.24
84	92.96	94.01	94.72	95.23	95.67	96.11	96.46	**96.69**	96.69	95.82	93.27
85	93.00	94.03	94.75	95.25	95.69	96.12	96.47	**96.71**	96.71	95.82	93.29
86	93.01	94.08	94.76	95.28	95.71	96.13	96.49	**96.72**	96.75	95.86	93.34
87	93.07	94.10	94.79	95.30	95.73	96.15	96.51	**96.75**	96.74	95.87	93.33
88	93.11	94.12	94.81	95.34	95.74	96.19	96.52	**96.77**	**96.77**	95.87	93.38
89	93.13	94.18	94.84	95.37	95.77	96.20	96.52	**96.79**	**96.79**	95.91	93.39
90	93.17	94.20	94.88	95.39	95.77	96.21	96.56	96.80	**96.82**	95.93	93.41
91	93.20	94.23	94.90	95.40	95.79	96.23	96.57	96.83	**96.82**	95.96	93.41
92	93.24	94.24	94.92	95.43	95.82	96.23	96.57	96.83	**96.87**	95.98	93.46
93	93.25	94.28	94.95	95.44	95.84	96.28	96.60	96.87	**96.86**	96.00	93.47
94	93.30	94.31	94.96	95.45	95.86	96.28	96.61	96.88	**96.89**	96.03	93.49
95	93.33	94.34	95.00	95.49	95.89	96.29	96.63	96.90	**96.90**	96.04	93.52
96	93.38	94.36	95.02	95.50	95.90	96.31	96.64	96.92	**96.93**	96.06	93.56

97	93.40	94.37	95.05	95.51	95.92	96.33	96.65	96.92	**96.94**	96.10	93.57
98	93.43	94.41	95.07	95.54	95.95	96.34	96.69	96.94	**96.95**	96.11	93.59
99	93.47	94.43	95.11	95.55	95.96	96.36	96.70	96.95	**96.98**	96.13	93.61
100	93.46	94.47	95.13	95.57	95.98	96.38	96.71	96.97	**96.99**	96.15	93.64

Table B.2
Average power supply reliability $R_{W\&Savg}$ versus active battery capacity B_{ac} with wind and solar mixed ratio varies from 100% to 0% for the years of 1998 to 2017 at Mexico City.

$R_{W\&Savg}$	W/S mixed ratio										
B_{ac}	100%	90%	80%	70%	60%	50%	40%	30%	20%	10%	0%
1	57.07	59.46	**59.85**	58.99	57.75	56.24	54.42	52.21	49.54	46.43	42.22
2	61.51	64.07	**64.75**	63.97	62.71	61.13	59.3	57.04	54.23	50.79	46.37
3	63.27	65.81	**66.41**	65.73	64.41	62.75	60.83	58.44	55.53	51.95	47.16
4	64.83	67.31	**68.12**	67.44	66.15	64.67	62.76	60.43	57.63	53.97	49.73
5	66.05	68.59	**69.51**	69.11	68.00	66.45	64.57	62.25	59.44	56.04	51.61
6	67.28	69.86	**70.89**	70.61	69.5	67.86	66.09	63.80	60.86	57.25	52.63
7	68.45	71.13	**72.23**	72.12	71.33	69.98	68.30	66.02	63.15	59.66	54.93
8	69.65	72.36	73.53	**73.54**	72.91	71.62	69.89	67.63	64.71	61.14	56.67
9	70.65	73.39	74.70	**74.87**	74.35	73.23	71.59	69.36	66.45	62.62	57.68
10	71.71	74.55	75.88	**76.25**	76.03	75.20	73.88	71.94	69.20	65.38	60.07
11	72.79	75.64	77.08	**77.47**	77.39	76.80	75.73	73.90	71.17	67.35	61.87
12	73.82	76.75	78.27	78.84	**78.95**	78.71	77.87	76.31	73.85	70.04	63.47
13	74.90	77.86	79.53	80.25	80.60	**80.72**	80.37	79.32	77.42	74.14	67.77
14	75.82	78.92	80.64	81.43	81.92	82.26	**82.28**	81.63	80.14	77.23	71.43
15	76.78	79.87	81.57	82.57	83.21	83.74	**84.05**	83.82	82.76	80.43	74.92
16	77.55	80.63	82.50	83.56	84.28	84.99	85.56	**85.71**	85.14	83.41	78.39
17	78.22	81.33	83.23	84.28	85.15	85.94	86.72	**87.17**	86.94	85.68	81.17
18	78.85	81.90	83.80	84.91	85.80	86.72	87.51	88.11	**88.20**	87.28	83.16
19	79.38	82.41	84.31	85.46	86.41	87.32	88.18	88.87	**89.02**	88.37	84.83
20	79.88	82.88	84.76	85.92	86.90	87.85	88.75	89.45	**89.74**	89.16	85.73
21	80.30	83.29	85.17	86.38	87.36	88.30	89.21	89.93	**90.21**	89.77	86.43
22	80.78	83.70	85.58	86.75	87.77	88.74	89.62	90.31	**90.59**	90.17	86.75
23	81.16	84.07	85.92	87.16	88.14	89.10	89.96	90.64	**90.92**	90.49	87.22
24	81.57	84.40	86.27	87.51	88.51	89.45	90.28	90.95	**91.17**	90.73	87.43
25	81.88	84.77	86.62	87.80	88.84	89.77	90.60	91.21	**91.38**	90.92	87.6
26	82.27	85.04	86.91	88.16	89.14	90.05	90.86	91.44	**91.61**	91.05	87.75
27	82.57	85.37	87.20	88.38	89.46	90.32	91.11	91.64	**91.80**	91.22	87.85
28	82.87	85.66	87.49	88.66	89.68	90.55	91.31	91.87	**91.96**	91.36	87.97
29	83.15	85.89	87.74	88.88	89.91	90.79	91.56	92.03	**92.11**	91.46	88.06
30	83.43	86.18	87.97	89.15	90.13	91.04	91.70	92.22	**92.25**	91.57	88.15
31	83.75	86.41	88.21	89.38	90.37	91.23	91.92	92.36	**92.37**	91.68	88.25
32	83.98	86.71	88.42	89.61	90.61	91.45	92.08	**92.52**	92.48	91.76	88.32
33	84.28	86.92	88.65	89.88	90.85	91.61	92.26	**92.63**	92.62	91.84	88.38
34	84.53	87.16	88.89	90.07	91.02	91.80	92.39	**92.76**	92.71	91.92	88.46
35	84.82	87.40	89.09	90.27	91.25	91.94	92.53	**92.91**	92.82	91.97	88.53
36	85.05	87.62	89.33	90.46	91.40	92.10	92.65	**93.00**	92.91	92.05	88.61
37	85.30	87.88	89.52	90.67	91.54	92.25	92.80	**93.11**	93.00	92.10	88.65
38	85.54	88.07	89.72	90.84	91.69	92.39	92.95	**93.24**	93.09	92.16	88.73
39	85.78	88.30	89.90	91.04	91.85	92.53	93.08	**93.33**	93.18	92.23	88.77
40	85.99	88.47	90.12	91.20	92.03	92.67	93.22	**93.42**	93.27	92.28	88.82

144

41	86.22	88.67	90.26	91.32	92.18	92.80	93.34	**93.54**	93.36	92.33	88.89
42	86.45	88.84	90.42	91.49	92.32	92.93	93.42	**93.65**	93.43	92.39	88.93
43	86.64	89.00	90.57	91.61	92.43	93.06	93.53	**93.72**	93.50	92.42	88.99
44	86.83	89.20	90.75	91.79	92.58	93.16	93.62	**93.80**	93.56	92.48	89.03
45	87.02	89.36	90.88	91.92	92.70	93.29	93.74	**93.91**	93.63	92.54	89.08
46	87.23	89.51	91.02	92.09	92.82	93.40	93.84	**93.99**	93.72	92.59	89.12
47	87.41	89.70	91.18	92.21	92.96	93.54	93.96	**94.08**	93.79	92.64	89.18
48	87.58	89.85	91.34	92.37	93.07	93.63	94.03	**94.15**	93.84	92.69	89.21
49	87.77	90.02	91.49	92.47	93.20	93.74	94.14	**94.21**	93.91	92.73	89.25
50	87.97	90.14	91.62	92.60	93.31	93.85	94.22	**94.30**	93.95	92.78	89.29
51	88.11	90.30	91.73	92.72	93.41	93.94	94.32	**94.37**	94.00	92.80	89.32
52	88.29	90.44	91.87	92.83	93.51	94.06	94.39	**94.44**	94.06	92.85	89.37
53	88.44	90.59	91.99	92.95	93.65	94.12	94.47	**94.50**	94.11	92.88	89.38
54	88.62	90.72	92.13	93.06	93.72	94.23	94.56	**94.59**	94.16	92.92	89.44
55	88.76	90.85	92.27	93.15	93.81	94.31	**94.62**	**94.62**	94.2	92.95	89.46
56	88.92	90.98	92.37	93.26	93.94	94.38	**94.70**	**94.70**	94.29	92.98	89.49
57	89.03	91.11	92.50	93.37	94.01	94.49	**94.76**	94.74	94.31	93.03	89.52
58	89.20	91.24	92.60	93.46	94.10	94.55	**94.83**	94.82	94.37	93.05	89.55
59	89.33	91.34	92.72	93.56	94.19	94.63	**94.91**	94.89	94.39	93.07	89.57
60	89.45	91.48	92.80	93.67	94.29	94.71	**94.95**	94.93	94.43	93.10	89.60
61	89.63	91.61	92.90	93.75	94.37	94.78	**95.02**	94.97	94.47	93.14	89.62
62	89.75	91.70	93.01	93.84	94.44	94.84	**95.10**	95.04	94.51	93.16	89.65
63	89.89	91.81	93.09	93.94	94.54	94.91	**95.14**	95.09	94.55	93.19	89.67
64	90.01	91.93	93.19	94.02	94.62	94.99	**95.20**	95.15	94.59	93.21	89.68
65	90.13	92.03	93.28	94.11	94.67	95.06	**95.26**	95.20	94.61	93.24	89.72
66	90.28	92.15	93.39	94.17	94.76	95.11	**95.33**	95.25	94.66	93.26	89.74
67	90.38	92.25	93.47	94.30	94.85	95.19	**95.36**	95.27	94.69	93.30	89.76
68	90.50	92.36	93.58	94.36	94.90	95.24	**95.44**	95.33	94.71	93.32	89.79
69	90.62	92.45	93.66	94.45	94.99	95.31	**95.47**	95.37	94.75	93.33	89.81
70	90.76	92.54	93.74	94.52	95.05	95.36	**95.52**	95.40	94.77	93.36	89.83
71	90.88	92.67	93.82	94.60	95.11	95.45	**95.56**	95.45	94.81	93.37	89.85
72	90.96	92.74	93.92	94.69	95.18	95.49	**95.61**	95.47	94.86	93.39	89.90
73	91.08	92.82	94.01	94.76	95.24	95.54	**95.67**	95.53	94.87	93.43	89.89
74	91.18	92.92	94.08	94.82	95.30	95.60	**95.70**	95.55	94.92	93.44	89.94
75	91.27	93.00	94.17	94.89	95.36	95.66	**95.75**	95.58	94.92	93.44	89.94
76	91.40	93.09	94.26	94.96	95.42	95.70	**95.79**	95.63	94.95	93.47	89.97
77	91.47	93.18	94.34	95.03	95.48	95.76	**95.83**	95.67	94.99	93.50	90.00
78	91.59	93.25	94.41	95.08	95.56	95.80	**95.88**	95.70	94.99	93.53	90.03
79	91.69	93.36	94.47	95.13	95.60	95.85	**95.91**	95.71	95.04	93.54	90.05
80	91.80	93.43	94.54	95.20	95.66	95.88	**95.96**	95.77	95.07	93.56	90.06
81	91.89	93.54	94.60	95.26	95.71	95.93	**96.00**	95.80	95.10	93.58	90.09
82	91.99	93.62	94.68	95.33	95.76	95.98	**96.02**	95.83	95.12	93.59	90.10
83	92.08	93.68	94.76	95.39	95.82	96.03	**96.06**	95.86	95.13	93.61	90.11
84	92.19	93.79	94.83	95.44	95.86	96.06	**96.10**	95.88	95.16	93.64	90.11
85	92.28	93.86	94.87	95.51	95.90	96.12	**96.13**	95.93	95.18	93.65	90.14
86	92.37	93.92	94.94	95.55	95.96	96.17	**96.16**	95.94	95.21	93.65	90.18
87	92.44	94.00	95.00	95.61	95.98	96.20	**96.21**	95.98	95.25	93.68	90.18
88	92.54	94.08	95.07	95.69	96.05	**96.25**	96.23	95.99	95.26	93.71	90.23
89	92.62	94.16	95.13	95.72	96.10	**96.28**	96.28	96.02	95.28	93.71	90.23
90	92.72	94.23	95.18	95.78	96.15	**96.33**	96.30	96.05	95.31	93.72	90.26
91	92.80	94.31	95.24	95.82	96.18	**96.36**	96.35	96.07	95.32	93.74	90.27
92	92.89	94.38	95.31	95.87	96.22	**96.39**	96.36	96.11	95.34	93.77	90.28
93	92.99	94.45	95.36	95.93	96.26	**96.43**	96.42	96.13	95.38	93.78	90.31

94	93.07	94.50	95.42	95.99	96.28	**96.47**	96.43	96.15	95.39	93.80	90.30
95	93.15	94.57	95.49	96.02	96.34	**96.50**	96.47	96.18	95.41	93.81	90.35
96	93.21	94.64	95.53	96.06	96.38	**96.52**	96.48	96.22	95.43	93.84	90.35
97	93.27	94.73	95.60	96.10	96.42	**96.57**	96.52	96.25	95.45	93.84	90.38
98	93.37	94.78	95.65	96.14	96.45	**96.58**	96.56	96.28	95.46	93.87	90.38
99	93.44	94.86	95.70	96.20	96.50	**96.62**	96.58	96.31	95.49	93.88	90.40
100	93.52	94.91	95.73	96.24	96.54	**96.66**	96.6	96.33	95.49	93.90	90.41

Table B.3
Average power supply reliability $R_{W\&Savg}$ versus active battery capacity B_{ac} with wind and solar mixed ratio varies from 100% to 0% for the years of 1998 to 2017 at Houston.

$R_{W\&Savg}$	W/S mixed ratio										
B_{ac}	100%	90%	80%	70%	60%	50%	40%	30%	20%	10%	0%
1	67.89	**69.25**	68.52	67.28	65.78	63.95	61.66	58.79	55.24	50.22	42.65
2	72.47	**73.87**	73.23	72.09	70.65	68.81	66.62	63.81	60.11	54.96	46.42
3	73.98	**75.38**	74.83	73.75	72.24	70.51	68.27	65.40	61.71	56.37	48.98
4	75.19	**76.75**	76.37	75.35	73.97	72.15	69.97	67.11	63.42	58.25	49.61
5	76.33	**77.90**	77.82	76.86	75.54	73.85	71.65	68.85	65.25	59.98	52.16
6	77.38	**79.10**	79.06	78.36	77.15	75.35	73.21	70.42	66.64	61.27	52.66
7	78.35	80.19	**80.31**	79.80	78.70	77.16	75.10	72.30	68.65	63.30	55.10
8	79.31	81.14	**81.49**	81.09	80.01	78.52	76.61	73.91	70.18	64.87	56.85
9	80.15	82.17	**82.53**	82.36	81.54	80.16	78.21	75.52	71.95	66.26	57.26
10	81.08	83.14	**83.75**	83.74	83.17	81.99	80.28	77.80	74.27	68.73	59.35
11	81.77	83.96	84.69	**84.95**	84.63	83.66	82.12	79.81	76.48	70.89	60.80
12	82.61	84.86	85.72	86.16	**86.21**	85.57	84.30	82.18	79.01	73.49	63.00
13	83.32	85.63	86.58	87.24	**87.58**	87.39	86.48	84.75	81.98	76.91	66.90
14	84.03	86.33	87.36	88.08	88.62	**88.66**	88.05	86.68	84.28	79.63	70.41
15	84.69	86.99	88.04	88.85	89.53	**89.74**	89.39	88.30	86.26	81.98	73.01
16	85.26	87.56	88.75	89.59	90.26	**90.62**	90.40	89.53	87.74	83.72	75.39
17	85.79	88.10	89.26	90.16	90.94	**91.24**	91.16	90.41	88.80	84.97	76.93
18	86.24	88.57	89.77	90.67	91.42	**91.79**	91.76	91.06	89.53	85.86	78.00
19	86.72	88.93	90.14	91.08	91.85	**92.23**	92.22	91.58	90.04	86.47	78.77
20	87.12	89.36	90.54	91.50	92.22	**92.64**	92.59	91.97	90.47	86.89	79.32
21	87.53	89.71	90.96	91.85	92.63	**93.01**	92.95	92.30	90.81	87.19	79.76
22	87.89	90.04	91.23	92.21	92.96	**93.33**	93.26	92.61	91.08	87.48	80.09
23	88.24	90.33	91.57	92.56	93.27	**93.60**	93.56	92.88	91.31	87.68	80.35
24	88.55	90.66	91.87	92.83	93.57	**93.90**	93.82	93.15	91.52	87.87	80.54
25	88.84	90.93	92.10	93.12	93.82	**94.12**	94.07	93.39	91.69	87.96	80.71
26	89.08	91.19	92.41	93.36	94.08	**94.39**	94.27	93.59	91.85	88.11	80.88
27	89.40	91.44	92.64	93.62	94.30	**94.61**	94.50	93.79	92.02	88.22	81.04
28	89.65	91.70	92.87	93.87	94.51	**94.82**	94.69	93.96	92.16	88.33	81.18
29	89.91	91.93	93.11	94.07	94.76	**95.01**	94.85	94.09	92.29	88.40	81.33
30	90.16	92.17	93.32	94.31	94.94	**95.19**	94.97	94.25	92.43	88.50	81.44
31	90.40	92.40	93.53	94.48	95.12	**95.36**	95.16	94.37	92.54	88.57	81.52
32	90.63	92.61	93.75	94.67	95.29	**95.50**	95.30	94.52	92.63	88.66	81.63
33	90.91	92.80	93.92	94.82	95.45	**95.65**	95.43	94.61	92.73	88.74	81.73
34	91.10	93.00	94.10	95.01	95.60	**95.78**	95.55	94.73	92.81	88.77	81.83
35	91.30	93.17	94.26	95.14	95.76	**95.91**	95.67	94.83	92.89	88.86	81.90
36	91.49	93.34	94.43	95.31	95.91	**96.05**	95.77	94.92	92.96	88.88	81.98
37	91.71	93.50	94.59	95.47	96.02	**96.16**	95.89	95.03	93.03	88.94	82.05

38	91.88	93.68	94.74	95.59	96.16	**96.30**	96.00	95.12	93.11	88.95	82.11
39	92.08	93.84	94.88	95.73	96.28	**96.41**	96.12	95.21	93.17	89.02	82.19
40	92.24	93.98	95.01	95.84	96.42	**96.51**	96.2	95.27	93.22	89.07	82.26
41	92.38	94.12	95.16	95.97	96.52	**96.62**	96.32	95.37	93.29	89.12	82.29
42	92.54	94.24	95.28	96.09	96.63	**96.72**	96.40	95.46	93.36	89.16	82.37
43	92.69	94.38	95.41	96.22	96.74	**96.83**	96.49	95.52	93.39	89.20	82.40
44	92.83	94.53	95.53	96.35	96.86	**96.90**	96.59	95.59	93.44	89.20	82.46
45	92.96	94.66	95.63	96.44	96.94	**96.99**	96.68	95.69	93.50	89.26	82.48
46	93.10	94.78	95.74	96.58	97.04	**97.08**	96.76	95.72	93.57	89.29	82.54
47	93.23	94.88	95.82	96.65	97.13	**97.17**	96.83	95.81	93.57	89.31	82.56
48	93.36	94.97	95.93	96.75	97.20	**97.24**	96.90	95.87	93.63	89.33	82.63
49	93.48	95.10	96.02	96.84	97.29	**97.31**	96.98	95.93	93.67	89.36	82.64
50	93.60	95.19	96.13	96.93	97.35	**97.38**	97.05	95.98	93.72	89.40	82.68
51	93.71	95.30	96.24	97.01	97.43	**97.44**	97.11	96.05	93.75	89.40	82.72
52	93.82	95.38	96.33	97.10	97.48	**97.51**	97.16	96.07	93.78	89.44	82.76
53	93.94	95.51	96.43	97.20	97.57	**97.58**	97.22	96.13	93.81	89.44	82.76
54	94.05	95.57	96.51	97.27	97.64	**97.64**	97.29	96.18	93.86	89.46	82.81
55	94.14	95.66	96.58	97.34	97.70	**97.71**	97.34	96.21	93.87	89.48	82.85
56	94.24	95.75	96.65	97.42	**97.76**	**97.76**	97.39	96.28	93.91	89.49	82.85
57	94.33	95.82	96.74	97.48	**97.82**	97.80	97.44	96.31	93.91	89.52	82.88
58	94.44	95.92	96.83	97.55	**97.89**	97.83	97.48	96.35	93.96	89.54	82.91
59	94.52	95.98	96.87	97.61	**97.95**	97.90	97.53	96.40	93.99	89.57	82.91
60	94.63	96.07	96.96	97.67	**98.00**	97.95	97.56	96.41	94.01	89.59	82.93
61	94.71	96.13	97.03	97.72	**98.04**	97.99	97.61	96.47	94.04	89.59	82.95
62	94.79	96.22	97.09	97.78	**98.10**	98.03	97.65	96.50	94.05	89.65	82.97
63	94.86	96.28	97.13	97.83	**98.14**	98.08	97.68	96.54	94.08	89.64	82.99
64	94.94	96.35	97.20	97.90	**98.18**	98.11	97.73	96.56	94.10	89.64	83.01
65	95.04	96.41	97.28	97.96	**98.22**	98.14	97.75	96.61	94.13	89.69	83.04
66	95.11	96.48	97.34	97.99	**98.25**	98.19	97.80	96.62	94.13	89.71	83.05
67	95.18	96.54	97.39	98.05	**98.29**	98.21	97.82	96.66	94.15	89.71	83.08
68	95.26	96.61	97.44	98.09	**98.33**	98.24	97.88	96.70	94.18	89.72	83.09
69	95.31	96.67	97.50	98.15	**98.37**	98.29	97.90	96.72	94.19	89.73	83.12
70	95.41	96.72	97.55	98.18	**98.42**	98.32	97.94	96.75	94.21	89.77	83.13
71	95.48	96.80	97.61	98.24	**98.46**	98.36	97.96	96.78	94.23	89.76	83.14
72	95.53	96.85	97.65	98.27	**98.50**	98.40	98.01	96.80	94.25	89.78	83.17
73	95.58	96.91	97.72	98.30	**98.54**	98.43	98.04	96.84	94.27	89.80	83.17
74	95.65	96.95	97.75	98.35	**98.57**	98.45	98.07	96.84	94.29	89.82	83.19
75	95.70	97.01	97.79	98.38	**98.61**	98.49	98.11	96.88	94.30	89.84	83.22
76	95.77	97.06	97.84	98.43	**98.64**	98.52	98.12	96.90	94.30	89.85	83.25
77	95.82	97.11	97.88	98.46	**98.68**	98.55	98.15	96.91	94.34	89.86	83.25
78	95.89	97.15	97.93	98.50	**98.70**	98.57	98.18	96.94	94.35	89.87	83.27
79	95.95	97.20	97.97	98.55	**98.74**	98.60	98.20	96.97	94.36	89.87	83.27
80	95.99	97.24	98.00	98.57	**98.77**	98.63	98.22	97.01	94.36	89.87	83.31
81	96.07	97.28	98.03	98.60	**98.80**	98.66	98.25	97.01	94.39	89.90	83.31
82	96.12	97.35	98.07	98.62	**98.82**	98.67	98.28	97.04	94.39	89.91	83.32
83	96.18	97.37	98.11	98.66	**98.85**	98.70	98.30	97.06	94.42	89.93	83.33
84	96.20	97.42	98.15	98.69	**98.87**	98.73	98.32	97.08	94.42	89.95	83.35
85	96.25	97.46	98.18	98.72	**98.89**	98.75	98.35	97.09	94.46	89.96	83.36
86	96.31	97.50	98.21	98.74	**98.91**	98.76	98.38	97.11	94.47	89.99	83.39
87	96.36	97.53	98.25	98.76	**98.93**	98.79	98.39	97.13	94.49	89.97	83.41
88	96.39	97.58	98.28	98.79	**98.95**	98.82	98.39	97.14	94.51	89.99	83.40
89	96.42	97.63	98.30	98.82	**98.96**	98.84	98.41	97.15	94.50	90.01	83.41
90	96.49	97.67	98.36	98.84	**98.99**	98.86	98.44	97.18	94.53	90.00	83.44

91	96.53	97.70	98.37	98.86	**99.00**	98.88	98.46	97.19	94.55	90.03	83.45
92	96.58	97.75	98.41	98.89	**99.01**	98.89	98.46	97.21	94.55	90.05	83.46
93	96.62	97.76	98.42	98.91	**99.04**	98.91	98.48	97.22	94.58	90.09	83.47
94	96.67	97.80	98.45	98.94	**99.05**	98.93	98.49	97.23	94.58	90.06	83.47
95	96.71	97.84	98.48	98.96	**99.07**	98.95	98.51	97.24	94.60	90.10	83.48
96	96.75	97.87	98.51	98.99	**99.09**	98.97	98.53	97.27	94.61	90.10	83.49
97	96.80	97.89	98.54	99.01	**99.10**	98.98	98.54	97.26	94.62	90.13	83.52
98	96.82	97.93	98.56	99.02	**99.12**	98.99	98.55	97.28	94.64	90.10	83.53
99	96.87	97.97	98.59	99.04	**99.13**	99.01	98.57	97.30	94.64	90.13	83.56
100	96.92	97.99	98.62	99.06	**99.15**	99.03	98.59	97.31	94.66	90.14	83.56

Table B.4
Average power supply reliability $R_{W\&Savg}$ versus active battery capacity B_{ac} with wind and solar mixed ratio varies from 100% to 0% for the years of 1998 to 2017 at Salt Lake City.

$R_{W\&Savg}$	W/S mixed ratio										
B_{ac}	100%	90%	80%	70%	60%	50%	40%	30%	20%	10%	0%
1	73.60	**73.81**	73.07	71.82	70.39	68.45	65.88	62.41	57.45	50.93	41.80
2	79.36	**79.76**	79.07	77.97	76.44	74.29	71.46	67.62	62.34	55.63	46.17
3	81.74	**82.08**	81.42	80.22	78.55	76.31	73.44	69.34	63.91	56.84	47.85
4	83.59	**83.89**	83.11	81.90	80.28	78.05	75.11	71.11	65.64	58.81	49.53
5	85.07	**85.29**	84.63	83.50	81.89	79.72	76.83	72.67	67.19	60.20	51.22
6	86.30	**86.64**	86.06	84.96	83.38	81.31	78.36	74.40	68.83	61.72	52.54
7	87.34	**87.70**	87.29	86.34	84.88	82.84	80.04	75.95	70.55	63.43	53.78
8	88.28	**88.68**	88.36	87.51	86.18	84.26	81.42	77.53	71.96	64.71	55.65
9	89.07	**89.52**	89.26	88.56	87.36	85.55	83.01	79.11	73.62	66.35	56.61
10	89.77	**90.25**	90.12	89.49	88.45	86.80	84.44	80.90	75.74	68.48	57.99
11	90.42	**90.91**	90.81	90.30	89.41	87.95	85.88	82.70	77.93	71.14	60.23
12	90.96	**91.52**	91.46	91.03	90.27	88.98	87.16	84.40	80.22	73.75	62.89
13	91.55	92.08	**92.09**	91.71	91.02	89.85	88.24	85.74	82.12	76.52	66.20
14	91.96	92.53	**92.57**	92.22	91.59	90.54	89.03	86.83	83.50	78.35	68.69
15	92.43	92.95	**93.01**	92.70	92.08	91.10	89.67	87.60	84.62	79.91	70.71
16	92.76	93.31	**93.35**	93.05	92.47	91.56	90.20	88.26	85.45	80.99	72.28
17	93.10	93.61	**93.68**	93.40	92.79	91.89	90.58	88.78	86.00	81.74	73.35
18	93.39	93.89	**93.91**	93.63	93.09	92.17	90.87	89.09	86.42	82.23	74.02
19	93.67	94.11	**94.15**	93.87	93.29	92.40	91.14	89.31	86.73	82.60	74.53
20	93.89	94.31	**94.34**	94.06	93.50	92.61	91.38	89.55	86.93	82.89	74.85
21	94.10	94.51	**94.52**	94.22	93.68	92.79	91.52	89.78	87.13	83.09	75.07
22	94.30	94.68	**94.67**	94.38	93.84	92.94	91.68	89.91	87.27	83.28	75.29
23	94.47	94.82	**94.83**	94.54	93.98	93.11	91.85	90.08	87.46	83.41	75.45
24	94.64	**94.97**	94.94	94.68	94.11	93.23	91.99	90.21	87.60	83.53	75.59
25	94.77	**95.10**	95.06	94.78	94.23	93.36	92.09	90.30	87.71	83.65	75.68
26	94.92	**95.22**	95.19	94.91	94.35	93.46	92.21	90.44	87.79	83.77	75.77
27	95.06	**95.34**	95.29	95.01	94.46	93.56	92.33	90.54	87.91	83.83	75.86
28	95.17	**95.46**	95.39	95.08	94.56	93.66	92.42	90.63	87.99	83.91	75.94
29	95.29	**95.57**	95.48	95.18	94.64	93.78	92.51	90.74	88.08	84.00	76.03
30	95.40	**95.66**	95.60	95.27	94.72	93.83	92.55	90.80	88.15	84.05	76.09
31	95.52	**95.74**	95.67	95.35	94.79	93.93	92.67	90.89	88.25	84.12	76.17
32	95.63	**95.83**	95.77	95.44	94.88	93.99	92.74	90.96	88.28	84.20	76.22
33	95.73	**95.93**	95.84	95.52	94.96	94.08	92.82	91.03	88.37	84.24	76.29
34	95.85	**96.01**	95.92	95.60	95.04	94.17	92.89	91.12	88.43	84.31	76.37

35	95.93	**96.12**	96.00	95.69	95.10	94.22	92.97	91.18	88.48	84.36	76.40
36	96.01	**96.17**	96.08	95.74	95.20	94.28	93.04	91.20	88.55	84.39	76.44
37	96.11	**96.26**	96.14	95.82	95.25	94.33	93.10	91.27	88.62	84.44	76.50
38	96.17	**96.32**	96.19	95.88	95.31	94.42	93.13	91.33	88.66	84.48	76.57
39	96.24	**96.40**	96.27	95.95	95.38	94.47	93.20	91.39	88.70	84.50	76.58
40	96.34	**96.44**	96.32	96.00	95.44	94.52	93.26	91.46	88.78	84.53	76.62
41	96.39	**96.52**	96.38	96.06	95.48	94.57	93.29	91.52	88.78	84.55	76.63
42	96.46	**96.59**	96.46	96.11	95.53	94.65	93.35	91.59	88.83	84.59	76.68
43	96.51	**96.63**	96.49	96.16	95.59	94.71	93.39	91.63	88.91	84.61	76.70
44	96.61	**96.69**	96.54	96.19	95.62	94.74	93.43	91.67	88.93	84.64	76.71
45	96.65	**96.73**	96.59	96.25	95.67	94.80	93.48	91.71	88.97	84.66	76.76
46	96.71	**96.80**	96.65	96.31	95.72	94.86	93.54	91.77	89.05	84.69	76.77
47	96.77	**96.84**	96.67	96.33	95.76	94.89	93.59	91.81	89.05	84.71	76.78
48	96.82	**96.90**	96.72	96.38	95.80	94.94	93.63	91.86	89.12	84.72	76.81
49	96.89	**96.94**	96.78	96.43	95.86	94.99	93.67	91.92	89.15	84.75	76.84
50	96.93	**96.97**	96.82	96.46	95.90	95.02	93.72	91.93	89.19	84.78	76.83
51	96.99	**97.03**	96.87	96.51	95.95	95.06	93.73	92.01	89.22	84.78	76.89
52	97.02	**97.05**	96.92	96.54	95.96	95.11	93.78	92.03	89.25	84.81	76.89
53	97.07	**97.11**	96.95	96.59	96.01	95.15	93.82	92.07	89.27	84.81	76.93
54	97.12	**97.14**	97.00	96.63	96.04	95.17	93.87	92.09	89.3	84.85	76.93
55	97.16	**97.19**	97.04	96.65	96.09	95.22	93.90	92.13	89.34	84.87	76.94
56	97.20	**97.23**	97.08	96.70	96.13	95.25	93.93	92.17	89.37	84.90	76.95
57	97.25	**97.26**	97.09	96.73	96.15	95.26	93.97	92.19	89.38	84.90	76.97
58	97.29	**97.31**	97.14	96.75	96.19	95.31	94.01	92.23	89.40	84.93	76.99
59	97.33	**97.33**	97.19	96.79	96.21	95.35	94.03	92.24	89.45	84.94	77.01
60	97.36	**97.38**	97.21	96.82	96.26	95.39	94.06	92.28	89.45	84.97	77.02
61	97.40	**97.40**	97.25	96.85	96.28	95.40	94.10	92.32	89.47	84.99	77.02
62	97.44	**97.45**	97.28	96.87	96.31	95.46	94.13	92.34	89.48	84.99	77.05
63	97.49	**97.48**	97.30	96.91	96.34	95.45	94.17	92.37	89.51	85.04	77.06
64	97.51	**97.49**	97.33	96.92	96.38	95.51	94.19	92.40	89.55	85.04	77.08
65	97.56	**97.53**	97.36	96.98	96.41	95.52	94.22	92.45	89.56	85.05	77.09
66	97.58	**97.56**	97.36	97.01	96.42	95.56	94.26	92.47	89.58	85.05	77.13
67	97.61	**97.59**	97.41	97.03	96.46	95.59	94.27	92.47	89.58	85.08	77.13
68	97.65	**97.62**	97.42	97.05	96.46	95.61	94.31	92.52	89.61	85.10	77.16
69	97.68	**97.64**	97.45	97.08	96.50	95.64	94.34	92.56	89.63	85.10	77.18
70	97.71	**97.67**	97.48	97.09	96.53	95.66	94.36	92.55	89.64	85.13	77.19
71	97.74	**97.68**	97.50	97.12	96.55	95.70	94.38	92.60	89.66	85.16	77.22
72	97.75	**97.72**	97.53	97.14	96.57	95.72	94.42	92.62	89.68	85.15	77.24
73	97.80	**97.75**	97.55	97.16	96.60	95.75	94.45	92.65	89.71	85.16	77.25
74	97.83	**97.77**	97.56	97.18	96.62	95.76	94.49	92.66	89.72	85.19	77.26
75	97.86	**97.80**	97.58	97.20	96.63	95.79	94.50	92.69	89.73	85.19	77.27
76	97.89	**97.82**	97.61	97.23	96.66	95.81	94.51	92.73	89.77	85.22	77.28
77	97.91	**97.84**	97.63	97.26	96.68	95.83	94.54	92.73	89.75	85.24	77.30
78	97.93	**97.86**	97.67	97.27	96.72	95.85	94.57	92.75	89.78	85.25	77.32
79	97.96	**97.89**	97.68	97.30	96.74	95.88	94.60	92.77	89.76	85.26	77.33
80	97.98	**97.90**	97.72	97.31	96.76	95.89	94.61	92.80	89.78	85.26	77.34
81	98.01	**97.93**	97.72	97.33	96.78	95.92	94.65	92.83	89.80	85.26	77.36
82	98.04	**97.96**	97.73	97.36	96.80	95.96	94.65	92.85	89.83	85.30	77.37
83	98.07	**97.98**	97.76	97.37	96.83	95.97	94.68	92.87	89.84	85.30	77.41
84	98.08	**97.99**	97.78	97.39	96.85	96.00	94.70	92.89	89.85	85.32	77.41
85	98.11	**98.02**	97.79	97.41	96.86	96.03	94.73	92.91	89.87	85.35	77.41
86	98.13	**98.03**	97.81	97.43	96.87	96.05	94.74	92.92	89.88	85.34	77.45
87	98.14	**98.06**	97.84	97.43	96.90	96.07	94.76	92.92	89.90	85.33	77.45

88	98.17	**98.08**	97.85	97.45	96.92	96.08	94.81	92.96	89.93	85.36	77.46
89	98.20	**98.11**	97.87	97.48	96.92	96.10	94.82	93.00	89.91	85.37	77.47
90	98.21	**98.12**	97.87	97.50	96.94	96.11	94.83	93.01	89.94	85.41	77.47
91	98.23	**98.14**	97.91	97.51	96.96	96.14	94.88	93.03	89.96	85.39	77.50
92	98.24	**98.15**	97.92	97.53	96.98	96.15	94.89	93.05	89.96	85.41	77.49
93	98.27	**98.17**	97.92	97.56	96.99	96.16	94.91	93.06	89.98	85.42	77.53
94	98.29	**98.19**	97.95	97.57	97.01	96.19	94.93	93.08	89.98	85.44	77.54
95	98.30	**98.19**	97.95	97.58	97.04	96.19	94.93	93.11	89.99	85.43	77.55
96	98.31	**98.22**	97.98	97.60	97.05	96.21	94.96	93.13	90.02	85.46	77.56
97	98.34	**98.24**	97.99	97.62	97.06	96.23	94.96	93.14	90.03	85.47	77.59
98	98.34	**98.25**	98.01	97.63	97.08	96.25	94.98	93.15	90.03	85.49	77.57
99	98.35	**98.27**	98.02	97.65	97.09	96.29	95.01	93.17	90.05	85.51	77.60
100	98.38	**98.28**	98.04	97.67	97.12	96.31	95.04	93.19	90.06	85.49	77.60

Table B.5
Average power supply reliability $R_{W\&Savg}$ versus active battery capacity B_{ac} with wind and solar mixed ratio varies from 100% to 0% for the years of 1998 to 2017 at Vancouver.

$R_{W\&Savg}$	W/S mixed ratio										
B_{ac}	100%	90%	80%	70%	60%	50%	40%	30%	20%	10%	0%
1	64.80	75.13	76.42	**76.43**	75.83	74.60	72.59	69.53	64.95	56.76	39.76
2	68.24	79.08	80.63	**80.76**	80.32	79.20	77.34	74.56	70.10	61.77	43.36
3	69.78	80.59	82.32	**82.44**	81.95	80.83	79.06	76.26	71.86	63.30	45.26
4	71.09	81.59	83.43	**83.67**	83.32	82.36	80.65	77.99	73.55	65.05	46.61
5	72.24	82.33	84.58	**84.83**	84.52	83.54	81.89	79.23	74.84	66.24	47.91
6	73.16	82.91	85.40	**85.85**	85.63	84.78	83.25	80.69	76.4	67.89	49.33
7	73.92	83.47	86.25	**86.84**	86.69	85.84	84.32	81.83	77.53	68.80	49.95
8	74.53	83.92	86.89	**87.64**	87.57	86.89	85.49	83.15	79.00	70.44	51.58
9	75.01	84.31	87.39	88.49	**88.54**	87.88	86.51	84.22	80.03	71.35	52.32
10	75.39	84.69	87.85	89.35	**89.54**	89.02	87.82	85.67	81.78	73.34	54.07
11	75.78	85.05	88.30	90.27	**90.77**	90.40	89.36	87.38	83.69	75.38	56.36
12	76.11	85.36	88.72	91.13	**91.83**	91.64	90.74	88.94	85.47	77.46	58.57
13	76.45	85.72	89.12	91.78	**92.68**	92.63	91.92	90.26	87.02	79.35	60.87
14	76.74	86.03	89.47	92.28	93.22	**93.29**	92.64	91.14	88.06	80.59	62.57
15	77.09	86.32	89.78	92.64	93.62	**93.75**	93.17	91.70	88.78	81.54	63.86
16	77.36	86.60	90.03	92.93	93.93	**94.09**	93.54	92.14	89.32	82.17	65.02
17	77.70	86.85	90.28	93.18	94.20	**94.35**	93.82	92.49	89.68	82.61	65.75
18	77.97	87.08	90.51	93.42	94.45	**94.61**	94.08	92.74	89.99	82.91	66.27
19	78.24	87.28	90.75	93.67	94.66	**94.81**	94.26	93.01	90.24	83.13	66.62
20	78.52	87.52	90.97	93.85	94.88	**94.99**	94.49	93.17	90.44	83.37	66.95
21	78.76	87.70	91.16	94.07	95.06	**95.16**	94.66	93.37	90.64	83.54	67.15
22	79.06	87.90	91.33	94.25	95.21	**95.34**	94.84	93.54	90.85	83.69	67.36
23	79.25	88.06	91.52	94.42	95.38	**95.49**	94.97	93.72	91.02	83.81	67.56
24	79.53	88.26	91.71	94.58	95.53	**95.63**	95.13	93.85	91.19	83.94	67.74
25	79.71	88.37	91.87	94.71	95.67	**95.75**	95.26	94.00	91.29	84.08	67.88
26	79.92	88.52	92.03	94.86	95.80	**95.89**	95.38	94.16	91.42	84.17	68.05
27	80.10	88.70	92.16	95.02	95.93	**96.01**	95.51	94.31	91.57	84.31	68.19
28	80.30	88.85	92.31	95.13	96.07	**96.11**	95.61	94.40	91.68	84.41	68.34
29	80.45	88.97	92.43	95.29	96.15	**96.21**	95.72	94.52	91.79	84.50	68.46
30	80.64	89.12	92.58	95.39	96.28	**96.32**	95.82	94.62	91.89	84.59	68.58
31	80.77	89.23	92.69	95.49	96.38	**96.42**	95.92	94.72	92.00	84.65	68.70

32	80.92	89.34	92.82	95.60	96.45	**96.50**	96.01	94.81	92.06	84.72	68.78
33	81.06	89.48	92.94	95.72	96.55	**96.59**	96.08	94.91	92.15	84.78	68.88
34	81.19	89.59	93.04	95.82	96.64	**96.66**	96.16	94.99	92.22	84.81	68.96
35	81.33	89.71	93.15	95.93	96.72	**96.75**	96.24	95.05	92.29	84.87	69.05
36	81.48	89.82	93.25	96.01	96.79	**96.81**	96.33	95.14	92.35	84.93	69.11
37	81.60	89.93	93.37	96.08	96.85	**96.87**	96.37	95.20	92.42	84.97	69.19
38	81.73	90.03	93.43	96.18	**96.94**	96.93	96.45	95.30	92.50	84.99	69.28
39	81.86	90.11	93.55	96.24	**96.99**	96.98	96.52	95.34	92.56	85.04	69.30
40	81.99	90.24	93.61	96.31	**97.08**	97.04	96.59	95.39	92.59	85.08	69.37
41	82.12	90.31	93.69	96.37	**97.12**	97.10	96.64	95.46	92.65	85.11	69.43
42	82.25	90.43	93.79	96.44	**97.19**	97.17	96.70	95.50	92.72	85.15	69.46
43	82.35	90.50	93.84	96.51	**97.25**	97.23	96.75	95.57	92.74	85.17	69.52
44	82.48	90.59	93.93	96.58	**97.30**	97.27	96.79	95.63	92.83	85.21	69.57
45	82.59	90.69	94.02	96.65	**97.36**	97.32	96.85	95.70	92.87	85.22	69.59
46	82.70	90.78	94.09	96.69	**97.41**	97.37	96.91	95.74	92.91	85.25	69.61
47	82.81	90.84	94.17	96.76	**97.46**	97.42	96.94	95.80	92.94	85.30	69.67
48	82.92	90.93	94.22	96.82	**97.51**	97.47	96.99	95.84	92.98	85.33	69.69
49	83.01	91.00	94.30	96.88	**97.56**	97.51	97.05	95.88	93.02	85.33	69.72
50	83.12	91.07	94.34	96.95	**97.61**	97.56	97.08	95.94	93.05	85.36	69.75
51	83.20	91.14	94.40	97.01	**97.65**	97.59	97.12	95.97	93.10	85.38	69.81
52	83.29	91.22	94.47	97.05	**97.71**	97.64	97.18	96.02	93.11	85.42	69.83
53	83.39	91.30	94.52	97.11	**97.74**	97.67	97.20	96.04	93.17	85.44	69.86
54	83.48	91.37	94.59	97.15	**97.81**	97.72	97.26	96.07	93.19	85.44	69.87
55	83.59	91.42	94.66	97.20	**97.84**	97.74	97.29	96.13	93.24	85.47	69.92
56	83.65	91.51	94.69	97.25	**97.88**	97.77	97.32	96.17	93.26	85.50	69.93
57	83.71	91.58	94.77	97.29	**97.93**	97.81	97.36	96.21	93.29	85.52	69.95
58	83.83	91.63	94.82	97.33	**97.97**	97.86	97.39	96.24	93.32	85.55	69.98
59	83.92	91.69	94.86	97.39	**98.00**	97.90	97.43	96.29	93.34	85.54	70.01
60	83.98	91.74	94.91	97.44	**98.03**	97.92	97.46	96.32	93.37	85.57	70.01
61	84.07	91.78	94.99	97.48	**98.07**	97.96	97.49	96.35	93.40	85.60	70.04
62	84.13	91.85	95.03	97.52	**98.09**	97.99	97.52	96.36	93.42	85.59	70.07
63	84.21	91.89	95.06	97.56	**98.12**	98.02	97.54	96.41	93.46	85.63	70.09
64	84.30	91.97	95.12	97.60	**98.16**	98.04	97.58	96.44	93.47	85.63	70.09
65	84.39	92.02	95.18	97.63	**98.19**	98.07	97.61	96.49	93.50	85.64	70.12
66	84.46	92.06	95.23	97.67	**98.22**	98.11	97.64	96.50	93.53	85.66	70.13
67	84.52	92.12	95.28	97.71	**98.24**	98.13	97.68	96.55	93.55	85.67	70.16
68	84.61	92.15	95.32	97.73	**98.28**	98.16	97.69	96.55	93.58	85.68	70.18
69	84.65	92.20	95.37	97.79	**98.30**	98.20	97.73	96.60	93.60	85.70	70.19
70	84.70	92.24	95.40	97.81	**98.34**	98.22	97.75	96.60	93.62	85.71	70.22
71	84.77	92.30	95.45	97.84	**98.36**	98.25	97.79	96.64	93.63	85.73	70.20
72	84.83	92.36	95.49	97.88	**98.38**	98.29	97.81	96.67	93.65	85.72	70.23
73	84.91	92.39	95.51	97.91	**98.41**	98.30	97.83	96.69	93.69	85.75	70.24
74	84.96	92.42	95.55	97.95	**98.43**	98.32	97.86	96.71	93.70	85.74	70.27
75	85.01	92.49	95.58	97.98	**98.45**	98.35	97.87	96.73	93.72	85.76	70.27
76	85.07	92.53	95.61	98.02	**98.49**	98.38	97.89	96.77	93.73	85.75	70.31
77	85.10	92.57	95.67	98.06	**98.50**	98.39	97.92	96.79	93.76	85.80	70.30
78	85.16	92.59	95.68	98.08	**98.52**	98.42	97.95	96.82	93.78	85.81	70.33
79	85.22	92.66	95.71	98.11	**98.56**	98.44	97.97	96.83	93.80	85.80	70.35
80	85.26	92.71	95.76	98.13	**98.57**	98.45	97.99	96.86	93.82	85.85	70.38
81	85.33	92.72	95.76	98.16	**98.59**	98.48	98.01	96.89	93.85	85.85	70.35
82	85.39	92.75	95.82	98.19	**98.62**	98.50	98.03	96.90	93.87	85.85	70.38
83	85.41	92.79	95.84	98.21	**98.64**	98.52	98.06	96.92	93.87	85.86	70.41
84	85.47	92.81	95.87	98.23	**98.66**	98.55	98.08	96.95	93.89	85.87	70.43

85	85.53	92.86	95.90	98.26	**<u>98.67</u>**	98.55	98.09	96.98	93.92	85.90	70.43
86	85.58	92.88	95.93	98.27	**<u>98.70</u>**	98.58	98.11	96.99	93.94	85.90	70.45
87	85.64	92.91	95.96	98.29	**<u>98.71</u>**	98.59	98.13	97.02	93.97	85.92	70.45
88	85.66	92.95	95.99	98.32	**<u>98.72</u>**	98.60	98.15	97.02	93.98	85.91	70.47
89	85.71	92.98	96.02	98.34	**<u>98.74</u>**	98.63	98.17	97.05	93.98	85.92	70.50
90	85.75	93.00	96.04	98.35	**<u>98.76</u>**	98.63	98.19	97.06	94.02	85.93	70.50
91	85.80	93.05	96.07	98.37	**<u>98.79</u>**	98.66	98.21	97.09	94.02	85.94	70.51
92	85.83	93.07	96.09	98.41	**<u>98.80</u>**	98.68	98.22	97.10	94.04	85.97	70.54
93	85.87	93.11	96.13	98.42	**<u>98.82</u>**	98.71	98.23	97.12	94.06	85.97	70.54
94	85.91	93.13	96.17	98.43	**<u>98.84</u>**	98.72	98.25	97.15	94.08	85.98	70.54
95	85.94	93.15	96.20	98.46	**<u>98.85</u>**	98.74	98.27	97.16	94.09	86.01	70.57
96	85.98	93.19	96.20	98.47	**<u>98.86</u>**	98.74	98.28	97.18	94.10	86.01	70.60
97	86.01	93.22	96.21	98.49	**<u>98.88</u>**	98.76	98.30	97.18	94.12	86.01	70.61
98	86.08	93.23	96.24	98.51	**<u>98.89</u>**	98.77	98.32	97.22	94.13	86.03	70.62
99	86.11	93.27	96.27	98.52	**<u>98.91</u>**	98.78	98.33	97.22	94.14	86.04	70.61
100	86.15	93.28	96.30	98.54	**<u>98.92</u>**	98.80	98.35	97.24	94.15	86.06	70.63

Reference

[1]   H. Chen *et al.*, "The impacts of climate change and human activities on biogeochemical cycles on the Q inghai‑T ibetan P lateau," *Global change biology,* vol. 19, no. 10, pp. 2940-2955, 2013.

[2]   J. Leider, "A Quantile Regression Study of Climate Change in Chicago, 1960-2010," *Department of Mathematics, Statistics and Computer Science, University of Illinois, Chicago,* 2012.

[3]   C. Xu *et al.*, "Climate change in Urumqi City during 1960–2013," *Quaternary international,* vol. 358, pp. 93-100, 2015.

[4]   M. Du, S. Kawashima, S. Yonemura, X. Zhang, and S. Chen, "Mutual influence between human activities and climate change in the Tibetan Plateau during recent years," *Global and Planetary Change,* vol. 41, no. 3-4, pp. 241-249, 2004.

[5]   Worldometer. "World population." https://www.worldometers.info/world-population/ (accessed.

[6]   R. J. Heffron, D. McCauley, and B. K. Sovacool, "Resolving society's energy trilemma through the Energy Justice Metric," *Energy Policy,* vol. 87, pp. 168-176, 2015.

[7]   N. Gunningham, "Managing the energy trilemma: The case of Indonesia," *Energy Policy,* vol. 54, pp. 184-193, 2013.

[8]   J. Oliver and B. Sovacool, "The energy trilemma and the smart grid: implications beyond the United States," *Asia & the Pacific Policy Studies,* vol. 4, no. 1, pp. 70-84, 2017.

[9]   R. J. Heffron, D. McCauley, and G. Z. de Rubens, "Balancing the energy trilemma through the Energy Justice Metric," *Applied energy,* vol. 229, pp. 1191-1201, 2018.

[10]   H. Ritchie and M. Roser, "Renewable Energy. Our World in Data," ed, 2019.

[11]   B. Lehner, G. Czisch, and S. Vassolo, "The impact of global change on the hydropower potential of Europe: a model-based analysis," *Energy Policy,* vol. 33, no. 7, pp. 839-855, 2005.

[12]   P. Voigtländer and M. Gattinger, "Potentiale: Wasserkraft," *Regenerativer Strom for Europa durch Fern. ubertragung elektrischer Energie. AFES-Press, Moosbach,* 1999.

[13]   J. Bairstow. "Global hydropower market 'to see compound growth rate of 2.4% until 2030'." Energy live news. https://www.energylivenews.com/2019/10/29/global-hydropower-market-to-see-compound-growth-rate-of-2-4-until-2030/ (accessed.

[14]   M. D. A. Al-Falahi, S. D. G. Jayasinghe, and H. Enshaei, "A review on recent size optimization methodologies for standalone solar and wind hybrid renewable energy system," (in English), *Energy Conversion and Management,* vol. 143, pp. 252-274, Jul 1 2017, doi: 10.1016/j.enconman.2017.04.019.

[15]   National Energy Administration. (2016). *China 13th Renewable Energy Development Five Year Plan (2016-2020).* [Online] Available: http://www.nea.gov.cn/2016-12/19/c_135916140.htm

[16]   "STATE RENEWABLE PORTFOLIO STANDARDS AND GOALS." http://www.ncsl.org/research/energy/renewable-portfolio-standards.aspx (accessed.

[17]   T. W. Power. "global wind data " https://www.thewindpower.net/country_list_en.php (accessed.

[18]   !!! INVALID CITATION !!! [2].

[19]   Y.-H. Wan, "Primer on wind power for utility applications," National Renewable Energy Lab.(NREL), Golden, CO (United States), 2005.

[20]   C. Miller and A. Davenport, "Guidelines for the calculation of wind speed-ups in complex terrain," *Journal of Wind Engineering and Industrial Aerodynamics,* vol. 74, pp. 189-197, 1998.

[21]   S. Lang and E. McKeogh, "LIDAR and SODAR measurements of wind speed and direction in upland terrain for wind energy purposes," *Remote Sensing,* vol. 3, no. 9, pp. 1871-1901, 2011.

[22]   J. Ashcroft, "The relationship between the gust ratio, terrain roughness, gust duration and the hourly mean wind speed," *Journal of Wind Engineering and Industrial Aerodynamics,* vol. 53, no. 3, pp. 331-355, 1994.

[23]   E. Friis-Christensen and H. Svensmark, "What do we really know about the sun-climate connection?," *Advances in Space Research,* vol. 20, no. 4-5, pp. 913-921, 1997.

[24]   K. Labitzke and H. Van Loon, "The signal of the 11-year sunspot cycle in the upper troposphere-lower stratosphere," *Space Science Reviews,* vol. 80, no. 3-4, pp. 393-410, 1997.

[25]   D. Shindell, D. Rind, N. Balachandran, J. Lean, and P. Lonergan, "Solar cycle variability, ozone, and climate," *Science,* vol. 284, no. 5412, pp. 305-308, 1999.

[26]   V. M. Mehta and T. Delworth, "Decadal variability of the tropical Atlantic Ocean surface temperature in shipboard measurements and in a global ocean-atmosphere model," *Journal of Climate,* vol. 8, no. 2, pp. 172-190, 1995.

[27]   M. Voiculescu, I. G. Usoskin, and K. Mursula, "Different response of clouds to solar input," *Geophysical research letters,* vol. 33, no. 21, 2006.

[28]   I. Usoskin, M. Voiculescu, G. Kovaltsov, and K. Mursula, "Correlation between clouds at different altitudes and solar activity: Fact or Artifact?," *Journal of atmospheric and solar-terrestrial physics,* vol. 68, no. 18, pp. 2164-2172, 2006.

[29]   Y. Qian, W. Wang, L. R. Leung, and D. P. Kaiser, "Variability of solar radiation under cloud‐free skies in China: The role of aerosols," *Geophysical Research Letters,* vol. 34, no. 12, 2007.

[30]   J. L. Lean, G. J. Rottman, H. L. Kyle, T. N. Woods, J. R. Hickey, and L. C. Puga, "Detection and parameterization of variations in solar mid‐and near‐ultraviolet radiation (200–400 nm)," *Journal of Geophysical Research: Atmospheres,* vol. 102, no. D25, pp. 29939-29956, 1997.

[31]   J. D. Haigh, "The role of stratospheric ozone in modulating the solar radiative forcing of climate," *Nature,* vol. 370, no. 6490, pp. 544-546, 1994.

[32]   F. S. Rowland, "Stratospheric ozone depletion," in *Twenty Years of Ozone Decline*: Springer, 2009, pp. 23-66.

[33]   M. M. Caldwell and S. D. Flint, "Stratospheric ozone reduction, solar UV-B radiation and terrestrial ecosystems," *Climatic change,* vol. 28, no. 4, pp. 375-394, 1994.

[34]   B. Tarroja, F. Mueller, J. D. Eichman, J. Brouwer, and S. Samuelsen, "Spatial and temporal analysis of electric wind generation intermittency and dynamics," *Renew Energ,* vol. 36, no. 12, pp. 3424-3432, 2011.

[35]   G. Ren, J. Liu, J. Wan, Y. Guo, and D. Yu, "Overview of wind power intermittency: Impacts, measurements, and mitigation solutions," *Applied Energy,* vol. 204, pp. 47-65, 2017.

[36]   G. Ren, J. Liu, J. Wan, Y. Guo, D. Yu, and J. Liu, "Measurement and statistical analysis of wind speed intermittency," *Energy,* vol. 118, pp. 632-643, 2017.

[37]   M. Alam, K. Muttaqi, and D. Sutanto, "A novel approach for ramp-rate control of solar PV using energy storage to mitigate output fluctuations caused by cloud passing," *Ieee T Energy Conver,* vol. 29, no. 2, pp. 507-518, 2014.

[38]   H. Holttinen, "Hourly wind power variations in the Nordic countries," *Wind Energy: An International Journal for Progress and Applications in Wind Power Conversion Technology,* vol. 8, no. 2, pp. 173-195, 2005.

[39] H. Holttinen, S. Rissanen, X. G. Larsén, and A. L. Løvholm, "Wind and load variability in the Nordic countries," 2013.

[40] G. Sinden, "Characteristics of the UK wind resource: Long-term patterns and relationship to electricity demand," *Energy policy,* vol. 35, no. 1, pp. 112-127, 2007.

[41] E. Wiemken, H. Beyer, W. Heydenreich, and K. Kiefer, "Power characteristics of PV ensembles: experiences from the combined power production of 100 grid connected PV systems distributed over the area of Germany," *Sol Energy,* vol. 70, no. 6, pp. 513-518, 2001.

[42] J. Marcos, L. Marroyo, E. Lorenzo, and M. García, "Smoothing of PV power fluctuations by geographical dispersion," *Progress in Photovoltaics: Research and Applications,* vol. 20, no. 2, pp. 226-237, 2012.

[43] T. Hurley and R. Watson, "An assessment of the expected variability and load following capability of a large penetration of wind power in Ireland," in *Proceedings of Global Wind Power Conference GWPC*, 2002, vol. 2.

[44] B. Hasche, "General statistics of geographically dispersed wind power," *Wind Energy,* vol. 13, no. 8, pp. 773-784, 2010.

[45] B. Tammelin and J. Nurmi, "PG3. 22 An Assessment of Variability of Wind Power Production in Finland," in *EWEC-CONFERENCE-*, 2001, pp. 1078-1081.

[46] G. Giebel, *On the benefits of distributed generation of wind energy in Europe*. VDI-Verlag, 2001.

[47] L. Landberg, "The availability and variability of the European wind resource," *International journal of solar energy,* vol. 18, no. 4, pp. 313-320, 1997.

[48] J. Widén, "Correlations between large-scale solar and wind power in a future scenario for Sweden," *Ieee T Sustain Energ,* vol. 2, no. 2, pp. 177-184, 2011.

[49] F. Santos-Alamillos, D. Pozo-Vázquez, J. Ruiz-Arias, V. Lara-Fanego, and J. Tovar-Pescador, "Analysis of spatiotemporal balancing between wind and solar energy resources in the southern Iberian Peninsula," *Journal of applied meteorology and climatology,* vol. 51, no. 11, pp. 2005-2024, 2012.

[50] F. Ueckerdt, R. Brecha, and G. Luderer, "Analyzing major challenges of wind and solar variability in power systems," *Renew Energ,* vol. 81, pp. 1-10, 2015.

[51] W. Katzenstein, E. Fertig, and J. Apt, "The variability of interconnected wind plants," *Energy policy,* vol. 38, no. 8, pp. 4400-4410, 2010.

[52] J. Apt, "The spectrum of power from wind turbines," *Journal of Power Sources,* vol. 169, no. 2, pp. 369-374, 2007.

[53] J. Jung and K.-S. Tam, "A frequency domain approach to characterize and analyze wind speed patterns," *Applied energy,* vol. 103, pp. 435-443, 2013.

[54] M. R. R. Tabar *et al.*, "Kolmogorov spectrum of renewable wind and solar power fluctuations," *The European Physical Journal Special Topics,* vol. 223, no. 12, pp. 2637-2644, 2014.

[55] J. Podesta, D. Roberts, and M. Goldstein, "Power spectrum of small‐scale turbulent velocity fluctuations in the solar wind," *Journal of Geophysical Research: Space Physics,* vol. 111, no. A10, 2006.

[56] T. Ma, H. Yang, L. Lu, and J. Peng, "Technical feasibility study on a standalone hybrid solar-wind system with pumped hydro storage for a remote island in Hong Kong," *Renewable energy,* vol. 69, pp. 7-15, 2014.

[57] H. Fathabadi, "Novel standalone hybrid solar/wind/fuel cell power generation system for remote areas," *Solar Energy,* vol. 146, pp. 30-43, 2017.

[58] A. Al-Badi and H. Bourdoucen, "Study and design of hybrid diesel–wind standalone system for remote area in Oman," *International Journal of Sustainable Energy,* vol. 31, no. 2, pp. 85-94, 2012.

[59] T. Ma, H. Yang, and L. Lu, "A feasibility study of a stand-alone hybrid solar–wind–battery system for a remote island," *Applied Energy,* vol. 121, pp. 149-158, 2014.

[60] W. He *et al.*, "The potential of integrating wind power with offshore oil and gas platforms," *Wind Engineering,* vol. 34, no. 2, pp. 125-137, 2010.

[61] A. A. M. Zin, M. Moradi, J. Tavalaei, A. Naderipour, A. H. Khavari, and M. Moradi, "Techno-economic analysis of stand-alone hybrid energy system for the electrification of Iran drilling oil rigs," *Telkomnika,* vol. 15, no. 2, p. 746, 2017.

[62] K. Zhou, J. Ferreira, and S. De Haan, "Optimal energy management strategy and system sizing method for stand-alone photovoltaic-hydrogen systems," *Int J Hydrogen Energ,* vol. 33, no. 2, pp. 477-489, 2008.

[63] N. b. S. Kaveh Mazloomi1, Hossein Moayedi, "Electrical Efficiency of Electrolytic Hydrogen Production," *International Journal of ELECTROCHEMICAL SCIENCE,* 2012.

[64] D. H. Program, "Hydrogen Fuel Cells." [Online]. Available: www.hydrogen.energy.gov

[65] P. Hoffmann, *Tomorrow's energy: hydrogen, fuel cells, and the prospects for a cleaner planet*. MIT press, 2012.

[66] D. Stolten and B. Emonts, *Hydrogen Science and Engineering, 2 Volume Set: Materials, Processes, Systems, and Technology*. John Wiley & Sons, 2016.

[67] M. R. Patel, *Wind and solar power systems: design, analysis, and operation*. CRC press, 2005.

[68] J. Kaldellis, E. Kondili, and A. Filios, "Sizing a hybrid wind-diesel stand-alone system on the basis of minimum long-term electricity production cost," *Applied Energy,* vol. 83, no. 12, pp. 1384-1403, 2006.

[69] A. S. Al Busaidi, H. A. Kazem, A. H. Al-Badi, and M. F. Khan, "A review of optimum sizing of hybrid PV–Wind renewable energy systems in oman," *Renewable and Sustainable Energy Reviews,* vol. 53, pp. 185-193, 2016.

[70] M. D. Al-Falahi, S. Jayasinghe, and H. Enshaei, "A review on recent size optimization methodologies for standalone solar and wind hybrid renewable energy system," *Energy conversion and management,* vol. 143, pp. 252-274, 2017.

[71] P. Chen and T. Thiringer, "Analysis of energy curtailment and capacity overinstallation to maximize wind turbine profit considering electricity price–wind correlation," *Ieee T Sustain Energ,* vol. 8, no. 4, pp. 1406-1414, 2017.

[72] R. Hosseinalizadeh, H. Shakouri, M. S. Amalnick, and P. Taghipour, "Economic sizing of a hybrid (PV–WT–FC) renewable energy system (HRES) for stand-alone usages by an optimization-simulation model: Case study of Iran," *Renewable and Sustainable Energy Reviews,* vol. 54, pp. 139-150, 2016.

[73] M. Smaoui, A. Abdelkafi, and L. Krichen, "Optimal sizing of stand-alone photovoltaic/wind/hydrogen hybrid system supplying a desalination unit," *Sol Energy,* vol. 120, pp. 263-276, 2015.

[74] R. Belfkira, L. Zhang, and G. Barakat, "Optimal sizing study of hybrid wind/PV/diesel power generation unit," *Sol Energy,* vol. 85, no. 1, pp. 100-110, 2011.

[75] C. E. C. Nogueira *et al.*, "Sizing and simulation of a photovoltaic-wind energy system using batteries, applied for a small rural property located in the south of Brazil," *Renewable and Sustainable Energy Reviews,* vol. 29, pp. 151-157, 2014.

[76] H.-C. Chen, "Optimum capacity determination of stand-alone hybrid generation system considering cost and reliability," *Applied Energy,* vol. 103, pp. 155-164, 2013.

[77] P. D. Diamantoulakis, V. M. Kapinas, and G. K. Karagiannidis, "Big Data Analytics for Dynamic Energy Management in Smart Grids," (in English), *Big Data Res,* vol. 2, no. 3, pp. 94-101, Sep 2015, doi: 10.1016/j.bdr.2015.03.003.

[78] T. Mastelic, A. Oleksiak, H. Claussen, I. Brandic, J. M. Pierson, and A. V. Vasilakos, "Cloud Computing: Survey on Energy Efficiency," (in English), *Acm Comput Surv,* vol. 47, no. 2, Jan 2015, doi: Artn 33

10.1145/2656204.

[79]   J. Minguez, M. Jakob, U. Heinkel, and B. Mitschang, "A SOA-based Approach for the Integration of a Data Propagation System," (in English), *Proceedings of the 2009 Ieee International Conference on Information Reuse and Integration,* pp. 47-52, 2008. [Online]. Available: <Go to ISI>://WOS:000274330000009.

[80]   B. S. Borowy and Z. M. Salameh, "Methodology for optimally sizing the combination of a battery bank and PV array in a wind/PV hybrid system," *Ieee T Energy Conver,* vol. 11, no. 2, pp. 367-375, 1996.

[81]   T. Markvart, "Sizing of hybrid photovoltaic-wind energy systems," *Sol Energy,* vol. 57, no. 4, pp. 277-281, 1996.

[82]   L. L. Bucciarelli Jr, "Estimating loss-of-power probabilities of stand-alone photovoltaic solar energy systems," *Sol Energy,* vol. 32, no. 2, pp. 205-209, 1984.

[83]   J. Gordon, "Optimal sizing of stand-alone photovoltaic solar power systems," *Solar cells,* vol. 20, no. 4, pp. 295-313, 1987.

[84]   G. Tina, S. Gagliano, and S. Raiti, "Hybrid solar/wind power system probabilistic modelling for long-term performance assessment," *Sol Energy,* vol. 80, no. 5, pp. 578-588, 2006.

[85]   H. Yang, L. Lu, and W. Zhou, "A novel optimization sizing model for hybrid solar-wind power generation system," *Sol Energy,* vol. 81, no. 1, pp. 76-84, 2007.

[86]   E. Koutroulis, D. Kolokotsa, A. Potirakis, and K. Kalaitzakis, "Methodology for optimal sizing of stand-alone photovoltaic/wind-generator systems using genetic algorithms," *Sol Energy,* vol. 80, no. 9, pp. 1072-1088, 2006.

[87]   H. Yang, W. Zhou, L. Lu, and Z. Fang, "Optimal sizing method for stand-alone hybrid solar–wind system with LPSP technology by using genetic algorithm," *Sol Energy,* vol. 82, no. 4, pp. 354-367, 2008.

[88]   G. Seeling-Hochmuth, "A combined optimisation concet for the design and operation strategy of hybrid-PV energy systems," *Sol Energy,* vol. 61, no. 2, pp. 77-87, 1997.

[89]   X. Pelet, D. Favrat, and G. Leyland, "Multiobjective optimisation of integrated energy systems for remote communities considering economics and CO2 emissions," *International journal of Thermal sciences,* vol. 44, no. 12, pp. 1180-1189, 2005.

[90]   R. Dufo-Lopez and J. L. Bernal-Agustín, "Multi-objective design of PV–wind–diesel–hydrogen–battery systems," *Renew Energ,* vol. 33, no. 12, pp. 2559-2572, 2008.

[91]   A. Berrada and K. Loudiyi, "Operation, sizing, and economic evaluation of storage for solar and wind power plants," *Renewable and sustainable energy Reviews,* vol. 59, pp. 1117-1129, 2016.

[92]   J. P. Fossati, A. Galarza, A. Martín-Villate, and L. Fontan, "A method for optimal sizing energy storage systems for microgrids," *Renew Energ,* vol. 77, pp. 539-549, 2015.

[93]   M. I. Blanco, "The economics of wind energy," *Renewable and sustainable energy reviews,* vol. 13, no. 6-7, pp. 1372-1382, 2009.

[94]   D. G. Caglayan, D. S. Ryberg, H. Heinrichs, J. Linßen, D. Stolten, and M. Robinius, "The techno-economic potential of offshore wind energy with optimized future turbine designs in Europe," *Applied Energy,* vol. 255, p. 113794, 2019.

[95]   E. Dupont, R. Koppelaar, and H. Jeanmart, "Global available solar energy under physical and energy return on investment constraints," *Applied Energy,* vol. 257, p. 113968, 2020.

[96]   P. Denholm, G. L. Kulcinski, and T. Holloway, "Emissions and energy efficiency assessment of baseload wind energy systems," *Environmental science & technology,* vol. 39, no. 6, pp. 1903-1911, 2005.

[97]   I. Komušanac, B. Ćosić, and N. Duić, "Impact of high penetration of wind and solar PV generation on the country power system load: the case study of Croatia," *Applied energy,* vol. 184, pp. 1470-1482, 2016.

[98]   R. Turconi, C. O'Dwyer, D. Flynn, and T. Astrup, "Emissions from cycling of thermal power plants in electricity systems with high penetration of wind power: Life cycle assessment for Ireland," *Applied energy,* vol. 131, pp. 1-8, 2014.

[99]   P. Denholm and M. Hand, "Grid flexibility and storage required to achieve very high penetration of variable renewable electricity," *Energy Policy,* vol. 39, no. 3, pp. 1817-1830, 2011.

[100]   P. Denholm and R. M. Margolis, "Evaluating the limits of solar photovoltaics (PV) in traditional electric power systems," *Energy policy,* vol. 35, no. 5, pp. 2852-2861, 2007.

[101]   M. Milligan *et al.*, "Integration of variable generation, cost-causation, and integration costs," *The Electricity Journal,* vol. 24, no. 9, pp. 51-63, 2011.

[102]   W. Katzenstein and J. Apt, "The cost of wind power variability," *Energy Policy,* vol. 51, pp. 233-243, 2012.

[103]   J. Chang, K. Madjarov, R. Baldick, A. Alvarez, and P. Q. Hanser, "Renewable integration model and analysis," in *IEEE PES T&D 2010*, 2010: IEEE, pp. 1-8.

[104]   S. Diaf and G. Notton, "Technical and economic analysis of large-scale wind energy conversion systems in Algeria," *Renewable and Sustainable Energy Reviews,* vol. 19, pp. 37-51, 2013.

[105]   A. A. Shata and R. Hanitsch, "Evaluation of wind energy potential and electricity generation on the coast of Mediterranean Sea in Egypt," *Renew Energ,* vol. 31, no. 8, pp. 1183-1202, 2006.

[106]   M. A. Ramli, A. Hiendro, and Y. A. Al-Turki, "Techno-economic energy analysis of wind/solar hybrid system: Case study for western coastal area of Saudi Arabia," *Renew Energ,* vol. 91, pp. 374-385, 2016.

[107]   D. Saheb-Koussa, M. Haddadi, and M. Belhamel, "Economic and technical study of a hybrid system (wind–photovoltaic–diesel) for rural electrification in Algeria," *Applied Energy,* vol. 86, no. 7-8, pp. 1024-1030, 2009.

[108]   L. Hirth, F. Ueckerdt, and O. Edenhofer, "Integration costs revisited–An economic framework for wind and solar variability," *Renew Energ,* vol. 74, pp. 925-939, 2015.

[109]   H. S. Chen, T. N. Cong, W. Yang, C. Q. Tan, Y. L. Li, and Y. L. Ding, "Progress in electrical energy storage system: A critical review," (in English), *Prog Nat Sci-Mater,* vol. 19, no. 3, pp. 291-312, Mar 10 2009, doi: 10.1016/j.pnsc.2008.07.014.

[110]   D. Rastler, *Electricity energy storage technology options: a white paper primer on applications, costs and benefits*. Electric Power Research Institute, 2010.

[111]   M. Beaudin, H. Zareipour, A. Schellenberglabe, and W. Rosehart, "Energy storage for mitigating the variability of renewable electricity sources: An updated review," *Energy Sustain Dev.,* vol. 14, no. 4, pp. 302-314, 2010.

[112]   H. Zhao, Q. Wu, S. Hu, H. Xu, and C. N. Rasmussen, "Review of energy storage system for wind power integration support," *Applied energy,* vol. 137, pp. 545-553, 2015.

[113]   T. Ayodele and A. Ogunjuyigbe, "Mitigation of wind power intermittency: Storage technology approach," *Renewable and Sustainable Energy Reviews,* vol. 44, pp. 447-456, 2015.

[114]   F. Díaz-González, A. Sumper, O. Gomis-Bellmunt, and R. Villafáfila-Robles, "A review of energy storage technologies for wind power applications," *Renewable and sustainable energy reviews,* vol. 16, no. 4, pp. 2154-2171, 2012.

[115]   A. Gallo, J. Simões-Moreira, H. Costa, M. Santos, and E. M. dos Santos, "Energy storage in the energy transition context: A technology review," *Renewable and Sustainable Energy Reviews,* vol. 65, pp. 800-822, 2016.

[116]   C. J. Rydh and B. A. Sandén, "Energy analysis of batteries in photovoltaic systems. Part II: Energy return factors and overall battery efficiencies," *Energy conversion and management,* vol. 46, no. 11-12, pp. 1980-2000, 2005.

[117] A. Jaiswal, "Lithium-ion battery based renewable energy solution for off-grid electricity: A techno-economic analysis," *Renewable and Sustainable Energy Reviews,* vol. 72, pp. 922-934, 2017.

[118] C. D. Parker, "Lead–acid battery energy-storage systems for electricity supply networks," *Journal of Power Sources,* vol. 100, no. 1-2, pp. 18-28, 2001.

[119] J. B. Greenblatt, S. Succar, D. C. Denkenberger, R. H. Williams, and R. H. Socolow, "Baseload wind energy: modeling the competition between gas turbines and compressed air energy storage for supplemental generation," *Energy Policy,* vol. 35, no. 3, pp. 1474-1492, 2007.

[120] A. Kaabeche and R. Ibtiouen, "Techno-economic optimization of hybrid photovoltaic/wind/diesel/battery generation in a stand-alone power system," *Solar Energy,* vol. 103, pp. 171-182, 2014.

[121] M. Wakihara, "Recent developments in lithium ion batteries," *Materials Science and Engineering: R: Reports,* vol. 33, no. 4, pp. 109-134, 2001.

[122] B. Dursun and B. Alboyaci, "The contribution of wind-hydro pumped storage systems in meeting Turkey's electric energy demand," *Renewable and Sustainable Energy Reviews,* vol. 14, no. 7, pp. 1979-1988, 2010.

[123] P. Bajpai and V. Dash, "Hybrid renewable energy systems for power generation in stand-alone applications: A review," *Renewable and Sustainable Energy Reviews,* vol. 16, no. 5, pp. 2926-2939, 2012.

[124] D. Ipsakis, S. Voutetakis, P. Seferlis, F. Stergiopoulos, and C. Elmasides, "Power management strategies for a stand-alone power system using renewable energy sources and hydrogen storage," *International journal of hydrogen energy,* vol. 34, no. 16, pp. 7081-7095, 2009.

[125] D. Ipsakis, S. Voutetakis, P. Seferlis, F. Stergiopoulos, S. Papadopoulou, and C. Elmasides, "The effect of the hysteresis band on power management strategies in a stand-alone power system," *Energy,* vol. 33, no. 10, pp. 1537-1550, 2008.

[126] E. Dursun and O. Kilic, "Comparative evaluation of different power management strategies of a stand-alone PV/Wind/PEMFC hybrid power system," *International Journal of Electrical Power & Energy Systems,* vol. 34, no. 1, pp. 81-89, 2012.

[127] M. S. Ismail, M. Moghavvemi, and T. Mahlia, "Design of an optimized photovoltaic and microturbine hybrid power system for a remote small community: case study of Palestine," *Energy conversion and management,* vol. 75, pp. 271-281, 2013.

[128] S. Abedi, A. Alimardani, G. Gharehpetian, G. Riahy, and S. Hosseinian, "A comprehensive method for optimal power management and design of hybrid RES-based autonomous energy systems," *Renewable and Sustainable Energy Reviews,* vol. 16, no. 3, pp. 1577-1587, 2012.

[129] N. Karami, N. Moubayed, and R. Outbib, "Energy management for a PEMFC–PV hybrid system," *Energy conversion and management,* vol. 82, pp. 154-168, 2014.

[130] H. Kim, S. Baek, E. Park, and H. J. Chang, "Optimal green energy management in Jeju, South Korea–On-grid and off-grid electrification," *Renewable energy,* vol. 69, pp. 123-133, 2014.

[131] G. Dalton, D. Lockington, and T. Baldock, "Feasibility analysis of renewable energy supply options for a grid-connected large hotel," *Renewable energy,* vol. 34, no. 4, pp. 955-964, 2009.

[132] D. Saheb-Koussa, M. Koussa, M. Belhamel, and M. Haddadi, "Economic and environmental analysis for grid-connected hybrid photovoltaic-wind power system in the arid region," *Energy Procedia,* vol. 6, pp. 361-370, 2011.

[133] A. Ozbilen, I. Dincer, G. Naterer, and M. Aydin, "Role of hydrogen storage in renewable energy management for Ontario," *International journal of hydrogen energy,* vol. 37, no. 9, pp. 7343-7354, 2012.

[134] C. Draxl, A. Clifton, B.-M. Hodge, and J. McCaa, "The wind integration national dataset (wind) toolkit," *Applied Energy,* vol. 151, pp. 355-366, 2015.

[135] M. Brower, "Development of eastern regional wind resource and wind plant output datasets," *Rep. No. NREL/SR-550,* vol. 46764, 2009.

[136] M. Sengupta, Y. Xie, A. Lopez, A. Habte, G. Maclaurin, and J. Shelby, "The national solar radiation data base (NSRDB)," *Renewable and Sustainable Energy Reviews,* vol. 89, pp. 51-60, 2018.

[137] I. Abouzahr and R. Ramakumar, "Loss of power supply probability of stand-alone wind electric conversion systems: a closed form solution approach," *Ieee T Energy Conver,* vol. 5, no. 3, pp. 445-452, 1990.

[138] J. King, A. Clifton, and B.-M. Hodge, "Validation of power output for the WIND Toolkit," National Renewable Energy Lab.(NREL), Golden, CO (United States), 2014.

[139] J. Zhang, C. Draxl, T. Hopson, L. Delle Monache, E. Vanvyve, and B.-M. Hodge, "Comparison of numerical weather prediction based deterministic and probabilistic wind resource assessment methods," *Applied Energy,* vol. 156, pp. 528-541, 2015.

[140] C. Draxl *et al.*, "Advancements in Wind Integration Study Data Modeling: The Wind Integration National Dataset (WIND) Toolkit," National Renewable Energy Lab.(NREL), Golden, CO (United States), 2013.

[141] M. Kaltschmitt, W. Streicher, and A. Wiese, *Renewable energy: technology, economics and environment*. Springer Science & Business Media, 2007.

[142] E. Elibol, Ö. T. Özmen, N. Tutkun, and O. Köysal, "Outdoor performance analysis of different PV panel types," *Renewable and Sustainable Energy Reviews,* vol. 67, pp. 651-661, 2017.

[143] D. Yang, "Kriging for NSRDB PSM version 3 satellite-derived solar irradiance," *Solar Energy,* vol. 171, pp. 876-883, 2018.

[144] D. Yang, "Spatial prediction using kriging ensemble," *Solar Energy,* vol. 171, pp. 977-982, 2018.

[145] D. Yang, "A correct validation of the national solar radiation data base (NSRDB)," *Renewable and Sustainable Energy Reviews,* vol. 97, pp. 152-155, 2018.

[146] J. A. Duffie, W. A. Beckman, and N. Blair, *Solar Engineering of Thermal Processes, Photovoltaics and Wind*. John Wiley & Sons, 2020.

[147] R. Thiéblemont, K. Matthes, N.-E. Omrani, K. Kodera, and F. Hansen, "Solar forcing synchronizes decadal North Atlantic climate variability," *Nature communications,* vol. 6, p. 8268, 2015.

[148] C. L. Archer and M. Z. Jacobson, "Supplying baseload power and reducing transmission requirements by interconnecting wind farms," *Journal of Applied Meteorology and Climatology,* vol. 46, no. 11, pp. 1701-1717, 2007.

[149] Y.-h. Wan, M. Milligan, and B. Parsons, "Output power correlation between adjacent wind power plants," *J. Sol. Energy Eng.,* vol. 125, no. 4, pp. 551-555, 2003.

[150] J. Schoukens, R. Pintelon, E. Van Der Ouderaa, and J. Renneboog, "Survey of excitation signals for FFT based signal analyzers," *IEEE Transactions on Instrumentation and Measurement,* vol. 37, no. 3, pp. 342-352, 1988.

[151] D. Crescini, A. Flammini, D. Marioli, and A. Taroni, "Application of an FFT-based algorithm to signal processing of LVDT position sensors," *IEEE Transactions on Instrumentation and Measurement,* vol. 47, no. 5, pp. 1119-1123, 1998.

[152] S. G. Johnson and M. Frigo, "A modified split-radix FFT with fewer arithmetic operations," *IEEE Transactions on Signal Processing,* vol. 55, no. 1, pp. 111-119, 2006.

[153] J. K. Kaldellis and D. Zafirakis, "The wind energy (r) evolution: A short review of a long history," *Renew Energ,* vol. 36, no. 7, pp. 1887-1901, 2011.

[154] L. He, S. Zhang, Y. Chen, L. Ren, and J. Li, "Techno-economic potential of a renewable energy-based microgrid system for a sustainable large-scale residential community in Beijing, China," *Renewable and Sustainable Energy Reviews,* vol. 93, pp. 631-641, 2018.

[155] Q. Yuan, K. Zhou, and J. Yao, "A new measure of wind power variability with implications for the optimal sizing of standalone wind power systems," *Renewable Energy,* vol. 150, pp. 538-549, 2020.

[156] B. P. Baddipadiga and M. Ferdowsi, "A high-voltage-gain dc-dc converter based on modified dickson charge pump voltage multiplier," *Ieee T Power Electr,* vol. 32, no. 10, pp. 7707-7715, 2016.

[157] Q. Yuan, K. Zhou, W. Lu, and J. Yao, "Big data driven optimal sizing of stand-alone photovoltaic energy systems," in *2018 13th IEEE Conference on Industrial Electronics and Applications (ICIEA)*, 2018: IEEE, pp. 679-684.

[158] R. Chedid and S. Rahman, "Unit sizing and control of hybrid wind-solar power systems," *Ieee T Energy Conver,* vol. 12, no. 1, pp. 79-85, 1997.

[159] S. Hakimi, S. M. Tafreshi, and A. Kashefi, "Unit sizing of a stand-alone hybrid power system using particle swarm optimization (PSO)," in *2007 IEEE international conference on automation and logistics*, 2007: IEEE, pp. 3107-3112.

[160] N. DiOrio, A. Dobos, and S. Janzou, "Economic analysis case studies of battery energy storage with SAM," National Renewable Energy Lab.(NREL), Golden, CO (United States), 2015.

[161] W. Kellogg, M. Nehrir, G. Venkataramanan, and V. Gerez, "Generation unit sizing and cost analysis for stand-alone wind, photovoltaic, and hybrid wind/PV systems," *Ieee T Energy Conver,* vol. 13, no. 1, pp. 70-75, 1998.

[162] D. B. Nelson, M. H. Nehrir, and C. Wang, "Unit sizing and cost analysis of stand-alone hybrid wind/PV/fuel cell power generation systems," *Renew Energ,* vol. 31, no. 10, pp. 1641-1656, 2006.

[163] A. Maheri, "Multi-objective design optimisation of standalone hybrid wind-PV-diesel systems under uncertainties," *Renew Energ,* vol. 66, pp. 650-661, 2014.

[164] T. U. S. E. I. Administration. "EIA introduces short-term forecasts for wholesale electricity prices." https://www.eia.gov/todayinenergy/detail.php?id=40793 (accessed.

[165] N. E. M. Association, *American National Standard for Electric Power Systems and Equipment-Voltage Ratings (60 Hertz).* National Electrical Manufacturers Association, 1996.

[166] T. U. S. E. I. Administration. "U.S. electric system is made up of interconnections and balancing authorities." https://www.eia.gov/todayinenergy/detail.php?id=27152 (accessed.

[167] E. I. Administration, *Annual energy review 2011*. Government Printing Office, 2012.

[168] E. Ela and B. Kirby, "ERCOT event on February 26, 2008: lessons learned," National Renewable Energy Lab.(NREL), Golden, CO (United States), 2008.

[169] U. S. E. I. Administration, *Annual Energy Review*. The Office, 2007.

[170] L. E. Jones, *Renewable energy integration: practical management of variability, uncertainty, and flexibility in power grids*. Academic press, 2017.

[171] E. Lannoye *et al.*, "Integration of variable generation: Capacity value and evaluation of flexibility," in *IEEE PES General Meeting*, 2010: IEEE, pp. 1-6.

[172] M. Joos and I. Staffell, "Short-term integration costs of variable renewable energy: Wind curtailment and balancing in Britain and Germany," *Renewable and Sustainable Energy Reviews,* vol. 86, pp. 45-65, 2018.

[173] L. Bird, J. Cochran, and X. Wang, "Wind and solar energy curtailment: Experience and practices in the United States," National Renewable Energy Lab.(NREL), Golden, CO (United States), 2014.

[174] M. Milligan and B. Kirby, "Calculating wind integration costs: Separating wind energy value from integration cost impacts," National Renewable Energy Lab.(NREL), Golden, CO (United States), 2009.

[175] J. Kabouris and F. Kanellos, "Impacts of large-scale wind penetration on designing and operation of electric power systems," *Ieee T Sustain Energ,* vol. 1, no. 2, pp. 107-114, 2010.

[176] J. Nazarko and Z. A. Styczynski, "Application of statistical and neural approaches to the daily load profiles modelling in power distribution systems," in *1999 IEEE transmission and distribution conference (Cat. No. 99CH36333)*, 1999, vol. 1: IEEE, pp. 320-325.

[177] J. Wu, T. Lee, K. Lo, J. Chen, and C. Lin, "A reliability-centered outage scheduling with considering daily load patterns and load transfer for electrical distribution feeders," in *2006 International Conference on Probabilistic Methods Applied to Power Systems*, 2006: IEEE, pp. 1-6.

[178] X. Li, X. Jiang, J. Qian, H. Chen, J. Song, and L. HUANG, "A classifying and synthesizing method of power consumer industry based on the daily load profile," *Automation of Electric Power Systems,* vol. 34, no. 10, pp. 56-61, 2010.

List of Publication

Articles in Journal

Q. Yuan, K. Zhou, and J. Yao, "A new measure of wind power variability with implications for the optimal sizing of standalone wind power systems," *Renewable Energy,* vol. 150, pp. 538-549, 2020.

Q. Yuan, K. Zhou, J. Yao, W. Luo, J. Yang, "Impacts of solar power variability on the optimal sizing of standalone photovoltaic systems", submitted to *IET Renewable Power Generation*, under review

Q. Yuan, K. Zhou, J. Yao, W. Luo, J. Yang, "Inspiration from wind and solar power variability to system economics and flexibility", submitted to *Energy Policy*, under review

Articles in Conference Proceeding

Q. Yuan, K. Zhou, W. Lu, and J. Yao, "Big data driven optimal sizing of stand-alone photovoltaic energy systems," in *2018 13th IEEE Conference on Industrial Electronics and Applications (ICIEA)*, 2018, pp. 679-684: IEEE.